CRANFIELD UNIVERSITY

VILIUS PORTAPAS

HANDLING QUALITIES OF HIGH ASPECT RATIO WING AIRCRAFT

SCHOOL OF AEROSPACE, TRANSPORT AND MANUFACTURING
Aerospace Engineering

PHD THESIS
Academic Year: 2017–2018

Supervisors: Dr Mudassir Lone and Dr Alastair Cooke

July 2018

CRANFIELD UNIVERSITY

SCHOOL OF AEROSPACE, TRANSPORT AND MANUFACTURING
Aerospace Engineering

PhD Thesis

Academic Year: 2017–2018

VILIUS PORTAPAS

Handling qualities of high aspect ratio wing aircraft

Supervisors: Dr Mudassir Lone and Dr Alastair Cooke

July 2018

This thesis is submitted in partial fulfilment of the requirements for the degree of PhD.

© Cranfield University 2018. All rights reserved. No part of this publication may be reproduced without the written permission of the copyright owner.

Abstract

To reduce the environmental impact of the aviation industry aircraft designers invest much effort to develop new and improve existing technologies to create new aircraft configurations. New high aspect ratio wings allow to improve aerodynamic efficiency while reducing aircraft weight through the use of new lightweight materials. However, their slenderness tends to introduce significant interaction between flight dynamics and aeroelastics. These interactions need to be identified in order to allow future pilots to anticipate behaviour of those aircraft. The literature review revealed a gap in the knowledge of flying and handling qualities (HQs) of large transport highly flexible wing aircraft. Hence, this thesis presents a comparison between rigid and flexible aircraft configurations carried out by the means of the pilot-in-the-loop simulations of flight test manoeuvres.

Firstly, the analysis of the extended equations of motion, which consider the structural flexibility, revealed significant flexibility impact on the lateral/directional dynamics of the aircraft. Then, the equations were integrated into the Simulation Framework for Flexible Aircraft (SFFA) that was developed by integrating the aeroservoelastic model CA^{2}LM with the engineering flight simulator EFS500. The simulation campaign was performed using the SFFA for the HARTEN aircraft model, which exhibited an unusually aft neutral point position. The results of the simulation campaign revealed minor differences in the longitudinal dynamics between the rigid and flexible aircraft. However, the lateral/directional dynamics showed significant differences, especially in the change of the Dutch roll shape from horizontal to vertical and the spiral mode from unstable to neutrally stable. It also highlighted the 'wing rocking' phenomenon and the 'wing ratcheting' significantly decreased roll performance. Finally, a new slalom task proved its applicability to efficiently assess HQs and revealed a degradation of HQs for the flexible aircraft configuration. The SFFA was also assessed and limiting hardware issues were indicated to support the comparison of aircraft HQs.

For the future it is recommended to identify a set of dynamic parameters that would allow to highlight deficiencies of flexible aircraft and to improve the SFFA allowing pilots to fully concentrate on the task.

Keywords: Aeroservoelasticity, Aircraft Dynamics, Flexible Aircraft, Flight Dynamics, Flying Qualities, Handling Qualities, Pilot-in-the-loop Simulation.

Acknowledgements

Firstly, I would like to express my gratitude to my supervisor Dr Mudassir Lone for giving me this opportunity to carry out the PhD research at Cranfield University. This would be impossible without his belief in me and his care of all the project matters. His endless advices, guidance and support allowed me to see the world from a different perspective. Thanks for bringing the world together here in Cranfield.

Secondly, I would like to express my gratitude to Dr Alastair Cooke and Dr James Whidborne for managing the Dynamics, Simulation and Control Group. Alastair's precise advices and guidance cleared my path in the blurry world of research.

Gaetan Dussart, David Hayes, Alessandro Pontillo, Simone Weber and Sezsy Yusuf deserved appreciations for their endless friendship and support, courtesy and respect, questions and answers, and a continuous drive of the group. All of you together with the recent joiners to the group Raheeg Alamin and Martin Carrizales created so many joyful moments without which life would have been much sadder here in Cranfield. Our tea time conversations induced many new ideas and solved many problems. I would also like to appreciate former member of the group Guillermo Lopez without whom the real-time flight simulator would have never been developed and this project would have hardly finished.

I would like to acknowledge Airbus for their sponsorship and support through the AWI project. Thanks to Dr Etienne Coetzee for his friendship and supervision during my stay at the Future Projects Office and all the support he provided afterwards. Thanks to PhD students and research associates from the University of Bristol AWI project group for their friendship, support and understanding during the AWI project workshops and international conferences.

I express my special gratitude to my family who always support me during my adventures and my journey through life. My parents Vladas and Valerija, my sister Egle and her family have always been an inspiration to me.

Contents

Abstract v

Acknowledgements vii

Nomenclature xxi

List of Abbreviations xxv

1 Introduction 1
- 1.1 Aim and objectives . . . 4
- 1.2 Scope of thesis . . . 5
- 1.3 Thesis outline . . . 5

2 Literature review 7
- 2.1 The use of high aspect ratio wings . . . 7
  - 2.1.1 Sailplanes . . . 7
  - 2.1.2 Commercial airliners . . . 9
- 2.2 Modelling flexible aircraft . . . 12
  - 2.2.1 Equations of motion for flexible bodies . . . 12
  - 2.2.2 Modelling and simulation of flexible aircraft . . . 14
- 2.3 Flight testing and handling qualities evaluation . . . 17
  - 2.3.1 Control Anticipation Parameter . . . 18
  - 2.3.2 C* criterion . . . 20
  - 2.3.3 Gibson Dropback criterion . . . 21
  - 2.3.4 Bandwidth criterion . . . 22
  - 2.3.5 Neal-Smith criterion . . . 23
  - 2.3.6 Experimental Behaviour Measurement Method . . . 25
  - 2.3.7 Discussion of time domain and frequency domain handling qualities criteria . . . 28
  - 2.3.8 Cooper-Harper Rating . . . 29
  - 2.3.9 Flight test manoeuvres . . . 32
  - 2.3.10 Handling qualities evaluation . . . 33

2.3.11 Importance of simulator motion cues on handling qualities assessment . . . 33

3 Equations of motion for flexible aircraft 35
3.1 Derivation of equations of motion . . . 35
3.1.1 Equation of accelerations . . . 36
3.1.2 Equation of forces . . . 38
3.1.3 Equation of moments . . . 38
3.2 Comparison with rigid body EoM . . . 39
3.2.1 Trim (static) results . . . 41
3.2.2 Dynamic response of aircraft . . . 41
3.3 Summary of the chapter . . . 43

4 Flight simulation framework 45
4.1 CA^{2}LM – MATLAB/Simulink based flight physics framework . . . 45
4.1.1 Aerodynamics of the wing, horizontal and vertical tailplanes . . . 45
4.1.2 Aerodynamics of the fuselage and nacelles . . . 49
4.1.3 Structural dynamics . . . 51
4.1.4 Environment and gravity models . . . 53
4.1.5 Equations of motion . . . 54
4.1.6 The use of the CA^{2}LM framework . . . 54
4.1.7 Upgrades to the CA^{2}LM framework . . . 58
4.1.8 Limitations of the CA^{2}LM framework . . . 61
4.2 EFS500 flight simulator . . . 61
4.2.1 Hardware . . . 61
4.2.2 Software . . . 65
4.3 Integration of the CA^{2}LM framework with the EFS500 . . . 66
4.4 Summary of the chapter . . . 70

5 HARTEN 71
5.1 HARTEN definition . . . 72
5.1.1 Wing, horizontal and vertical tailplanes . . . 73
5.1.2 Fuselage and engines . . . 75
5.2 Definition of HARTEN configurations for testing . . . 75
5.2.1 Mass configurations . . . 75
5.2.2 Flexibility configurations . . . 76
5.2.3 Flight conditions . . . 77
5.3 Longitudinal static stability . . . 77

6 Flight simulation campaign 81
6.1 Preparation for the test campaign . . . 82
6.1.1 Aircraft structural flexibility configurations . . . 82
6.1.2 Test pilots . . . 83

6.1.3 Flying and handling qualities evaluation metrics 84
6.2 Test manoeuvres 84
6.2.1 Stall conditions test 85
6.2.2 Short period pitching oscillation mode test 86
6.2.3 Phugoid mode test 86
6.2.4 Steady heading sideslip test 87
6.2.5 Roll mode test 87
6.2.6 Spiral mode test 88
6.2.7 Dutch roll mode test 88
6.2.8 Slalom task for the HQs assessment 89

7 Flight simulation results **93**
7.1 Comparison between rigid and flexible aircraft dynamics 93
7.1.1 Stall performance 93
7.1.2 Longitudinal dynamics 96
7.1.3 Lateral/directional dynamics 101
7.1.4 Slalom task 111
7.2 Assessment of SFFA 114
7.2.1 Software 114
7.2.2 Hardware 116
7.3 Summary of the chapter 117
7.3.1 Summary of longitudinal and lateral/directional FQs and HQs . . 117
7.3.2 Discussion of SFFA 119

8 Conclusions and further work **121**
8.1 Conclusions 121
8.2 Further work 123
8.2.1 Handling qualities of flexible aircraft 123
8.2.2 Simulation Framework for Flexible Aircraft 124
8.3 Contribution to knowledge 125
8.4 Dissemination of results 126
8.4.1 Technical presentations 126
8.4.2 Conference papers 126
8.4.3 Journal articles 127

A Data of SUGAR, eta sailplane and Lilienthal hang glider **143**
A.1 The Subsonic Ultra Green Aircraft Research, or SUGAR, Freeze design concept 143
A.2 Lilienthal hang glider 144
A.3 eta sailplane on final 145
A.4 Aspect ratio of eta sailplane 146
A.5 Aerodynamic efficiency of eta sailplane 147

A Unsteady aerodynamic state-space model matrices **149**

B Time histories for Gibson Dropback criterion **151**

C Data for the static margin definition of HARTEN **153**

D Stall simulation data **155**
D.1 Stall conditions test, pilot 1, rigid A/C – ST(1)R 156
D.2 Stall conditions test, pilot 1, flexible A/C – ST(1)F 161
D.3 Stall conditions test, pilot 2, rigid A/C – ST(2)R 166
D.4 Stall conditions test, pilot 2, flexible A/C – ST(2)F 171

E Longitudinal modes simulation data **177**
E.1 SPPO mode, pilot 1, rigid A/C – SP(1)R 178
E.2 SPPO mode, pilot 1, flexible A/C – SP(1)F 183
E.3 SPPO mode, pilot 2, rigid A/C – SP(2)R 188
E.4 SPPO mode, pilot 2, flexible A/C, frequency sweep input – SP(2)F-FS . . 193
E.5 SPPO mode, pilot 2, flexible A/C, elevator doublet input – SP(2)F-PD . . 198
E.6 Phugoid mode, pilot 1, rigid A/C – PH(1)R 203
E.7 Phugoid mode, pilot 1, flexible A/C – PH(1)F 208
E.8 Phugoid mode, pilot 2, rigid A/C – PH(2)R 213
E.9 Phugoid mode, pilot 2, flexible A/C – PH(2)F 218

F Lateral/directional modes simulation data **223**
F.1 Steady heading sideslip, pilot 1, rigid A/C – SH(1)R 224
F.2 Steady heading sideslip, pilot 1, flexible A/C – SH(1)F 229
F.3 Steady heading sideslip, pilot 2, rigid A/C – SH(2)R 234
F.4 Steady heading sideslip, pilot 2, flexible A/C – SH(2)F 239
F.5 Roll mode, pilot 1, flexible A/C – RM(1)F 244
F.6 Roll mode, pilot 2, rigid A/C – RM(2)R 249
F.7 Roll mode, pilot 2, flexible A/C – RM(2)F 254
F.8 Spiral mode, pilot 1, rigid A/C – SM(1)R 259
F.9 Spiral mode, pilot 2, rigid A/C – SM(2)R 264
F.10 Spiral mode, pilot 2, flexible A/C – SM(2)F 269
F.11 Dutch roll, pilot 1, rigid A/C – DR(1)R 274
F.12 Dutch roll, pilot 2, rigid A/C – DR(2)R 279
F.13 Dutch roll, pilot 2, flexible A/C – DR(2)F 284

G Slalom task simulation data **289**
G.1 Slalom task, pilot 2, rigid A/C – SL(2)R 290
G.2 Slalom task, pilot 2, flexible A/C – SL(2)F 295
G.3 Slalom task, pilot 3, rigid A/C – SL(3)R 300
G.4 Slalom task, pilot 3, flexible A/C – SL(3)F 305

List of Figures

1.1 AR impact on lateral static stability 2
1.2 Recent aircraft investigated for the structural flexibility impact on HQs . . 3
1.3 Helios Prototype in flight and its disintegration 3
1.4 Examples of HAR wing commercial aircraft concepts 4

2.1 Examples of past and current gliders 8
2.2 AR increase during years 10
2.3 Wing deflection of Boeing 787 aircraft under ground, 1g and ultimate loading 11
2.4 Currently investigated configurations of HAR wing aircraft 12
2.5 Rigid body and structural dynamics frequencies for conventional and flexible aircraft 14
2.6 Artificial wing elongation using the linear structural dynamics theory . . . 16
2.7 Definition of the Gibson Dropback criterion 22
2.8 Definition of the bandwidth criterion 24
2.9 Diagram of the experimental behaviour measurement method application 27
2.10 Cooper-Harper Rating scale 31

3.1 Axes system for equations of motion analysis 36
3.2 Comparison of EoM sets A and B for rigid and flexible body cases during pitch doublet disturbance 42
3.3 Comparison of EoM sets A and B for rigid and flexible body cases during aileron doublet disturbance 42
3.4 Comparison of EoM sets A and B for rigid and flexible body cases during rudder doublet disturbance 43

4.1 Structural representation of the CA^{2}LM framework 46
4.2 Aerodynamic model of the wing, HTP and VTP 47
4.3 Axes systems used in the CA^{2}LM framework 48
4.4 Stall angles of attack for NASA SC(2)-0010/0610 aerofoils 49
4.5 Sources of flexible fuselage and engine nacelle modelling methods 51
4.6 Aerodynamic and structural frames in the CA^{2}LM framework 52
4.7 The AX-1 aircraft model and its main specifications 55

4.8 Effect of airspeed on the longitudinal HQs of AX-1 model 56
4.9 Ailerons deflection ξ, angular rate, load factor n, wing root bending moment M_{root} and wing root torsion T_{root} and roll, pitch and yaw rates at aileron excitation frequency of 1.1634 Hz 57
4.10 Wing root bending moment M_{root} at different aileron excitation frequencies 58
4.11 New trim routine of the CA^{2}LM framework 60
4.12 Cockpit environment of the EFS500 flight simulator 63
4.13 Overall setup of the EFS500 flight simulator 64
4.14 EFS500 simulator network 64
4.15 PFD and EHSI displays in EFS500 flight simulator cockpit 65
4.16 Flight dynamics computer (Node 2) process flow 66
4.17 EFS500 simulator network with the Speedgoat real-time machine 68
4.18 Interface between the PFD computer and the Speedgoat real-time machine 68

5.1 HARTEN - Airbus UK proposed medium size flexible wing transport aircraft concept 71
5.2 Dimensions of the HARTEN fuselage and engines 75
5.3 Rigid and flexible wing deformations at the trim state 77
5.4 di_H/dC_L dependency on CG for different altitudes 78

6.1 Definition of the slalom task 90

7.1 Main parameters of the stall condition for each test case 94
7.2 Phugoid at the η limited stall condition during ST(1)R test 95
7.3 Dutch rolling of the aircraft as witnessed by the pilot during ST(1)F test . 95
7.4 Oscillation parameters 97
7.5 Main parameters of the SPPO mode tests using pitch doublet input 98
7.6 Main parameters of the SPPO mode tests using frequency sweep input . . 98
7.7 Main parameters of the phugoid mode tests using pulse input 101
7.8 Trends (linear fits) of main SHSS parameters 102
7.9 Main parameters for roll mode 105
7.10 Main parameters of the spiral mode 107
7.11 Coupling between the roll rate p and sideslip β 108
7.12 Main parameters for Dutch roll mode 109
7.13 Comparison of Φ and β parameters during Dutch roll mode 110
7.14 Adverse yaw during slalom tests 113
7.15 Slip and throttle indications on the PFD 115
7.16 The sidestick of the EFS500 116

A.1 NASA/Boeing SUGAR concept aircraft 143
A.2 Lilienthal hang glider 144
A.3 eta sailplane on final 145
A.4 Aspect ratio of eta sailplane 146

A.5 Aerodynamic efficiency of eta sailplane 147

B.1 Time histories of pitch rate q and pitch angle θ for minimum, maximum and inflection points of Fig. 4.8 152

C.1 $iH(C_L)$ variability with CG change at 5000 ft 153
C.2 $iH(C_L)$ variability with CG change at 10000 ft 154
C.3 $iH(C_L)$ variability with CG change at 15000 ft 154
C.4 $iH(C_L)$ variability with CG change at 20000ft 154

D.1 Test card (ST(1)R) 156
D.2 Time histories of altitude and velocities 157
D.3 Time histories of longitudinal parameters 158
D.4 Time histories of lateral parameters 159
D.5 Time histories of directional parameters 160
D.6 Test card (ST(1)F) 161
D.7 Time histories of altitude and velocities 162
D.8 Time histories of longitudinal parameters 163
D.9 Time histories of lateral parameters 164
D.10 Time histories of directional parameters 165
D.11 Test card (ST(2)R) 166
D.12 Time histories of altitude and velocities 167
D.13 Time histories of longitudinal parameters 168
D.14 Time histories of lateral parameters 169
D.15 Time histories of directional parameters 170
D.16 Test card (ST(2)F) 171
D.17 Time histories of altitude and velocities 172
D.18 Time histories of longitudinal parameters 173
D.19 Time histories of lateral parameters 174
D.20 Time histories of directional parameters 175

E.1 Test card (SP(1)R) 178
E.2 Time histories of altitude and velocities 179
E.3 Time histories of longitudinal parameters 180
E.4 Time histories of lateral parameters 181
E.5 Time histories of directional parameters 182
E.6 Test card (SP(1)F) 183
E.7 Time histories of altitude and velocities 184
E.8 Time histories of longitudinal parameters 185
E.9 Time histories of lateral parameters 186
E.10 Time histories of directional parameters 187
E.11 Test card (SP(2)R) 188
E.12 Time histories of altitude and velocities 189

E.13 Time histories of longitudinal parameters . . . 190
E.14 Time histories of lateral parameters . . . 191
E.15 Time histories of directional parameters . . . 192
E.16 Test card (SP(2)F-FS) . . . 193
E.17 Time histories of altitude and velocities . . . 194
E.18 Time histories of longitudinal parameters . . . 195
E.19 Time histories of lateral parameters . . . 196
E.20 Time histories of directional parameters . . . 197
E.21 Test card (SP(2)F-PD) . . . 198
E.22 Time histories of altitude and velocities . . . 199
E.23 Time histories of longitudinal parameters . . . 200
E.24 Time histories of lateral parameters . . . 201
E.25 Time histories of directional parameters . . . 202
E.26 Test card (PH(1)R) . . . 203
E.27 Time histories of altitude and velocities . . . 204
E.28 Time histories of longitudinal parameters . . . 205
E.29 Time histories of lateral parameters . . . 206
E.30 Time histories of directional parameters . . . 207
E.31 Test card (PH(1)F) . . . 208
E.32 Time histories of altitude and velocities . . . 209
E.33 Time histories of longitudinal parameters . . . 210
E.34 Time histories of lateral parameters . . . 211
E.35 Time histories of directional parameters . . . 212
E.36 Test card (PH(2)R) . . . 213
E.37 Time histories of altitude and velocities . . . 214
E.38 Time histories of longitudinal parameters . . . 215
E.39 Time histories of lateral parameters . . . 216
E.40 Time histories of directional parameters . . . 217
E.41 Test card (PH(2)F) . . . 218
E.42 Time histories of altitude and velocities . . . 219
E.43 Time histories of longitudinal parameters . . . 220
E.44 Time histories of lateral parameters . . . 221
E.45 Time histories of directional parameters . . . 222

F.1 Test card (SH(1)R) . . . 224
F.2 Time histories of altitude and velocities . . . 225
F.3 Time histories of longitudinal parameters . . . 226
F.4 Time histories of lateral parameters . . . 227
F.5 Time histories of directional parameters . . . 228
F.6 Test card (SH(1)F) . . . 229
F.7 Time histories of altitude and velocities . . . 230
F.8 Time histories of longitudinal parameters . . . 231

F.9 Time histories of lateral parameters 232
F.10 Time histories of directional parameters 233
F.11 Test card (SH(2)R) 234
F.12 Time histories of altitude and velocities 235
F.13 Time histories of longitudinal parameters 236
F.14 Time histories of lateral parameters 237
F.15 Time histories of directional parameters 238
F.16 Test card (SH(2)F) 239
F.17 Time histories of altitude and velocities 240
F.18 Time histories of longitudinal parameters 241
F.19 Time histories of lateral parameters 242
F.20 Time histories of directional parameters 243
F.21 Test card (RM(1)F) 244
F.22 Time histories of altitude and velocities 245
F.23 Time histories of longitudinal parameters 246
F.24 Time histories of lateral parameters 247
F.25 Time histories of directional parameters 248
F.26 Test card (RM(2)R) 249
F.27 Time histories of altitude and velocities 250
F.28 Time histories of longitudinal parameters 251
F.29 Time histories of lateral parameters 252
F.30 Time histories of directional parameters 253
F.31 Test card (RM(2)F) 254
F.32 Time histories of altitude and velocities 255
F.33 Time histories of longitudinal parameters 256
F.34 Time histories of lateral parameters 257
F.35 Time histories of directional parameters 258
F.36 Test card (SM(1)R) 259
F.37 Time histories of altitude and velocities 260
F.38 Time histories of longitudinal parameters 261
F.39 Time histories of lateral parameters 262
F.40 Time histories of directional parameters 263
F.41 Test card (SM(2)R) 264
F.42 Time histories of altitude and velocities 265
F.43 Time histories of longitudinal parameters 266
F.44 Time histories of lateral parameters 267
F.45 Time histories of directional parameters 268
F.46 Test card (SM(2)F) 269
F.47 Time histories of altitude and velocities 270
F.48 Time histories of longitudinal parameters 271
F.49 Time histories of lateral parameters 272
F.50 Time histories of directional parameters 273

F.51 Test card (DR(1)R) . . . 274
F.52 Time histories of altitude and velocities . . . 275
F.53 Time histories of longitudinal parameters . . . 276
F.54 Time histories of lateral parameters . . . 277
F.55 Time histories of directional parameters . . . 278
F.56 Test card (DR(2)R) . . . 279
F.57 Time histories of altitude and velocities . . . 280
F.58 Time histories of longitudinal parameters . . . 281
F.59 Time histories of lateral parameters . . . 282
F.60 Time histories of directional parameters . . . 283
F.61 Test card (DR(2)F) . . . 284
F.62 Time histories of altitude and velocities . . . 285
F.63 Time histories of longitudinal parameters . . . 286
F.64 Time histories of lateral parameters . . . 287
F.65 Time histories of directional parameters . . . 288

G.1 Test card (SL(2)R) . . . 290
G.2 Time histories of altitude and velocities . . . 291
G.3 Time histories of longitudinal parameters . . . 292
G.4 Time histories of lateral parameters . . . 293
G.5 Time histories of directional parameters . . . 294
G.6 Test card (SL(2)F) . . . 295
G.7 Time histories of altitude and velocities . . . 296
G.8 Time histories of longitudinal parameters . . . 297
G.9 Time histories of lateral parameters . . . 298
G.10 Time histories of directional parameters . . . 299
G.11 Test card (SL(3)R) . . . 300
G.12 Time histories of altitude and velocities . . . 301
G.13 Time histories of longitudinal parameters . . . 302
G.14 Time histories of lateral parameters . . . 303
G.15 Time histories of directional parameters . . . 304
G.16 Test card (SL(3)F) . . . 305
G.17 Time histories of altitude and velocities . . . 306
G.18 Time histories of longitudinal parameters . . . 307
G.19 Time histories of lateral parameters . . . 308
G.20 Time histories of directional parameters . . . 309

List of Tables

3.1 Trim angles of attack for each test case 41

4.1 Computer node function and aircraft model dependency 66
4.2 Speedgoat real-time target machine specifications 67

5.1 HARTEN comparison to similar size aircraft 72
5.2 Definition of the wing, HTP and VTP of the HARTEN aircraft 74
5.3 Definition of primary control surfaces of the HARTEN aircraft 74
5.4 Mass distribution along the fuselage for $CG_{1\text{-}4}$ test cases 76
5.5 Rigid and flexible wing vertical deformations with respect to reference . . 76
5.6 Flight testing envelope 78

6.1 Test matrix 91

7.1 Main parameters of the stall conditions 94
7.2 SPPO mode parameters 97
7.3 SPPO mode levels of flying qualities 99
7.4 Phugoid mode parameters 100
7.5 Main parameters of the SHSS tests 102
7.6 Roll mode parameters 104
7.7 Spiral mode parameters 106
7.8 Dutch roll parameters 109
7.9 CHR scores during the slalom task 112

Nomenclature

A	Amplitude *or* state matrix
A	Coefficients matrix of the Modified Strip Theory
A_i	Coefficients of indicial functions
a	Acceleration of a node *or* semi-major axis of the ellipsoid *or* speed of sound
$(a_n)_w$	Lift-curve slope of a nacelle
B	Input matrix
b	Wingspan *or* semi-manor axis of the ellipsoid
b_i	Exponents of indicial functions
C	Output matrix
C_D	Drag coefficient
C_{Dc}	Viscous cross-flow drag contribution
C_L	Lift coefficient
C_l	Rolling moment coefficient
C_m	Pitching moment coefficient
C_N	Normal force coefficient
C_{Nc}	Cross-flow normal force coefficient
$C_{N\alpha}$	Zero AoA normal force slope coefficient
C_n	Yawing moment coefficient
C_{PL}	Geometric coefficient
c	Chord length
c_{ctrl}	Control surface chordwise position from the corresponding aerodynamic surface leading edge
c_e	Elevator chordwise position from the HTP leading edge
c_r	Rudder chordwise position from the VTP leading edge
D	Drag *or* feedthrough matrix
DB	Dropback
d	Nodal deformations
e	Oswald efficiency number *or* the first ellipsoidal eccentricity
$\vec{F}$	Forces vector
F_i	Modal force *or* wing control surface geometric properties
f	Ellipsoidal flattening
GM	Earth's gravitational constant

g	Gravitational acceleration
g_e	Theoretical gravity at the equator
g_h	Gravitational acceleration above the ellipsoid
g_p	Theoretical gravity at the poles
h	Geodetic height
h_n	Neutral point
I	Inertia matrix
i	Number of node of a flexible body
i_H	Incidence angle of the HTP
K	Structural stiffness
L	Lift *or* moment around x-axis
L_n	Nacelle lift force
l	Length of a nacelle
M	Mach number *or* moment around y-axis
$\vec{M}$	Moments vector
M_{root}	Wing root bending moment
m	Mass
N	Moment around z-axis *or* total number of nodes of a flexible body
n_z	Normal load factor
p	Aircraft roll rate
q	Aircraft pitch rate *or* dynamic pressure
q_{max}	Maximum pitch rate
q_{ss}	Steady state pitch rate
Re	Reynolds number
r	Aircraft yaw rate
$\vec{r}$	Position vector of a node
s	Wingspan
T	Period of oscillation
T_2	Time to double
T_P	Thrust provided
$T_{P_{max}}$	Maximum thrust
T_{P_τ}	Engine time constant
T_{root}	Wing root torsion moment
T_i	Indicial time constants
t	Time
U	Body velocity in x-axis
u	Velocity of a node in x-axis
u	Input vector
V	Body velocity in y-axis
V_{HTP}	HTP volume ratio
V_S	Stall speed
V_V	Vertical velocity

V_{VTP}	VTP volume ratio
v	Velocity of a node in y-axis
$\vec{v}_0$	Vector of linear velocities U, V, W
W	Body velocity in z-axis
w	Velocity of a node in z-axis *or* width of a nacelle
X	Body force in x-axis
x	Modal displacement *or* position of a node in x-axis
$\mathbf{x}$	State vector
x_e	Hinge location of a control surface
Y	Body force in y-axis
y	Position of a node in y-axis
Z	Body force in z-axis
z	Position of a node in z-axis

Greek alphabet

α	Angle of attack
α_{eff}	Effective AoA
α_{ind}	Indicial AoA
α_n	AoA of a nacelle
β	Sideslip angle or Prandtl-Glauert compressibility correction factor
β_n	Sideslip angle of a nacelle
Γ	Downwash circulation strength
γ	Flight path angle *or* local dihedral angle
δ_{ctrl}	Control input angle
ζ	Damping *or* rudder deflection angle
η	Elevator deflection angle *or* relative position along the span
Θ	Local twist angle *or* pitch angle
Θ_m	Modeshape matrix
λ	Local sweep angle
$\tau_{\pm 30^\circ}$	Roll performance time constant
τ_r	Roll mode time constant
Φ	Bank angle
ϕ	Phase *or* geodetic latitude
ξ	Aileron deflection angle
Ψ	Yaw angle
ω	Frequency
$\vec{\omega}_0$	Vector of body angular velocities $\{p, q, r\}$
ω_{BW}	Bandwidth frequency
ω_d	Damped frequency
ω_n	Natural frequency

List of Abbreviations

A/C	Aircraft
AGL	Above ground level
AoA	Angle of attack
AR	Aspect ratio
ATPL	Airline transport pilot licence
AWI	Agile Wing Integration
BAC	Body axes centre
BW	Bandwidth
CAL	Cornell Aeronautical Laboratory
CA^2LM	Cranfield Accelerated Aircraft Loads Model
CAP	Control anticipation parameter
CG	Centre of gravity
CHR	Cooper-Harper Rating
CPU	Central processing unit
DCM	Direction cosine matrix
DoF	Degrees of freedom
EAS	Equivalent airspeed
EBMM	Experimental behaviour measurement method
EFIS	Electronic flight instrument system
EFS	Engineering flight simulator
EHSI	Electronic horizontal situation indicator
EoM	Equations of motion
FCS	Flight control system
FCU	Flight control unit
FFS	Full flight simulator
FQ	Flying quality
FS	Frequency sweep
GUI	Graphical user interface
HALE	High Altitude Long Endurance
HAR	High aspect ratio
HARTEN	High Aspect Ratio Technology ENabler aircraft model
HQ	Handling quality
HQDT	Handling qualities during tracking

HTP	Horizontal tailplane
IG	Image generation
ILS	Instrument landing system
ISA	International standard atmosphere
LOES	Low order equivalent system
LSS	Longitudinal static stability
MAC	Mean aerodynamic chord
MLW	Maximum landing weight
MST	Modified Strip Theory
MTOW	Maximum take-off weight
MZFW	Maximum zero fuel weight
NASA	National Aeronautics and Space Administration
OS	Operating system
PD	Pitch doublet
PFD	Primary flight display
PIO	Pilot induced oscillation
RAM	Random-access memory
RoD	Rate of descent
RWY	Runway
SFFA	Simulation Framework for Flexible Aircraft
SHSS	Steady heading sideslip
SPPO	Short period pitching oscillation
SSD	Solid-state drive
SSSP	Sinusoidal signal pump (frequency sweep)
TR	Taper ratio
UDP	User datagram protocol
USAF	United State Air Force
VTP	Vertical tailplane

Chapter 1

Introduction

Over the last few decades the society has witnessed significant achievements in aviation. Air travel has become so affordable that the number of passengers is about to double in the next 20 years and airlines keep introducing longest ever revenue flights, which range for about 15000 km and last for more than 17 hours, to connect the most distant places of our planet. This was made possible only by a continuous development and improvement of airliner efficiency. Economic and social benefits that the aviation industry induces globally are very appreciated and well understood [1, 2]. However, they come with a cost of a negative environmental impact, which the aviation sector is highly criticised for. To reduce this impact, international aviation organizations ICAO, IATA, ECAC set the environmental targets to significantly reduce emissions from aircraft [3, 4] or, in other words, to improve aircraft efficiency. This improvement can be achieved in two ways: 1) by providing straighter flight paths and, thus, reducing the operational costs and emissions due to air navigation peculiarities, and 2) by increasing aircraft efficiency by improving its design and systems. Three domains, where aircraft efficiency could be improved the most, are the aerodynamics, the propulsion and the structural weight. Improvements in the propulsion system of commercial airliners have long been the main driving factor of the efficiency increasing process, but every further improvement of an engine adds less efficiency for a higher cost. On the other hand, it is common knowledge among designers and engineers that increasing wing aspect ratio (AR) reduces aircraft induced drag. High aspect ratio (HAR) unswept wings are usually seen in sailplane designs to provide very high lift-to-drag ratios, but could not be used for large transport aircraft in the past because of arising structural issues due to the much higher wing loading in commercial transport aircraft. The use of HAR wings in sailplanes design provided the following advantages:

1. Less induced drag. About 40% of total drag in cruise is induced drag [5], thus reducing it would lead to a significant reduction of total drag.

2. More equal lift distribution. Due to a longer and narrower wing it becomes similar to elliptical distribution, which is known for its preferable properties.

3. Higher maximum lift coefficient [6].

However, there are some disadvantages of using the HAR wings too:

1. Lateral static stability is reduced as the $C_{l_{\beta_{wing}}}$ increases its value with increasing AR [7] as shown in Fig. 1.1.

2. An increase in wing root bending moment due to an increased AR is an essential problem for large transport aircraft.

3. A decrease in stall angle of attack as the effective angle of attack at the tips is higher [6].

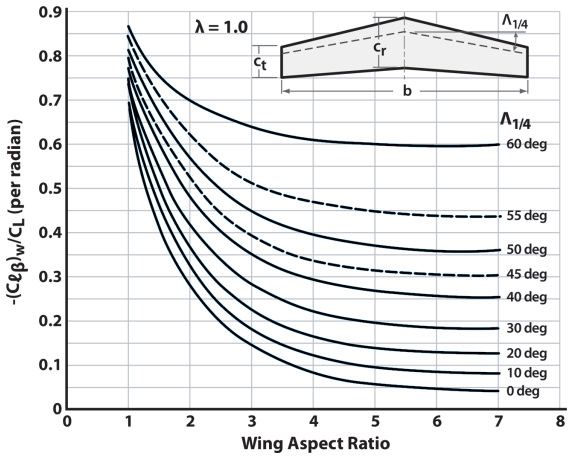

Figure 1.1: AR impact on lateral static stability (reproduced from Ref. [7])

With the development of composite materials and novel manufacturing technologies [8], previous structural issues have been solved. Moreover, the use of composite materials also allows us to reduce the overall weight of an aircraft. As the AR increases larger wing deformations develop, which affect the flying (FQs) and handling (HQs) qualities of such flexible aircraft. As aircraft are controlled by pilots, their perception of HQs of these new flexible configurations is very important for further designs of airframes and flight control systems. It is also important to assess the changes in flight dynamics when the airframe becomes flexible.

Previous approaches to assess HQs of flexible aircraft were based mainly on the longitudinal HQs [9–12]. Pilots, placed in front of an aircraft, experienced different dynamics than the ones at the centre of gravity (CG) due to the bending of long slender fuselages. Thus, it was important to investigate the way that the pilots' perception of HQs was altered. One of such assessments was done by Waszak et al. [13] at the NASA Langley Visual/Motion Simulator facility for the Rockwell B-1 aircraft. It set the foundation for the future investigations of flexible aircraft HQs. Recently, Damveld [11] and Andrews [12] investigated the impact of the fuselage flexibility on military and commercial jets shown in Fig. 1.2. Damveld's investigation was based on the development of new meth-

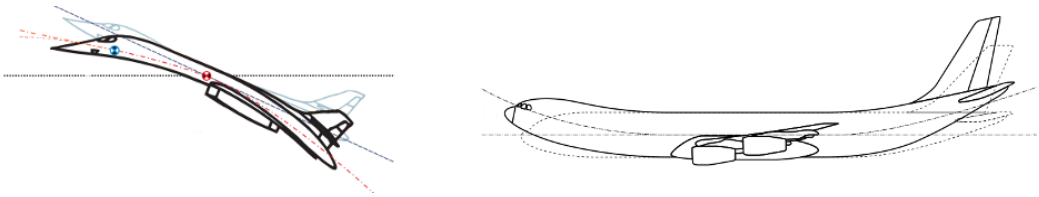

(a) Flexible military jet (reproduced from Ref. [11])

(b) Flexible commercial jet (reproduced from Ref. [12])

Figure 1.2: Recent aircraft investigated for the structural flexibility impact on HQs

(a) Helios Prototype

(b) In-flight disintegration of Helios Prototype

Figure 1.3: Helios Prototype in flight and its disintegration (reproduced from Ref. [14])

ods to investigate and quantify the longitudinal HQs and was compared to the findings of the previous research done by Waszak et al. Andrews, on the other hand, considered not only the fuselage flexibility, but also the wing flexibility. However, the commercial aircraft in his investigation had a relatively rigid wing. During Andrew's project the AX-1 model was developed - the foundational part of the Cranfield Accelerated Aeroplane Loads Model (CA^{2}LM).

As large aircraft were fitted with relatively rigid wings, the unmanned aerial vehicles (UAV) were used as test beds for HAR wings technologies. Much effort was made in the USA to develop the technologies and methodologies both to manufacture and investigate the HAR wing UAVs. The High Altitude Long Endurance (HALE) and Helios Prototype are the most famous examples of the HAR wing UAVs. The Helios Prototype flying wing is shown in Fig. 1.3(a). Helios is also a well-known example of the in-flight disintegration (shown in Fig. 1.3(b)) of a highly flexible wing.

As the manufacturing technologies advanced, the researchers started looking at HAR flexible wing applicability to large commercial aircraft. The Subsonic Ultra Green Aircraft Research (SUGAR) is well-known research into the applicability of HAR low swept wings for commercial transport. Led by Boeing and NASA the aircraft concept aims

(a) NASA/Boeing SUGAR concept (see App. A.1)

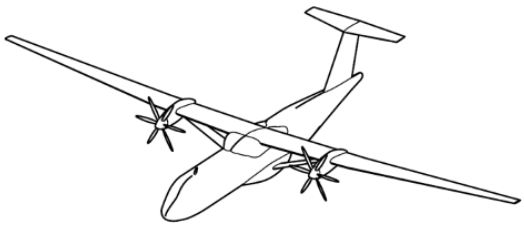

(b) Airbus HARTEn concept (reproduced from Ref. [15])

Figure 1.4: Examples of HAR wing commercial aircraft concepts

to reduce the CO_2 emission by more than 70%. Airbus along with its academic partners Cranfield University and the University of Bristol suggested the HARTEn concept aircraft [15]. Both concepts consider not only HAR wings, but many other novel technologies, which allow an increase in aircraft efficiency. These two concepts are shown in Fig. 1.4.

These new HAR wings concepts not only increase aircraft efficiency, but also introduce new aircraft dynamics. As the structural issues of HAR wings were analysed in the Helios report (Ref. [14]), the FQs or HQs analysis of such aircraft has never been done before. As mentioned before, the longitudinal HQs due to the fuselage flexibility or due to the relatively rigid wing flexibility were usually tested. However, the impact of high wing deformations on FQs and HQs of a large transport aircraft is still unknown. Moreover, the pilot-in-the-loop simulations were never done for HAR highly flexible wing aircraft. Such simulations demonstrate the differences between rigid and flexible aircraft in terms of flight dynamics. Moreover, the opinions collected from professional test pilots allow us to assess and de-risk such configurations with more confidence.

1.1 Aim and objectives

The aim of this project is to investigate the differences between rigid and flexible wing aircraft dynamics by the use of the pilot-in-the-loop flight simulation techniques. The aim is met through the following objectives:

1. The development of extended equations of motion (EoM), which consider the structural flexibility, their analysis and implementation into the simulation framework.

2. The development of the new simulation framework, capable of the pilot-in-the-loop real-time simulations, by integrating the aeroservoelastic framework with the engineering flight simulator.

3. The development of new tasks to assess HQs of new aircraft configurations using the pilot-in-the-loop flight simulations.

4. The assessment of FQs and HQs of a new highly flexible wing aircraft configuration during a pilot-in-the-loop flight simulation campaign.

1.2 Scope of thesis

Pilot-in-the-loop simulations of the HARTEN aircraft within the CA^{2}LM framework and assessment of FQs and HQs of the aircraft are the scope of this research. As the linear structural dynamics model is used within the CA^{2}LM framework, only the wing dihedral change due to the structural flexibility and low frequency structural dynamics are of interest in this research. The low fidelity Modified Strip Theory (MST) model along with the Leishman unsteady aerodynamic model are used within the CA^{2}LM framework in order to provide real-time simulations. The CA^{2}LM framework is utilised by test pilots through the interface provided by the EFS500 hardware framework. Both of them integrated into the Simulation Framework for Flexible Aircraft (SFFA) provide the pilot-in-the-loop simulation capability, which is used to test FQs and HQs of the HAR wing aircraft. The testing is carried out by three professional test pilots, each of them presenting communities of academia, commercial aviation and flight testing. The HAR wing flexibility effect is assessed by comparing aircraft response to a pilot input between the flexible and rigid aircraft configurations. The FQs evaluation is based on simulating standard open-loop flight test manoeuvres. The HQs are assessed by using the newly developed closed-loop slalom task. The scope of this research also includes the assessment of this new slalom task applicability for the HQs evaluation as well as the assessment of the SFFA. All simulations are carried out for the Airbus HAR wing aircraft HARTEN. Bare airframe with ailerons, elevator and rudder is tested for FQs and HQs. The qualitative rather than quantitative assessment of FQs and HQs is the scope of this thesis due to all the limitations mentioned above.

1.3 Thesis outline

The chapters of this thesis describe the process needed to develop a simulation framework to carry out pilot-in-the-loop simulations and assessment of the flying and handling qualities of HAR highly flexible wing aircraft.

Chapter 2 reviews the use of HAR wings within sailplanes and approaches to use HAR wings within the commercial aviation. It also reviews the approaches to model and simulate flexible aircraft within the research community. The HQs assessment criteria are also reviewed along with the flight test manoeuvres.

Chapter 3 presents the derivation of the extended EoM that take into account the structural flexibility effect. An investigation of their impact on the response of rigid and

flexible aircraft is also provided.

Chapter 4 introduces the new simulation framework, which is needed to carry out the real-time pilot-in-the-loop flight simulations. The review of two parts of the new simulator - the aeroservoelastic framework and the engineering flight simulator - is provided along with a discussion on the integration process. The limitations and upgrades to the aeroservoelastic framework are also discussed and an example of its use is given.

Chapter 5 reviews the example aircraft model used in this project to assess the differences between rigid and flexible aircraft. Its longitudinal static stability (LSS) is also assessed in the chapter.

Chapter 6 reviews the flight simulation campaign. The structural flexibility test cases are defined and the experience of test pilots and FQs and HQs evaluation metrics are discussed in the chapter. The test manoeuvres carried out during the flight simulation campaign are also defined and their execution procedures are provided. The new slalom task developed to assess HQs of new aircraft configurations more efficiently is also introduced in the chapter.

Chapter 7 presents the findings and results from the flight simulation campaign along with a discussion. The assessment of FQs and HQs is carried out as a comparison between rigid and flexible aircraft configurations. The FQs investigation is divided into longitudinal and lateral/directional dynamics. Then the slalom task results are presented to assess the difference in HQs between rigid and flexible aircraft. The assessment of the new simulation framework is presented at the end of the chapter.

Chapter 8 concludes the thesis and also suggests the future directions in the research on HQs of highly flexible aircraft and the development of the new simulation framework. The summary of publications in which the findings of this research have been disseminated completes this chapter.

Chapter 2

Literature review

This chapter reviews the literature on the following topics: 1) the use of high aspect ratio wings, 2) developments of EoM for flexible aircraft, and 3) HQs criteria for aircraft assessment.

2.1 The use of high aspect ratio wings

Benefits of HAR wings were realised decades ago [16]. Known for their high aerodynamic efficiency they have been widely used in sailplane design to increase their performance and competitiveness during gliding competitions. However, their use for large transport aircraft was limited due to much higher wing loading leading to excessive flight loads and consequent structural weight implications. Hence, the option to significantly increase wing aspect ratio was never considered. When manufacturing technologies improved and new materials were developed, the use of HAR wings for large transport aircraft became possible. Engineers developed techniques to produce highly flexible wings and many concepts of aircraft with such wings emerged. However, such aircraft operate under much higher wing loading and velocities than sailplanes. Hence, much effort is made to investigate handling characteristics of highly flexible wing large transport aircraft taking into consideration already known characteristics of sailplane dynamics.

2.1.1 Sailplanes

Sailplanes are the first aircraft type that come to mind when thinking about HAR wing aircraft. For many years they served aircraft designers as a platform for testing methods to increase aerodynamic performance. Starting from the Lilienthal hang glider in early 20^{th} century, sailplane designs have improved along with advances in engineering sciences.

Sailplanes are widely known for their long and slender HAR wings. Wings used to be very low aspect ratio at the very beginning of aviation - the Lilienthal hang glider shown in Fig. 2.1(a) had an AR of 4 [17]. Although engineers understood the importance of the aspect ratio in reducing the induced drag and increasing the aerodynamic performance,

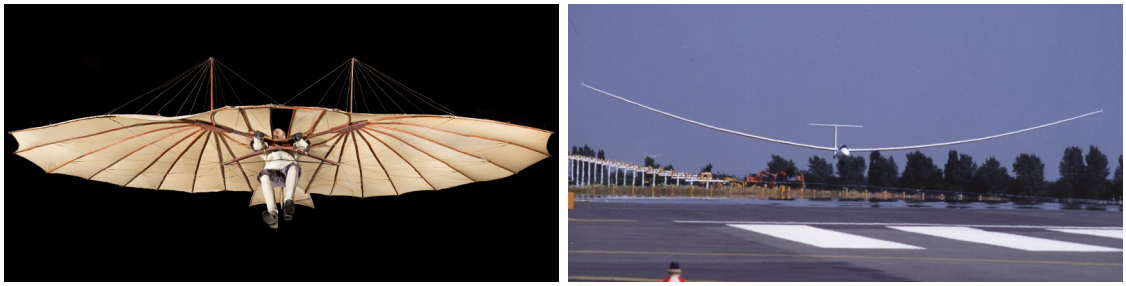

(a) Lilienthal hang glider (see App. A.2) (b) eta sailplane (see App. A.3)

Figure 2.1: Examples of past and current gliders

HAR wings were not viable due to lack of suitable lightweight materials. Thus, other ways to change the aspect ratio for different phases of flight were considered, e.g. the use of the Fowler-type flap let the AR vary from 26.8 to 36.2 in case of the British Sigma sailplane [17]. However, with advances in manufacturing and material engineering in the 1960s-1970s HAR wings became viable through the use of reinforced glass-fibres. This allowed even higher AR wings to be produced. Currently, the eta sailplane shown in Fig. 2.1(b) has an AR of 51.33 (see App. A.4) and achieves a lift-to-drag ratio of 70 (see App. A.5).

The use of HAR wings not only increases the aerodynamic efficiency, but also brings with it some structural and control issues. Back in 1965, Jakubov noted that high performance gliders exhibited low torsional rigidity of their high aspect ratio (AR=25-30) wings [18]. Thus, the “elastic wing twisting resulted in a decrease in pitching moment and elevator trim angles” [18]. This significantly affected the long period dynamics of those sailplanes.

Another issue of HAR flexible wings is their time varying deformation in flight due to changing loads, which affect their dihedral angle and lateral/directional stability. Although early sailplanes had no dihedral, its positive effect on HQs was already anticipated [17]. Later, when the dihedral effect was better understood, negative wing dihedral was implemented within the Ku-4 Austria (1932) sailplane to compensate for the excessive dihedral due to wing bending under flight load.

The adverse yaw, being another significant drawback of HAR wings, is an undesired behaviour of the aircraft due to asymmetric lift distribution when the down deflected aileron creates more lift and as a result, more induced drag [19]. The issue brings one of the biggest challenges for a designer to minimise the adverse yaw effect by setting an appropriate dihedral angle.

As sailplanes, due to their HAR wings, possessed many unknown flight dynamic phenomena, much work was required to investigate and define their HQs. Morelli investigated longitudinal motion of the sailplane through definition of the ‘stick fixed’ neutral

point, which was estimated to be at 48% MAC [20]. He concluded that if the CG is aft of the neutral point, the motion would be aperiodic and divergent, and in case of forward CG, the motion would be oscillatory. Moreover, with the CG shifted forward, the period of the motion would become shorter. For the lateral/directional dynamics it was noted that winglets help to reduce the induced drag by minimising the wingtip vorticity and improve aileron efficiency by minimising cross-flow, which in turn improves HQs [17]. Moreover, in the future HQs may be improved using small computer-controlled moving surfaces [17] to provide lateral control, when the wing is highly deflected and ailerons lose their efficiency. Such surfaces (*spoilers*) are in few cases used now for rolling an aircraft during high velocity flight phases. However, this might be the only means of lateral controls for aircraft with high wing deformations.

As discussed, different aspects of sailplanes were thoroughly investigated in the past. Many issues due to HAR wings were discovered, investigated and solved during those years. However, high lift-to-drag ratio, which is the outcome of using a HAR wing, is the strongest lure for every aircraft designer and new domains for using HAR wings are under investigation.

2.1.2 Commercial airliners

Manufacturers of commercial airliners are interested in any means to increase aircraft efficiency as this usually leads to higher profit margins for their users, i.e. airlines. The well-known Breguet range equation (2.1) [21, 22] identifies three areas where the aircraft efficiency could be increased, i.e. aerodynamics, propulsion and structures.

$$Range = \frac{a}{g}\frac{ML}{D}\frac{1}{SFC}\ln\left(\frac{W_i}{W_f}\right) \tag{2.1}$$

The propulsion parameter SFC was the main driver of recent approaches to increase the overall aircraft efficiency providing the most benefits. However, every increment in the efficiency of the propulsion system becomes more and more costly. Moreover, the design of engines does not depend on aircraft manufacturers as they are provided by external suppliers. On the other hand, both aerodynamic and structural parameters, ML/D and W_i/W_f, are defined by aircraft manufacturers and play a significant role in the overall aircraft design. Previously considered as independent parameters they are becoming highly interdependent when considering a more integrated design process of the future aircraft concepts. As this thesis considers only HAR wings aircraft, a brief discussion on their interplay is provided below.

The commercial aviation industry is currently starting to actively look into using HAR wings to increase the aerodynamic efficiency as it is directly attributed to the design of its airframe and, mostly, the wing. The use of new materials with higher than usual specific stiffness and strength allows a significant increase in the wing aspect ratio with a little or no weight penalty. This in turn allows an increase in ML/D parameter as the induced drag reduces. Reduction of the induced drag is even more signified when flying at a constant

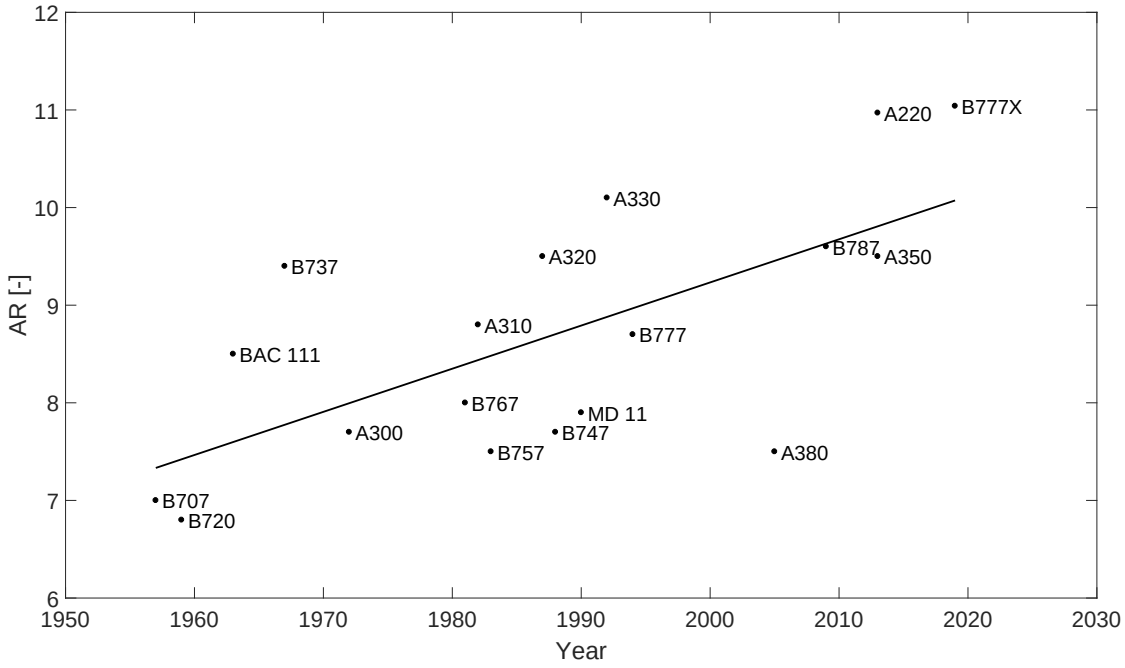

Figure 2.2: AR increase during years

altitude and Mach number the overall weight of the aircraft reduces and thus the angle of attack must be also reduced. Hence, to employ previously discussed advantages the main aircraft manufacturers - Airbus and Boeing - are investing significant resources to investigate the feasibility of HAR wings for commercial use. Figure 2.2 shows the trend of AR increase from early to the latest designs of commercial aircraft. As seen from the figure, the highest currently achieved AR is around 11, while current research is looking into AR between 18 and 20.

The use of composite materials allows designers to increase AR while maintaining or even reducing the mass of wings. As seen in Fig. 2.2, AR of a new Boeing 787 (B787) is around 9.6, while AR of two decades older Boeing 777 (B777) is around 8.7. The composition of their structures is significantly different: an older B777-300 consists of 12% composites and 50% aluminium, while a newer B787-800 consists of 50% composites and 20% aluminium [23]. An increased AR and an increased use of composite materials results in high wing deflections (see Fig. 2.3) for B787: the wingtip deflects around 3.66 m (12% of semi-span) under cruise conditions and up to 7.93 m (26% of semi-span) under 'ultimate' loading [23]. Such high deflections are not the case for B777, nevertheless its wingspan is only 1 m larger (61 m) than that of the B787 (60 m). Moreover, recently introduced Bombardier C Series aircraft possess wings with the aspect ratio of 11. However, due to a small wingspan (35.05 m) the flexibility of the wing is not as evident as in the case of large transport aircraft. Hence, it can be said that some clear current and future trends of the industry are:

1. To increase wing AR in order to increase the aerodynamic efficiency by reducing the induced drag.

2. To use more composite materials in order to reduce structural mass.

Figure 2.3: Wing deflection of Boeing 787 aircraft under ground, 1g and ultimate loading (reproduced from Ref. [23])

Both trends will result in even more flexible wings. It means that flight dynamics and HQs of such aircraft need to be thoroughly investigated and well understood before they enter the market. One way of carrying out such investigation is by modelling and investigating them using computational simulation methods and wind tunnel testing.

Some initiatives to investigate flexible wing transport aircraft have been launched in recent years. The first one, NASA's Subsonic Ultra Green Aircraft Research [24], tends to explore the use of the truss braced flexible wing. Launched in 2009-2010, it aims to investigate viability of new technologies, like hybrid propulsion or laminar flow wings. The research has been based on the high wing T-tail configuration medium size aircraft with the Maximum Take-Off Weight (MTOW) of 68100 kg, which is shown in Fig. 2.4(a). Its wing AR is around 19.55 and its span is 51.6 m.

The second initiative, Airbus High Aspect Ratio Technology ENabler [15], aims to explore the use of the HAR flexible wings mounted on a classically configured aircraft. It was launched in 2014 among Airbus UK, Cranfield University and the University of Bristol as part of the Agile Wing Integration (AWI) project. This research initiative aims to investigate laminar flow and HAR wing technologies' application to commercial aircraft. Much attention has been given to explore HQs of such aircraft. The most recent proposed model is based on the low wing T-tail configuration medium size aircraft with MTOW of around 80000 kg, as shown in Fig. 2.4(b). Its wing AR is around 17.7 and wingspan is 50 m.

As discussed, the AR of wings is inevitably increasing within the large transport aircraft design. The wingtip deflection of 26% semi-span [23] will soon become conventional rather than an unconventional feature. Thus, flexibility effects must be taken into account when investigating flight dynamic parameters of such aircraft. These should be accounted for through an in-depth study of non-linear structural dynamics and flight dynamic EoM for flexible aircraft.

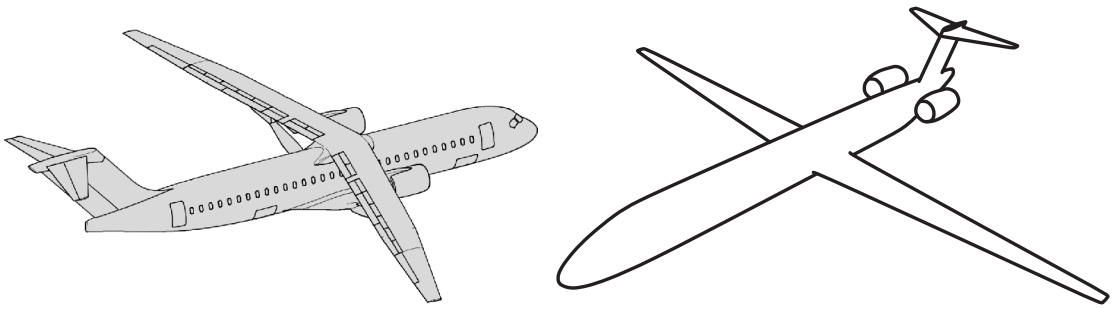

(a) NASA SUGAR (reproduced from Ref. [24]) (b) Airbus HARTEN

Figure 2.4: Currently investigated configurations of HAR wing aircraft

2.2 Modelling flexible aircraft

The majority of aircraft models have been developed assuming the airframe to be rigid. Thus, it is rational to model them as a mass point with inertia properties of the aircraft assigned to that point. As wings become more flexible, inertia properties variation in time becomes more significant. Thus, a model of a very flexible aircraft as a mass point is not valid any more. Hence, such aircraft are modelled as sets of mass points, representing their mass distribution, constrained in space. Corresponding changes must be made to equations of motion, i.e. they must be amended with additional terms to account for the structural flexibility. Moreover, the structural dynamic equations of motion have to be improved to account for structural non-linearities in case of high structural deformations. All these models are usually combined in modelling and simulation frameworks to investigate their impact on aircraft configurations of interest. As this thesis aims to investigate flight dynamics rather than structural dynamics, only past developments of flight dynamic EoM are discussed in the following sections along with flight simulation frameworks.

2.2.1 Equations of motion for flexible bodies

Equations of motion equate forces and moments acting on the body to motion parameters of that body, i.e. rotational and translational accelerations. These are then integrated to calculate velocities and body position and attitude in space. The classical equations of motion have assumed a body to be rigid and modelled it as a point with particular inertia and mass properties [25, 26]. However, in the case of a flexible structure, a body cannot be assumed as a single point, but rather as a set of points constrained and distributed in space, representing an elastic body.

Different approaches to model flexible bodies have been applied over the years. It was shown in early stages of flexible body research that the motion of a “slightly deformable body” could be defined through three separate parts: translation, rotation and vibration.

However, Hemp [27] concluded that rotation and vibration are coupled unless both of these motions are small.

An idea of having a supersonic transport suggested that an aircraft might be a slender flexible body [28]. It was noted that the classical approach of modifying EoM by the use of 'modified derivatives' is very inefficient as it includes only a steady state deformation of the airframe and could not be applied over a broad range of flight conditions [28]. A different approach was suggested, which included the motion of each point into linear and angular momentum equations. The mean axes system was introduced to reduce the inertial coupling between the overall motion of a body and its relative deformations [28].

As previous approaches were usually applied to small deformations, the approach to derive equations limited by small strains rather than small deformations was taken by Veubeke [29]. A mean rigid body motion was modelled along with a relative body motion which took into account deformations. The proposed approach minimised the mean square of relative displacements. Nevertheless, it preserved the zero momentum condition and linearised the angular momentum condition in such a way that the relative deformations were represented by expansion in natural elastic vibration modes. Hamilton's principle [30] was used to derive the equations by using the concept of quasi-coordinates.

The interest in large spacecraft with distributed structural flexibility revived an interest in floating reference frames [31]. The linearised Tisserand frame was suggested as the most advantageous choice because of the following characteristics: 1) it optimally follows a body, and 2) constraint relationship is easily evaluated. However, the rigid body motion was still kept separate from structural motion.

The idea to separate rigid and flexible body modes was criticised by Waszak and Schmidt [9]. They argued that this practice might be applied for relatively rigid aircraft where the frequencies of rigid and flexible modes are significantly apart (see Fig. 2.5). However, with the introduction of new composite materials it was argued that the frequency separation would be significantly reduced. Thus, the need to change the design practice was highlighted. A new way proposed developing flexible integrated vehicle models initially and then simplifying these models according to the application. However, sufficiently small structural deformations were usually assumed for a new model [9] and a set of normal vibration modes was used. The elastic and rigid body motions were coupled through the use of generalised forces.

Much work on multi-body equations of motion was done by Udwadia [32–36]. General form of the explicit equations of motion, applicable to holonomic and non-holonomic systems, was obtained. Such sets of EoM allow the decomposition of multi-body systems into subsystems with known equations of motion and then combine them to obtain EoM of the overall system. However, general formulation of equations of motion, introduced by Udwadia, had not seen much success in the domain of aeronautical engineering. Thus, the discussion on which approach is the most suitable to model a flexible aircraft continued. Meirovitch and Tuzcu criticised the mean axes system in Ref. [37], arguing that in times when the computational power was inadequate to solve complex equations, the concept of mean axes was appealing due to its promise of inertial decoupling of the EoM.

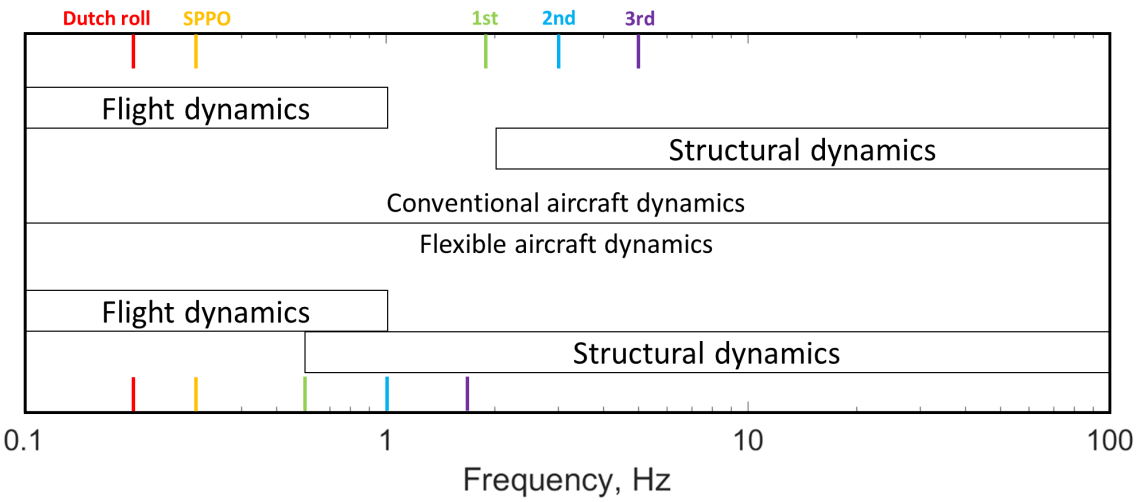

Figure 2.5: Rigid body and structural dynamics frequencies for conventional and flexible aircraft

However, it turned out to be a "blind alley" for aircraft, as EoM were still coupled through the aerodynamic forces and the use of mean axes resulted in increased complexity [37].

Schmidt, the most prominent advocate of the mean axes system, responded with a demonstration of "the mean-axis formulation" that "leads to useful and valid equations of motion of a deformable body" in Ref. [38]. He argued that "a quite valid and very useful dynamic model of relatively low dynamic order may be obtained from the mean-axis formulation". Although equations of motion have been investigated for many years, the discussion on applying those equations for flexible bodies [39] or discovering more convenient axes systems to model those equations [40] is still going on.

While different approaches to model equations of motion bring different perspectives and insights into flight dynamics, examples of their applications are their best advocates. Hence, many simulation frameworks were developed to show advantages of each approach and investigate dynamics of different aircraft configurations.

2.2.2 Modelling and simulation of flexible aircraft

Numerous high and low fidelity flexible aircraft simulation frameworks were developed in the past.

A good starting point for a review of flexible aircraft simulators is the report produced by Waszak et al. back in 1987 [13]. The Rockwell B-1B bomber, which has a high fineness ratio and thus flexible fuselage, was modelled and this established the basis for the future research into flexible aircraft flight dynamics and HQs. Later many researchers (e.g. Refs. [11, 41]) compared their results against the ones from Ref. [13]. However, the focus of this model was to explore the fuselage flexibility impact on the longitudinal flight dynamics.

Modelling of the Light Eagle aircraft showed that the separation of rigid body and structural dynamics cannot be justified [42]: the same conclusion as seen in many discussions about the equations of motion. To develop the model Schoor utilised two-dimensional strip model, which was a common choice between flexible aircraft modellers [9, 13]. The structural model was based on the linear beam theory, thus preventing it from being used for large wing deformations.

A whole integrated aeroelastic package ASWING was developed by Drela and presented in Ref. [43]. It made use of non-linear beams, which allowed large deformations to be modelled. Aerodynamic model was more advanced too - it utilised the vortex lattice method with unsteady lifting lines with wing-aligned trailing vorticity. Compressibility effects were modelled in a traditional way via the Prandtl-Glauert compressibility factor. Being much more advanced than the previous models, it also modelled stall and its effect on lift and drag.

With the advance of new technologies came new requirements for surveillance aircraft. Thus, the HALE concept was introduced. The requirements being 1) a substantial loiter period, and 2) long range, led to configurations of HAR wings, providing very high lift-to-drag ratios [44]. Thus, in order to produce computational models of such aircraft it was decided to couple a finite-state airloads model with the structural model, defined as a set of beams. The airloads model included both an inflow model and a dynamic stall model, developed by ONERA. Results of the validation exercise in Ref. [44] indicated a need to include higher order non-linear effects to predict aeroelastic effects more accurately.

Effects of non-linearities on the flight parameters have been investigated since the first models of flexible aircraft were introduced. On the one hand, it was shown that both linear and non-linear geometrical models resulted in wing deflections with negligible differences for a wingtip deflection of around 25% semi-span [45]. Moreover, both bending and twisting of the wing could be predicted “quite accurately”. The main drawback of applying the linear structural theory for highly deformable wings was indicated to be its fore-shortening effect, which means that the wing becomes artificially elongated as shown in Fig. 2.6. On the other hand, it was clear that significantly different structural frequencies and modeshapes result from non-linear models [44–46]. These changes significantly affect longitudinal flight dynamic modes and the trim solutions [46, 47]. For the U-shape wing configuration those non-linearities might lead to the absence of the short period pitching oscillation (SPPO) mode, while the phugoid mode might become unstable. Moreover, the flutter speed might change by more than 50%, as it was shown in Ref. [45]. It was also noted in Ref. [47] that using the linear structural theory to predict aircraft performance would lead to incorrect estimation of the flight envelope. For example, the stall speed turned out to be higher for flexible aircraft rather than for the rigid one [47]. It was shown in Refs. [48] and [49] that modelling stall non-linearities decreased the flutter speeds drastically due to coupling between the low frequency stall dynamics and structural modes. On the other hand, the linear analysis led to over-prediction of the flutter speed - the situation that is very dangerous for flights within that speed region [49].

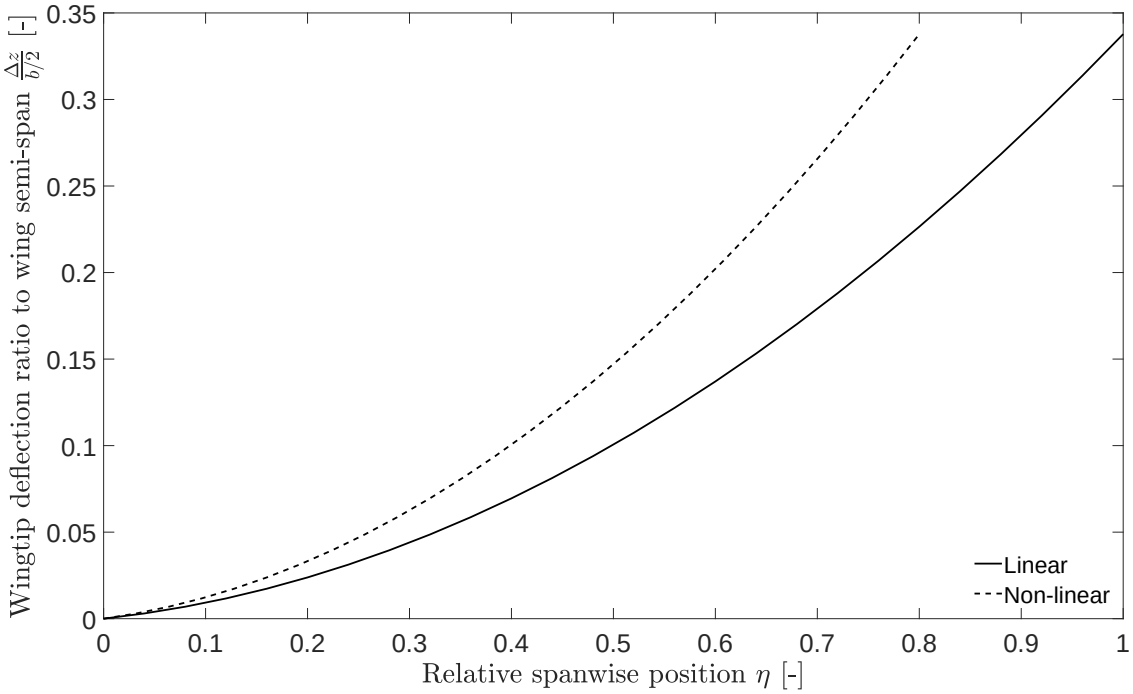

Figure 2.6: Artificial wing elongation using the linear structural dynamics theory

The low frequency modes, which involved wing flexibility, were fully coupled with the flight dynamic modes [47]. However, the coupling between high frequency wing aeroelastic modes and flight dynamic modes was very little [47]. Moreover, those structural frequencies were found to vary as a function of wingtip displacement [47]. It affected both longitudinal modes (phugoid and SPPO) and the trim solution [47]. These results showed that the non-linear behaviour of long flexible wings need to be well understood and highlighted the need for a complete and consistent non-linear dynamic analysis and simulation tools [49].

The geometrically-exact beam theory along with large motion aerofoil aerodynamic theory resulted in a model presented by Patil and Hodges in Ref. [46]. The framework was used to model a flexible very high aspect ratio ($AR = 30$) flying-wing concept.

Another framework, which tightly couples the non-linear 6 degrees of freedom (DoF) EoM with the non-linear aeroelastic equations, was presented in Ref. [50]. It was shown that higher-order formulations are required to capture dynamics of a flexible aircraft. Moreover, it was shown that the longitudinal dynamics can be captured by the linearised or, even, rigid-body solutions. However, for lateral/directional manoeuvres the non-linear structural model is required.

More recent models of flexible wing aircraft involve morphing mechanisms [51] and more advanced aerodynamic and structural models [52–54]. Models to simulate flying wings or flexible transport category aircraft were discussed in Refs. [55, 56].

The discussion above indicates the presence of numerous different fidelity aeroservoelastic models. Each of them has its own advantages and disadvantages. To assess HQs of an aircraft real-time aerodynamic and structural dynamic models are required. Combining these models with a flight simulation environment will allow the pilot-in-the-loop testing of new aircraft configurations.

2.3 Flight testing and handling qualities evaluation

Every new manufactured aircraft must pass the basic flight testing to show that it meets the airworthiness requirements laid down in CS-25 specifications [57]. Their flight control and other systems are tested in flight according to in-house manufacturer requirements. The overall testing campaign may take a couple of weeks. However, for new configurations of aircraft (such as the flexible wing aircraft within the framework of this project), an extensive testing campaign must be planned. As this project aims to assess the HQs of the conceptual aircraft design, the real in-flight tests cannot be carried out. Thus, the aeroservoelastic model integrated with the flight simulation hardware provides a capability of the pilot-in-the-loop testing of such concepts. An important part of such a testing campaign is the methodology used to assess the results. Having in mind that the structural flexibility becomes more significant variable in the flight dynamics it is vital to assess the limitations of the most popular currently used HQs evaluation methods. Hence, this section reviews existing methodologies and their applicability within the flexible aircraft domain.

The research of HQs has been of high interest for the flight dynamics community from the very first flights in the beginning of the 20^{th} century. At that moment the term 'Handling Qualities' did not exist and all discussions and investigations of aircraft were based on the stability and controllability. Thus, researchers derived the basic principles of the stability derivatives of aircraft, which are still successfully used nowadays. They also understood the importance of the aircraft-pilot system and tried to correlate the in-flight measured characteristics with the opinions of test pilots. One of the first trials to correlate in-flight measurements with a pilot's opinion is attributed to H.A. Soule [58]. The testing campaign consisted of eight monoplanes and biplanes flown to acquire the data of their long and short period dynamics that were later used to define the longitudinal stability of aircraft. The longitudinal oscillations were induced by deflecting an elevator - the technique still used nowadays. Moreover, pilots' opinions about the aircraft handling characteristics were collected. However, at the end it was concluded that the theoretically defined longitudinal stability characteristics had no correlation with the pilots' opinions.

The importance of investigating the overall aircraft-pilot system rather than aircraft independently was understood early in the research of HQs. As mentioned previously in Ref. [58], the trial of correlating some quantifiable stability parameters with pilots' observations was unsuccessful as points of view about desirable handling characteristics of engineers and pilots were grounded on different experience and understanding. The base for the research was laid down and even more discussions on the pilots' understanding of

HQs evolved [59, 60]. The importance of *quantifying* pilot's opinion was emphasised by Hill [61]. Lack of understanding between pilots and engineers was a problem also indicated by the prominent aircraft engineer O.C. Koppen [62]. This gap appeared because of lack of precision defining minimum stability requirements. Moreover, lack of numerical criteria was indicated as a critical issue as most of the requirements were qualitative rather than quantitative. Lack of written definitions of minimum requirements for lateral stability was indicated as another issue. Hence, the process to define the requirements for satisfactory FQs started. R.R. Gilruth grouped FQs requirements into three main groups [63]:

1. Longitudinal stability and control requirements, which characterised pitch motion and elevator controls.

2. Lateral stability and control requirements, which characterised both roll and yaw motions and corresponding controls, i.e. rudder and ailerons.

3. Stall requirements, which characterised aircraft behaviour at stall conditions.

The aeroelasticity effects became increasingly important during the years and engineers started to investigate their impact on FQs relatively early [64]. The aeroelastic analysis of an example aircraft with a backward swept wing of AR = 9.43 was presented in Ref. [65]. The analysis revealed the wing aerodynamic centre motion and the wing lift-curve slope change due to the wing flexibility. It was concluded that the wing aerodynamic centre moved forward and the wing lift-curve slope reduced due to the wing bending. Thus, the destabilising effect of the wing aerodynamic centre forward shift was counteracted by the stabilising effect of the wing lift-curve slope.

The advancement of HQs analysis methods and the requirements to quantify HQs clearly indicated the future developments of the domain. As a result, new criteria were developed and they are reviewed in this section.

2.3.1 Control Anticipation Parameter

The Control Anticipation Parameter (CAP) is one of the first HQs evaluation criteria. It is defined as the ratio between the instantaneous pitch acceleration $\dot{q}_0$ and the steady state normal load factor $n_{z_{ss}}$ and represents the strength of the anticipation signal received by the pilot [66]:

$$CAP = \frac{\dot{q}_0}{n_{z_{ss}}} \approx \frac{\omega_{sp}^2}{n_{z_\alpha}} \tag{2.2}$$

It is shown in Eq. 2.2 that the parameter could be approximated by the ratio between the short period mode frequency ω_{sp}^2 and the normal load factor per unit angle of attack n_{z_α}, while the parameters $\dot{q}_0$ and $n_{z_{ss}}$ are those sensed by the inner ear of a human body [25].

Knowing CAP allows the pilot to anticipate the lag between his/her control input and the aircraft response [66–68].

CAP was first suggested by Bihrle in 1966 as it had been noted that the pilot's ability to perform precise flight path tasks depends on the short period dynamic characteristics of an aircraft [66]. These characteristics might be the mode natural frequency ω_{sp} and its damping ζ_{sp} or associated coefficients $2\zeta_{sp}\omega_{sp}$ and ω_{sp}^2. Focusing only on the short period dynamics CAP ignores the long period phugoid dynamics [25].

On the one hand, CAP is defined by human sensitivity to the motion. The instantaneous pitch acceleration $\dot{q}_0$ is sensed by the *cristae ampullaris*, which are situated in the semi-circular canals and are responsible for sensing angular accelerations. The steady state normal load factor $n_{z_{ss}}$ is sensed by *otoliths*, which form another part of the inner ear for sensing linear accelerations. Hence, the ratio is a good measure of the pilot's anticipation of an aircraft response to his/her control input [25, 66] as it gives an indication of the steady state normal load factor $n_{z_{ss}}$ change from the instantaneous pitch acceleration $\dot{q}_0$ [67, 68]. The lower acceptable value of CAP is defined by the human sensitivity and is usually around 16 $\frac{deg/sec^2}{g}$ for any human [66]. The higher acceptable values of CAP are around 50 $\frac{deg/sec^2}{g}$ [66]. However, higher acceptable values are subjective as they depend on the pilot's understanding of the controllable aircraft and his/her preferred control strategy. Hence, a different acceptable value for every individual exists.

On the other hand, CAP is defined by the airframe characteristics, as discussed in Ref. [66]:

$$CAP = \frac{W\bar{c}C_{m_{C_L}} + \frac{1}{4}S\bar{c}^2\rho g C_{m_q}}{-I_{yy}\left(1 + \frac{C_{m_{C_L}}}{l_t/\bar{c}}\right)} \tag{2.3}$$

where W is weight, $\bar{c}$ - mean aerodynamic chord, $C_{m_{C_L}}$ - static margin derivative, S - wing area, C_{m_q} - damping derivative, I_{yy} - moment of inertia around y- axis, l_t - distance from the $c_{1/4}$ of tail to $c_{1/4}$ of wing.

The short period mode's frequency depends on the previously discussed airframe parameters, as shown in Ref. [66]:

$$\omega_{sp}^2 = \frac{L_\alpha}{W}\left(\frac{W\bar{c}C_{m_{C_L}} + \frac{1}{4}S\bar{c}^2\rho g C_{m_q}}{-I_{yy}}\right) \tag{2.4}$$

where $L_\alpha = p_{dyn}SC_{L_\alpha}$.

Providing that $\frac{C_{m_{C_L}}}{l_t/\bar{c}}$ in Eq. 2.3 is small enough to be neglected and $n_\alpha = L_\alpha/W$, then Eq. 2.3 approximates to:

$$CAP \approx \frac{\omega_{sp}^2}{n_\alpha} \tag{2.5}$$

which brings a reader to Eq. 2.2 and a conclusion that the CAP connects airframe characteristics, flight conditions [26, 69] and human performance characteristics.

CAP was developed during the time when rigid structure, conventional second-order-like response aircraft formed the majority of industrial cases [70]. The short period and long period modes formed the longitudinal dynamics of such aircraft. However, for the modern flexible wing aircraft it is no longer the case as the structural flexibility introduced additional modes of frequencies near the short period mode. Thus, the coupling between the flexible body modes and the rigid body dynamic modes appears. Gautrey and Cook have shown in Ref. [70] that even in the case of the non-conventional dynamic response aircraft the amended CAP, called the Generic CAP, could still be applied as:

$$GCAP = \frac{\dot{q}_0}{n_{z_{ss}}} \equiv \frac{\dot{q}_0}{n_{z_{peak}}} \frac{n_{z_{peak}}}{n_{z_{ss}}} = \frac{\dot{q}_0}{n_{z_{peak}}} \left(1 + \exp\left(\frac{-\zeta_{sp}\pi}{\sqrt{1+\zeta_{sp}^2}} \right) \right) \tag{2.6}$$

The above equation is applicable for a reduced order model for which the response to a unit step input is second-order-like. On the other hand, Field states that the CAP criterion is not applicable to other than conventional response types since the 'mathematical basis for the criterion is no longer applicable' [71]. Hence, the criteria should not be used for augmented response systems, such as highly flexible aircraft that require significant augmentation via a flight control system.

With advancements of flight control systems, CAP criterion lost its significance to other criteria. Nevertheless, C* and C*U criteria are similar to CAP and use the same parameters. Both of these are much more used, especially for flight control systems development by main aircraft manufacturers [72, 73].

2.3.2 C* criterion

C* is another criterion to evaluate longitudinal HQs of aircraft and is widely used in flight control systems (FCS) design. As in the case of CAP, the C* criterion takes into account the normal acceleration n_z. However, the pitch rate q is used instead of the pitch acceleration $\dot{q}$. These two parameters - n_z and q - have been considered as the most significant motion cues for a pilot [71, 72, 74–77]. It is assumed that at lower speeds the pitch rate is felt by the pilot after the control input. At higher speeds even for a small control input resulting in a very small pitch rate significant normal acceleration is felt. Hence, normal acceleration becomes the main motion cue for a pilot.

Proposed in 1966 the C* criterion was intended to account for higher order dynamics [71]. However, it was shown in Ref. [78] that the criterion correlated only for configurations with negligible control system dynamics. On the other hand, being based on the time history envelope, the criterion overcame an issue of adequately describing HQs of augmented response aircraft, while traditional criteria, based on the single index or combinations of them, were inadequate [75].

The C* criterion blended the normal acceleration n_z and the pitch rate q through the following equation [74]:

$$C^* = n_z + \frac{V_{co}}{g} q \tag{2.7}$$

where V_{co} is the crossover velocity. Both motion cues n_z and q are equally important at the crossover velocity V_{co} (around 240 kt or 400 ft/s) [72, 77].

The choice of the crossover velocity has been criticised as it is an arbitrary boundary [72] and is not based on any experimental background [75]. Moreover, the validity of the criterion has been questioned [77, 78] as both the pitch rate and the normal acceleration are interconnected and cannot be controlled independently.

Regardless of the criticism above, the C* criterion has been widely used within FCS implementations. One of the biggest drawbacks of the criterion within the FCS application is its tendency to provide neutral speed stability to an aircraft [76]. This means that in the case of any change of the airspeed of an aircraft, there is no tendency to return to the trim velocity.

As flight control systems became more complex, a need for a more adequate criterion was clear. Thus, the C*U criterion was proposed.

C*U – augmentation of C* criterion

The C*U criterion was proposed to overcome the issue of airspeed stability during manoeuvring. Thus, the speed stability term U has been introduced [76]:

$$C^*U = C^* - K_V U_{err} \tag{2.8}$$

where K_V is the airspeed stability gain and U_{err} - the difference between the longitudinal airspeed and the reference speed.

The C*U was introduced as a control law rather than a handling qualities criterion. The C*U control law provides speed stability, which means that the pitch attitude is changed to return an aircraft to a reference airspeed [73].

Initially the C*U criterion was developed and applied for the conventional rigid aircraft Boeing 777. However, recently it has been successfully applied to the relatively flexible wing aircraft Boeing 787 [23] and is widely applied by other aircraft manufacturers as well.

2.3.3 Gibson Dropback criterion

The Gibson Dropback criterion [69, 79] is a well-known metric to assess longitudinal HQs and assist in the design of command and stability augmentation systems. The key advantage of this criterion is that it is time domain based and so effects of non-linear dynamics can be considered. Such effects cannot be captured through approaches based on low order equivalent systems (LOES) [80]. The key parameters for evaluating the Gibson Dropback criterion are:

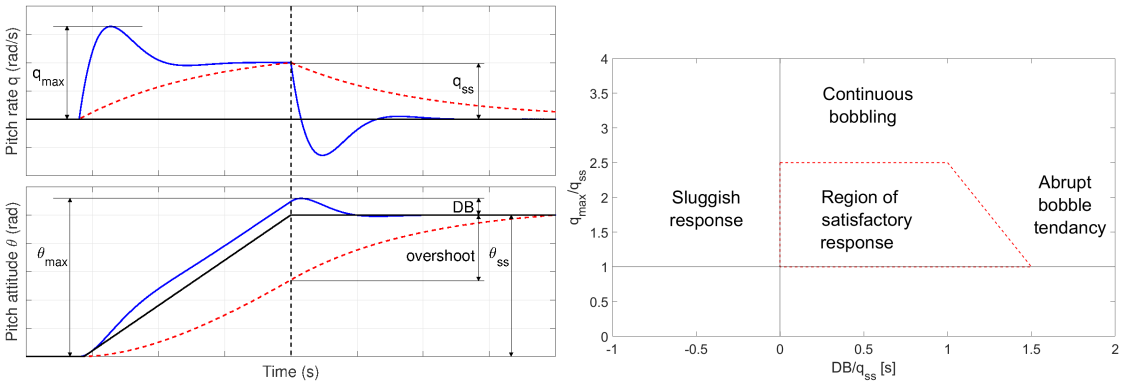

(a) Definition of q_{max}, q_{ss} and DB terms

(b) Boundaries of satisfactory response region

Figure 2.7: Definition of the Gibson Dropback criterion

1. Pitch rate overshoot ratio $\frac{q_{max}}{q_{ss}}$.

2. Attitude dropback (DB) to steady state pitch rate ratio $\frac{DB}{q_{ss}}$.

The parameters q_{max} and DB are illustrated in Fig. 2.7(a). From the pilot's perspective these parameters show the controllability and stability of an aircraft:

- q_{max} provides information about how responsive the aircraft is to an elevator input;
- DB demonstrates aircraft's pitch stability.

However, the criterion is based on ratios of these parameters to q_{ss} and extensive pilot opinion gathered to outline regions of satisfactory and undesirable response characteristics, as shown in Fig. 2.7(b). The boundaries used in this study are based on research conducted on large transport aircraft in Ref. [75].

All of the above discussed criteria - CAP, C*, C*U and Gibson Dropback - are based on the time domain analysis of aircraft response. However, criteria based on the frequency domain analysis of aircraft response play a significant part in the analysis of HQs.

2.3.4 Bandwidth criterion

The bandwidth criterion is the most basic analysis tool of aircraft HQs in the frequency domain. It allows the evaluation of the closed loop aircraft-pilot system in the high gain tasks.

The bandwidth is defined in the classical control theory as "that frequency at which the closed loop amplitude is down -3 dB from the low frequency value" [81, 82]. However, the use of the bandwidth as a HQs requirement is based on the overall stability of the

aircraft-pilot system. For the system to be stable, the gain phase difference must be more than $-\pi$ [81]. It was shown in Ref. [81] that 45° margin should be added to the previous requirement of the stable system to take into account a pilot's time delay. This margin represents a tracking task "of full attention, but less than maximum effort" [71, 83]. Considering the gain margin, the factor of 2 in gain is typically used to establish the crossover frequency [82], thus leading to the gain margin of -6 dB. Thus, the complete bandwidth definition is as defined in Ref. [82]:

> "The bandwidth of the specified response to a particular control input is defined as the lowest frequency for which the phase margin is at least 45° and the gain margin is at least 6 dB."

The testing experience showed that aircraft with high bandwidth should have rapid and well damped response, while aircraft with low bandwidth would have sluggish and wallowing response [67, 68].

Figure 2.8 shows the Bode diagram where both gain margin $\omega_{BW_{gain}}$ and phase margin $\omega_{BW_{phase}}$ criteria are explained graphically. The overall bandwidth of the aircraft-pilot system would be the lowest of those two.

The bandwidth criterion was developed as the simplest frequency based HQs analysis tool to assess the modern flight control systems. The new control systems added complexity to the unconventional HQs and the frequency domain analysis was supposed to add valuable insight into these HQs [26]. In simple words, the bandwidth could be described as the parameter, which defines the frequency "below which the pilot can follow all commands, and above which he cannot" [71]. It will be shown later that many other frequency domain criteria are based on the bandwidth theory too.

Despite its ease to use, the bandwidth criterion has some limitations. The first limitation is its dependence on tasks [71], which would impose different boundaries for different response types and, thus, requires in-flight test data, which is very expensive to get. Another limitation is its dependence on linearised aircraft models as the bandwidth theory is based on the transfer functions representing the ratio between the response of aircraft and the input of pilots. This makes the criterion valid only for a limited flight task or flight condition. Another highly important limitation is based on the initial development of the criterion - it was developed to investigate "unconventional HQs" that appeared due to complex flight control systems. However, currently another variable is getting significance, i.e. an increase of the structural flexibility reduce the structural frequencies that affect the HQs even more. Hence, the bandwidth criterion loses its theoretical reasoning when aircraft non-linear behaviour is taken into account.

2.3.5 Neal-Smith criterion

The introduction of complex flight control systems led to the development of another - the Neal-Smith - criterion [78, 84] as the previously used C* criterion did not show satisfactory agreement with new complex FCS dynamics. Moreover, the new method considered

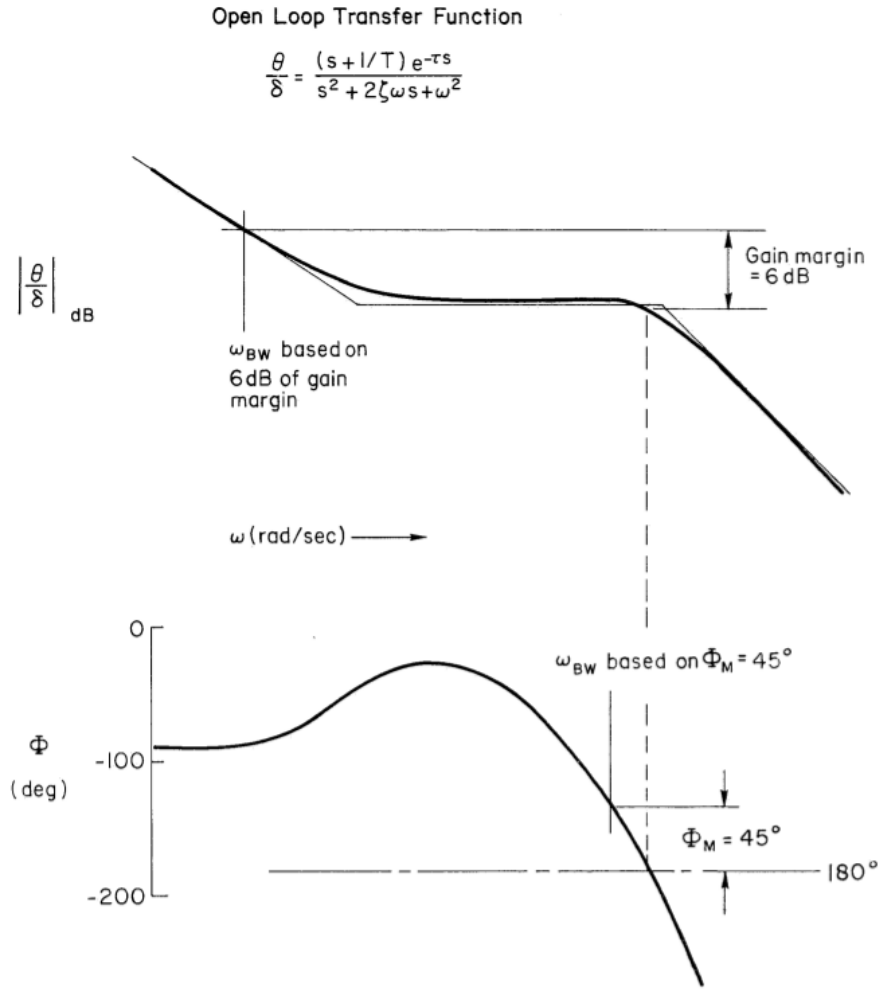

Figure 2.8: Definition of the bandwidth criterion (reproduced from Ref. [82])

a closed loop system rather than an open loop system, which was the case of the C* criterion. It is also based on the previously discussed bandwidth theory. A thorough procedure of deriving the new criterion was presented in Refs. [78, 84]. The Neal-Smith criterion takes into account three parameters of the system dynamics, particularly (as defined in Refs. [78, 84]):

1. Bandwidth, which measures the responsiveness of an aircraft to the pilot's input. It is the frequency at which the closed loop Bode phase ($\angle|\theta/\theta_c|$) equals $-90°$.

2. Droop, which shows how slowly the nose settles down on target. It is measured as the maximum excursion of closed-loop Bode amplitude ($|\theta/\theta_c|$) below the 0 dB line for ω_{BW}.

3. Closed loop resonance ($|\theta/\theta_c|_{max}$), which relates the damping ratio and magnitude

of oscillations in pitch attitude. It is defined as the magnitude of any resonant peak in the closed loop Bode plot.

The following performance standards were determined according to pilot comments:

1. $\omega_{BW_{min}} = 3.5\frac{rad}{sec}$ for $\angle|\theta/\theta_c| \geq -90^\circ$ at $\omega = 3.5$.
2. $|\theta/\theta_c| \geq -3dB$ for $\omega \leq \omega_{BW}$.

The above results were acquired for the fighter's missions, which required precision in controlling the pitch attitude, e.g. tracking task during the air superiority missions.

2.3.6 Experimental Behaviour Measurement Method

The need for an objectively quantifiable method was indicated in Ref. [11]. Hence, the experimental behaviour measurement method (EBMM) has been developed at Delft university based on their previous work done in the pilot modelling and evaluation domain. The EBMM was first introduced in 2009 by HJ Damveld in Ref. [11]. The development of the method was based on the fact that previous HQs evaluation methods, particularly Cooper-Harper Rating, were rather subjective than objective. It was shown in Ref. [11] that EBMM meets the previous requirement of a quantifiable HQs assessment method.

EBMM is based on the quantification of the pilot behaviour. One of the possible ways to quantify a pilot's behaviour is to ask a pilot to reduce the error between some parameters shown on the primary flight display (PFD), e.g. the difference between the actual pitch attitude and the target pitch attitude. This is similar to the air-to-air refuelling task, where the pilot has to follow some arbitrary target. By introducing some forcing function the error varies within certain limits. This forces the pilot to counteract those variations. Continuously increasing the bandwidth of the forcing function leads to an increasing crossover frequency. The crossover frequency [81, 85, 86] is defined as the frequency at which the magnitude of the open-loop dynamics crosses over 0 dB. It is a very important parameter as this frequency determines both the performance and stability of the system. At some point the pilot-aircraft system will reach the point from which an increasing bandwidth will lead to a decreasing crossover frequency. This point is called crossover-regression frequency and can be used to quantify HQs of the open-loop aircraft-pilot system. The crossover frequency regression could be explained as a pilot's control strategy to optimise the performance within the boundaries of workload and stability. During the high-bandwidth tasks, well-trained and experienced pilots will almost always show crossover regression by nature [11].

To carry out the EBMM test four essential steps have to be taken. These steps are shown in Fig. 2.9 and are as follows:

1. The design of forcing functions with an increasing bandwidth. The frequency range within the forcing functions should be clearly defined. For example, the forcing function could include the short period mode frequency or frequencies of structural

flexible modes. In general, the frequencies should be of the phenomenon that is intended to be tested, e.g. structural flexibility effect on HQs. The design of the forcing function needs to be such that the crossover-regression frequency is situated between the lowest and the highest bandwidth. Designing the power spectra of forcing functions is an iterative process as the crossover-regression frequency of an aircraft is not known a priori.

2. The testing phase, where test pilots perform the tracking task. The initial goal during the task is to reduce the error between prescribed parameters. As the analysis of the method is based on the pilot behaviour, thus the error, an aircraft's response and the pilot's control inputs are recorded for the further data analysis.

3. The data analysis, which is carried out for the recorded data. The first step is done in the time domain, when the error and control input signals are averaged for each forcing function and each pilot. The purpose of this averaging is to reduce the remnant and to increase the signal-to-noise ratio. Then the pilot describing functions and the crossover frequencies have to be obtained by the use of the system identification methods.

4. The analysis of the crossover frequencies is the last step. The crossover frequencies are plotted along with the forcing function bandwidths for each pilot. Thus, the crossover-regression frequency is found for each pilot from the resulting plot. Then the average crossover frequency and error bars per forcing function bandwidth could be calculated.

The forcing function has two goals within the EBMM, which are:

1. To force the occurrence of the crossover-regression and quantify the frequency at which it occurs.

2. To enable system identification of the effective open-loop pilot describing function at a wide frequency range.

To reach the goals the forcing function should meet the following requirements [11]:

1. The forcing function should be defined as a multi-sine signal due to its high signal-to-noise ratio.

2. The separation between frequencies should be relatively small to assure the detection of important properties of the pilot describing function. Thus, usually the logarithmic spacing is used when defining the forcing function.

3. The forcing function should take the range of frequencies from below the crossover frequency to at least one decade beyond the crossover frequency in order to determine the crossover frequency and effective time delay.

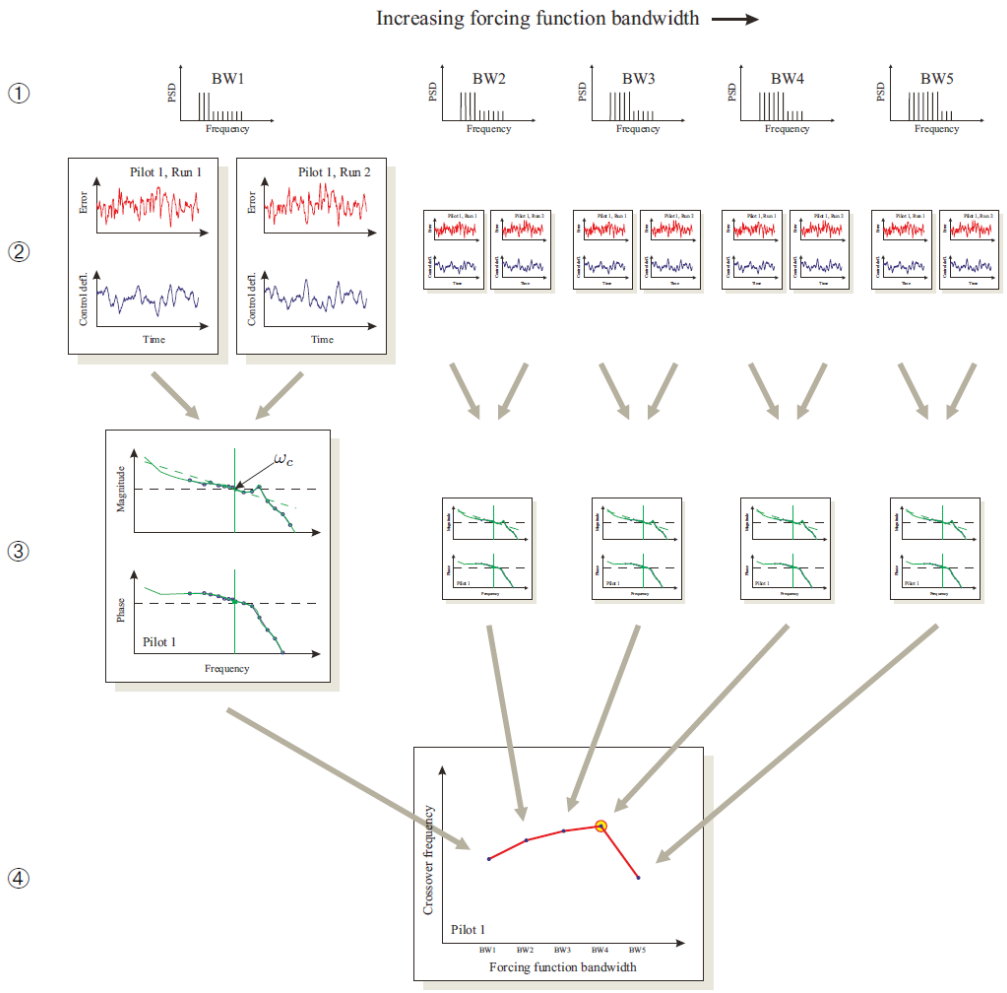

Figure 2.9: Diagram of the experimental behaviour measurement method application (reproduced from Ref. [11])

4. The forcing function should be random appearing to avoid the precognitive behaviour. This requirement is met by implementing multiple sines in the forcing function.

5. An unambiguous monotonic relation between the independent variables and the dependent variable - the crossover frequency - should be obtained to detect when the pilot shows the crossover-regression. To meet the requirement, ideally there would be only one independent variable, which magnitude would be increased until the crossover-regression occurs. The value of that independent variable will be a measure of HQs.

The multi-sine function is defined as follows:

$$f(t) = \mu_f + \sum_{i=1}^{N} A_i \sin(\omega_i t + \phi_i) \tag{2.9}$$

where μ_f is the mean of the forcing function, N - number of sines, ω_i - frequencies of sines, A_i - amplitudes of sines and ϕ_i - phases of sines.

Multiple forcing functions of increasing bandwidth are used to test the open-loop system. Increasing the bandwidth of the forcing function forces a test pilot to use a high-bandwidth control technique. However, in the simulator environment, when there is no stress or anxiety present, experienced pilots automatically compensate to avoid high-bandwidth control technique. This compensation is a change in the behaviour, which is defined as the output of a human operator in response to an input. Thus, the bandwidth at which the compensation appears is a measure for the maximum bandwidth of the aircraft and is a measure of HQs. It is important to notice that inexperienced pilots usually do not show crossover-regression by nature, thus only professional test pilots should be used at this stage. Then the system identification methods are applied to sets of data to identify describing function of each pilot. Moreover, this method also allows researchers to identify the crossover frequencies of each pilot.

The crossover frequency is understood to be dependent on the forcing function bandwidth. Thus, plotting both the crossover frequencies and the forcing function bandwidths allows an engineer to define their interrelationship. The usual trend is that the crossover frequency increases with the forcing function bandwidth. However, when the pilot reaches a certain point of the forcing function bandwidth, the crossover frequency starts to decrease. This point is defined as the crossover-regression frequency. The crossover-regression frequencies of multiple pilots allow to evaluate HQs of a tested aircraft.

Defining aircraft HQs by the crossover-regression frequency is a purely quantifiable metric, which does not include any subjective opinions of pilots. Of course, different pilots are different humans, who exhibit different behaviour. Thus, some subjectivity still exists. However, the subjectivity is reduced by choosing test pilots with similar training and flying experience.

2.3.7 Discussion of time domain and frequency domain handling qualities criteria

The review of the main HQs criteria revealed limitations of them to be applied for the flexible aircraft investigation. The first observation shows that the most of the criteria were developed using relatively rigid aircraft. The complexity of the dynamics between rigid and flexible aircraft is fundamentally different. Thus, applicability of these traditional HQs criteria for assessing flexible aircraft configurations is fundamentally questionable. Regarding the time domain criteria their applicability to assess the complex systems was

shown through the use of C* and C*U criteria. GCAP criterion showed its applicability for the analysis of complex flight control systems too. However, once again, it was developed for the complex control systems of relatively rigid aircraft, thus ignoring airframe flexibility. Considering the frequency domain criteria, their applicability to investigate complex flight control systems has been proven during decades of their use. However, only EBMM criterion was developed taking into account the flexibility effects and showed its applicability using the example of longitudinally flexible aircraft. Also all of the criteria were developed to investigate longitudinal dynamics rather than lateral/directional dynamics, which is of high interest for this doctoral research.

The Gibson Dropback criterion was applied for the analysis of a flexible aircraft HQs during this project. It will be shown later in Ch. 4 that it can reveal the deficiencies of the aircraft arising due to its wing flexibility. However, the trial to apply the EBMM technique during the pilot-in-the-loop testing failed while one of the test pilots commented that the aircraft oscillation due to the forcing function was similar to the turbulence as the aircraft kept its flight path straight with little lateral oscillations. The pilot simply refused to control the aircraft as the task seemed to be unrealistic for the large transport aircraft.

From the discussion above it is clear that some generic HQs criterion has to be developed on this occasion taking into account the structural flexibility of an aircraft wing. However, the criterion will need to be validated by some real flight tests - the objective, which is very problematic to achieve as there are no large flexible aircraft flying. Thus, the classical pilot rating method will be used during this project to assess HQs of the flexible aircraft.

2.3.8 Cooper-Harper Rating

The Cooper-Harper Rating (CHR) is the most used HQs evaluation metric. It was first introduced in 1969 [87]. The initial idea was to merge two scales - the Cooper scale and the Cornell Aeronautical Laboratory (CAL) scale - into one common scale [88], as the scales used before were usually adapted to the individual investigator needs. This prevented results to be compared if they were derived using different scales. Thus, the CHR method overcame this issue of quantifying HQs of aircraft. The CHR method is based on a human factors survey, created for the needs of aircraft HQs evaluation, and concluded the lessons from earlier rating scales [89]. With time, the CHR method became the most popular method within the flight testing community as it “is, far and away, the most important and common HQs flight testing technique in existence” [89]. Moreover, it is the only significant method to answer the question “Do the aircraft HQs enable the pilot to complete his mission?” [89].

On the other hand, the CHR method has some limitations. The problem of repeatability to acquire the CHR score has been discussed in Refs. [90, 91]. This issue is known as the Cooper-Harper pilot rating variability. Some of the sources of this variability are discussed in Refs. [90, 91]. First of all so called ‘intrapilot’ variability occurs when a single pilot is not capable to assign the same score for exactly the same test case. This

highly depends on the environment and pilot's attitude during the testing phase. The issue might be mitigated by additional runs to reduce the standard deviation. The 'interpilot' variability occurs when couple of pilots assign different scores for exactly the same test case. Again it depends on the natural difference between pilots and their perceived workload [90]. The 'interpilot' variability might be reduced by selecting test pilots of similar experience and training. Due to both sources of variability, the confidence of Cooper-Harper ratings is reduced. To overcome these issues additional testing is required with more pilots. Moreover, the test condition such as the free flight time before assigning the score should be set the same for different pilots. Other factors, which contribute to the variability of the CHR evaluations are as follows [90]:

- the format of questions and statements in the CHR scale decision tree;
- the pilot's objectiveness;
- cultural and linguistic differences.

An issue of the scale's lack of diagnostic power to assess multidimensional concepts[1] was reported in Ref. [88].

The CHR scale is shown in Fig. 2.10. The use of the scale requires the pilot to make binary decisions to answer the questions about an aircraft flown:

1. If an aircraft is controllable, which leads to the next question or evaluation of an aircraft as 'impossible to fly' (CHR 10).
2. If the adequate performance is achieved, which leads to the next question or evaluation of an increased pilot workload and not adequate performance (CHR 7-9).
3. If an aircraft is satisfactory without improvement, which leads to an evaluation of desirable performance (CHR 1-3) or adequate performance (CHR 4-6).

An aircraft performance is better if the CHR score is lower. Sometimes test pilots tend to provide decimal ratings or half-point ratings. However, this should be avoided, because these ratings imply a confidence that simply cannot exist given the highly subjective nature of nearly every element of the CHR scale [89]. The CHR method requires the desired and adequate performance limits of the pilot-aircraft system in the task, the definition of a task and the flight environment. Hence, the CHR method evaluates an aircraft for a given task rather than an aircraft itself [89].

The scale is based not only on the quantification of the aircraft performance, but on the pilot's comments, which come along with the score and are the most important results of the CHR evaluation [89]. Neither CHR scores nor the pilot's opinion should be ignored

[1] Multidimensional concepts are assessments that take into account multiple variables at the same instance, e.g. the handling qualities of an aircraft and the pilot workload during the task. The best example of such a multidimensionality is the NASA-TLX workload scale [92].

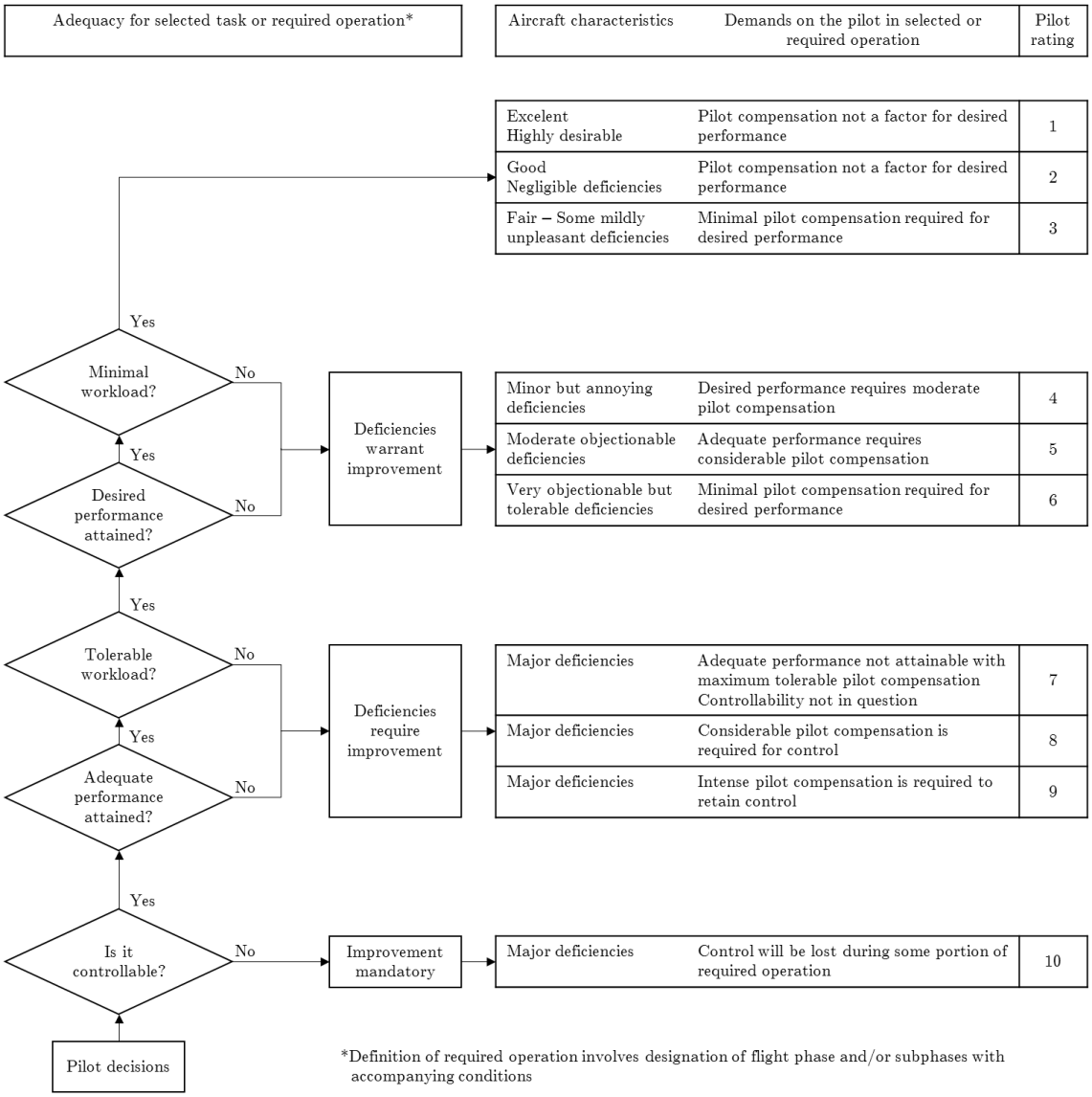

Figure 2.10: Cooper-Harper Rating scale

when discussing HQs of an aircraft as both are useless without each other when using the CHR method.

Although there is no more important, more used and more efficient flight testing technique in aircraft HQs testing [89], the CHR method is not the only method to evaluate HQs of an aircraft. The method was even criticised in Ref. [11] as being not properly quantifiable, as it highly depends on the pilot's opinion. Moreover, as all the classical methods the CHR method was developed with testing experience of relatively rigid aircraft, while future research is aiming to investigate very flexible aircraft. However, the method will be used later in this project as it is well known for every test pilot. To apply the CHR method, well defined flying task has to be developed or appropriate flight test manoeuvres have to be chosen.

2.3.9 Flight test manoeuvres

All previous criteria are based on precisely flown tasks. Moreover, to excite flight or structural modes of interest, particular manoeuvres may be designed. Hence, it is important to understand the background for each manoeuvre.

A flight test manoeuvre is a vital part of a flight testing procedure along with appropriate rating scales or assessment criteria. More than 20 flight test manoeuvres have been described in Ref. [93]. The manoeuvres are classified by their purposes, applicable classes and flight categories, their operational applications. The guide on how to select an appropriate manoeuvre for the user specified testing case is provided too. The proper choice of a manoeuvre can be done evaluating the following five parameters:

1. Environment - conventional or high angle of attack.
2. Axes to be tested - longitudinal, lateral/directional or axial.
3. Data to be collected - quantitative or qualitative.
4. Precision of the performance - no capture, gross capture, moderate or tight control.
5. Type of a manoeuvre - individual manoeuvre, sequence of manoeuvres or freestyle manoeuvre.

The use of the guide allows a flight test engineer to easily choose a manoeuvre and anticipate what results should be obtained during the testing.

The handling qualities during tracking (HQDT) task has been seen as one of the most suitable tasks to exhibit an aircraft to the pilot induced oscillations (PIO). The HQDT techniques and the testing process were extensively discussed in Ref. [94]. It was stated that the HQDT task allows a rapid evaluation of the mission effectiveness of an aircraft relatively early in the flight test programme. The method uses the CHR scale to evaluate an aircraft within its manoeuvre environment. The HQDT technique shows aircraft deficiencies that conventional methods would not discover otherwise. The Air Force Flight

Test Center publication 'Handling Qualities Testing' confidently states that the HQDT technique is perhaps the most important HQs testing technique at the disposal of a flight tester [89]. The HQDT technique was applied for a flexible aircraft HQs investigation in Ref. [13]. Waszak et al. showed that increasing flexibility of an aircraft decreases its HQs by degrading the tracking performance. The results indicated that there were fundamental differences between the dynamics of rigid and elastic aircraft. These differences led to increased tracking errors, degraded HQs and changes in the frequency content of the pilot inputs [13].

2.3.10 Handling qualities evaluation

Having discussed the main HQs criteria, it is a common sense that any testing starts from the very basic manoeuvres, i.e. stall test, SPPO, Dutch roll, etc. Only when basic aircraft dynamic parameters are known, the previously discussed criteria should be applied. However, to evaluate different dynamic modes and stability of an aircraft some clear criterion must be used.

One of the most thorough specification of FQs is provided in military specifications MIL-F-8785C [95]. However, it specifically defines flying qualities instead of handling qualities. Nevertheless, the document is still extensively used nowadays within the flight test community as it provides clarity in aircraft and flight phases classification. It classifies FQs into three levels of acceptability:

1. Those adequate for the mission.

2. Those adequate to accomplish the mission, but with some degradation in effectiveness and/or some increase in pilot workload.

3. Those leading to a safe flight, but with excessive pilot workload and/or inadequate effectiveness of the mission.

Hence, results of the research of aircraft FQs should be referenced to those three levels of acceptability for the comparison with other tested aircraft as this is a widely used metric.

2.3.11 Importance of simulator motion cues on handling qualities assessment

Motion cues are essential part of a realistic aircraft simulation for handling qualities assessment [96–98] as well as for pilot training [99]. The usual solution for motion cueing within the industry is the hexapod (Stewart) platform [100], which allows a 6-DoF motion of a simulator [101]. However, adding the motion to an existing fixed-base flight simulator is a very complex and expensive task. As a fixed-base flight simulation is an option for HQs assessment, it is vital to understand the effect that the absence of the motion cues has on pilots' perception of a simulated aircraft.

At early stage of the motion cueing research it was shown that the simulation of angular motions is more important than that of translational motions [96, 97]. Moreover, it was also shown that the human perception of accelerations is based on the vestibular system, while the human visual system is tuned to perceive velocities [97, 102]. Thus, for certain flight simulation tasks, such as a take-off, motion cues would enhance sensations of aircraft motion before simulated velocity builds up sufficiently to be noticeable [102–104]. However, to simulate relatively constant motion patterns the visual system of a flight simulator is enough [102].

As it was mentioned above, motion cues become more helpful when there are significant changes in accelerations. On the one hand, it is a case of marginally stable or difficult vehicles due to their design peculiarities [96]. On the other hand, it also could be the case of a flexible aircraft dynamics [98]. The issue with the latter case is a phase shift between the visual display and the simulator motion [98]. The phase shift also appears in the case of a rigid aircraft simulation, but as manoeuvres occur in a short period of time, the phase shift is more likely to be unnoticeable. However, as flexible aircraft usually have less damped structural oscillations, the phase shift may lead a pilot to the motion sickness and a reduction in perceived fidelity [98]. Moreover, the amplitude of the motion signals due to structural oscillations becomes smaller after being processed by the simulator motion drive algorithms [98]. Hence, scaling down of the oscillating motion signals may lead to overly optimistic perceived HQs of a simulated aircraft [98].

A big issue regarding the simulator motion cueing is uncertainty on which motion cues directly influence pilots' perception and control behaviour [105]. During the simulations of a helicopter Schroeder showed that yaw rotational cues had no significant effect on hovering flight simulation, while lateral translational cues significantly improved pilot-vehicle performance and lowered pilot-rated compensation [106]. However, as mentioned above, motion cues help pilots, who are unfamiliar with the realistic motion cues encountered in an aircraft, to catch up immediately with that aircraft behaviour [107]. Moreover, motion cueing also improves pilot performance for difficult control tasks as well as subjective handling qualities [108]. Another important aspect to be considered regarding the motion cues is that the cockpit of a transport aircraft is located at a significant distance from CG. Thus, the motion cues of the simulator should be representative to the cockpit position rather than the CG position [109].

Discussion above shows many advantages of motion-based flight simulations as well as many uncertainties on the suitability of some motion cues for particular flight tasks. Although motion cues help pilots to get used to aircraft dynamics and perceive their HQs better, they may also introduce biases due to the pilot station offset from the aircraft CG position or the phase shift between visual and motion cueing systems.

Chapter 3

Equations of motion for flexible aircraft

This chapter presents the derivation of the equations of motion for a flexible body and assessment of their impact on the motion parameters of that body.

3.1 Derivation of equations of motion

Equations of motion equate forces and moments acting on a body to motion parameters of that body. Primary motion parameters of any body are linear and angular accelerations, which are calculated by the use of the Newton's second law and the Euler's equations accordingly:

$$\begin{aligned} \text{Forces} &= \text{Mass} \times \text{Linear Accelerations} \\ \text{Moments} &= \text{Moments of Inertia} \times \text{Angular Accelerations} \end{aligned} \tag{3.1}$$

Mass and its distribution within any body are known a priori, thus moments of inertia can be calculated at any instance of time. It is clear that in case of a rigid body mass position does not change and such a body can be approximated as a mass point with defined inertia properties. For a long time it was a valid approximation as aircraft used to be relatively rigid structures. This also simplified the definition of EoM. Thus, most flight dynamics textbooks (e.g. Refs. [25] and [26]) present the derivation of classical EoM for a rigid body along with the explanations due to rigid body assumptions. Such an approximation is not valid any more in case of a flexible body, where masses move within the body frame and, as a consequence, moments of inertia change constantly. Structural flexibility affects linear and angular accelerations and equations defining them must account for that effect. Thus, a set of EoM for flexible bodies had to be derived to further investigate dynamics of flexible aircraft within the framework of this project. The derivation of EoM for flexible bodies was based on the same principles as for rigid bodies, thus the approach used by Cook [26] was chosen as a starting point.

3.1.1 Equation of accelerations

To begin derivation of the accelerations' equation, let's first define some arbitrary body and its reference axes, as shown in Fig. 3.1.

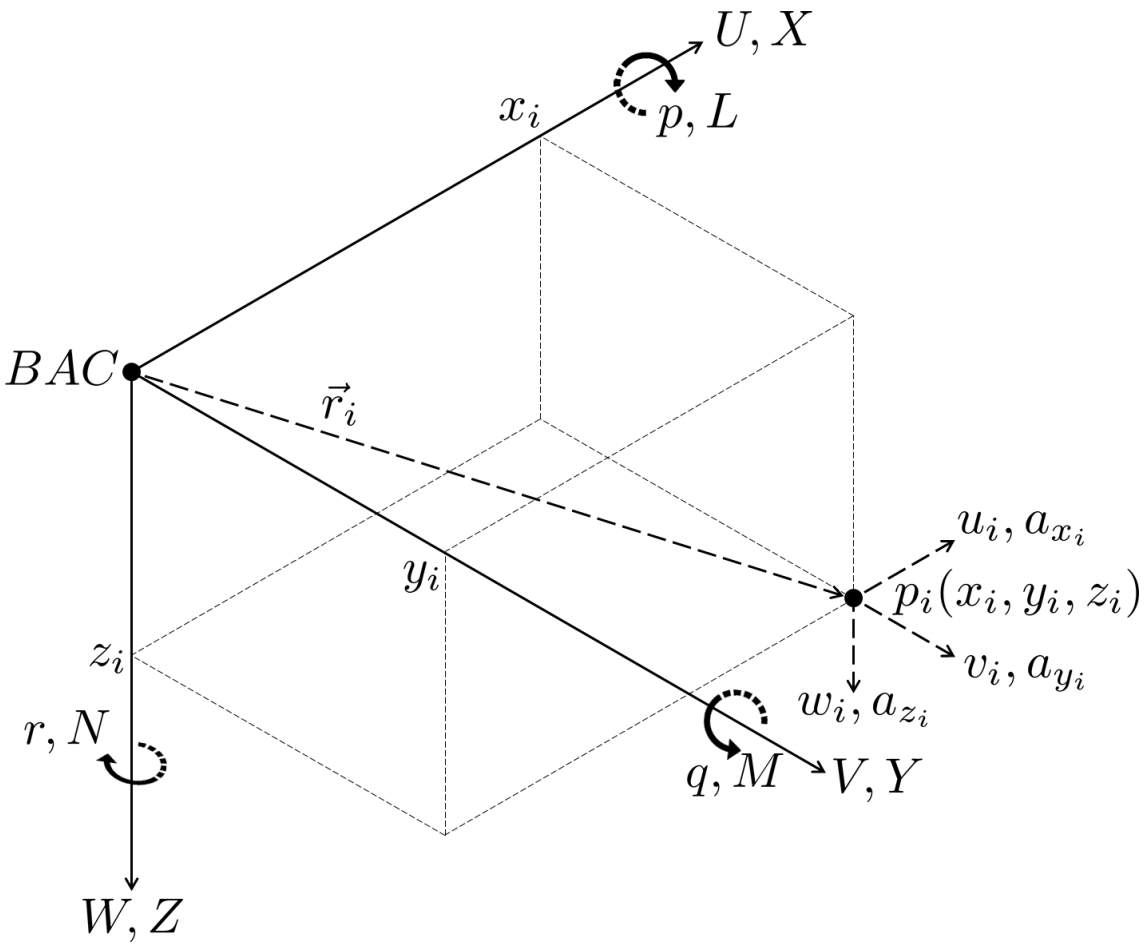

Figure 3.1: Axes system for equations of motion analysis

The body is defined in a coordinate system of orthogonal axes *oxyz* with its origin point *o*, referred to as the body axes centre (BAC). The motion of the body with respect to some external reference frame is described through its linear and angular velocities U, V, W and p, q, r. Corresponding forces and moments are defined as X, Y, Z and L, M, N.

Now let's consider some arbitrary point p_i within the body frame, which position is defined by a vector $\vec{r}_i(x_i, y_i, z_i)$ from BAC. Assuming that the body is flexible the point p_i can move within the body frame and the vector $\vec{r}_i$ becomes dependant on time, i.e. $\vec{r}_i = f(x_i, y_i, z_i, t)$. Then accelerations and velocities of p_i in some external reference

frame can be defined as a_{x_i}, a_{y_i}, a_{z_i} and u_i, v_i, w_i:

$$\begin{aligned} u_i &= U + \dot{x}_i - ry_i + qz_i \\ v_i &= V + \dot{y}_i - pz_i + rx_i \\ w_i &= W + \dot{z}_i - qx_i + py_i \end{aligned} \tag{3.2}$$

It is assumed at this point that the point p_i has only translational and no rotational motion within the body frame as the latter one would be negligible.

Accelerations of the point p_i can now be defined as derivatives of velocities and two terms due to the overall body's angular motion:

$$\begin{aligned} a_{x_i} &= \dot{u}_i - rv_i + qw_i \\ a_{y_i} &= \dot{v}_i - pw_i + ru_i \\ a_{z_i} &= \dot{w}_i - qu_i + pv_i \end{aligned} \tag{3.3}$$

Substituting u_i, v_i, w_i from equations (3.2) into equations (3.3) leads to the following definition of accelerations of the point p_i:

$$\begin{aligned} a_{x_i} &= \dot{U} - rV + qW - x_i(q^2 + r^2) + y_i(pq - \dot{r}) + z_i(pr + \dot{q}) + \ddot{x}_i - 2r\dot{y}_i + 2q\dot{z}_i \\ a_{y_i} &= \dot{V} - pW + rU + x_i(pq + \dot{r}) - y_i(p^2 + r^2) + z_i(qr - \dot{p}) + \ddot{y}_i - 2p\dot{z}_i + 2r\dot{x}_i \\ a_{z_i} &= \dot{W} - qU + pV + x_i(pr - \dot{q}) + y_i(qr + \dot{p}) - z_i(p^2 + q^2) + \ddot{z}_i - 2q\dot{x}_i + 2p\dot{y}_i \end{aligned} \tag{3.4}$$

The overall accelerations of a point p_i defined in equations (3.4) include terms due to the overall body motion in space and internal motion of the point p_i within the body itself. At this stage it is important to notice that as the EoM were implemented in the MATLAB/Simulink code, the vectorised form was used for all subsequently derived equations. The terms of equations (3.4), expressed in a vectorised form, are:

1. Terms due to the overall body motion:

$$\begin{Bmatrix} \dot{U} - rV + qW \\ \dot{V} - pW + rU \\ \dot{W} - qU + pV \end{Bmatrix} = \dot{\vec{v}}_0 + \vec{\omega}_0 \times \vec{v}_0$$

2. Terms due to the arbitrary point p_i offset from BAC:

$$\begin{Bmatrix} -x_i(q^2 + r^2) + y_i(pq - \dot{r}) + z_i(pr + \dot{q}) \\ x_i(pq + \dot{r}) - y_i(p^2 + r^2) + z_i(qr - \dot{p}) \\ x_i(pr - \dot{q}) + y_i(qr + \dot{p}) - z_i(p^2 + q^2) \end{Bmatrix} = \vec{\omega}_0 \times (\vec{\omega}_0 \times \vec{r}_i) + \dot{\vec{\omega}}_0 \times \vec{r}_i$$

3. Terms due to the arbitrary point p_i internal motion:

$$\begin{Bmatrix} \ddot{x}_i - 2r\dot{y}_i + 2q\dot{z}_i \\ \ddot{y}_i - 2p\dot{z}_i + 2r\dot{x}_i \\ \ddot{z}_i - 2q\dot{x}_i + 2p\dot{y}_i \end{Bmatrix} = \ddot{\vec{r}}_i + 2\vec{\omega} \times \dot{\vec{r}}_i$$

Hence, equations (3.4) expressed in a vectorised form are:

$$\vec{a}_i = \dot{\vec{v}}_0 + \dot{\vec{\omega}}_0 \times \vec{v}_0 + \vec{\omega}_0 \times (\vec{\omega}_0 \times \vec{r}_i) + \dot{\vec{\omega}}_0 \times \vec{r}_i + \ddot{\vec{r}}_i + 2\vec{\omega} \times \dot{\vec{r}}_i \tag{3.5}$$

Equation (3.5) introduced additional terms when compared to the classical rigid body EoM, i.e. two terms due to the internal motion of the point p_i, which represents the flexibility of the body.

Equation (3.5) can now be substituted into equations (3.1) to express forces and moments acting on the body.

3.1.2 Equation of forces

The overall forces acting on the body are calculated as the sum of forces acting on N points p_i, which form that body:

$$\vec{F} = \sum_{i=1}^{N} \delta m_i \vec{a}_i \tag{3.6}$$

Substituting $\vec{a}_i$ with the expression from equation (3.5) results in the following expression of forces:

$$\begin{aligned} \vec{F} = & \underbrace{\dot{\vec{v}}_0 \sum_{i=1}^{N} \delta m_i + \vec{\omega}_0 \times \vec{v}_0 \sum_{i=1}^{N} \delta m_i}_{\text{Overall body motion force}} + \underbrace{\vec{\omega}_0 \times \left(\vec{\omega}_0 \times \sum_{i=1}^{N} \delta m_i \vec{r}_i \right)}_{\text{Centrifugal force}} \\ & + \underbrace{\dot{\vec{\omega}}_0 \times \sum_{i=1}^{N} \delta m_i \vec{r}_i}_{\text{Euler force}} + \underbrace{\sum_{i=1}^{N} \delta m_i \ddot{\vec{r}}_i}_{\text{Inertial force}} + \underbrace{2\vec{\omega}_0 \times \sum_{i=1}^{N} \delta m_i \dot{\vec{r}}_i}_{\text{Coriolis force}} \end{aligned} \tag{3.7}$$

The equation of forces for flexible bodies includes four additional terms, each representing some source of force, i.e. centrifugal, Euler, inertial and Coriolis. Two of them, i.e. centrifugal and Euler forces, appear because the centre of gravity is different from the body axes centre. Their impact on the dynamics of the body is presented later in this chapter.

3.1.3 Equation of moments

The derivation of the equation of moments is not as straightforward as in the case of forces' equation. Nevertheless, the overall moments acting on the body are calculated as the sum of moments acting at N points p_i, which form that body:

$$\vec{M} = \sum_{i=1}^{N} \delta m_i \vec{r}_i \times \vec{a}_i \tag{3.8}$$

Substituting $\vec{a}_i$ with the expression from equation (3.5) results in the following expression of moments:

$$\begin{aligned}\vec{M} = &\overbrace{\sum_{i=1}^{N} \delta m_i \vec{r}_i \times \dot{\vec{v}}_0}^{\text{Term 1}} + \overbrace{\sum_{i=1}^{N} \delta m_i \vec{r}_i \times (\vec{\omega}_0 \times \vec{v}_0)}^{\text{Term 2}} + \overbrace{\sum_{i=1}^{N} \delta m_i \vec{r}_i \times (\vec{\omega}_0 \times (\vec{\omega}_0 \times \vec{r}_i))}^{\text{Term 3}} \\ &+ \underbrace{\sum_{i=1}^{N} \delta m_i \vec{r}_i \times \left(\dot{\vec{\omega}}_0 \times \vec{r}_i\right)}_{\text{Term 4}} + \underbrace{\sum_{i=1}^{N} \delta m_i \vec{r}_i \times \ddot{\vec{r}}}_{\text{Term 5}} + \underbrace{2\sum_{i=1}^{N} \delta m_i \vec{r}_i \times \left(\vec{\omega}_0 \times \dot{\vec{r}}_i\right)}_{\text{Term 6}}\end{aligned} \tag{3.9}$$

Terms 3, 4 and 6 may be replaced with the following expressions:

- $\sum_{i=1}^{N} \delta m_i \vec{r}_i \times (\vec{\omega}_0 \times (\vec{\omega}_0 \times \vec{r}_i)) = \vec{\omega}_0 \times (I\vec{\omega}_0)$;
- $\sum_{i=1}^{N} \delta m_i \vec{r}_i \times \left(\dot{\vec{\omega}}_0 \times \vec{r}_i\right) = I\dot{\vec{\omega}}_0$;
- $2\sum_{i=1}^{N} \delta m_i \vec{r}_i \times \left(\vec{\omega}_0 \times \dot{\vec{r}}_i\right) = \dot{I}\vec{\omega}_0 + \vec{\omega}_0 \times \sum_{i=1}^{N} \delta m_i \left(\vec{r}_i \times \dot{\vec{r}}_i\right)$.

Substituting these expressions into equation (3.9) results in the following expression:

$$\begin{aligned}\vec{M} = &\sum_{i=1}^{N} \delta m_i \vec{r}_i \times \dot{\vec{v}}_0 + \sum_{i=1}^{N} \delta m_i \vec{r}_i \times (\vec{\omega}_0 \times \vec{v}_0) + \vec{\omega}_0 \times (I\vec{\omega}_0) \\ &+ I\dot{\vec{\omega}}_0 + \sum_{i=1}^{N} \delta m_i \vec{r}_i \times \ddot{\vec{r}} + \dot{I}\vec{\omega}_0 + \vec{\omega}_0 \times \sum_{i=1}^{N} \delta m_i \left(\vec{r}_i \times \dot{\vec{r}}_i\right)\end{aligned} \tag{3.10}$$

Inertia matrix I and its time derivative $\dot{I}$ are:

$$I = \sum_{i=1}^{N} \delta m_i \begin{bmatrix} y_i^2 + z_i^2 & -x_i y_i & -x_i z_i \\ -x_i y_i & x_i^2 + z_i^2 & -y_i z_i \\ -x_i z_i & -y_i z_i & x_i^2 + y_i^2 \end{bmatrix} \qquad \dot{I} = \sum_{i=1}^{N} \delta m_i \begin{bmatrix} 2y_i\dot{y}_i + 2z_i\dot{z}_i & -\dot{x}_i y_i - x_i\dot{y}_i & -\dot{x}_i z_i - x_i\dot{z}_i \\ -\dot{x}_i y_i - x_i\dot{y}_i & 2x_i\dot{x}_i + 2z_i\dot{z}_i & -\dot{y}_i z_i - y_i\dot{z}_i \\ -\dot{x}_i z_i - x_i\dot{z}_i & -\dot{y}_i z_i - y_i\dot{z}_i & 2x_i\dot{x}_i + 2y_i\dot{y}_i \end{bmatrix}$$

3.2 Comparison with rigid body EoM

A comparison between the extended and the classical EoM is presented in this section. Two sets of EoM are referred to as set A and set B. Set A defines the classical EoM, which are as follows:

$$\begin{aligned}\vec{F} &= \dot{\vec{v}}_0 \sum_{i=1}^{N} \delta m_i + \vec{\omega}_0 \times \vec{v}_0 \sum_{i=1}^{N} \delta m_i \\ \vec{M} &= \vec{\omega}_0 \times (I\vec{\omega}_0) + I\dot{\vec{\omega}}_0\end{aligned}$$

Set B defines the extended EoM, which are as follows:

$$\vec{F} = \dot{\vec{v}}_0 \sum_{i=1}^{N} \delta m_i + \vec{\omega}_0 \times \vec{v}_0 \sum_{i=1}^{N} \delta m_i + \vec{\omega}_0 \times \left(\vec{\omega}_0 \times \sum_{i=1}^{N} \delta m_i \vec{r}_i \right) + \dot{\vec{\omega}}_0 \times \sum_{i=1}^{N} \delta m_i \vec{r}_i + \sum_{i=1}^{N} \delta m_i \ddot{\vec{r}}_i + 2\vec{\omega}_0 \times \sum_{i=1}^{N} \delta m_i \dot{\vec{r}}_i$$

$$\vec{M} = \sum_{i=1}^{N} \delta m_i \vec{r}_i \times \dot{\vec{v}}_0 + \sum_{i=1}^{N} \delta m_i \vec{r}_i \times (\vec{\omega}_0 \times \vec{v}_0) + \vec{\omega}_0 \times (I\vec{\omega}_0) + I\dot{\vec{\omega}}_0 + \sum_{i=1}^{N} \delta m_i \vec{r}_i \times \ddot{\vec{r}} + \dot{I}\vec{\omega}_0 + \vec{\omega}_0 \times \sum_{i=1}^{N} \delta m_i \left(\vec{r}_i \times \dot{\vec{r}}_i \right)$$

Both sets of equations were implemented in the CA^{2}LM framework (see Ch. 4) for their analysis. The comparison between EoM was carried out for flexible and rigid aircraft cases to identify the influence of additional terms.

Tested aircraft definition

The HARTEN aircraft, which is the test case here, will be fully defined later in Ch. 5. However, a brief definition of the HARTEN configuration is provided here.
Two test cases of HARTEN structural flexibility are defined for the EoM analysis:

1. Rigid aircraft, whose structural deflections are equal to zero. Zero structural flexibility was achieved by setting the CA^{2}LM simulation variable 'structural_feedback' to zero value, so that no structural deflections were propagated within the simulations.

2. Flexible aircraft, which exhibits wing flexibility with its Young's modulus of 8×10^9 Pa. The fuselage, horizontal (HTP) and vertical (VTP) tailplane rigidity was artificially increased by setting the Young's modulus to 6.89×10^{15} Pa.

Aircraft masses were distributed in such a way that the CG was situated at 20% MAC to represent a typical aircraft configuration.

Four cases in total were analysed, which were as follows:

1. Classical EoM applied to the rigid body.

2. Extended EoM applied to the rigid body.

3. Classical EoM applied to the flexible body.

4. Extended EoM applied to the flexible body.

The difference between 1 and 2 indicates the influence of terms, representing BAC offset from the CG. The difference between 3 and 4 indicates the influence of terms, representing both BAC offset from the CG and the structural flexibility impact as I and its time derivative, and $\vec{r}_i$ and its time derivatives are time dependent variables. It was expected that the difference between cases 1 and 2 should not have a significant impact

on the aircraft response, while the difference between cases 3 and 4 would significantly affect the body dynamics. Results of aircraft trim conditions and aircraft response to longitudinal and lateral/directional control inputs when the flight dynamics were governed by extended or classical EoM are presented in the following subsections.

3.2.1 Trim (static) results

The aircraft was trimmed for a level flight at 110 m/s velocity and 10000 ft altitude. The trim angles of attack α_{trim} for each case are shown in Table 3.1.

Table 3.1: Trim angles of attack for each test case

Case	1	2	3	4
α_{trim} [°]	3.87	3.85	5.41	5.31

As seen from the results above, higher angles of attack were determined when applying the classical EoM (cases 1 and 3). When considering the rigid body, the difference between the extended (case 2) and classical (case 1) EoM was around 0.5%. However, in case of the flexible body, the difference between the extended (case 4) and classical (case 3) EoM was around 1.9%. Hence, as expected, the difference between the static solutions using extended and classical EoM is very small. This finding also suggests that additional terms in the extended EoM, arising due to the body flexibility, should not be ignored in the future studies of highly flexible aircraft as they become more significant with the increase of structural flexibility[1]. The difference in α_{trim} arose due to the higher wing deformation for the flexible aircraft and, thus, higher required angle of attack to maintain the same lift. The explanation of the difference is elaborated later in the example given in Ch. 4.

This concludes the analysis of the classical and extended EoM for the static case, which suggests that the difference between sets A and B is very small. The next step is to investigate the difference of EoM for dynamic cases, which, it is believed, should suggest more significant differences between aircraft responses governed by the classical and extended EoM.

3.2.2 Dynamic response of aircraft

The control doublet input, shown in Figs. 3.2–3.4, was applied to the elevator, ailerons and rudder to investigate extended equations' effect on longitudinal and lateral/directional dynamics of the aircraft. The response of both rigid and flexible aircraft cases is shown also in Figs. 3.2–3.4. It was chosen to compare angular accelerations $d\vec{\omega}/dt$, as they are one of primary solutions of the equations of motion and define a change of the body's attitude in space.

[1]The example of flexible aircraft provided in the case study here is hardly realistic at the moment of writing this thesis. However, the author believes that as the aircraft structural flexibility (especially one of the wings) will continue to increase, this case study suggests the significance of using the extended EoM.

The aircraft response to the elevator doublet input is shown in Fig. 3.2. It is clear from both rigid and flexible aircraft cases that longitudinal dynamics are affected very little by the wing's flexibility as long as the fuselage is relatively rigid. Important to emphasize here is the fact that the classical EoM does not capture exactly the same dynamics as the extended EoM. Moreover, they damp the response much heavier and makes it lag versus the extended EoM.

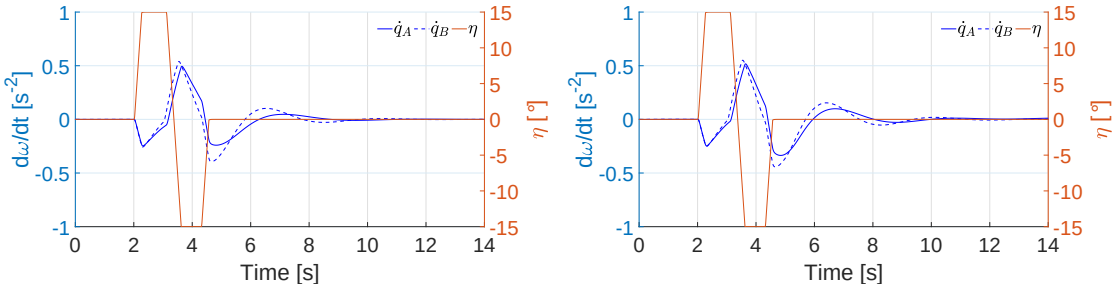

(a) Rigid (b) Flexible

Figure 3.2: Comparison of EoM sets A and B for rigid and flexible body cases during pitch doublet disturbance

Figure 3.3 presents the aircraft response to the ailerons doublet input. For this lateral perturbation both A and B sets of EoM follow the same dynamics and magnitudes for the rigid case. However, for the flexible case dynamics are followed, but the magnitudes of oscillations differ. The roll acceleration is underpredicted by up to 51.4% for the classical EoM versus the extended EoM, as seen in subfigure 3.3(b). Hence, the main finding here is the inability of classical EoM to capture the peaks of the oscillations.

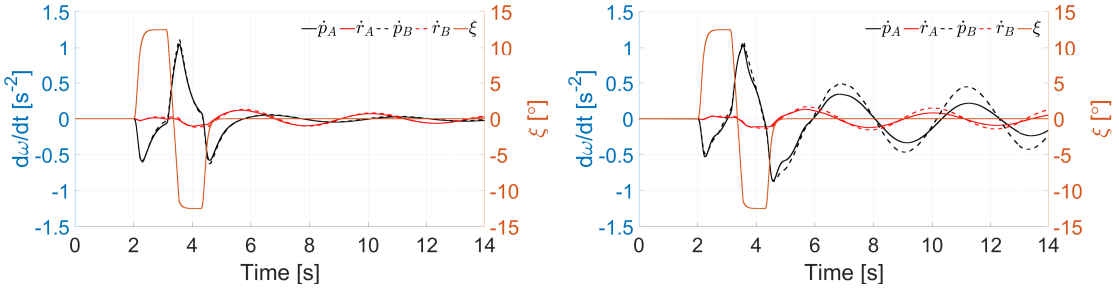

(a) Rigid (b) Flexible

Figure 3.3: Comparison of EoM sets A and B for rigid and flexible body cases during aileron doublet disturbance

Finally, Fig. 3.4 presents the aircraft response to the rudder doublet input. This input

is used to induce the Dutch roll mode, thus it covers both lateral and directional dynamics. Again, the main difference is observed for the flexible aircraft case in capturing the peaks of the oscillations. The ignorance of the flexibility terms in the classical equations leads to higher damping when compared to the extended equations.

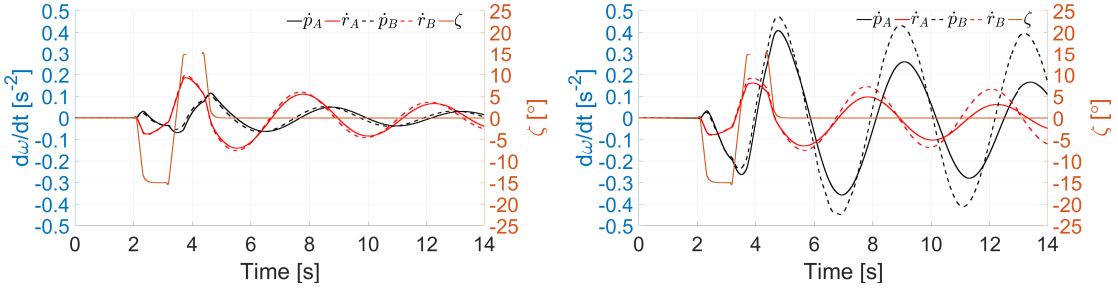

(a) Rigid

(b) Flexible

Figure 3.4: Comparison of EoM sets A and B for rigid and flexible body cases during rudder doublet disturbance

3.3 Summary of the chapter

The development of the extended EoM for flexible bodies has shown that new terms arise due to the body's structural motion in time. The comparison between the classical EoM and the extended EoM was carried out for rigid and flexible aircraft cases to identify the most significant terms of the extended EoM. Comparing trim results showed that for the static flight conditions both sets of EoM predicts similar trim angles of attack. However, the error between the α_{trim} results acquired using the classical and extended EoM increased with increased aircraft flexibility, thus showing the significance of using the extended EoM. Nevertheless, the difference was very small - around 1.9% for the most flexible aircraft case. The longitudinal response showed that terms due to the assumption of the different CG and BAC positions made the largest difference. However, in lateral/directional dynamics these terms were less significant, while the terms due to body's flexibility were of higher significance. It can be concluded that both the classical and extended EoM captured the similar dynamics. However, the classical EoM did not capture the peaks of the oscillations and showed an increased damping for the flexible aircraft case. These observations suggest that the extended EoM should be used when modelling flexible aircraft and flexibility effects should not be ignored as they tend to affect the dynamics of flexible aircraft significantly.

Chapter 4

Flight simulation framework

This chapter introduces the newly developed Simulation Framework for Flexible Aircraft (SFFA). As the framework is based on previously developed simulation tools - the MATLAB/Simulink based CA^{2}LM framework and the C++ based EFS500 real-time flight simulator - they must be thoroughly investigated to discover the most appropriate integration process and limitations of each of them. Thus, the CA^{2}LM framework is firstly reviewed - its aerodynamic and structural dynamic models, upgrades and new developments of the framework are discussed. Then the EFS500 flight simulator is reviewed - its current architecture and state of both software and hardware are discussed. The integration of CA^{2}LM and EFS500, using the Speedgoat real-time target machine, is presented at the end of the chapter along with the a priori known limitations of the new framework.

4.1 CA^{2}LM – MATLAB/Simulink based flight physics framework

CA^{2}LM is the flight physics framework for modelling of flexible aircraft configurations. It consists of the following components/models:

- the Modified Strip Theory (MST) based aerodynamic model;
- the linear structural dynamic model;
- the equations of motion for a flexible body;
- the environment model.

All of them are shown in Fig. 4.1 and discussed in detail in this section.

4.1.1 Aerodynamics of the wing, horizontal and vertical tailplanes

Aerodynamics of the wing, HTP and VTP are modelled using the MST and the Leishman unsteady aerodynamic model. Such a modelling approach combines capability of the

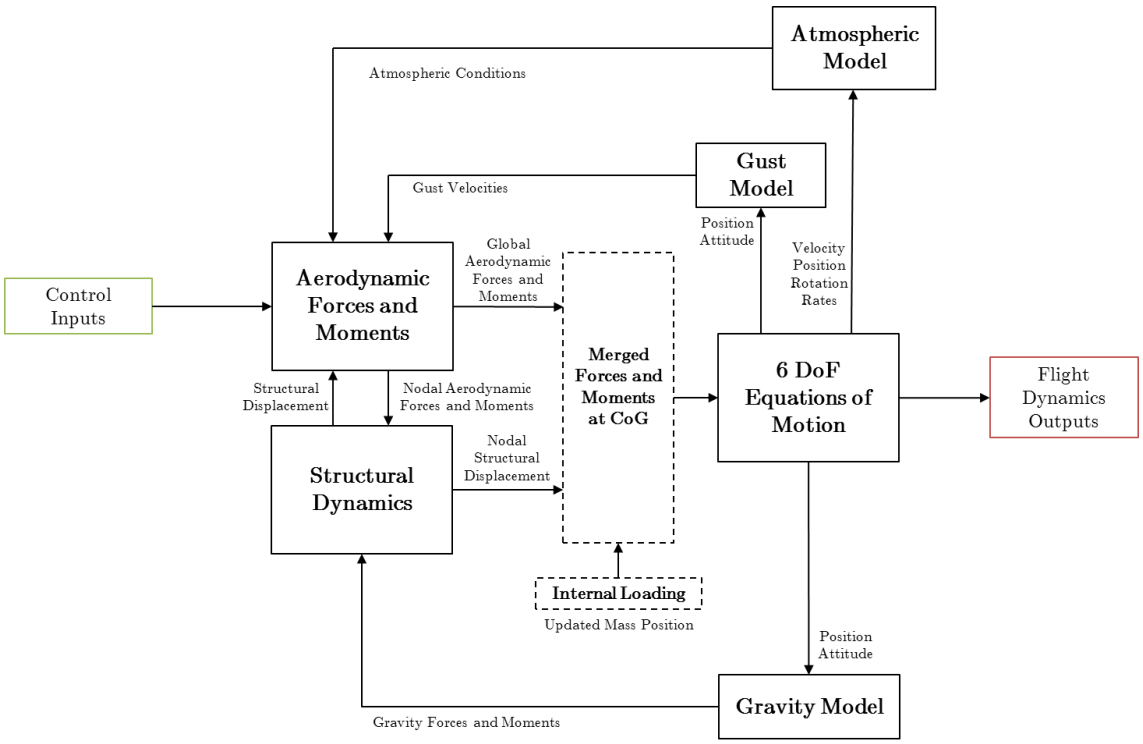

Figure 4.1: Structural representation of the CA^{2}LM framework

real-time pilot-in-the-loop simulations, while allowing to capture the aerodynamic effects necessary for the aeroservoelastic analysis of an aircraft [12, 110, 111]. The modelling of aerodynamics is further detailed in Fig. 4.2.

The Leishman unsteady aerodynamic model [112–114] is applied in the state-space form [115]:

$$\begin{aligned} \dot{x} &= A\mathbf{x} + B\mathbf{u} \\ y &= C\mathbf{x} + D\mathbf{u} \end{aligned} \tag{4.1}$$

The matrices A, B, C and D are shown in App. A. The state vector $\mathbf{x}$ and input vector $\mathbf{u}$ are of the following form:

$$\begin{aligned} \mathbf{x} &= [x_1 \;\; x_2 \;\; x_3 \;\; \ldots \;\; x_n]^T \\ \mathbf{u} &= [u_1 \;\; u_2 \;\; u_3 \;\; u_4]^T \end{aligned} \tag{4.2}$$

Each aerodynamic node has a 15 element state vector $\mathbf{x}$ associated with it that takes into account circulatory and non-circulatory terms. An input vector $\mathbf{u}$ consists of the angles of attack α at each aerodynamic node, their rates of change $\dot{\alpha}$, angles of control surfaces ξ, η, ζ and their angular rates $\dot{\xi}$, $\dot{\eta}$, $\dot{\zeta}$ [12, 116]. The framework currently uses 58 (35 - wing, 15 - HTP, 8 - VTP) aerodynamic nodes for unsteady aerodynamics. This results in 870 unsteady aerodynamic states.

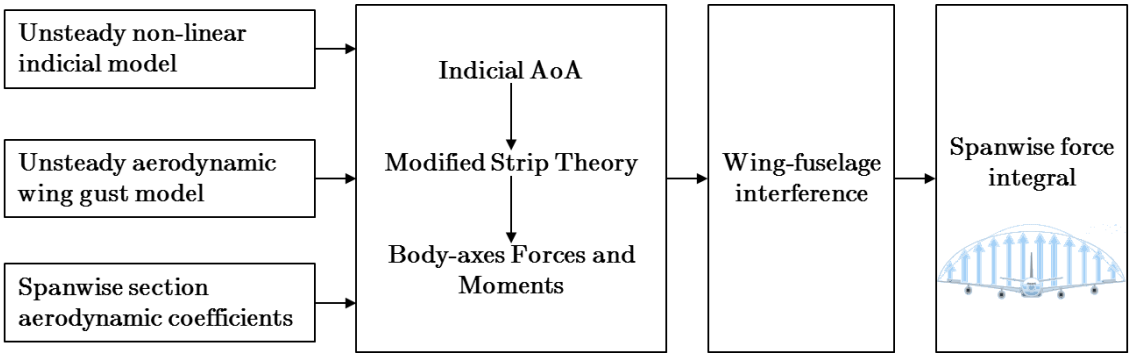

Figure 4.2: Aerodynamic model of the wing, HTP and VTP

The unsteady aerodynamic model is based on the Theodorsen and Wagner functions. The Theodorsen function [117] is used to model harmonic aerofoil oscillation [12]. The Wagner function [118] models aerodynamic forces due to a step change in incidence [12]. As the Wagner function is only applicable to incompressible flow, Leishman applied the Prandtl-Glauert correction factor to account for the compressibility effect [114]. The unsteady wind gusts are modelled as the Kussner function [119]. As in the case of the Wagner function, the Kussner function applies only to incompressible flow. However, Leishman proposed an approximation as a function of Mach number [120]. The resulting angles of attack due to the unsteady aerodynamics and the unsteady gust are then summed up to form the indicial angle of attack α_{ind}.

The steady aerodynamic coefficients are calculated from the pre-computed look up tables. The viscous drag coefficient, α_0, drag and pitching moment coefficients at α_0 along with α_{ind} are then acquired. To take into account 3D effects, an indicial angle of attack (α_{ind}) is added to the steady state angle of attack (α) and an effective angle of attack (α_{eff}) is calculated:

$$\alpha_{eff} = \alpha + \alpha_{ind} \tag{4.3}$$

Applying the resulting angle of attack to MST allows the calculation of forces, moments and downwash circulation on a user defined wing planform [121, 122]. Even though the original MST assumes the chordwise rather than the spanwise flow [123], the spanwise variation of the wing loading in the CA^{2}LM framework is accounted for by applying the correction factor to the given local lift-curve slope [12, 122].

The MST approach allows the calculation of forces acting on aerodynamic surfaces in the wind axis system. These are then transferred into the body axis system via the application of the following direction cosine matrix (DCM):

$$DCM = \begin{bmatrix} \cos\theta_i \cos\lambda_i & \cos\lambda_i \sin\theta_i \sin\gamma_i - \sin\lambda_i \cos\gamma_i & \cos\lambda_i \sin\theta_i \cos\gamma_i + \sin\lambda_i \sin\gamma_i \\ \cos\theta_i \sin\lambda_i & \sin\gamma_i \sin\theta_i \sin\lambda_i + \cos\gamma_i \cos\lambda_i & \sin\lambda_i \sin\theta_i \cos\gamma_i - \cos\lambda_i \sin\gamma_i \\ -\sin\theta_i & \cos\theta_i \sin\gamma_i & \cos\gamma_i \cos\theta_i \end{bmatrix} \tag{4.4}$$

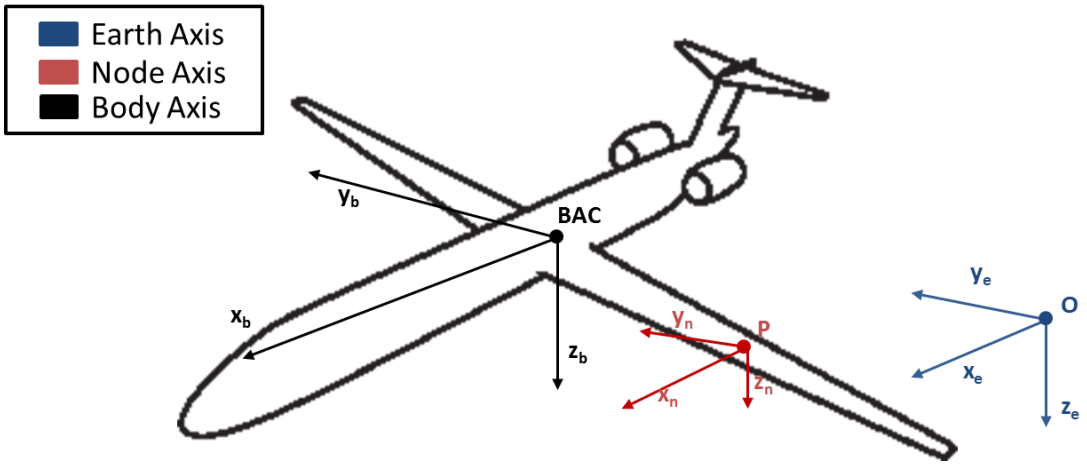

Figure 4.3: Axes systems used in the CA^{2}LM framework

where θ_i is the local twist angle and includes local angle of attack α_i, λ_i is the local sweep angle and includes local sideslip angle β_i and γ_i is the local dihedral angle. The various axes systems used in the model are shown in Fig. 4.3.

The aerodynamic model also estimates the wing downwash effect on the tailplane. Downwash circulation strength (Γ) is given by [12]:

$$\Gamma = sV\mathbf{A}(\alpha_{ind} - \alpha_{C_L=0}) \tag{4.5}$$

where s is the span of a wing, V is the velocity, $\mathbf{A}$ is the coefficients matrix for the MST approach and $\alpha_{C_L=0}$ is zero lift angle of attack. Circulation is then evaluated through a reduced order state-space model to get the indicial angle of attack for the tailplane. This implementation of the MST approach and unsteady aerodynamics provided a satisfactory balance between computational accuracy and cost [12].

Aerofoils used to model aerodynamic surfaces

To model the aerodynamics of the wing, HTP and VTP, two aerofoils are used:

- cambered NASA SC(2)-0610 aerofoil for the wing;
- symmetrical NASA SC(2)-0010 aerofoil for the HTP and VTP.

The use of supercritical aerofoils allows the framework to be used at high subsonic Mach numbers. To better understand the limitations of the CA^{2}LM framework, it is important to define the range of angles of attack at which the framework is valid. Thus, it was defined in Ref. [116] that the CA^{2}LM framework, previously known as AX-1, is valid between Mach 0.05 and 0.8 for angles of attack from $-10°$ to $+15°$. However, extra care should be taken when considering higher limits of Mach number as the Prandtl-Glauert correction factor is usually considered valid up to around Mach 0.7 [124] and relatively

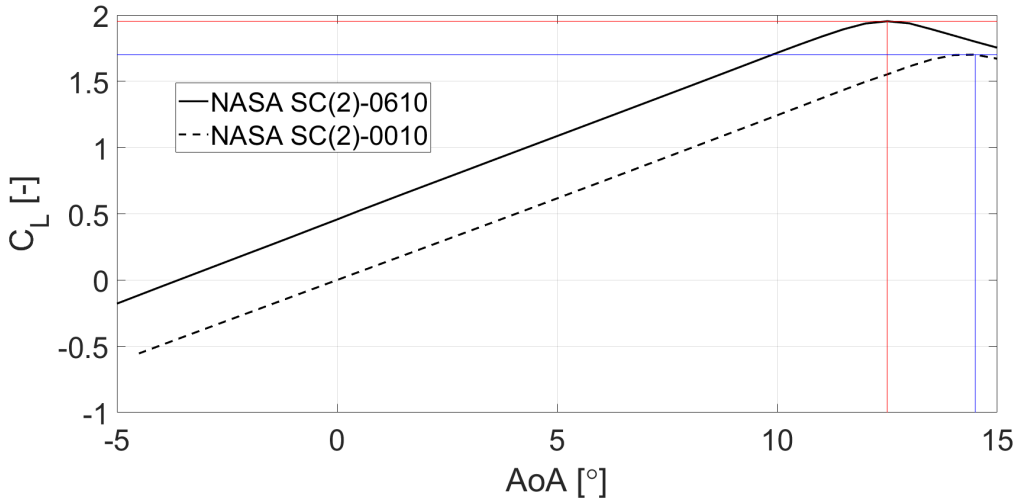

Figure 4.4: Stall angles of attack for NASA SC(2)-0010/0610 aerofoils

low angles of attack [125]. The range of AoA is important to know due to the fact that the aerodynamic stall model is absent and, as a consequence, the aircraft would not stall even above the limit AoA. Hence, by knowing the range of valid AoA allows to consider only reliable data.

To define the stall angle of attack at the particular condition that was used for the further flight test campaign, both aerofoils were analysed using the XFOIL program [126, 127], which was developed to design and analyse subsonic isolated aerofoils. The XFOIL was used as an integrated aerodynamic solver of the XFLR5 software package.

$C_L(\alpha)$ polars of both aerofoils are presented in Fig. 4.4. It is clear from the figure that the stall AoA for the NASA SC(2)-0610 aerofoil is around 12.5°. Analysis was done for $M = 0.3$ and $Re = 30 \times 10^6$ flight conditions, which represent flight conditions during the testing campaign. This being the lowest stall angle of both aerofoils, it should be considered as a limiting AoA for the validity of simulations, i.e. all flight conditions with $\alpha > 12.5°$ should be disregarded.

Note: The stall angles of attack calculated by the means of the XFOIL program for particular 2D aerofoils are for the illustrative purpose only. Thus, it was considered that the 2D aerofoil data from the main lifting surface is enough and no efforts were made to develop and analyse an overall aircraft model for the stall AoA. The assessment of the overall aircraft model by using high fidelity tools would give a reasonable indication of the potential stall AoA. However, this goal was out of scope for the current thesis.

4.1.2 Aerodynamics of the fuselage and nacelles

Aerodynamics of the fuselage and nacelles are modelled following the ESDU methodology based on empirical test data [128–131].

For small aeroplanes (e.g. Airbus A320 or Boeing 737) their fuselage can be modelled as a rigid body. However, for large aeroplanes (e.g. Airbus A340) the fuselage is long and slender and flexibility effects become more expressed. As the previous research on long slender aircraft [9, 11, 13] showed, the longitudinal fuselage flexibility changes characteristics of the flight dynamics and affects a pilot's perception of an aircraft handling qualities. Hence, the fuselage flexibility is modelled too to have a fully capable framework to model flexible aircraft. Thus, its aerodynamic model includes appropriate changes due to flexibility [12].

The fuselage was divided into fore and aft parts to model the flexibility effect. The forebody of the fuselage is modelled as a slender axi-symmetric body of revolution according to Refs. [130, 131] and the normal force coefficient is calculated as follows:

$$C_N = C_{N\alpha} \sin\alpha \cos\alpha + \frac{4}{\pi}\frac{L}{D} C_{PL} C_{Nc} \tag{4.6}$$

where $C_{N\alpha}$ is the normal force slope at zero angle of attack from Ref. [130], C_{PL} - geometric coefficient from Ref. [132] and C_{Nc} - cross-flow normal force coefficient as a function of Mach number and angle of attack from Ref. [131]. The aftbody of the fuselage is modelled again as a slender axi-symmetric body of revolution according to Ref. [129] and the change in normal force is calculated as follows:

$$\Delta C_N = \Delta C_{N\alpha} \sin\alpha \cos\alpha \left(1 - \sin^{0.6}\alpha\right) + \Delta C_{Dc} \sin^2\alpha \tag{4.7}$$

where $\Delta C_{N\alpha}$ is the inviscid contribution, ΔC_{Dc} - viscous cross-flow contribution. Flexibility is considered via changes in angles of attack and sideslip for the forebody and aftbody due to respective deformations as shown in Fig. 4.5.

Engine dynamics are modelled by a simple first order system:

$$\frac{T_P}{T_{P_\tau}} = \frac{T_{P_{max}}}{1 + \tau_P s} \tag{4.8}$$

where $T_{P_{max}}$ and τ_P are the maximum thrust and engine time constant and T_{P_τ} is the throttle setting.

Nacelles are modelled as annular aerofoils according to [128] to calculate the aerodynamic forces and moments. The lift force of each nacelle is expressed as follows:

$$L_n = qwl(a_n)_w \alpha_n \tag{4.9}$$

where q is dynamic pressure, w - width of the nacelle, l - length of the nacelle, $(a_n)_w$ - lift-curve slope of the nacelle and α_n - angle of attack of the nacelle. The same procedure is applied to calculate the sideslip angle β_n and the side force of the nacelle.

Forces and moments from the aerodynamic surfaces, fuselage and engines are calculated and concentrated at the aerodynamic nodes in the CA^{2}LM framework. However,

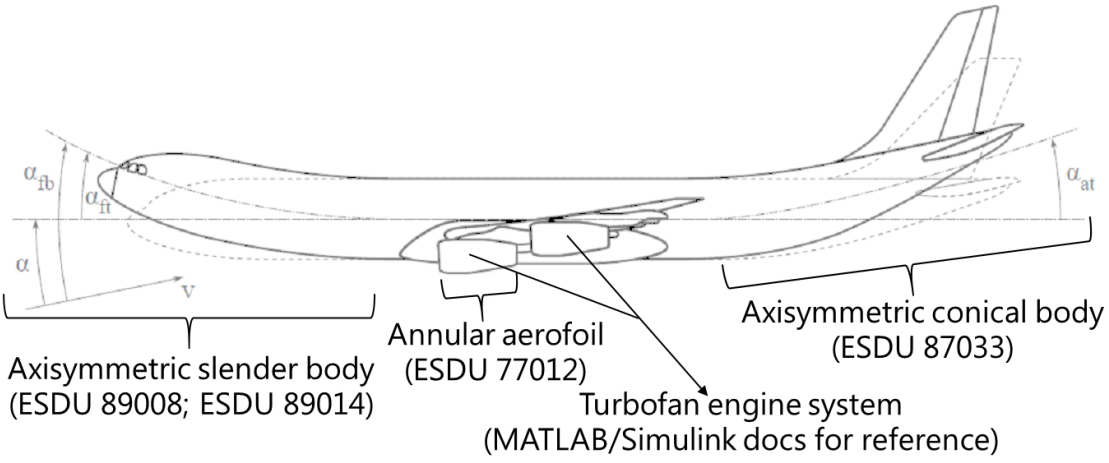

Figure 4.5: Sources of flexible fuselage and engine nacelle modelling methods (reproduced from Ref. [12])

forces and moments for the structural dynamics calculations are evaluated at the structural nodes. Therefore, the forces and moments from the aerodynamic frame must be transferred to the structural frame. On the other hand, structural deflections have to be transferred from the structural frame to the aerodynamic frame to account for the flexibility contribution to aerodynamic forces and moments. This transfer of forces and moments between aerodynamic and structural frames is carried out by a 1-D interpolation between aerodynamic and structural nodes. Higher order interpolation schemes may be applied in the future as the wings will become more flexible and their models will be more discretised to achieve higher simulation accuracy. However, their viability to provide more accurate real-time calculations should be investigated considering their potential of being applied.

One could ask for the reason for different numbers of aerodynamic and structural nodes. As it has been shown in Ref. [12] the amount of aerodynamic nodes is optimal at around 35 nodes per wingspan. However, the amount of structural nodes differs for different aircraft models and providers of them. Hence, it is more convenient to have independent frames and to interpolate loads and deflections between different frames rather than change the amount of nodes for different models. Moreover, too many nodes has its own drawback of too high computational cost. Thus, a high number of structural nodes does not mean a high number of aerodynamic nodes or vice versa. Both aerodynamic and structural frames are shown in Fig. 4.6.

4.1.3 Structural dynamics

Once the aerodynamic loading has been transferred to the structural frame, airframe deformations can be calculated. The structural dynamics in the CA^{2}LM framework are

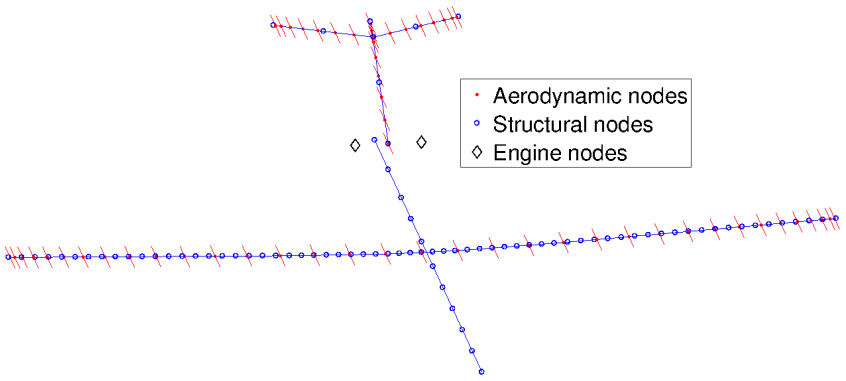

Figure 4.6: Aerodynamic and structural frames in the CA^{2}LM framework

modelled in the modal form, which means that the overall deformation of the structure depends on the sum of modeshapes. Thus, aerodynamic forces and moments F_{aero} are firstly converted into modal forces F_i using the resulting modeshape matrix (Θ_m):

$$F_i = \Theta_m^T F_{aero} \tag{4.10}$$

Then, the structural equation of motion is applied to solve for modal accelerations ($\ddot{x}$), velocities ($\dot{x}$) and displacements (x):

$$\ddot{x}_i = \frac{F_i}{m_i} - 2\zeta_i \omega_{n_i} \dot{x}_i - \omega_{n_i}^2 x_i \tag{4.11}$$

where m_i is the modal mass, ω_{n_i} is the modal natural frequency, ζ_i is the modal damping ratio and i represents the mode of interest.

Finally, the transition from the modal domain to structural domain is done to get the structural deformations. Linear and angular deformations at each node are obtained by solving the following equations:

$$\begin{aligned} d &= \Theta_m x \\ \dot{d} &= \Theta_m \dot{x} \\ \ddot{d} &= \Theta_m \ddot{x} \end{aligned} \tag{4.12}$$

This is the implementation of the linear structural dynamics model. Widely accepted opinion states that wingtip deflections of less than 10% of semi-span can be treated as linear deformations. Thus, the CA^{2}LM framework is valid for small deformations. However, large wing deformations are of interest in this research. Hence, one could argue that such a structural dynamics model is invalid for modelling large deformations as a nonlinear structural model should be used. Nonetheless, Patil and Hodges showed in Ref. [45] that the linear structural model predicts deformations with the same accuracy as the nonlinear structural model for the static case. For dynamic loading case the linear structural model

could not capture same dynamics of the structure as the nonlinear one. Due to this limitation current version of the CA^{2}LM framework should be used only for investigations of low frequency phenomena that consider pilot-structure interaction.

Another important point to notice is that out-of-plane bending, in-plane bending and torsion of each structural node are modelled within the CA^{2}LM framework. However, the experience of the pilot-in-the-loop simulations has shown that both in-plane bending and torsion of the most deformed aircraft component, i.e. the wing, are of negligible magnitude and insignificantly affect flying and handling qualities of flexible aircraft.

The modeshape data are essential for the analysis due to the way the framework is programmed. Thus, the modal data in the CA^{2}LM framework are generated by an external structural solver – NASTRAN. The modal data are computed by the use of the NASTRAN 103 modal solver. Modal frequencies, modal masses and the modeshape matrix are the outputs from the solver.

The CA^{2}LM framework considers only the first 12 flexible modes as it aims to analyse flight dynamics phenomena that typically have low frequencies. The modeshape matrix is independent of time for the relatively rigid aeroplane models currently implemented in the framework. It is important to notice that only small deflections are modelled for such aircraft. Hence, it is assumed that the properties of each beam vary linearly. However, recent developments in highly flexible HALE-like aircraft have introduced wingtip deflections of more than 25% of the wing semi-span. Static deflections of highly flexible wings can still be modelled correctly using the linear theory as it was published in Ref. [45]. Nevertheless, for the future implementations of highly flexible aeroplanes nonlinear approach to model structural deformations should be considered.

4.1.4 Environment and gravity models

The gravitational constant is calculated according to WGS-84 model [133] and applied to calculate forces and moments at the CG position for solving equations of motion. Additionally it is applied to calculate forces and moments of each structural node to solve the structural equation of motion. The following equation is used to calculate the gravitational constant:

$$g = g_e \frac{1 + k sin^2\phi}{\sqrt{1 - e^2 sin^2\phi}} \tag{4.13}$$

where $k = \frac{b g_p}{a g_e} - 1$, a and b - semi-major and semi-minor axes of the ellipsoid, g_e and g_p - theoretical gravity at the equator and poles, e - the first ellipsoidal eccentricity, ϕ - geodetic latitude. Then the gravity above the ellipsoid g_h is calculated by

$$g_h = g \left[1 - \frac{2}{a} \left(1 + f + m - 2 f sin^2\phi \right) h + \frac{3}{a^2} h^2 \right] \tag{4.14}$$

where $m = \frac{\omega^2 a^2 b}{GM}$, ω - angular velocity of the Earth, GM - Earth's gravitational constant, f - ellipsoidal flattening, h - geodetic height.

Atmospheric properties such as air density and temperature are modelled as International Standard Atmosphere (ISA) properties following the methodology provided in Ref. [134].

4.1.5 Equations of motion

Equations of motion are a vital part of the framework as they equate the forces and moments to motion variables. However, the traditional equations of motion for a rigid body should be changed with the ones for a flexible body. The development of equations of motion for a flexible aircraft is discussed in Ch. 3.

4.1.6 The use of the CA^{2}LM framework

Having the aerodynamic and structural models reviewed, the example of applying the CA^{2}LM framework to solve real problems is provided below.

Example

Capabilities of the CA^{2}LM framework are presented in this example. The first example focuses on handling qualities analysis following the Gibson Dropback criterion (as published in Ref. [135]). The second example demonstrates the capability of performing failure case assessments (as published in Ref. [136]). Both studies are based on the AX-1 model which is representative of a large transport aircraft.

The AX-1 model

The aircraft model, to which the testing was previously done, is the AX-1 model. It represents a large transport aircraft with relatively rigid wing. The model with its specifications is shown in Fig. 4.7. To analyse the structural flexibility effect on handling qualities of the aircraft, three cases were considered:

1. Original stiffness of the wing K.
2. 15% lower stiffness of the wing $K - 15\%$.
3. 30% lower stiffness of the wing $K - 30\%$.

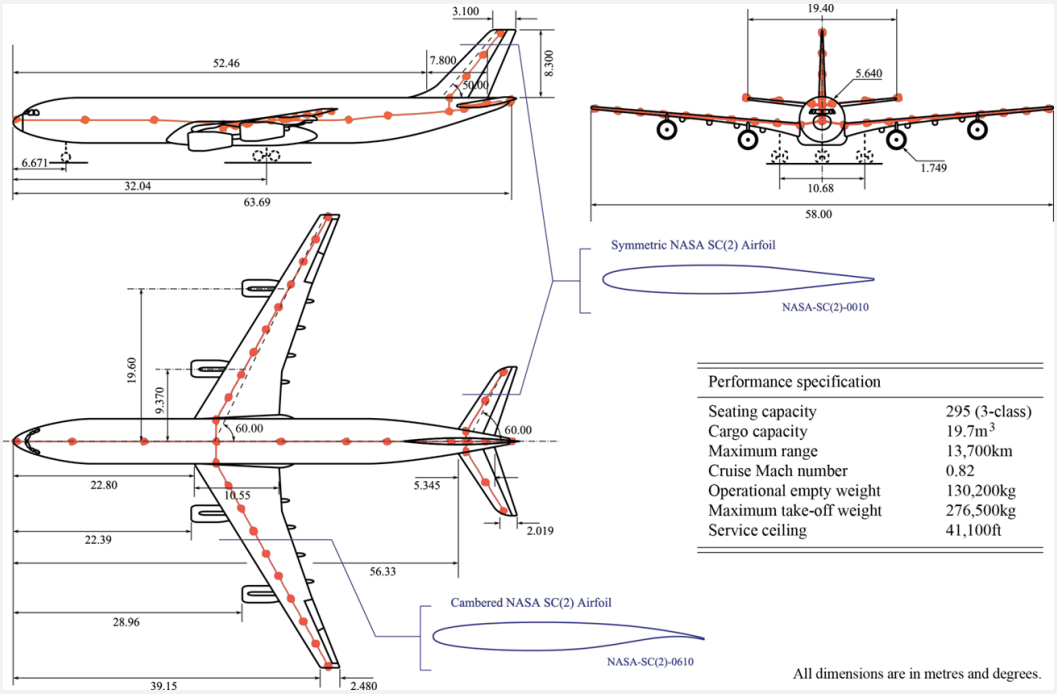

Figure 4.7: The AX-1 aircraft model and its main specifications (reproduced from Ref. [135])

Time domain handling qualities analysis

For this study, the AX-1 model was trimmed at an altitude of 10,000 ft and the DB criterion was evaluated at several airspeeds and airframe stiffnesses. As the AX-1 airframe is relatively stiff, it was decided to reduce the stiffness by 15% and 30%. The assessment was carried out by specifying a five second elevator pulse input of 5°. Figure 4.8 shows the variation of longitudinal handling qualities with varying airspeed and structural stiffness. It should be noted that no stability augmentation system has been implemented and consequently the majority of the cases are not in the satisfactory region.

The trends observed in Fig. 4.8 can be explained by considering the effects arising due to the deformation of a flexible wing in comparison with a stiffer tailplane. In comparison to a rigid wing, a wing with lower stiffness deforms more significantly due to change in angle of attack caused by the elevator deflection. This deformation leads to a loss in overall wing lift due to a reduction in effective wingspan and results in a relatively higher pitching moment contribution from the tailplane. Therefore, the difference between the aircraft's maximum pitch attitude and the steady state attitude increases as wing stiffness is reduced. Hence, there is an increase in *DB* as structural stiffness is reduced. No significant effects were observed

for q_{max}.
Time histories of minimum, maximum and inflection points in Fig. 4.8 are plotted in App. B. This is the input data for the Gibson DB criterion analysis. The response of flexible configurations shows that a steady state after the elevator input is not reached after a considerable amount of time. This observation might lead to a conclusion that the Gibson DB criterion should not be used for handling qualities analysis with complex models containing nonlinear structural deflections.

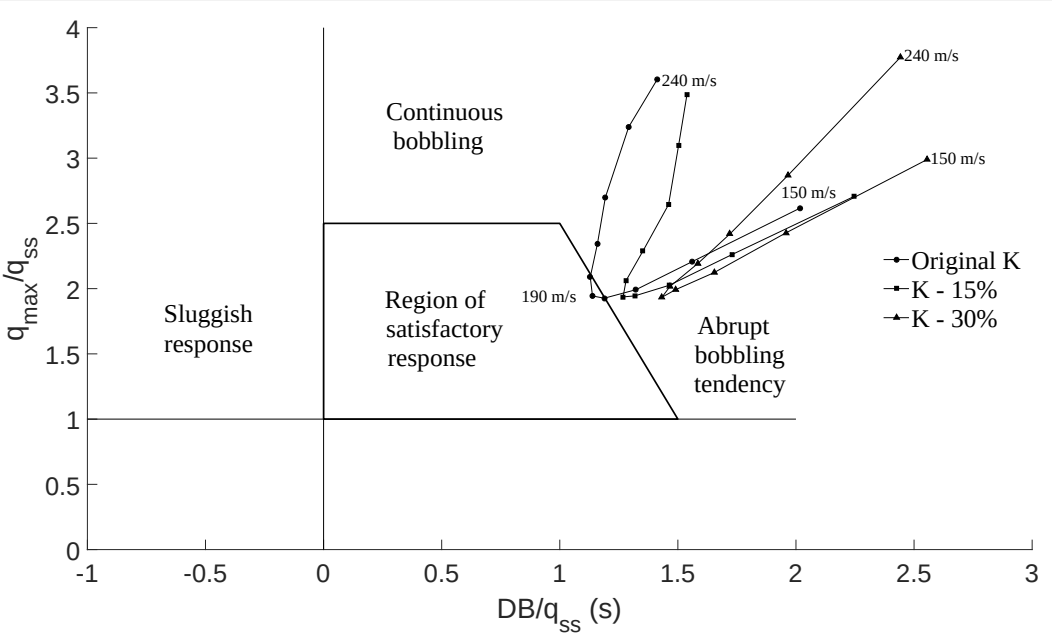

Figure 4.8: Effect of airspeed on the longitudinal HQs of AX-1 model

Aileron soft failure simulation

A control surface failure scenario is one of many extreme cases that need to be considered for flight loads evaluation. Here a soft aileron failure is simulated where the port aileron actuator fails whilst the starboard aileron remains at the original trim setting. The main results obtained from the simulation are shown in Fig. 4.9. The port aileron is forced to undergo a limit cycle oscillation at a constant frequency of 1.16 Hz, which corresponds to the first wing structural bending mode. The amplitude of this oscillation is set to $\pm 15^{\circ}$.
The frequency content of the roll rate and yaw rate signals show that the failure has excited a low frequency lateral-directional mode corresponding to periods of $Tp = 10.24$ s and $Tr = 10.92$ s in roll and yaw respectively. These correspond to the usual frequencies of the aircrafts Dutch roll mode. The load factor n_g only exhibits large transients when the aileron failure is initiated.

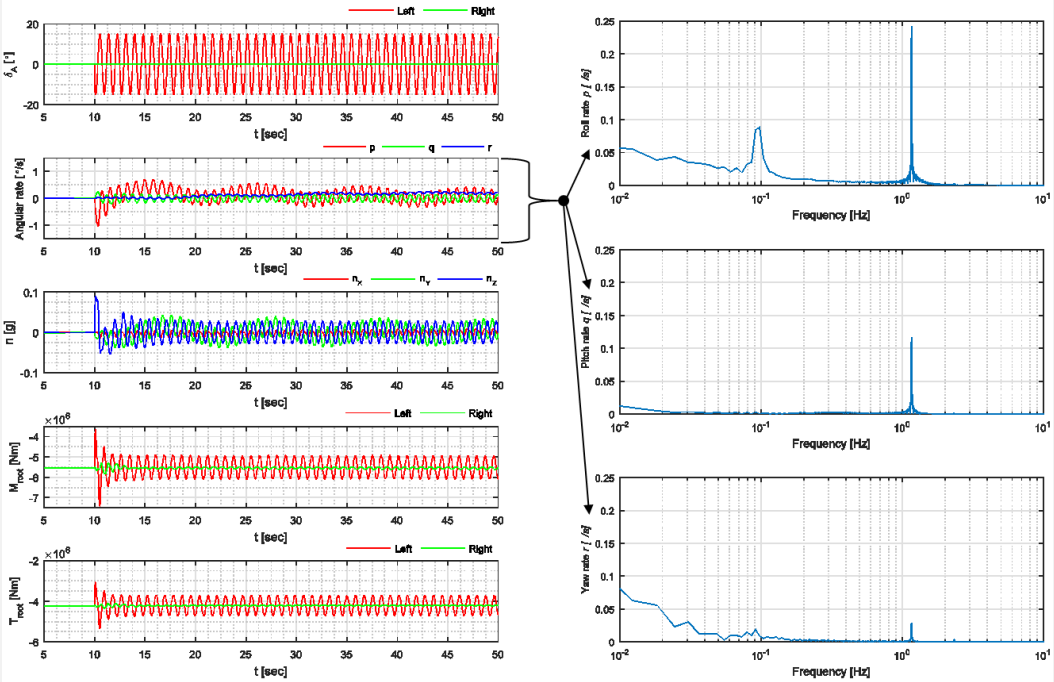

Figure 4.9: Ailerons deflection ξ, angular rate, load factor n, wing root bending moment M_{root} and wing root torsion T_{root} and roll, pitch and yaw rates at aileron excitation frequency of 1.1634 Hz

Figure 4.10 shows the frequency content of the wing root bending moment M_{root} at different aileron excitation frequencies. At a frequency of 1.245 Hz, slightly higher than the frequency of the first structural mode of the wing (1.1634 Hz), the first aeroelastic mode appears and a resulting resonance is observed. Upon magnification (bottom right subfigure) another two peaks can be observed at 2.5 Hz and 3 Hz. These correspond to aeroelastic modes associated with wing flexible modes numbers 5 and 11. At the frequency of 0.9 Hz M_{root} is higher than at the frequency of 1.1 Hz, which can be explained by the fact that the forcing function frequency is getting closer to rigid body frequencies.

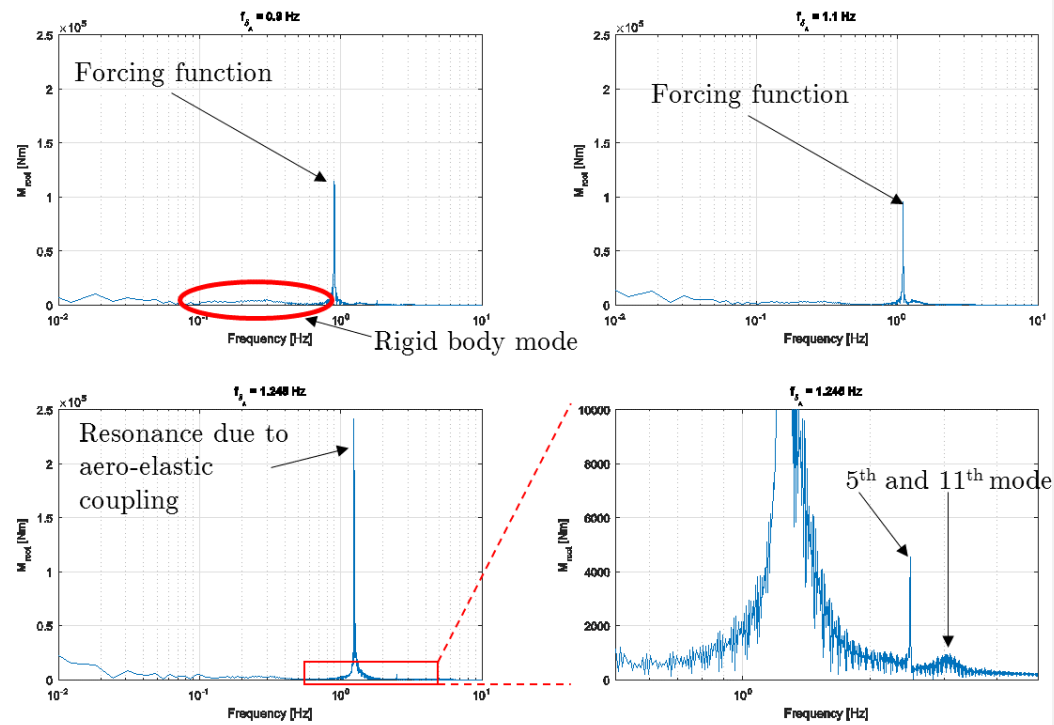

Figure 4.10: Wing root bending moment M_{root} at different aileron excitation frequencies

The main advantage of the CA^{2}LM framework is its suitability for the real-time pilot-in-the-loop simulations. This will be discussed later, after the EFS500 flight simulator and CA^{2}LM integration with EFS500 will be reviewed. However, the CA^{2}LM framework can be fully utilised to simulate and analyse an aircraft without the pilot as control inputs can be defined by the user. Such a case is presented and discussed in the example above.

4.1.7 Upgrades to the CA^{2}LM framework

A wide range of possible applications of CA^{2}LM is a significant advantage of this framework. However, one of the biggest limitations of the framework was the difficulty to implement new aircraft configurations. Due to its Simulink blocks based architecture, the framework had many stages of layers ('sub-systems' in Simulink terminology) with many 'hard-coded' values. Thus, any change in the size of the structural model led to a complex process of changing many variables in numerous different places. Hence, it was decided to change the Simulink blocks based architecture into Simulink functions based architecture, which allowed to significantly reduce the number of layers from 14 to 3. Moreover, this conversion allowed to condense equations into scripts instead of having each term of an equation as a separate Simulink block. The change of the 'hard-coded' variables into variables, which are initialised in the very beginning before running the

Simulink model, allows to rapidly implement new aircraft configurations. These changes cleared the framework and made it easier to modify, especially when implementing new aircraft models.

Another significant modification to the CA^{2}LM framework was development of the new trim routine. Any testing of aircraft usually starts from an aircraft being in an equilibrium (*or* trim) state. Thus, a set of control parameters, defining the trim state of an aircraft, has to be found. The trim routine was based on the MATLAB in-built 'trim' function in the previous version of the framework. However, being a purely mathematical operation, it used to solve the trim problem with some control settings, which being mathematically correct sometimes were physically unrealistic, e.g. engine throttle setting of 110%, while the obvious maximum value is 100%. The main cause for this was the function's sensitivity to initial conditions, which were set by the user. Thus, a more manageable trim routine was developed to overcome the issue.

The new trim routine, developed for the CA^{2}LM framework and shown in Fig. 4.11, overcomes the issue by setting the maximum limits for the range of control settings. Moreover, it does not require precise initial control settings. As it is based on multiple iterations of the simulation with different control settings, it provides a realistic set of controls without precise initial conditions as minimum and maximum inputs are used during the first loop. The new trim routine is as follows:

1. Initial conditions are set for all aircraft controls to zero values. Only the throttle control variable is assigned with some "reasonable" number to provide a flight condition.

2. Three control variables are then varied in a loop. The model is run for a period of time for forces and moments to become stable[1] for each setting of a variable. When the forces and moments become stable, their values are recorded and the next setting is applied to the model. Control variables, which are changed during the trimming process, are:

   tailplane setting i_H;

   throttle setting τ;

   rudder setting ζ.

3. When forces and/or moments for each setting of a control variable have been recorded, each control variable is then interpolated against the governing force or moment to be zero. These forces and moments are:

   vertical force Z for i_H;

   longitudinal force X for τ;

[1] Due to aeroelastic coupling and unsteady aerodynamics it takes a certain amount of time for a steady loading and deformation of the structure to establish. The amount of time depends on the structural flexibility and flight conditions.

yawing moment N for ζ.

It is then assumed that with the defined control setting an aircraft would be in an equilibrium state regarding corresponding forces or moments.

4. In current implementation only three parameters, i.e. Z, X and N, are taken into consideration when trimming an aircraft. The ailerons are not considered as aircraft, modelled within the CA^{2}LM framework, are usually symmetrical. However, omitting three parameters, i.e. Y, L and M, from the trimming procedure introduces errors when considering an equilibrium flight. Thus, the procedure is then repeated six times to minimize the error between the resulting force or moment value and its zero value.

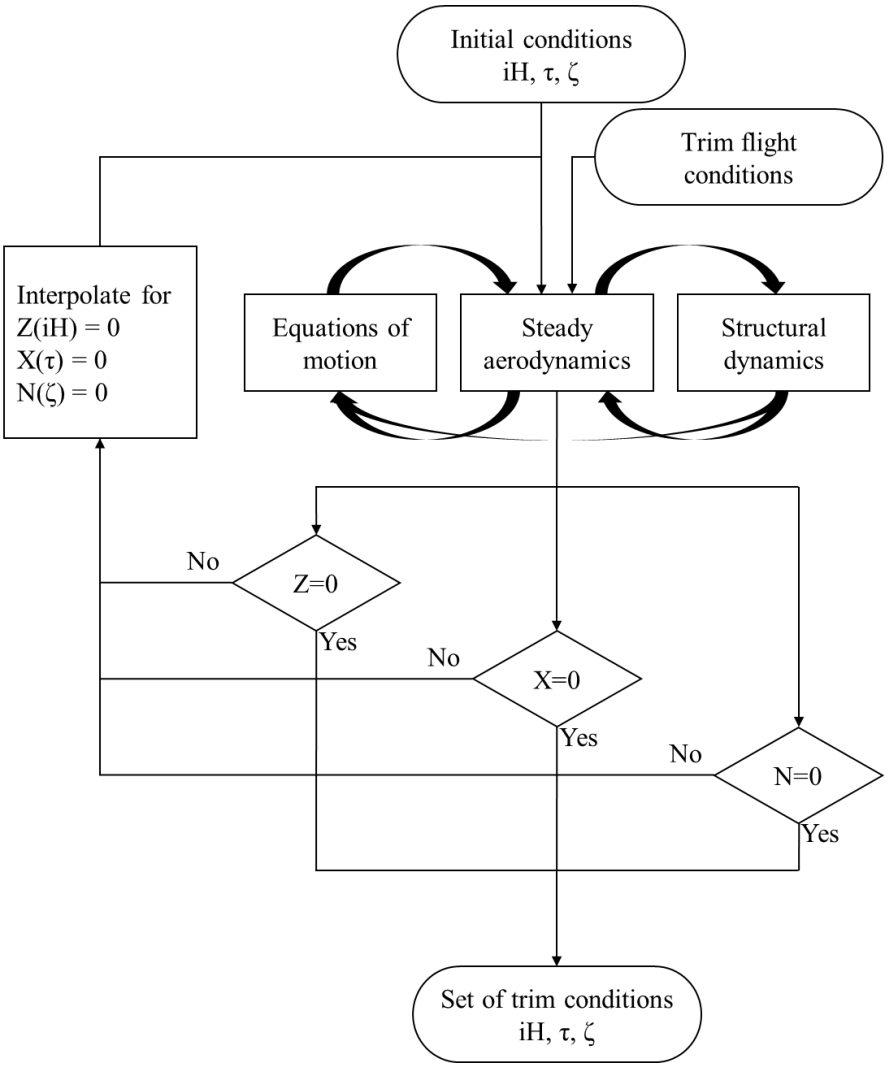

Figure 4.11: New trim routine of the CA^{2}LM framework

4.1.8 Limitations of the CA^{2}LM framework

Even though certain steps, discussed above, were taken to overcome the limitations of the CA^{2}LM framework, there are still many of them. The major ones are:

1. Absence of the aerodynamic stall model, which obliges the user to disregard results for flight conditions when the angle of attack is above 12.5°.

2. Linear structural model, which prevents the user from investigating flexibility effect on flight dynamics in high frequency dynamic events.

Despite these limitations the ultimate goal is to integrate the CA^{2}LM framework with the EFS500 flight simulator hardware to provide the environment for the pilot-in-the-loop testing capability. Hence, the next section provides an overview of the EFS500 flight simulator.

4.2 EFS500 flight simulator

The target simulator for the integration of the CA^{2}LM framework is the engineering flight simulator EFS500. The EFS500 provides a platform for the pilot to interface with the CA^{2}LM framework and constitutes another important part of a new simulation framework. It is an engineering flight simulator designed to demonstrate aircraft stability and control along with aircraft performance in real time, which is achieved by:

1. Modelling only the rigid body dynamics excluding any structural dynamics.

2. Aerodynamic and flight dynamic coefficients being modelled by simple empirical formulations.

Its hardware architecture and software are presented in the following subsections.

4.2.1 Hardware

The EFS500 simulator comprises the following elements [137]:

- *Cockpit environment*, which provides a generic single seat cockpit layout with a central stick, sidestick, rudder pedals and throttle lever. The flap selector, gear switch and other additional switches are also included in the cockpit, which is shown in Fig. 4.12.

- *Artificial loading system*, which allows force feedback response to the central stick and rudder pedals.

- *Computer system*, which consists of eight computers that provide flight dynamics model, cockpit displays, avionics, instructor operating station and image generation capability.

- *Sound generation system*, which generates environmental and warning sounds.
- *Image generation system*, which is comprises three projectors and a spherical screen, which provides a field of view of $140^\circ \times 40^\circ$ as shown in Fig. 4.13.

Computers in the simulator are connected into a segregated Ethernet network and communicate broadcasting information from each node sequentially. The communication sequence is controlled by the I/O system node operating at a frequency of 50Hz. The overall system architecture is shown in Fig. 4.14.

Each of the eight computers performs the following tasks:

1. The I/O system computer is based on a Raspberry Pi system to interface between the control inputs of the simulator hardware (i.e. control stick, right-hand stick, pedals, throttle) and the computer system. It has 32 analogue/digital input channels and four analogue/digital output channels. Moreover, this computer synchronises the computer system to broadcast packets of data at a frequency of 50 Hz.

2. The flight dynamics computer provides equations of motion, an aerodynamic model, engine models, flight control laws, dynamics of targets and the weather model. Moreover, it renders the primary flight display (PFD) as seen in Fig. 4.15(a).

3. The navigation and avionics computer computes navigation equations for the aircraft sensors, manages radio and flight control unit (FCU) panels and generates aircraft sounds. Moreover, it renders the electronic horizontal situation indicator (EHSI) as seen in Fig. 4.15(b).

4. The instructor operating station provides an interface of commanding different flight conditions and data recording via the touch screen GUI. It provides a capability of rapid repositioning of an aircraft on the map, plots simulator output data, allows failures of different aircraft systems, controls autopilot and flight plan.

5-7. The image generation (IG) computers are equipped with high performance nVidia graphics cards. They provide an OpenFlight visual database and render it in response to the data received from other computers, i.e. aircraft position, its attitude, weather conditions, time of day. Moreover, the head-up display may be displayed by IG computers.

8. The MATLAB computer provides an interface for the rapid implementation and testing of control laws.

All computers are connected into a local network by the 16-channel Ethernet switch. As the flight dynamics software runs at 50 Hz, so every other computer has to run at the same frequency. It is very important not to exceed 20 ms frame time when performing computations, thus the time margin is included in each computer.

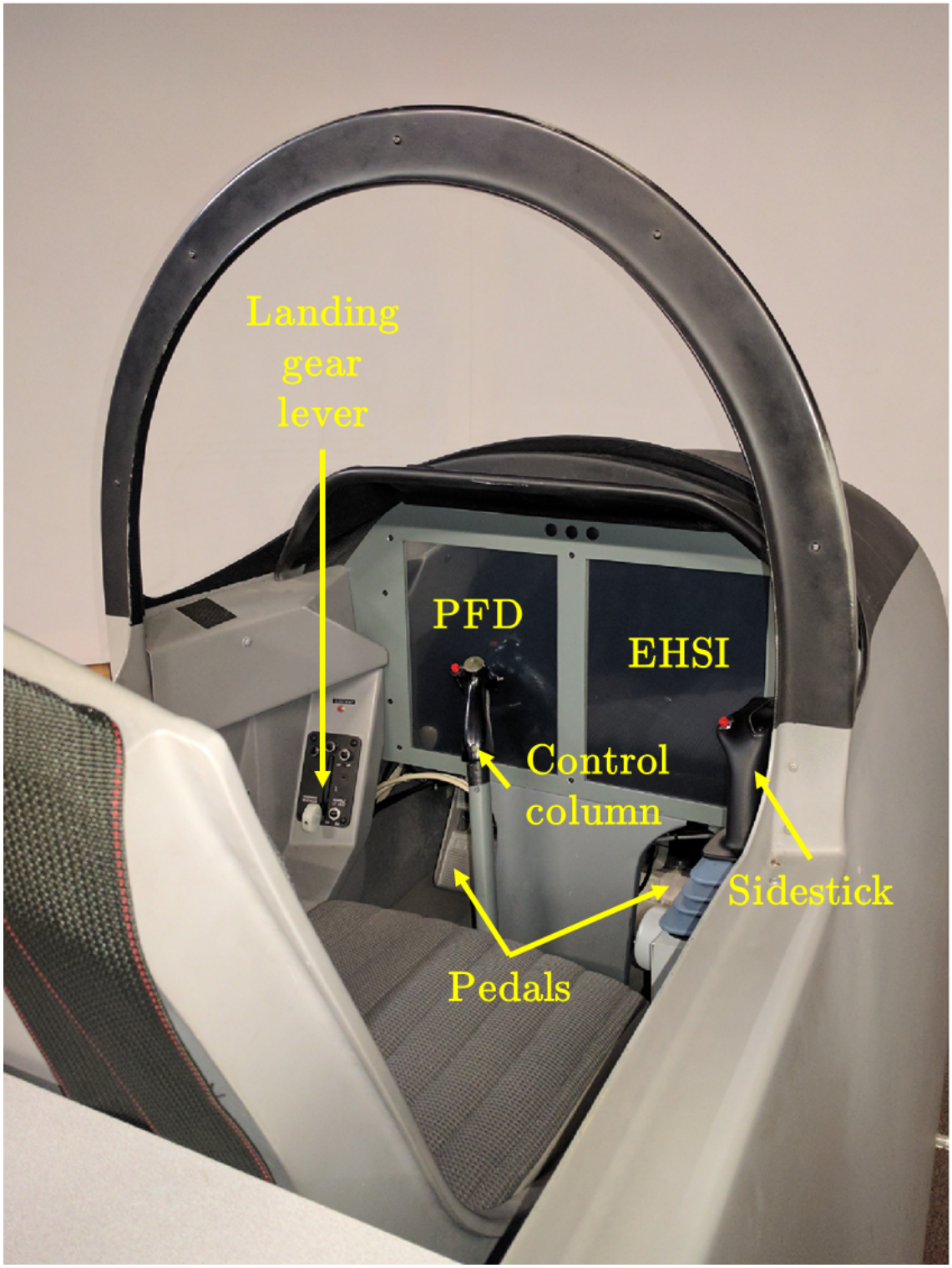

Figure 4.12: Cockpit environment of the EFS500 flight simulator

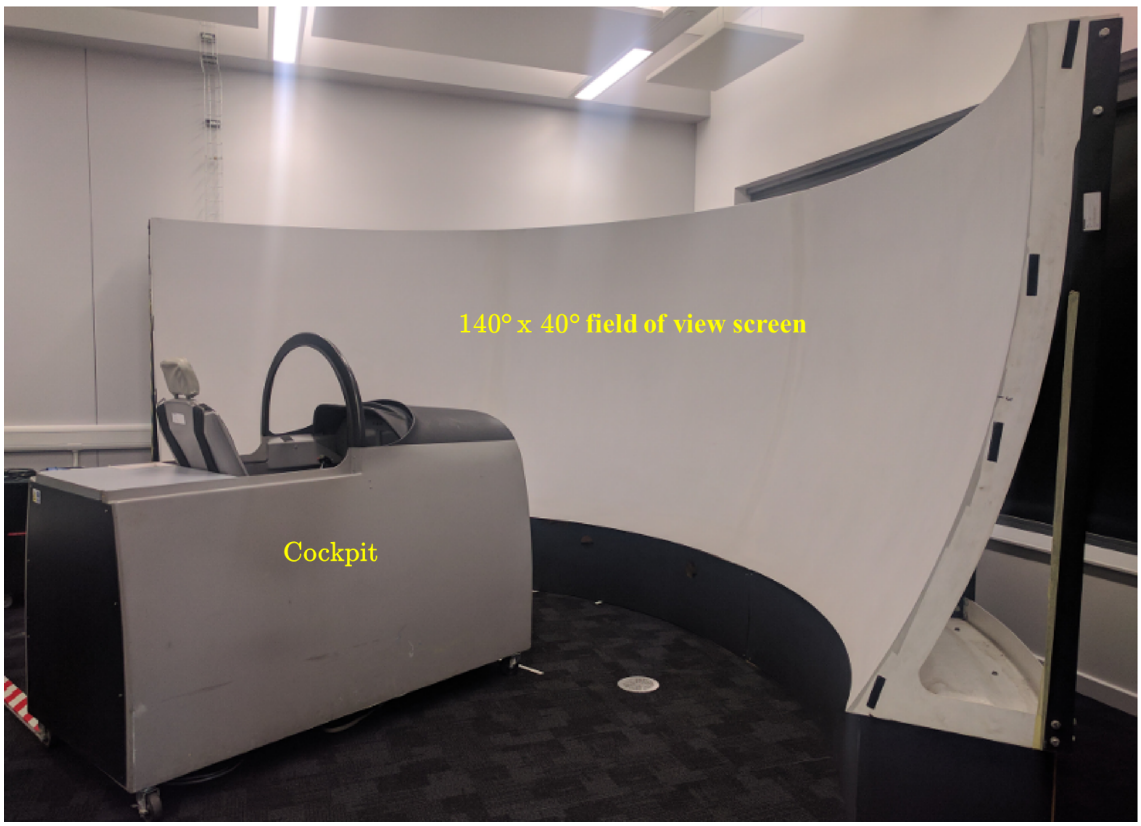

Figure 4.13: Overall setup of the EFS500 flight simulator

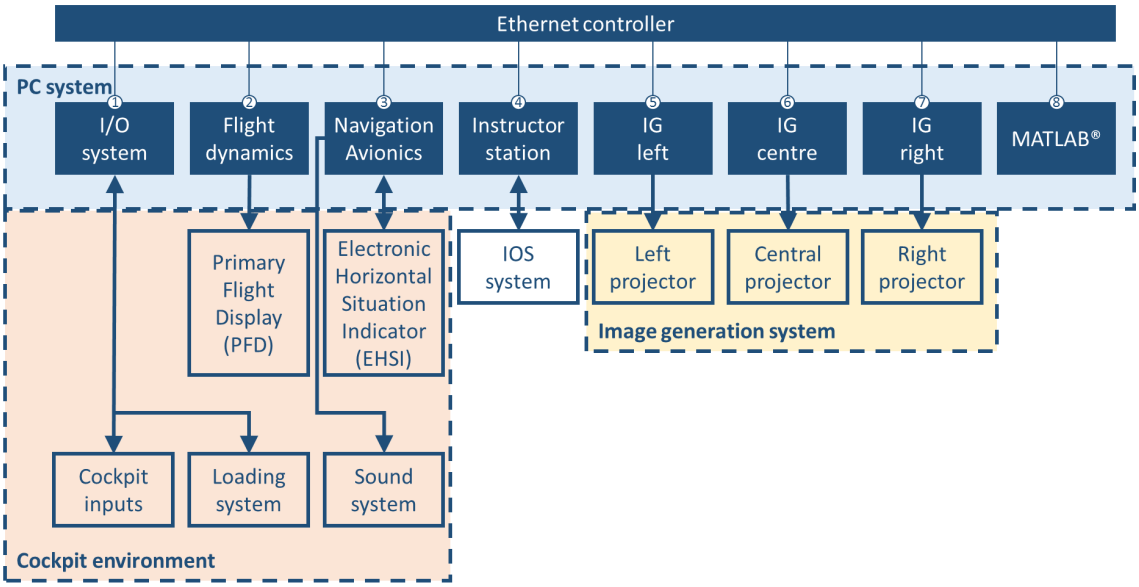

Figure 4.14: EFS500 simulator network (reproduced from Ref. [138])

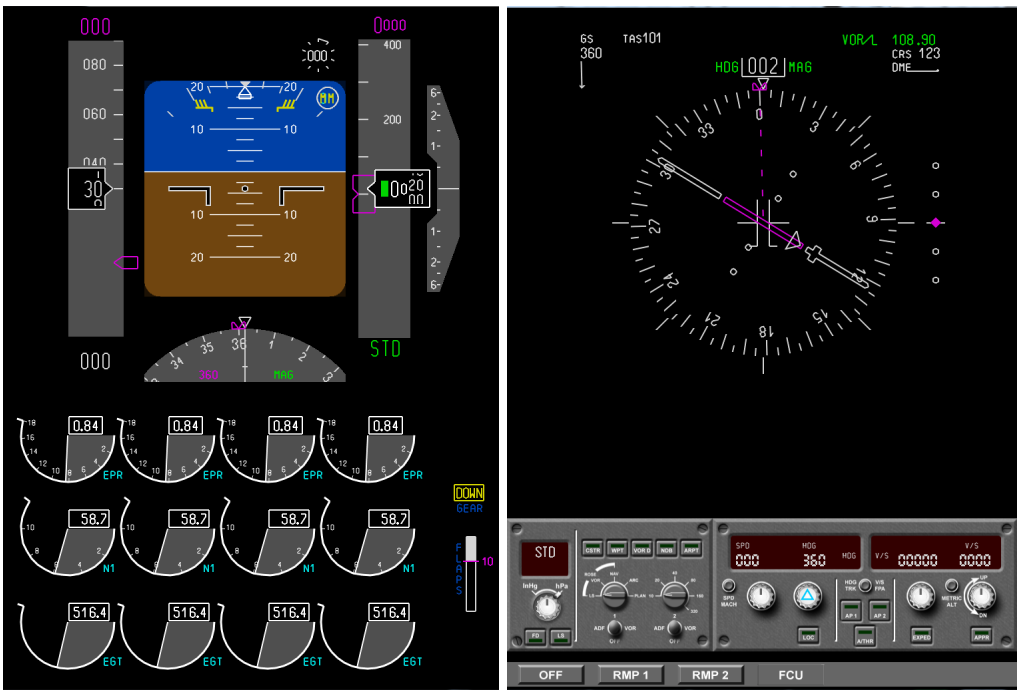

(a) PFD (b) EHSI

Figure 4.15: PFD and EHSI displays in EFS500 flight simulator cockpit

4.2.2 Software

The simulator runs custom coded software developed mostly in the C programming language. The code is distributed within the computers, allowing rapid modifications of the code and recompilation of the applications. Although most of simulator's software is written in the C programming language, image generation computers use the C++ programming language to interface with the OpenSceneGraph graphics library. All the nodes use the 'gcc' compiler for both C and C++ applications.

The simulator software is intended to be as modular as possible and the modification of the aircraft model only affects particular nodes. Details of each node function are presented in Table 4.1. Some of the nodes, like the instructor operating station, the I/O system or the image generation node, are not affected by changes in the aircraft model.

Only one application is executed per node as part of the original network design of the simulator. The flight dynamics computer (Node 2) process flow is shown in Fig. 4.16.

It is important to notice that the application is idle while the network data is being transferred. This architecture of the process flow relies on the network transaction time, which is supposed to be notably smaller than the total available slot time, i.e. less than 20 ms. In case smaller time steps or higher number of nodes in the architecture are required,

Table 4.1: Computer node function and aircraft model dependency

Node	Name	Function	A/C dependent
1	I/O system	Acquires data from cockpit and enables load system	No
2	Flight dynamics	Computes flight dynamics and renders PFD	Yes
3	Navigation & avionics	Computes avionics and renders EHSI	Yes
4	Instructor station	Runs instructor software enabling simulation control	No
5	IG left	Renders left area of the 3D environment	No
6	IG centre	Renders central area of the 3D environment	No
7	IG right	Renders right area of the 3D environment	No
8	MATLAB	Rapid implementation and testing of flight control laws	N/A

the time spent in network transactions may significantly reduce the time available for calculations.

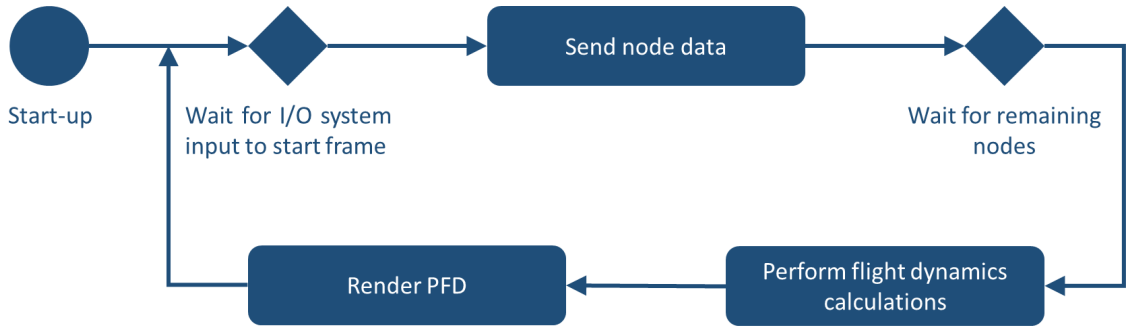

Figure 4.16: Flight dynamics computer (Node 2) process flow

Knowing the details of the EFS500 flight simulator allows the integration of the CA^{2}LM framework with the simulator. The CA^{2}LM framework is slower than the real time, thus it needs some means to be sped-up. The speedgoat real-time machine is used for that purpose, which is discussed in the next section.

4.3 Integration of the CA^{2}LM framework with the EFS500

To allow the interaction between the CA^{2}LM framework, developed in MATLAB/Simulink environment, and the EFS500 flight simulator, developed in C/C++ programming lan-

guages, both architectures must be compatible. There are two main areas that need to be compatible between the CA^{2}LM framework and the EFS500 flight simulator:

1. *Timing*, as both systems need to run in real time in order to perform the pilot-in-the-loop simulations. The EFS500 flight simulator is running in real time by default, but the CA^{2}LM framework is much slower than the real time. To increase the simulation speed, the Speedgoat real-time target machine is used.

2. *Data interfaces*, as the information exchange between the two systems must be compatible. The Simulink Real-Time software needs to be capable of sending enough information for the EFS500 flight simulator to work, while the simulator should feed the the real-time device with the expected control inputs.

The simulation timing requirement imposes the need for the CA^{2}LM framework to run in real time. At the current level of implemented aircraft model complexity, the CA^{2}LM framework is capable of performing 100 iterations per second on a standard i7-4770 desktop computer. Considering that the time step used in the framework is 0.001 s (1000 Hz), the CA^{2}LM framework needs to be sped-up by a factor of 10. In order to obtain the required performance improvement, it was decided to use the Speedgoat real-time target machine, whose specifications are presented in Table 4.2.

Table 4.2: Speedgoat real-time target machine specifications

Element	Model
CPU	Intel i7-6700K
RAM	8192MB
Storage	60GB SSD
Ethernet	2 + 1 Gigabit
OS	FreeDOS / Simulink Real-Time kernel

The implementation of the CA^{2}LM framework in the Speedgoat device required some changes in the model. Firstly, the data interface between the EFS500 and the CA^{2}LM framework needed to be compatible and compliant with the real-time requirement. An option would be to synchronise both systems, with the CA^{2}LM framework executing the simulation time step when the simulator network has finished the data transaction. As the CA^{2}LM framework, with the current aircraft model implemented, executed the simulation at 1000 Hz and the EFS500 ran at 50 Hz, a synchronised system was not suitable. It was decided to use an asynchronous system instead, with both the simulator system and the CA^{2}LM framework running freely and exchanging information asynchronously. The aeroservoelastic framework integration is therefore independent of its simulation frequency.

Since the PFD computer was originally responsible for flight dynamics calculations, it was decided that it will also be responsible for interfacing with the CA^{2}LM framework (see Fig. 4.17). The primary data interface to the Speedgoat real-time machine is

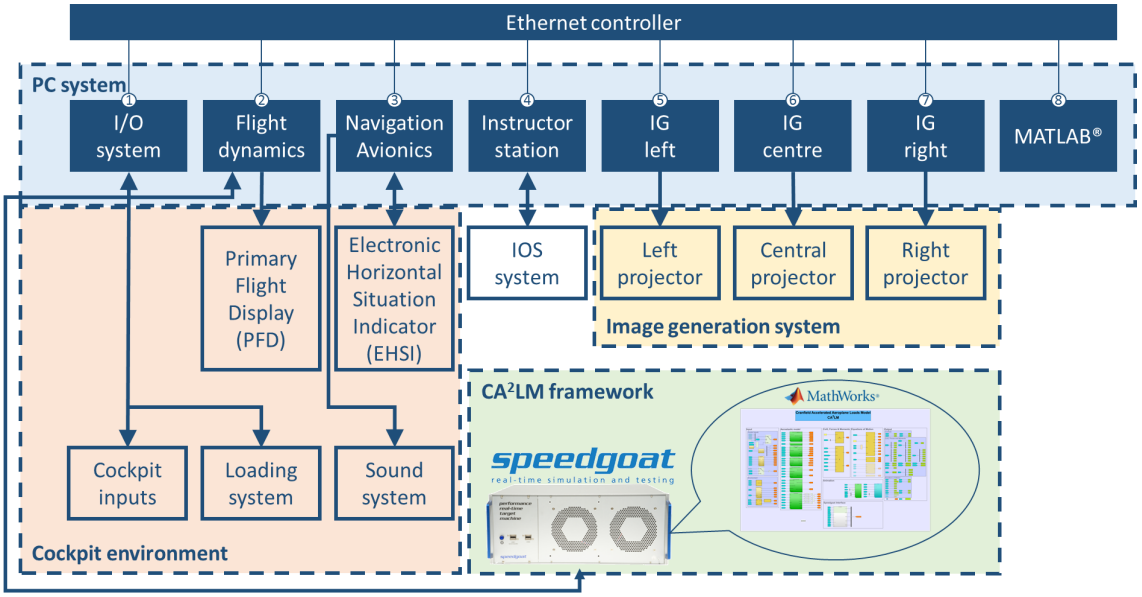

Figure 4.17: EFS500 simulator network with the Speedgoat real-time machine

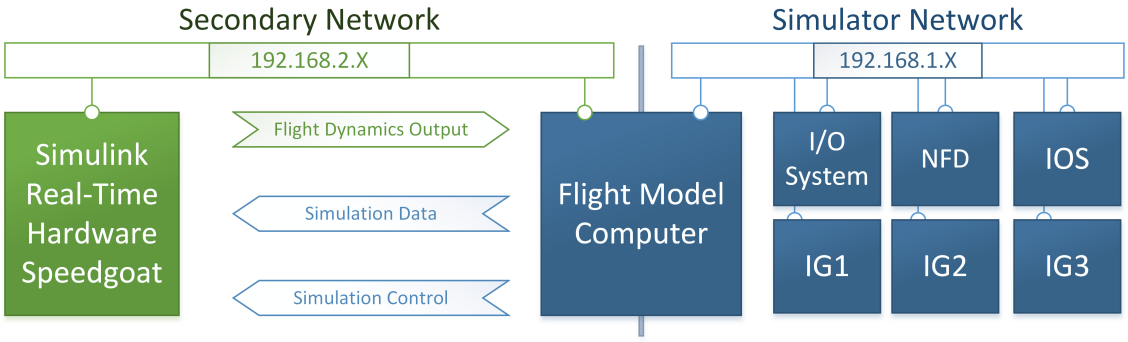

Figure 4.18: Interface between the PFD computer and the Speedgoat real-time machine

the Ethernet port. The architecture of the EFS500 network requires that no other data, except for the simulation data, is sent using the simulator network. Therefore, communication between the PFD computer and the real-time machine is done using a secondary Ethernet network independent of the main simulator network. The resultant architecture, presented in Fig. 4.18, comprises two separate networks with the PFD computer acting as the gateway between them. To allow this architecture, a secondary Ethernet port has been installed in the PFD computer.

Communication in the secondary network uses user datagram protocol (UDP) packets. In order to enable full control of the simulation, three packets have been defined:

- *Flight dynamics output packet*, which is used for the Speedgoat machine to send the most recent set of computed data to the flight model computer. This contains

position, attitude, translational and angular velocities of an aircraft along with flight conditions data. The information could be potentially sent at 1000 Hz, but it is sub-sampled and sent at 50 Hz, matching the frequency of the EFS500 simulator.

- *Simulation data packet*, which contains the simulation information that is generated in other simulator nodes. It includes control status, simulation status and ground altitude, which is computed in the Node 2 computer.

- *Simulation control packet*, which contains simulation modifiers, such as simulation start/stop flag, aircraft repositioning flag or simulation restore flag.

UDP interfaces in the real-time machine and the PFD computer are configured as non-blocking, always using the most recent value to allow systems to run asynchronously.

The Speedgoat real-time target machine requires the CA^{2}LM framework to be loaded into the target machine at each simulation. Two changes to the CA^{2}LM framework have been made to allow the compilation of the framework for the real-time target machine. The changes are following:

1. *Disabling (or 'commenting out' in MATLAB/Simulink terminology) Level-2 S-Functions*, which are used to generate visualisation of the airframe flight and structural dynamics during the simulation. Level-2 S-Functions can be compiled into real-time machines as long as C or Fortran code is provided, but the visualisation code within the CA^{2}LM framework is not available in those languages. Since the visualisation functions are redundant for the real-time simulations, the functions are simply disabled when targeting the Speedgoat real-time machine.

2. *Break of algebraic loops*, which introduce issues additionally to the previously discussed ones. Simulink is capable of solving algebraic loops in a discretised model when running in normal mode, but they need to be removed before compiling the model for a real-time machine. Algebraic loops can also slow down the simulation. Hence, the 'unit delay' blocks were added to break algebraic loops.

After making these modifications and specifying the required configuration in the 'Model Configuration Dialogue' window, the model is compiled and loaded into the real-time device. The report from the device indicates that the computation time for each time step is 0.7 ms, or approximately 70% of the available time. Hence, as the model runs in real time it can be integrated into the EFS500 simulator.

To comply with the UDP interface, Speedgoat real-time machine network configuration blocks were added along with the following 3 UDP interfaces:

- *UDP receiver for simulator data*, connected to a packet decoder ('Byte Unpack') to provide simulation parameters.

- *UDP receiver for simulator control*, connected to a packet decoder ('Byte Unpack') to extract the simulation commands such as stop or reposition.

- *UDP sender for output data*, preceded by a 'Byte Pack' element to send the output of the simulation to the PFD computer.

To ensure smooth integration of the CA^{2}LM framework with the EFS500 simulator the number of modifications has been kept to a minimum. Following the description in Table 4.1, the only nodes that should be modified regarding the model are Nodes 2 and 3, featuring flight dynamics, avionics and screens rendering. However, only the flight dynamics code running in the Node 2 computer was modified, encapsulating all the changes in the simulator into one single computer.

Additionally to installing an Ethernet port to communicate to the Speedgoat real-time target machine, the following changes were made on the Node 2 computer code to allow the integration of the CA^{2}LM framework:

1. The original flight dynamics code was circumvented in the EFS500 simulator.
2. The bypass was implemented to allow the data from the CA^{2}LM framework to be used instead of the original flight dynamics code.

4.4 Summary of the chapter

The flight simulation framework, used during the flight testing campaign, was reviewed in this chapter.

The CA^{2}LM framework was reviewed in detail through the discussion of the aerodynamic, the structural dynamic, environment and gravity models. The equations of motion, governing the flexible aircraft, were discussed previously in Ch. 3. As the simulator provides the capability to model and test flexible aircraft, its applicability was demonstrated using two examples - HQs testing using the Gibson Dropback criterion and wing structural loading estimation using the aileron soft failure scenario. Despite its limitations with respect to the angle of attack and linear structural model, it is still a useful framework for the investigation of flexible aircraft handling qualities.

The EFS500 flight simulator, which provides the interface between the pilot and the CA^{2}LM framework, was discussed in detail too. Its composition of eight computers, visualisation system and the cockpit environment was reviewed. A thorough review of its suitability for testing an aircraft will be provided in Ch. 7 in the form of the SFFA analysis after the testing campaign.

Finally, the CA^{2}LM framework and the EFS500 flight simulator integration process was reviewed. The speedgoat real-time machine is used to speed up the CA^{2}LM framework to achieve the real-time simulation of the flexible aircraft. The speedgoat real-time target machine, which only runs the Simulink model, sends/gets data to/from the 'Flight dynamics' computer of the EFS500 simulator, to which it is connected.

As discussed in this chapter, the recently developed flight simulation framework aims to test HQs of flexible aircraft. Thus, the next chapter reviews a tested flexible aircraft.

Chapter 5

HARTEN

High Aspect Ratio Technology ENabler (HARTEN) is the test case for defining differences in handling characteristics between relatively rigid and highly flexible wing aircraft. The HARTEN model was developed during the AWI project workshop in July 2017. The aerodynamic data, dimensions of the aircraft and its flight envelope were provided by the Future Projects Office of Airbus UK. The detailed structural NASTRAN model of the HARTEN aircraft was provided by the University of Bristol.

HARTEN represents a medium size transport aircraft and is shown in Fig. 5.1. The main feature differentiating HARTEN from other similar aircraft is its high aspect ratio flexible wing. The T-tail with engines at the back configuration has been previously seen in many aircraft families such as Boeing 727, Fokker 70/100, MD 80/90 or Bombardier CRJ [139]. Main advantages of the T-tail configuration are: 1) the end-plate effect, allowing to reduce the size of the VTP, and 2) the HTP clearance from the disturbed flow from the wing [6]. Moreover, the use of the T-tail configuration allows aft-fuselage mounted engines configuration, which eliminates wing-engine interference and allows a shorter landing gear [6]. However, wings of above mentioned aircraft have aspect ratios lower than 10 and have been manufactured using traditional methods and materials. Hence, they are relatively rigid structures exhibiting only small deformations.

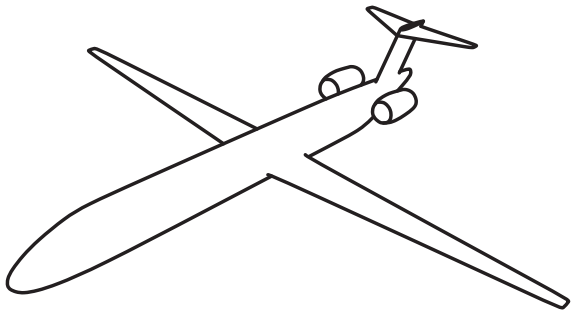

Figure 5.1: HARTEN - Airbus UK proposed medium size flexible wing transport aircraft concept

When considering weights of aircraft, HARTEN compares to the Airbus A321 or Boeing 737 series aircraft. For the interest of the reader comparison of main parameters of HARTEN and similar size aircraft, i.e. Airbus A321-251N and Boeing 737-10, is presented in Table 5.1. Data for A321-251N, B737-10 and HARTEN were extracted from type-certificate data sheets [140, 141], internal communication report [142] and publicly available online data. The HAR wing is the main difference between HARTEN and A321/B737 configurations, the other differences being the engines position and the empennage configuration.

Table 5.1: HARTEN comparison to similar size aircraft

Parameter	Airbus A321-251N	Boeing 737-10	HARTEN
Wing			
Span [m]	35.8	35.9	50.0
Area [m]	128.0	127.0	141.1
MAC [m]	4.2	4.0	3.1
AR [–]	10.0	10.2	17.7
Fuselage			
Length [m]	44.5	43.8	43.9
Diameter [m]	4.0	3.8	4.0
Mass			
MTOW [kg]	89000	92000	93500
MLW [kg]	77300	N/D	84200
MZFW [kg]	73300	N/D	78700
Fuel capacity [kg]	18510	20650	16600
Performance			
M_{cr} [–]	0.78	0.79	0.75
Range [nm]	3500	3300	2500

This chapter further defines the HARTEN aircraft model used for the flight testing campaign. Its dimensions and masses are given along with the flight envelope and the CG range for the test. Relatively rigid and highly flexible airframe configurations, used in the flight testing campaign, are defined in this chapter as well. The static longitudinal stability of both rigid and flexible configurations is defined as a function of the neutral point position with respect to the mean aerodynamic chord.

5.1 HARTEN definition

The HARTEN aircraft was modelled within the CA^{2}LM framework following the file "C5_v2_wing.tux_xml" provided by Airbus UK on 09/08/2017. The structural definition

of HARTEN was provided as a set of the following NASTRAN input files by the University of Bristol on 12/07/2017:

1. "harus_cbeam.dat", which defines beam elements of the aircraft model.
2. "harus_conm2.dat", which defines concentrated masses at grid points.
3. "harus_grid.dat", which defines grid points of the aircraft model.
4. "harus_mat.dat", which defines properties of materials, used to model the aircraft. It is the file where Young's modulus is defined and changed to alter the structural flexibility of the aircraft.
5. "harus_pbeam.dat", which defines the properties of the previously defined beam elements.
6. "harus_rbe2.dat", which defines the rigid bodies with independent DoF and dependent DoF.

Each definition above is taken from Ref. [143].

HARTEN was modelled to have the overall mass of 79167 kg for the flight testing campaign. This is an assumed mass of the HARTEN aircraft after the mission has been flown and the aircraft is approaching its final destination for landing. The nose of the aircraft is the coordinate reference point (datum) for longitudinal positions. The cabin floor level is the coordinate reference point (datum) for vertical positions.

5.1.1 Wing, horizontal and vertical tailplanes

HARTEN is a traditionally configured low-wing T-tail aircraft model. The wing of the aircraft is placed at 23.0 m from the horizontal datum. The VTP is situated at 42.9 m and the HTP at 43.9 m. The structural beam of the wing is at 24.7 m, which is 39.1% from the wing leading edge at the wing root and 42.0% from the wing leading edge at the position of MAC.

Main parameters of the HARTEN aircraft lifting surfaces are presented in Table 5.2. Two parameters that are not presented in the table, but are very important for the further stability studies of HARTEN, are volume ratios of HTP and VTP, V_{HTP} and V_{VTP}. They allow rapid estimation of the longitudinal and directional static stability of the aircraft and are derived from data in Table 5.2.

V_{HTP} is around 1.55, depending on the CG position. This is a larger value than traditional similar size transport aircraft have. According to Cook [26] V_{HTP} is usually around 0.5–1.3. However, Raymer [6] provides V_{HTP} value of 1 as typical for jet transports. Raymer also notes that due to aft-mounted engines the tail arm reduces by around 5%. Moreover, due to the all-moving HTP the V_{HTP} may be reduced by 10–15% and T-tail configuration allows to reduce it by another 5% [6]. Thus, V_{HTP} of around 0.85 would be

Table 5.2: Definition of the wing, HTP and VTP of the HARTEN aircraft

Parameter	Wing	HTP	VTP
Area [m^2]	141.1	32.9	59.1
Span [m]	50.0	11.2	5.9
MAC [m]	3.1	3.1	5.0
$\lambda_{c/4}$ [°]	0.5	31.0	37.5
AR [–]	17.7	3.8	2.3
TR [–]	0.3	0.4	1.0
Mass [kg]	20121	917	830

appropriate selection for the HARTEN model. However, it is about 82% larger and the effect of this will be discussed later in this chapter.

V_{VTP} is around 0.15, depending on the CG position. Raymer [6] provides V_{VTP} value of 0.09 as typical for jet transports. Due to the end-plate effect of the T-tail configuration, the V_{VTP} could be reduced by about 5%. Hence, the current V_{VTP} is about 67% larger when compared to similar aircraft designs.

Control surfaces

HARTEN is controlled by means of the traditional control surfaces - the ailerons, the elevator and the rudder. Their specifications are presented in Table 5.3. The HARTEN aircraft is also equipped with the all-moving HTP that has a range of $\pm 10°$.

Table 5.3: Definition of primary control surfaces of the HARTEN aircraft

Parameter	Aileron	Elevator	Rudder
c_{ctrl}/c [–]	0.45	0.6	0.5
η position [–]	0.72-0.97	0.10-0.90	0.00-1.00
Range [°]	$\pm 25°$	$\pm 30°$	$\pm 30°$
Actuator dynamics	$\frac{-1.77s+399}{s^2+48.2s+399}$	$\frac{-8.42s+2046}{s^2+102.87s+2046}$	$\frac{12.6s^2-1185s+27350}{s^3+77.7s^2+3331s+27350}$

Raymer [6] provides with usual values of elevator and rudder chordwise positions for jet transports, correspondingly $c_e/c = 0.25$ and $c_r/c = 0.32$. The elevator and rudder of HARTEN are thus oversized by 140% and 56% correspondingly. This oversize of the elevator and the rudder suggests the actions taken by the aircraft designers to compensate for too large HTP and VTP. This also suggests that the design procedure should be altered to avoid such conservative designs and mass penalties in the future.

5.1.2 Fuselage and engines

Dimensions of HARTEN fuselage and engines are shown in Fig. 5.2. The fuselage mass was 50419 kg, distributed along eleven nodes (N1–N11 as in Fig. 5.2). This distribution of the aircraft mass into eleven nodes is the default feature of the CA^{2}LM framework in order to provide capabilities to change the CG position and model fuselage flexibility effects. The engine mass was 3440 kg each. Engines were placed at 38.3 m from the datum and 1.8 m above the datum.

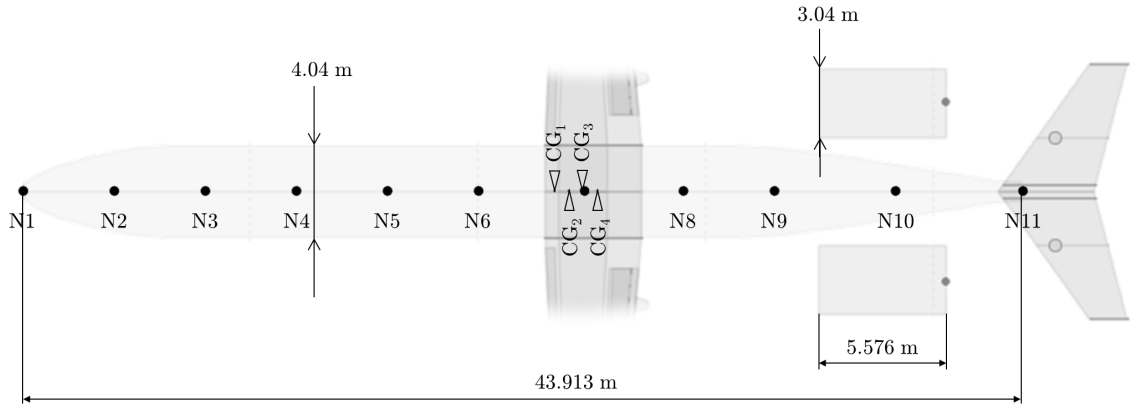

Figure 5.2: Dimensions of the HARTEN fuselage and engines

5.2 Definition of HARTEN configurations for testing

Configurations, defined in this section, were used for all the following tests of the HARTEN aircraft.

5.2.1 Mass configurations

The CG position of HARTEN was altered by redistributing the masses of the fuselage nodes. The following CG positions were defined for various test cases and are shown in Fig. 5.2:

1. CG_1 at 0% of MAC, which corresponded to 23.339 m from the datum.
2. CG_2 at 20% of MAC, which corresponded to 23.967 m from the datum.
3. CG_3 at 40% of MAC, which corresponded to 24.595 m from the datum.
4. CG_4 at 60% of MAC, which corresponded to 25.223 m from the datum.

Mass distribution for the above defined CG cases is presented in Table 5.4.

Table 5.4: Mass distribution along the fuselage for $CG_{1\text{-}4}$ test cases

Node	N1	N2	N3	N4	N5	N6	N7	N8	N9	N10	N11
x_{datum}	0	4	8	12	16	20	24.66	29	33	38.32	43.913
CG_1	200	350	500	2900	10000	23319	10000	2100	500	350	200
CG_2	200	350	500	2530	5000	23319	15000	2470	500	350	200
CG_3	200	350	500	1400	3000	23319	14000	6600	500	350	200
CG_4	200	350	500	1500	2000	23319	10000	7500	3500	1350	200

5.2.2 Flexibility configurations

Two significantly different wing structural flexibility configurations were defined to identify differences in handling characteristics between rigid and flexible wing aircraft. These configurations were: 1) rigid (R), with the corresponding wing Young's modulus of 8×10^{10} Pa, and 2) flexible (F), with the corresponding wing Young's modulus of 8×10^{9} Pa. Other parts of the HARTEN aircraft were modelled as relatively rigid and their Young's modulus was equal to 6.89×10^{15} Pa. To show the difference between rigid and flexible wings, the aircraft was trimmed for one flight condition at 10000 ft and 110 m/s flight velocity. Figure 5.3 shows the difference between rigid and flexible wing deformations and data from the figure along with the dihedral angle variations are shown in Table 5.5. The wing flexibility was expressed as the ratio of the wing vertical deformation Δz to the wing semi-span $b/2$, which is an industrially accepted standard. The validity of modelling large wing deformations using the linear structural model was discussed in Ch. 4. The most significant issue, however, for such a large deformation as seen in the figure is the artificial wing elongation that increases its length by approximately 11.5% for the discussed case. This large deformation of the wing increased its effective dihedral angle γ. It will be shown in Ch. 7 that this change significantly changes lateral/directional dynamics of the aircraft. Hence, this very large deformation of the wing provides insight into handling characteristics of the aircraft.

Table 5.5: Rigid and flexible wing vertical deformations with respect to reference

A/C config / Parameter	Reference	Rigid	Flexible
$\frac{\Delta z}{b/2}$ [–]	N/A	6.2%	49.4%
$\Delta\gamma$ [°]	N/A	3.5	26.3
γ [°]	2.5	6.0	28.8

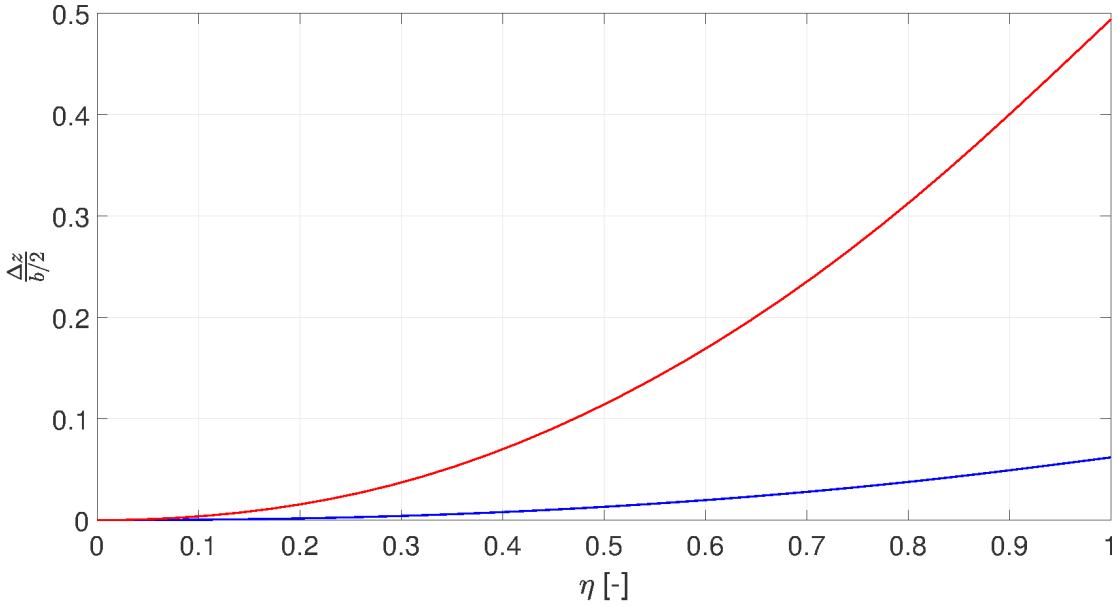

Figure 5.3: Rigid and flexible wing deformations at the trim state

5.2.3 Flight conditions

The HARTEN aircraft was trimmed for a set of different flight conditions to examine the flight envelope of both the aircraft and the CA^{2}LM framework. Trim sets are presented in Table 5.6. As seen in the table, not every mass configuration and/or flexibility configuration could be trimmed using the CA^{2}LM trim routine. The successfully trimmed sets of data were used to define the longitudinal static stability and for the flight testing campaign as the initial flight conditions.

5.3 Longitudinal static stability

The longitudinal static stability of the HARTEN aircraft was investigated by the use of the CA^{2}LM framework alone. A set of flight trim conditions, presented in the previous section, was used to define the LSS, which is usually defined by the neutral point position h_n and the static margin K_n. The neutral point h_n is defined as such a position of the CG, where $C_{m_\alpha} = 0$. To define h_n the $\frac{di_H}{dC_L}$ gradients were acquired for each CG position. The same procedure was repeated for different altitudes to investigate altitude effect on the LSS. These data are presented in App. C. Final results, derived from the ones in the appendix, are shown in Fig. 5.4.

The difference between $\frac{di_H}{dC_L}$ gradients of rigid and flexible configurations at the same CG position shows higher HTP deflection needed to compensate a change in AoA or flight

Table 5.6: Flight testing envelope

EAS, m/s / Altitude, ft	110	150	190	230
5,000	$CG_1(R,F)$ $CG_2(R,F)$ $CG_3(R,F)$ $CG_4(R,F)$	$CG_1(R,F)$ $CG_2(R,F)$ $CG_3(R,F)$ $CG_4(R,F)$	$CG_1(R,F)$ $CG_2(R,F)$ $CG_3(R,F)$ $CG_4(R,F)$	$CG_1(R,F)$ $CG_2(R,F)$ $CG_3(R,F)$ $CG_4(R,F)$
10,000	$CG_1(R,F)$ $CG_2(R,F)$ $CG_3(R,F)$ $CG_4(R,F)$	$CG_1(R,F)$ $CG_2(R,F)$ $CG_3(R,F)$ $CG_4(R,F)$	$CG_1(R,F)$ $CG_2(R,F)$ $CG_3(R,F)$ $CG_4(R,F)$	$CG_1(R,F)$ $CG_2(R,F)$ $CG_3(R,F)$ $CG_4(-,F)$
15,000	$CG_1(R,F)$ $CG_2(R,F)$ $CG_3(R,F)$ $CG_4(R,F)$	$CG_1(R,F)$ $CG_2(R,F)$ $CG_3(R,F)$ $CG_4(R,F)$	$CG_1(R,F)$ $CG_2(R,F)$ $CG_3(R,F)$ $CG_4(R,F)$	$CG_1(R,F)$ $CG_2(R,F)$ $CG_3(-,F)$ $CG_4(-,F)$
20,000	$CG_1(-,-)$ $CG_2(-,-)$ $CG_3(-,-)$ $CG_4(-,-)$	$CG_1(R,-)$ $CG_2(R,-)$ $CG_3(R,F)$ $CG_4(R,F)$	$CG_1(R,F)$ $CG_2(R,F)$ $CG_3(R,F)$ $CG_4(R,F)$	$CG_1(R,F)$ $CG_2(R,F)$ $CG_3(R,F)$ $CG_4(-,F)$

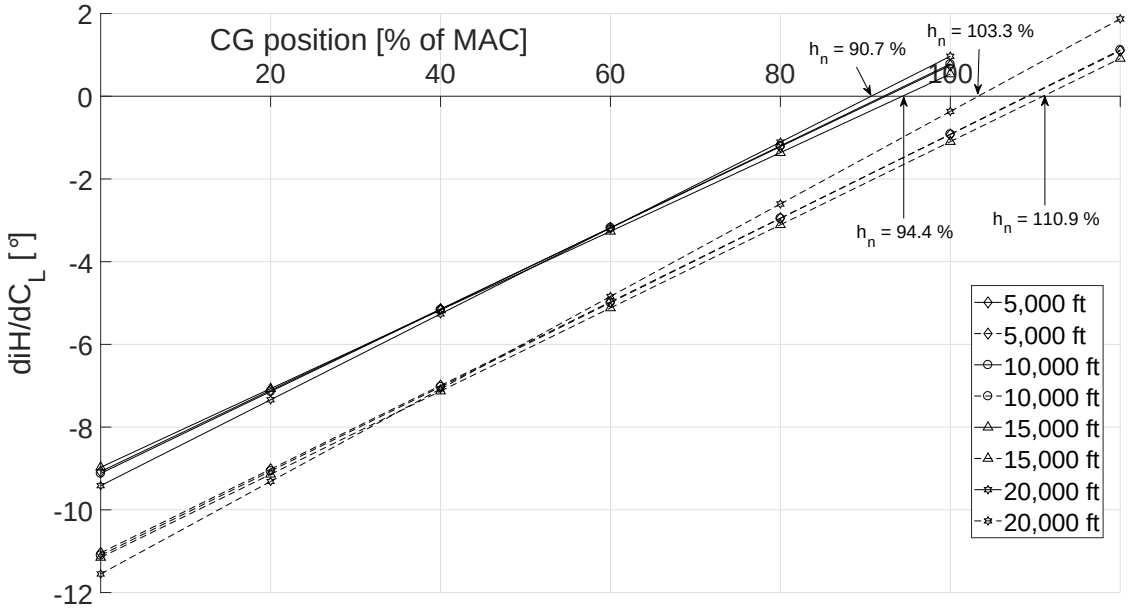

Figure 5.4: $\frac{di_H}{dC_L}$ dependency on *CG* for different altitudes: rigid (—) and flexible (– –) cases

velocity for flexible configuration. Due to reduced effective wingspan in the flexible wing case the loss of lift is counteracted by an increasing AoA to provide the same amount of lift. Thus, HTP has to be deflected more to increase angle of attack. This also affects trimmed flight conditions, i.e. the initial AoA and the pitch attitude are higher for flexible configuration aircraft.

The horizontal offset of the neutral point h_n is more than 10% aft for the flexible wing configuration compared to the rigid one. As the neutral point coincides with the aerodynamic centre position of the aircraft [25, 144], such an aft displacement of h_n is expected for the flexible wing aircraft. As the wing becomes deformed, it requires higher AoA to produce the same amount of lift. As mentioned before, higher AoA is achieved by increased pitch attitude, which is achieved by higher i_H angle. This means that the lift produced by the tail is larger, while the lift from the wing stays the same, when comparing flexible and rigid wing cases. Hence, the relative influence of the tail increases and the aerodynamic centre of the aircraft moves back.

The usual position of the neutral point h_n is around 40% MAC for traditional jet transport aircraft. However, as seen in Fig. 5.4, h_n is around 92% MAC for the rigid and 108% MAC for the flexible cases of the HARTEN aircraft. These unusually high values are the first indication of too large HTP, which was discussed earlier in this chapter in terms of V_{HTP} coefficient. Too large HTP, leading to excessive longitudinal stability, also requires larger elevator for the aircraft to be controlled. This suggests that the reduction of HTP size should be considered. It would also allow to reduce some mass, which is always one of the design objectives.

On the other hand, high h_n values give wider range of the static margin K_n. This provides more freedom to distribute the payload along the aircraft, which might be an appealing feature for the potential users of such an aircraft.

Chapter 6

Flight simulation campaign

This chapter reviews the flight simulation campaign, organised to assess and compare FQs and HQs of the rigid and flexible HARTEN aircraft configurations. The newly developed SFFA was used to perform this simulation campaign. Firstly, the flight conditions and aircraft configurations are defined. Then a brief review of test pilots' experience is provided and the metrics, used to evaluate FQs and HQs, are defined. The chapter ends with the review of test manoeuvres and an introduction of a new slalom task. Two main objectives of the flight simulation campaign were:

1. To assess the change in FQs and HQs between rigid and flexible aircraft.

2. To assess software and hardware of the SFFA.

Notes on the flight simulator configuration for the campaign

1. The fixed-base flight simulator was used for the current research due to:
   - its operational and physical availability for the simulation campaign;
   - its advantages, discussed in subsection 2.3.11, allowing to reduce the level of ambiguity of evaluating HQs of a novel aircraft concept.
2. The pilots experienced dynamics at the aircraft CG position, rather than at the cockpit position. This choice was justified by the fact that the simulated aircraft fuselage was rigid and there were no motion cues within the simulator. Hence, the pilots would see the same dynamics on the screen regardless of their positioning.

6.1 Preparation for the test campaign

Preparation for the test campaign consisted of the following steps:

1) test cases definition;

2) selection of test pilots;

3) selection of flying and handling qualities evaluation metrics.

6.1.1 Aircraft structural flexibility configurations

To meet the first objective of the flight test campaign two test cases of the aircraft structural flexibility were defined as follows:

- **R** - HARTEN rigid configuration with Young's modulus of the wing equal to 8×10^{10} Pa;
- **F** - HARTEN flexible configuration with Young's modulus of the wing equal to 8×10^{9} Pa.

Such choice of the rigid configuration Young's modulus was based on the usual values of aluminium alloys [145]. The Young's modulus of the flexible configuration was reduced by the power of ten to provide significant increase in the wingtip deflection. This choice also allowed avoidance of an additional test case of 2.5g manoeuvre, which usually provides ultimate structural load testing condition, as this would be difficult to achieve without motion cues and load indication for a pilot within the SFFA. The Young's modulus for all other parts was 6.89×10^{15} Pa. Modal damping $\zeta_i = 3\%$ (see equation 4.11) was chosen to represent industrially acceptable value for both configurations. All tests were done with the aircraft CG position at 20% MAC[1]. The aircraft was flown in clean configuration, i.e. no slats and no flaps were used as they are not modelled within the CA^{2}LM framework. Both rigid and flexible aircraft configurations were tested for the same test manoeuvres to find out an impact of an increased airframe flexibility to their handling qualities.

The aircraft was exposed to the same initial flight conditions at the beginning of each test. The initial trimmed flight conditions were as follows:

- altitude - 10000 ft;
- EAS - 110 m/s or 204 kt;

[1]Such CG position was chosen after discussion with some Airbus A321 (similar size and purpose aircraft) line pilots, who emphasized aircraft's tendency to be 'nose heavy' in the final stages of flights and also mentioned usual CG positions in the range of 20%–30% for A321 depending on a flight length. Similar CG position (25%) was also used in the recent NASA research [146] and could be inferred from the usual pilot training material [147].

- AoA - 3.8° for the rigid aircraft configuration;
- AoA - 5.3° for the flexible aircraft configuration.

Each test was flown by all or some of the pilots according to their experience and estimated contribution to each test.

6.1.2 Test pilots

Three test pilots, all with wide flying experience, participated in the test campaign. Short reviews of their experience are presented below.

(1) - Pilot 1 was a microlight aircraft test pilot with more than 1500 flight hours in more than 90 different types and sizes of aircraft. He holds a PhD degree in Aerospace Engineering from the University of Southampton, where he investigated airworthiness evaluation techniques. The pilot is a professor, a Chartered Engineer and an expert witness in legal cases related to air accidents. The pilot largely contributed with advice, assessments and expertise from the perspectives of aeronautical engineering and flight testing.

(2) - Pilot 2 was an active test pilot with more than 12000 flight hours in more than 100 different types and sizes of aircraft. The pilot attended the Empire Test Pilot School and the USAF Test Pilot School. For many years the pilot served the Royal Air Force as a pilot, a flying instructor, an experimental/research test pilot before being appointed as the chief test pilot here at Cranfield University. The pilot holds an Airline transport pilot licence (ATPL) licence with type rating instructor/examiner and synthetic flight instructor/examiner for the Jetstream 31/32 and the Full Flight Simulator (FFS) ratings. The pilot largely contributed with advice, assessments and expertise from the perspectives of flight testing and piloting techniques and flight simulator testing.

(3) - Pilot 3 was an active commercial aircraft pilot with more than 7000 flight hours in total, 3000 of which were pilot-in-command hours on Airbus A320/321 and Boeing 787. His experience covers more than 25 types of aircraft. The pilot got his test pilot experience at Calspan (US), International Test Pilots School (ITPS, Canada) and National Test Pilot School (NTPS, US). The pilot has also accumulated more than 300 hours performing the FFS testing for CAE - one of the biggest providers of flight simulators. The pilot largely contributed with advice, assessments and expertise from the perspectives of potential user of such an aircraft in commercial aviation and flight simulators testing.

Pilots, according to their experiences, were asked to fly different test cases of the HARTEN aircraft and different manoeuvres. All three pilots had particular strengths due to their background: Pilot 1 was very knowledgeable in the fields of aeronautical engineering and airworthiness, Pilot 2 possessed wide flight testing experience and Pilot 3 had wide experience in commercial flying and flight simulators testing. This choice of pilots allowed to cover the test campaign from academic, commercial flying and flight testing points of view. As the objectives of test campaign were to test the new configurations of aircraft and to assess the SFFA, it was decided that three highly experienced pilots were

enough for the campaign. Moreover, all of them had flight testing background and experience, which was of the highest importance for the simulation campaign. Experience of selected pilots also allowed them to comply with the flight simulation requirements set by the author. Their capabilities allowed the collection of high value data during the test campaign and evaluate it via classical metrics.

6.1.3 Flying and handling qualities evaluation metrics

Traditional metrics, most widely used in research community, were used to evaluate the flying and handling qualities of new aircraft configurations. Tests 1-7 were evaluated according to MIL-F-8785C requirements [95] and CS 25 requirements [57]. Even though MIL-F-8785C requirements were developed for military aircraft, they have been the ones mostly used within the research community. Moreover, they provide quantitative distinction between good and bad FQs. CS 25 requirements, in contrast to MIL-F-8785C, provide only qualitative requirements, e.g. the only CS 25 requirements for an aircraft dynamic stability are that the SPPO must be heavily damped and the Dutch roll must be positively damped and controllable with primary controls, while MIL-F-8785C provide particular quantitative requirements. The HARTEN aircraft qualified as class II (medium transport) aircraft and the initial flight conditions fell within flight phase category A ($\geq 1.2V_S$ and 10000 ft altitude) according to MIL-F-8785C. MIL-F-8785C requirements covered all tests, except the steady heading sideslip (SHSS) and slalom task. The aircraft were then assigned Level 1, Level 2 or Level 3 flying qualities, where Level 1 stands for the best ones, according to the demonstrated performance in the particular test.

The slalom task was evaluated using the CHR scale. Each pilot was asked to attribute CHR score along with comments explaining that particular score. Initial objective was to attribute the CHR scores for longitudinal and lateral/directional HQs separately. However, Pilot 3 refused to assess the HQs due to “lack of experience in flight testing”.

Pilot comments were also recorded as one of the most valuable outcomes of the simulation campaign. The SFFA was exclusively assessed according to pilot comments, while FQs and HQs assessment included both comments and quantitative parameters to validate the comments.

The evaluation metrics discussed above were applied to the most widely used test manoeuvres to assess the main longitudinal and lateral/directional modes of the tested aircraft. The following section briefly reviews each test manoeuvre with further explanations of the purpose of each manoeuvre and how the manoeuvre was executed.

6.2 Test manoeuvres

The following set of static/dynamic modes was chosen to assess flying and handling qualities of rigid and flexible aircraft configurations:

ST - Stall to define the aircraft stall speed and the reason for the stall, i.e. if it is aerodynamically driven stall or the elevator deflection limited stall.

SP - SPPO mode to assess the aircraft's longitudinal response to pilot's input.

PH - Phugoid mode to evaluate the long term longitudinal dynamics of the aircraft.

SH - SHSS to assess the aileron and rudder efficiency.

RM - Roll mode to define the roll performance of the aircraft.

SM - Spiral mode to define the aircraft stability during turns.

DR - Dutch roll mode to define the aircraft dynamics in response to sideslip.

SL - Slalom task to assess the overall performance of the aircraft and identify deficiencies of the simulator.

Each of the modes along with the techniques, used to induce them, are described below.

6.2.1 Stall conditions test

Definition. — The stall conditions test aims to determine the stall speed, the cause of the stall and the aircraft's behaviour during and after the stall. It is the simplest and the most primary test in assessing handling characteristics of any aircraft. The stall speed, which defines one of the most important speeds of the aircraft - the approach speed - is defined during the test. Moreover, the angle of attack at the stall speed allows an engineer to find out if the stall is primarily driven by the aerodynamic stall or by some other limiting factors, e.g. the elevator deflection $\Delta\eta$ limit. The latter being the case means that the main aerodynamic surface, i.e. the wing, is not utilised at its full efficiency at low speed, which is achieved just before the aerodynamic stall. Moreover, an aircraft's behaviour changes depending on the cause of the stall: the behaviour is hardly predictable in case of aerodynamic stall. However, if the aerodynamic stall is not achieved due to lack of the elevator authority, the aircraft exhibits $\Delta\eta$ limited stall, in which case full control of the aircraft in all three axes is usually maintained. Thus, it is highly important to understand this behaviour as the stall prevention and the post-stall recovery procedure will depend on it [148, 149].

Execution. — The test starts with an aircraft at the initial flight conditions. The stall test is performed by increasing the angle of attack of an aircraft. Firstly, the throttle is set to idle, i.e. zero thrust value is assumed in the simulation. Secondly, the control column is deflected aft to increase the angle of attack and decrease the velocity of an aircraft. The control column is deflected at such a pace to maintain the velocity decrease of 1 kt/s. At certain velocity V_S the angle of attack reaches its aerodynamic stall angle or $\Delta\eta$ limited angle and cannot be increased any more. This velocity V_S is then assumed to be the aerodynamic stall speed or $\Delta\eta$ limited stall speed.

6.2.2 Short period pitching oscillation mode test

Definition. — The SPPO mode test aims to assess the short term longitudinal aircraft response to the pilot's elevator input or any other aircraft disturbance from an equilibrium state. The SPPO is the most important dynamic mode of all. Whenever the aircraft is disturbed from its pitch equilibrium point, the mode is excited. It manifests itself as an oscillation, in which principal variables are the pitch rate and the angle of attack [150]. The typical period of the mode is between 1 s and 2 s or a little more [148], translating into frequencies of less than 0.5 Hz and up to 1-2 Hz. These frequencies coincide with the region of the human pilot natural frequencies, thus undesirable coupling between an aircraft and a pilot may arise. Hence, it is vital for the SPPO mode to be well damped.

Execution. — The test starts with the simulation of the datum flight conditions, which is defined above. Two test methods were applied to estimate parameters of both damped and undamped SPPO modes:

1. An elevator doublet input excites the mode and provides damping ζ_{sp} and frequency $\omega_{d_{sp}}$. This input is the most common one used to excite the mode [149], as it excites the SPPO mode while suppressing the phugoid mode. Although the input is easy to implement it does not contain much spectral power [151].

2. A sinusoidal signal pump (SSSP, or frequency sweep) provides the undamped natural frequency $\omega_{n_{sp}}$. The relative damping is not available as the input is continuously forced by the pilot to cover a wide range of possible mode frequencies. This technique provides a broad spectral range as a range of frequencies are excited [151]. The frequency at which the pilot's control column input is out of phase with the aircraft's pitch attitude defines $\omega_{n_{sp}}$.

6.2.3 Phugoid mode test

Definition. — The phugoid mode test aims to assess the long term longitudinal aircraft response to the pilot's elevator input or any other aircraft disturbance from an equilibrium state. The phugoid mode is a lightly damped low frequency oscillation in speed and height, where the exchange between potential and kinetic energy takes place [149]. The principal variables of the mode are the pitch attitude and the speed [150]. The angle of attack should remain substantially constant during the oscillation. The typical period of the mode is in the range of 40 s to 100 s [148]. The damping appears mostly due to the rate of change of drag of the aircraft with speed change. The phugoid manifests itself as a trimming problem, which does contribute to an increased pilot workload [152]. However, as it is a gentle, slow and easily controlled longitudinal mode it is of little interest for handling qualities [148]. Nevertheless, it has to be well investigated to understand its influence on other dynamic modes.

Execution. — The test starts with the simulation of the datum flight conditions, which is defined above. Then the mode is excited by a small, but long elevator input.

6.2.4 Steady heading sideslip test

Definition. — The aim of the SHSS test is to assess the lateral/directional control characteristics of the aircraft and effectiveness of corresponding controls. The SHSS test is the primary test for the lateral/directional qualities' investigation. It allows a pilot to assess the efficiency of corresponding control surfaces, i.e. ailerons and rudder. Moreover, it allows a pilot to estimate the aircraft's roll and yaw dynamics. The goal during the SHSS test is to compensate the sideslip, introduced by rudder input, by aileron input so that constant heading of an aircraft is maintained during the test. By assessing the inputs' magnitude and the sideslip and bank angles the pilot develops the perception of the aircraft's lateral/directional controllability. As will be shown later in the discussion, it is more a qualitative rather than a quantitative test.

Execution. — The test begins with a trimmed flight exposed to initial conditions, as discussed above. Firstly, a pilot makes rudder input to create the sideslip. Then the sideslip is compensated by rolling the aircraft. Capability to maintain steady heading means equal authority of ailerons and rudder for that particular case. The test is done continuously increasing the rudder deflection until ailerons reach their maximum deflection and cannot provide the rolling moment to compensate the moment from the rudder.

6.2.5 Roll mode test

Definition. — The roll mode test aims to assess an aircraft response to a pilot's lateral stick input. The roll mode is a non-oscillatory mode that "manifests itself as an exponential lag characteristic in rolling motion"[26]. It is a very important characteristic for a pilot as it defines the roll performance of an aircraft in terms of the time required to accelerate to and reach a steady state roll rate. As the roll mode appears to a pilot as "a lag in roll response to controls"[26], it is defined by the time constant τ_r, which is "typically around 1 s or less"[26]. τ_r is defined as the time to reach 63.2% of the steady state roll rate after initiating the roll manoeuvre. The time constant for the current case example (flight phase category A, class II aircraft) should be less than 1.4 s for Level 1 handling qualities [95].

Execution. — The test begins with a trimmed flight exposed to initial conditions, as discussed above. A pilot then banks an aircraft to angle of $\pm 30^\circ$. Then a pilot makes lateral stick input to roll the aircraft to an opposite bank angle of approximately the same magnitude.

6.2.6 Spiral mode test

Definition. — The spiral mode test aims to assess the aircraft's tendency to converge/diverge during the roll manoeuvre. The spiral mode is non-oscillatory mode and manifests itself as an exponential convergence or divergence in roll attitude [26]. It is the lateral static stability mode [26] and if unstable will produce a divergent spiral descent. The time constant T_2 of the mode is usually as large as 100 s [26]. The spiral mode is a long period mode, thus it has a little effect on handling qualities of an aircraft [149]. Hence, it does not cause any further problems even when it is unstable as long as time to double amplitude T_2 is more than 20 s [148]. However, in case of the unstable mode the aircraft tends to slowly diverge into a spiral dive when disturbed from a straight and level flight. In case when T_2 is lower than the Dutch roll period, the spiral mode will require more attention during precise manoeuvring tasks. This mode may become even more dangerous when external visual cues are poor or absent. Investigation of the mode allows an engineer to assess the balance between the size of the VTP and sufficiency of the wing dihedral angle [148].

Execution. — The test begins with a trimmed flight exposed to initial conditions, as defined above. Then an aircraft is rolled to 15° bank angle by ailerons or rudder input. When stabilised at 15° bank angle all control inputs are removed and aircraft's behaviour is investigated. In case of stable spiral mode, the aircraft will reduce the bank angle and eventually return to wings level flight. In case of neutral spiral mode stability, the aircraft will maintain the bank angle. In case of unstable spiral mode, the aircraft will increase the bank angle and enter the spiral dive.

6.2.7 Dutch roll mode test

Definition. — The Dutch roll mode test aims to assess the aircraft's tendency to roll-yaw coupling when yawing. The Dutch roll mode is an oscillation with a tightly coupled rolling and yawing motion with small damping [149]. The principal variables are the sideslip angle and the yaw rate [150]. The mode is the directional equivalent of the SPPO mode. One characteristic of the motion is that the sinusoidal changes in sideslip cause a change in the rolling motion. The phase shift between the cause and the effect means that the forward going wing is low and the wingtips describe an elliptical path. The key parameter to evaluate the mode is the ratio of bank angle to sideslip angle $\frac{\Delta\Phi}{\Delta\beta}$ [149]. Low ratio is usually more acceptable for a pilot as the yaw dominates the mode.

Execution. — The test starts with a trimmed flight exposed to initial conditions, as defined above. A pilot excites the mode by the rudder doublet input. The ratio between bank and sideslip angles is then assessed by a pilot, visually observing aircraft motion on the screen, and by the test engineer, analysing data recordings, for comparison.

6.2.8 Slalom task for the HQs assessment

Definition. — The slalom task aims to assess an aircraft's capability to perform a real life high gain task. It helps to assess the aircraft's capabilities in challenging situations, such as flight path corrections during the final approach stage. Those complex situations require the aircraft to perform well longitudinally, laterally and directionally. Thus, most of the aircraft deficiencies, if any, manifest themselves during the test, when the pilot performs this closed loop high gain task. At the end of the task a pilot assigns CHR scores for longitudinal and lateral/directional handling qualities of an aircraft.

Execution. — The test begins with a trimmed flight exposed to initial condition, as defined above. Then a pilot flies an aircraft through a series of flying spheres. Depending on which sphere (smaller or bigger) is flown through, the desired or adequate levels of performance are attributed to an aircraft-pilot combination. However, if the pilot misses both of the spheres, the aircraft is defined as uncontrollable.

Example of the slalom task

The offset landing manoeuvre together with the slalom manoeuvre (see Ref. [153] for the explanation of both manoeuvres) were chosen as the base to develop the slalom task. The hypothetical situation was developed with respect to ILS approach procedure. To apply the task at different altitudes and places of the scenery, the target airway was defined by the coloured spheres. The task was also amended with the additional capability allowing to assign CHR scores. This was achieved by placing two spheres at the same point in space and defining their diameters according to the performance level to be achieved, i.e. adequate or desired.

Hypothetical situation

Let's assume that the aircraft is on the glideslope for landing at some arbitrary runway RWY. The aircraft is descending through the cloud on the centreline of RWY. The cloud base is at 200 ft AGL, which is in accordance with CAT 1 ILS minimum. Out of the cloud the pilot notices that the aircraft is off the RWY centreline by 2.5°, which corresponds to full vertical needle deflection of the ILS indicator. This gives a lateral offset of 432 ft *or* 0.071 nm. Distance from 200 ft AGL to the touchdown point is approximately 3816 ft *or* 0.628 nm on a standard 3.0° glideslope.

Distances between circles

Lateral distance between circles was chosen to be 0.071 nm. However, the longitudinal distance was increased to 1.2 nm, because of the high flight velocity as the

aircraft was flown in the clean configuration. The circles and distances are given in Fig. 6.1.

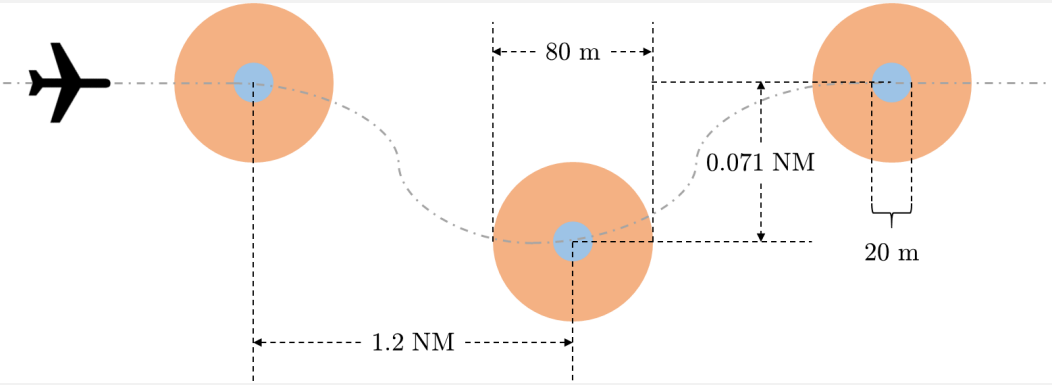

Figure 6.1: Definition of the slalom task

Sizing of circles

Figure 6.1 also presents two sets of circles, i.e. outer orange and inner blue. They define adequate (orange circles) and desired (blue circles) performance of aircraft-pilot couple for the CHR evaluation. If both circles are missed the aircraft is assumed to be uncontrollable. The sizes of adequate and desired circles were chosen according to sizes of runways, i.e. the desired circle had a diameter of 20 m, which is usually the width of a touchdown zone, and the adequate circle had diameter of 80 m, which is the width of the widest runways at large aerodromes.

Other assumptions

The test was carried out at 10000 ft altitude and the aircraft was flown in clean configuration. Thus, no attempt to land was performed. This reduced the workload of pilots and should have positively affected CHR scores. However, it still supported HQs evaluation, especially allowing to distinguish between three main groups, i.e. desired, adequate and uncontrollable.

The overall test campaign is summarised in Table 6.1 in the test matrix form. Each test code consists of: 1) test name (first two letters), 2) pilot number, and 3) structural stiffness case, e.g. SP(1)R is the short period pitching oscillation mode (SP) test carried out by Pilot 1 (1) for the rigid (R) case aircraft.

The findings of the testing campaign will be presented in the next chapter.

Table 6.1: Test matrix

Tests		Pilot 1	Pilot 2	Pilot 3
Stall conditions		ST(1)R ST(1)F	ST(2)R ST(2)F	Nil
Longitudinal modes	Short period pitching oscillation	SP(1)R SP(1)F	SP(2)R SP(2)F	Nil
	Phugoid	PH(1)R PH(1)F	PH(2)R PH(2)F	Nil
Lateral/directional modes	Steady heading sideslip	SH(1)R SH(1)F	SH(2)R SH(2)F	Nil
	Roll mode / Roll performance	RM(1)F	RM(2)R RM(2)F	Nil
	Spiral	SM(1)R	SM(2)R SM(2)F	Nil
	Dutch roll	DR(1)R	DR(2)R DR(2)F	Nil
Slalom task		Nil	SL(2)R SL(2)F	SL(3)R SL(3)F

Chapter 7

Flight simulation results

Findings and results of the flight simulation campaign are presented in this chapter. The chapter is split in two parts according to the simulation campaign objectives to indicate the differences between rigid and flexible aircraft and to assess the SFFA. The first part presents the comparison of flight dynamics between the rigid and flexible aircraft configurations through simulating a series of longitudinal and lateral/directional modes. The second part presents the assessment of the simulation framework based on the comments from the pilots.

7.1 Comparison between rigid and flexible aircraft dynamics

7.1.1 Stall performance

Two stall cases were tested during the campaign. The first case exhibited η limited stall before reaching the aerodynamic stall angle of attack. During the second case trial, the aerodynamic stall angle of attack of 12.5° was exceeded due to absence of the aerodynamic stall model within the simulation framework. However, the artificial limit of 15°, set within the CA^{2}LM framework, was reached and the stall settled around this value.

Time histories of four tests are provided in Apps. D.1–D.4. Main parameters of the flight phase approaching stall conditions and the stall itself are extracted in Fig. 7.1. Table 7.1 presents flight parameters at the stall point.

Tests ST(1)R and ST(1)F were flown with the elevator deflection limited to $\pm 15.7°$, while tests ST(2)R and ST(2)F were flown with the elevator deflection limited to $\pm 30.0°$. Both cases showed difference in the stall speed V_S and rate of descent RoD, i.e. ST(1) cases exhibited higher V_S, but lower RoD as angles of attack were lower, while ST(2) cases exhibited lower V_S and higher RoD as angles of attack were higher.

Pilot 1 described the stall as a "fairly stable mush[1]" as he maintained the "full control

[1] A partly or nearly stalled condition.

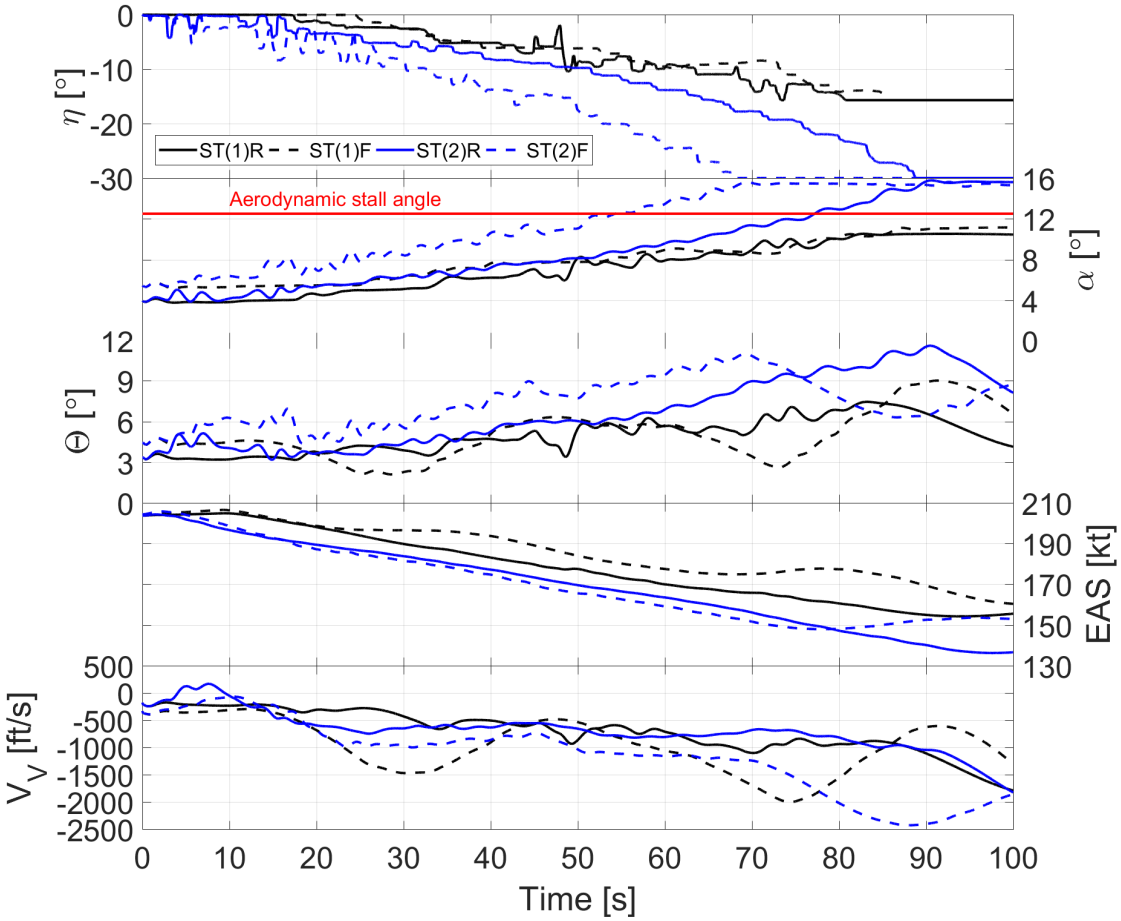

Figure 7.1: Main parameters of the stall condition for each test case

Table 7.1: Main parameters of the stall conditions

Test	V_S [kt]	RoD [ft/min]	AoA [°]	Θ [°]	γ [°]
ST(1)R	154	1400	10.5	5.5	-5.0
ST(1)F	160	1600	11.2	5.5	-5.7
ST(2)R	136	1600	15.0	9.1	-5.9
ST(2)F	148	1700	15.0	8.9	-6.1

over the aircraft in all three axes" during ST(1)R test. The aircraft reached a maximum pitch attitude of about 5.5° at the corresponding AoA of 10.5°. As this was elevator limited flight condition, the aerodynamic stall angle was not reached. Thus, such a case represents too small authority of the elevator. The authority of the elevator was increased for ST(2)R as mentioned above. This showed an increase in maximum AoA. However, as there was no aerodynamic stall model, the aerodynamic stall condition was not reached. The plateau seen at about $AoA = 15°$ appeared due to internal limits of the CA^{2}LM frame-

work, which were discussed in Ch. 4. For the rigid aircraft case “little rolling excursions” and its tendency to phugoid at the stall condition (see Fig. 7.2) were noticed by Pilot 1.

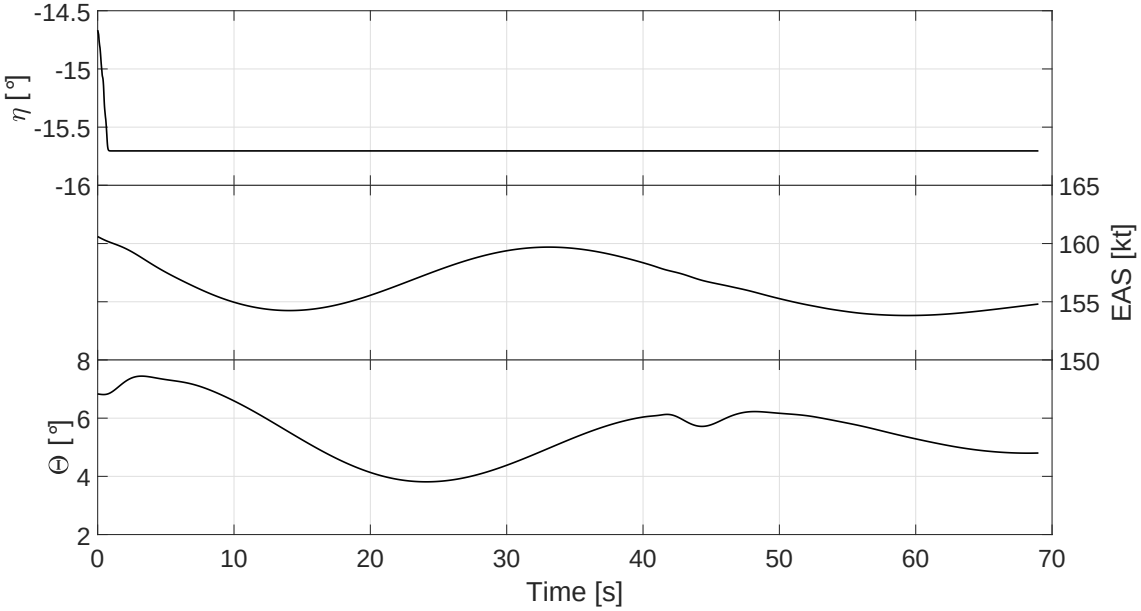

Figure 7.2: Phugoid at the η limited stall condition during ST(1)R test

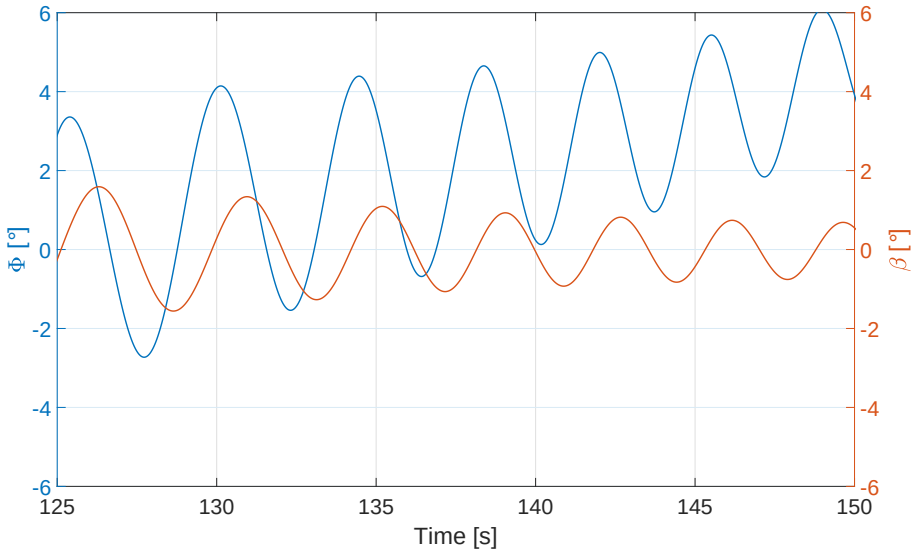

Figure 7.3: Dutch rolling of the aircraft as witnessed by the pilot during ST(1)F test

ST(1)F and ST(2)F tests revealed an interesting phenomenon - the ‘wing rocking’, which was induced at the flight phase of maximum AoA. This phenomenon is understood as a lateral/directional instability and is usually observed at high angles of attack for low

AR wing aircraft[2] [154, 155]. It is "triggered by flow asymmetries, developed by negative roll damping, and sustained by nonlinear aerodynamic roll damping" [154]. The 'wing rocking' manifested itself as an oscillation of the aircraft around its longitudinal axis at high AoA and disappeared when the AoA was reduced. Due to an increased wing dihedral angle this oscillation also coupled with the directional dynamics and induced the Dutch roll mode. Pilot 1 commented that the aircraft was "Dutch rolling on its own" as seen in Fig. 7.3. Nevertheless, the control of the aircraft was never lost by any of the pilots during this and further tests.

Comparison between the rigid and the flexible aircraft showed an increase by 4%-9% in V_S and 6%-14% in RoD. An increase in AoA was about 7% during ST(1) test cases, while the artificial limit of AoA was reached in both cases of ST(2). Allowing higher α by increasing η range resulted in lower stall velocities. However, the flight path angle γ and RoD increased.

The discussion above showed an importance of an aerodynamic stall model. The missing model did not allow to fully assess one of the most important and critical speeds - the stall speed V_S. However, it was shown that the elevator effectiveness can be assessed by this test.

The stall performance test, being the very basic test of an aircraft handling characteristics, revealed differences between the rigid and the flexible aircraft configurations – both V_S and RoD were higher for flexible aircraft, as well as the flight path angle γ. The 'wing rocking' phenomenon due to an increased wing dihedral angle was revealed during the test at high AoA. Also the rigid aircraft tendency to phugoid was revealed.

7.1.2 Longitudinal dynamics

The SPPO and phugoid modes were simulated to define the longitudinal dynamics of the aircraft.

SPPO mode

Two techniques were applied to assess the SPPO parameters – the pitch doublet (PD) input and the frequency sweep (FS) input. Time histories of five tests are provided in Apps. E.1–E.5. Main parameters of the SPPO mode are presented in Table 7.2. The parameters in Table 7.2 were extracted from Fig. 7.5 and Fig. 7.6.

[2]Although the HARTEN is considered as a high AR wing aircraft, but due to the wing's flexibility, especially under high loading at the maximum AoA, the effective wingspan is significantly reduced. This makes the HARTEN to be considered as a low AR aircraft in terms of aerodynamic phenomenon, such as the 'wing rocking'.

Table 7.2: SPPO mode parameters

Test	Method	T_{sp} [s]	$\omega_{d_{sp}}$ [Hz]	$\omega_{n_{sp}}$ [Hz]	ζ_{sp} [-]
SP(1)R-PD	PD	3.9	0.26	0.28	0.37
SP(1)R-FS	FS	1.6	N/A	0.63	N/A
SP(1)F	PD	3.7	0.27	0.28	0.30
SP(2)R	PD	3.9	0.26	0.28	0.39
SP(2)F-FS	FS	1.8	N/A	0.56	N/A
SP(2)F-PD	PD	3.7	0.27	0.29	0.33

Definition of damping ζ and natural frequency ω_n

The damping of the oscillations was calculated using the logarithmic decrement method [156]:

$$\zeta = \frac{\Delta}{\sqrt{\Delta^2 + 4\pi^2}}, \quad \text{where} \quad \Delta = \frac{1}{n} \ln \left(\frac{y_i - y_f}{y_{i+n} - y_f} \right)$$

y_i is the amplitude of the first peak, n - number of peaks taken into account and y_f - steady value of the signal after the oscillation was damped out. These parameters are visualised in Fig. 7.4.

The natural frequency of the damped oscillation ω_n was then calculated by the following equation [156]:

$$\omega_n = \frac{\omega_d}{\sqrt{1 - \zeta^2}}, \quad \text{where} \quad \omega_d = \frac{1}{T_d} \quad \text{and} \quad T_d = \frac{t(y_{i+n}) - t(y_i)}{n}$$

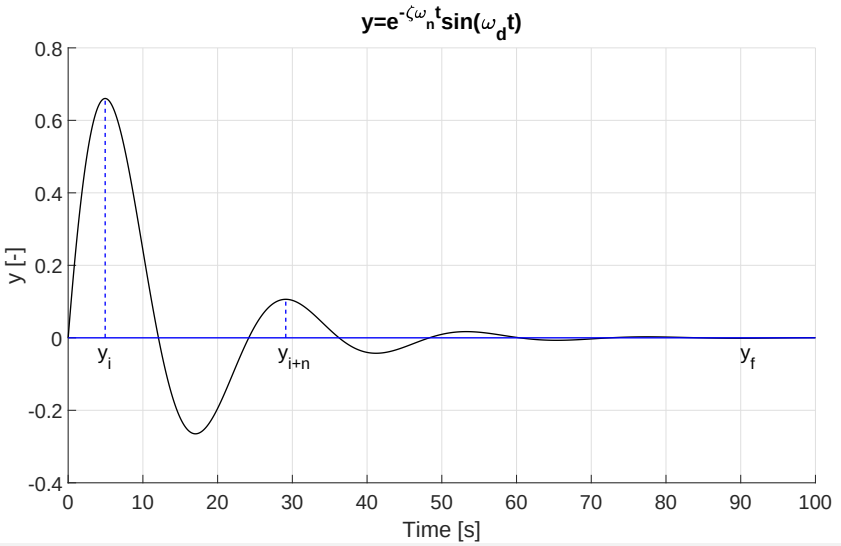

Figure 7.4: Oscillation parameters

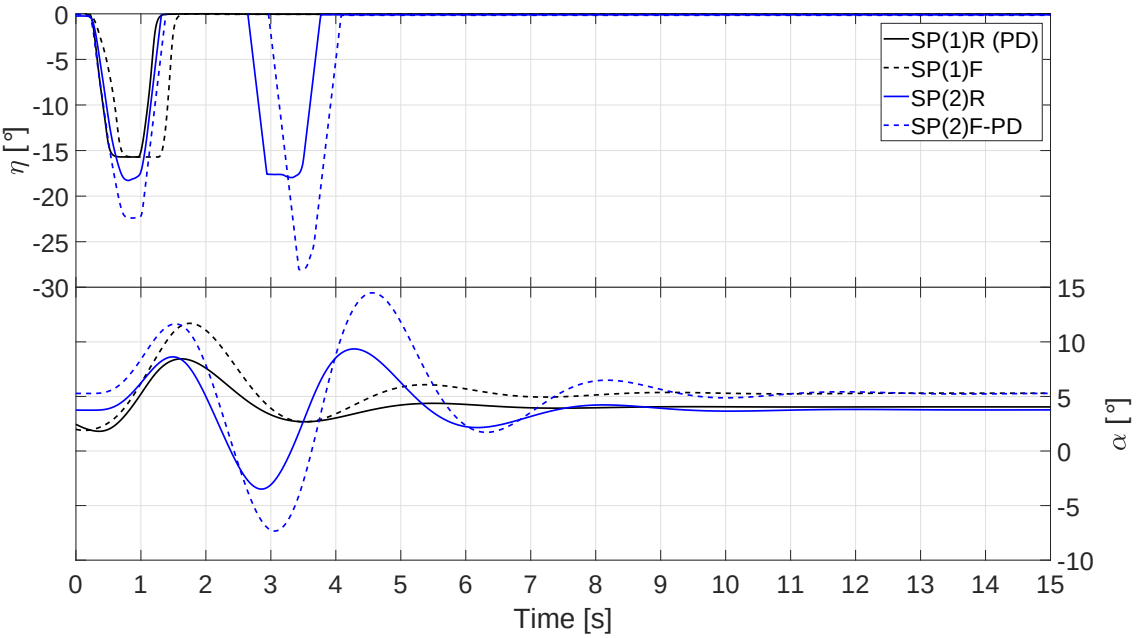

Figure 7.5: Main parameters of the SPPO mode tests using pitch doublet input

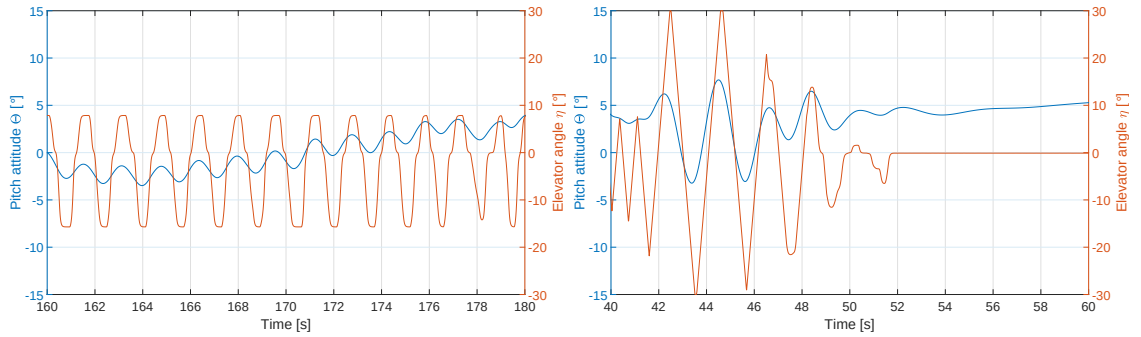

(a) SP(1)R (FS)

(b) SP(2)F-FS

Figure 7.6: Main parameters of the SPPO mode tests using frequency sweep input

Parameters of the SPPO mode from Table 7.2 were compared against the flying qualities requirements, as stated in MIL-F-8785C [95], i.e. the SPPO damping ζ_{sp} and the SPPO frequency $\omega_{n_{sp}}$ and acceleration sensitivity n/α. Results are provided in Table 7.3.

As seen from different requirements (e.g. CS 25 and FAR 25) the damping is the main parameter of concern of the short period mode. CS 25 requirements [57] state that "any short period oscillation ... must be heavily damped". However, no numbers are given to determine how well the oscillation should be damped. This leaves the only possibility to

Table 7.3: SPPO mode levels of flying qualities according to Ref. [95]

Test	ζ_{sp} criterion		$\omega_{n_{sp}}$ & n/α criterion		
	ζ_{sp} [-]	Level	$\omega_{n_{sp}}$ [rad/s]	n/α [g/rad]	Level
SP(1)R (PD)	0.37	1	1.76	4.7	1
SP(1)R (FS)	N/A	N/A	3.96	9.7	1
SP(1)F	0.30	2	1.76	8.8	1
SP(2)R	0.39	1	1.76	6.8	1
SP(2)F-FS	N/A	N/A	3.52	13.9	1
SP(2)F-PD	0.33	2	1.82	15.4	2

assess damping against MIL-F-8785C requirements, as was done in Table 7.3. Results show that the relatively rigid aircraft exhibited higher damping than the flexible one and Pilot 1 assessed both configurations as heavily damped or "deadbeat". The rigid aircraft met Level 1 requirements, while the flexible aircraft met Level 2 requirements. As stated in TABLE IV of Ref. [95], the damping ratio for Level 1 flying qualities should be between 0.35 and 1.30. Thus, the HARTEN aircraft lies within the lower limit of the requirement for Level 1 / Level 2 qualities.

The frequency and acceleration sensitivity analysis showed mostly Level 1 flying qualities, except for the SP(2)F-PD test case, where Level 2 qualities were obtained. The largest difference in $\omega_{n_{sp}}$ appeared between the pitch doublet and the frequency sweep testing techniques. As seen from Tables 7.2 and 7.3, the natural frequencies acquired using the frequency sweep technique were twice higher than using the classical doublet input. Pilot 1 noted that two different periods were "not what one would expect to see". For comparison $\omega_{n_{sp}}$ of B747 was extracted from data in Ref. [157] and was about 0.7-0.8 Hz. Considering it as a realistic test case, one could conclude that the frequency sweep technique leads to more realistic results (0.56-0.63 Hz for HARTEN). However, no significant differences were noticed between rigid and flexible aircraft frequencies using the frequency sweep technique. Pilot 2 also evaluated the flexible aircraft as "qualitatively similar to rigid". On the other hand, the acceleration sensitivity showed significant differences between the two configurations. n/α was about twice larger for the flexible configuration using the pitch doublet input. As the wing of the aircraft becomes more flexible, it tends to deflect more under the same increase of the angle of attack. This means that the structural nodes of the wing develop larger structural accelerations, which in turn result in higher overall body acceleration. The differences in n/α magnitudes of SP(1) and SP(2) test cases are attributed to the maximum elevator deflection angle, which was discussed in Ch. 5. The overall comparison of damping, natural frequency and acceleration sensitivity parameters showed that flying qualities degrade from Level 1 in case of the rigid aircraft to Level 2 in case of the flexible aircraft. Tests were biased by the different experience of Pilots 1 and 2. For example, the more experienced Pilot 2 managed to keep the altitude constant during the test, while the less experienced Pilot 1 let the aircraft drift down. However, it is assumed that the drift down of 1000 ft did not

significantly affect the testing conditions.

From the data above it is clear that the wing flexibility negligibly affects period and frequency of the SPPO mode. However, the flexibility effect was more significantly expressed on the damping of the mode. The natural frequency and acceleration sensitivity analysis showed higher n/α values for the flexible configuration. ζ_{sp} and n/α parameters were mostly affected by the inertia changes in vertical plane, which appeared due to increased wing deformations.

Phugoid mode

Phugoid is another longitudinal mode. Traditionally, its importance to aircraft handling qualities is low. However, the HARTEN aircraft tendency to phugoid was noticed by Pilots 1 and 2 during the previous two tests. According to pilots, the phugoid was the dominant longitudinal mode. Thus, it cannot be neglected and must be well investigated.

Time histories of the phugoid mode tests are provided in Apps. E.6–E.9. Main parameters of the phugoid mode are presented in Table 7.4 and Fig. 7.7.

Table 7.4: Phugoid mode parameters

Test	T_{ph} [s]	$\omega_{d_{ph}}$ [Hz]	$\omega_{n_{ph}}$ [Hz]	ζ_{ph} [-]
PH(1)R	49.7	0.020	0.020	0.031
PH(1)F	55.8	0.018	0.018	0.038
PH(2)R	52.1	0.019	0.019	0.023
PH(2)F	55.5	0.018	0.018	0.029

The drift of altitude from the trim condition of 10000 ft to around 6500 ft at the end of the test was present in PH(1)R test case, as seen in Fig. 7.7. This was induced by the prolonged elevator input η, which was twice longer for PH(1)R test case compared to other cases. Moreover, initial 'nose-down' manoeuvre is not the traditional way to induce the mode. And as it was a prolonged manoeuvre, the flight path line was set to be with a descent angle. Hence, the oscillation appeared along the descending flight path. The elevator input made by Pilot 1 for PH(1)F case was similar to the inputs of Pilot 2 and, thus, the oscillation was along the horizontal flight path.

The data analysis shows that there is no significant difference between the rigid and the flexible aircraft configurations regarding period of the mode. Period of around 50-55 s was within the range defined in Ch. 6. However, the damping of the mode increased by more than 20% for the flexible aircraft. Nonetheless, the damping was very low in both cases - around 2-3% - that was noticed by both pilots. Pilot 1 even noticed during PH(1)R test that the aircraft "started phugoiding without me making an input" - the tendency, which is the outcome of the low damping. ζ_{ph} in the range between 0% and 4% results in Level 2 flying qualities [95].

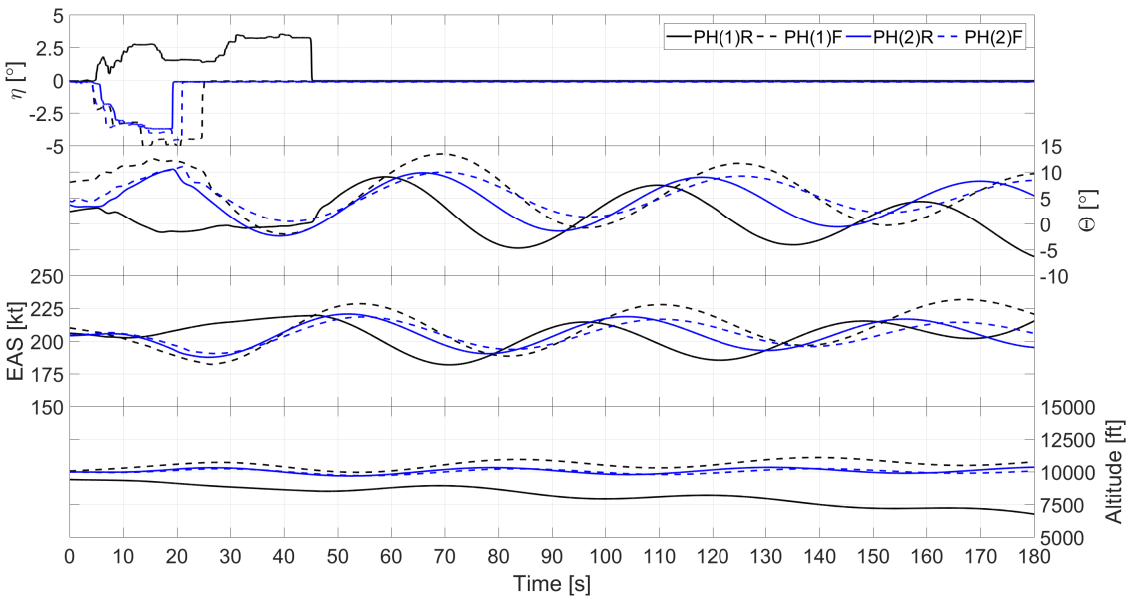

Figure 7.7: Main parameters of the phugoid mode tests using pulse input

Summary of longitudinal dynamics

Rigid aircraft exhibited Level 1 flying qualities regarding the SPPO mode requirements, while the flexible aircraft exhibited Level 2 qualities. Considering the phugoid mode requirements, both rigid and flexible aircraft exhibited Level 2 qualities. The low damping of the phugoid mode and high damping of the SPPO mode made the phugoid dominant longitudinal mode, which was also acknowledged by Pilots 1 and 2.

7.1.3 Lateral/directional dynamics

The lateral/directional dynamics of the HARTEN aircraft were assessed through a series of simulations, which are reviewed below.

Steady heading sideslip

The SHSS test allowed to evaluate the authority of ailerons and rudder. Time histories of SHSS tests are provided in Apps. F.1–F.4. However, only test data generated by Pilot 2 are discussed here to compare dynamics of rigid and flexible aircraft. SH(1) tests were flown with much lower precision, hence it was decided to omit these tests from the further discussion. Main parameters of the SHSS tests are presented in Table 7.5 and Fig. 7.8.

The SHSS was the most difficult test to fly due to the simulator hardware issues, discussed later in the next section. The absence of the slip indicator, too stiff sidestick and too large free play of the pedals were the most significant deficiencies of the simulator, which stopped the pilots from adequately controlling the aircraft in lateral/directional

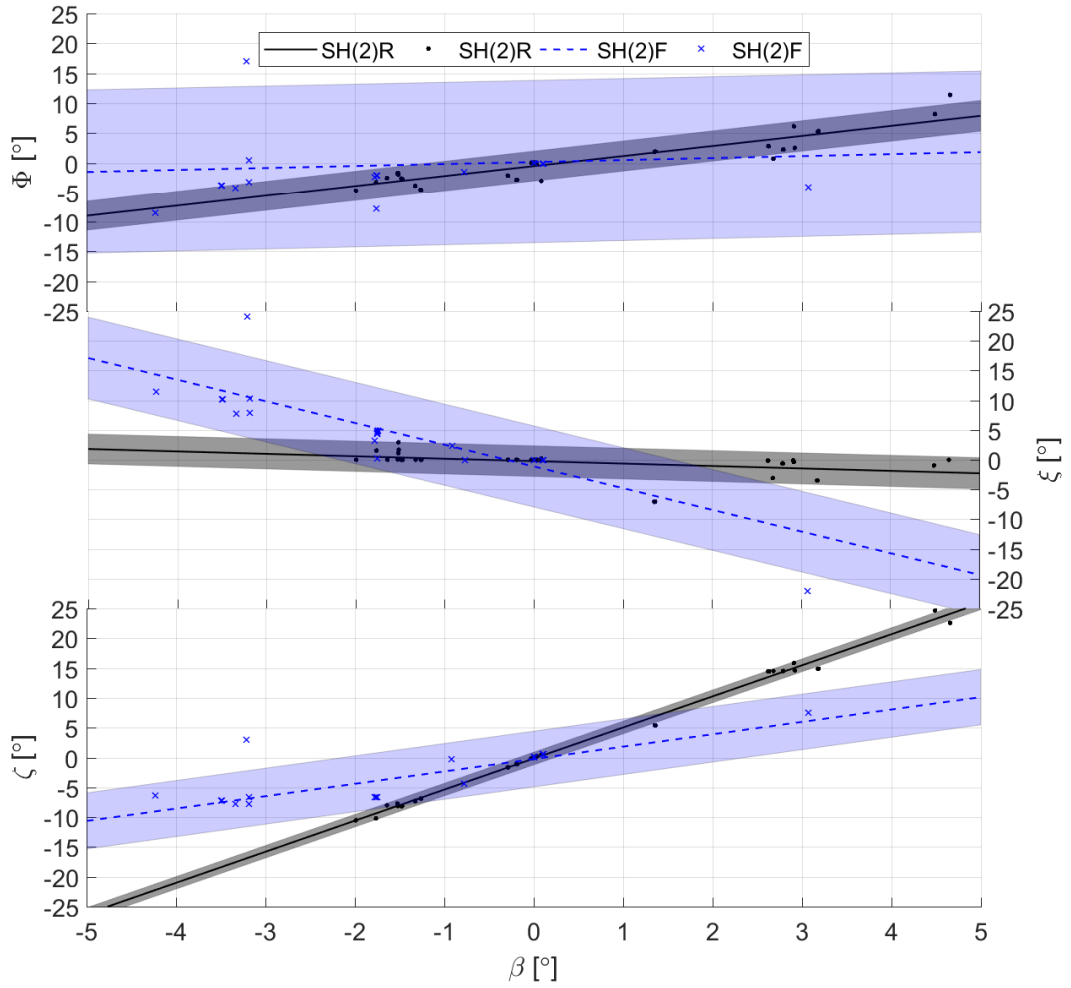

Figure 7.8: Trends (linear fits) of main SHSS test parameters. The shaded areas represent 95% confidence intervals

Table 7.5: Main parameters of the SHSS tests

Test	$d\Phi/d\beta$	$d\xi/d\beta$	$d\zeta/d\beta$
SH(2)R	1.69 ± 0.19	-0.41 ± 0.19	5.21 ± 0.08
SH(2)F	0.33 ± 1.37	-3.65 ± 0.68	2.08 ± 0.47

planes. Nonetheless, the test revealed the differences between rigid and flexible aircraft and they are discussed below.

CS 25.177 states that "in straight, steady, sideslips over the range of sideslip angles appropriate to the operation of the aeroplane, the aileron and rudder control movements and forces must be substantially proportional to the angle of sideslip in a stable sense" [57]. The SHSS test showed the compliance of the HARTEN aircraft with this requirement.

Data points in Fig. 7.8 represent steady heading conditions ($\frac{d\Psi}{dt} = \pm 0.5^\circ/s$, representing half value of the smallest heading reading unit, and $\frac{d^2\Psi}{dt^2} = \pm 0.01^\circ/s^2$, essentially assuring no change in heading) with sideslip induced and maintained by ailerons and the rudder. $\frac{d\zeta}{d\beta}$ must be positive and $\frac{d\xi}{d\beta}$ must be negative for an aircraft to exhibit lateral/directional stability [149]. Common practice also states that $\frac{d\Phi}{d\beta}$ must be positive in case of lateral/directional stability. Both rigid and flexible aircraft configurations met these requirements as seen in Fig. 7.8 and Table 7.5. However, $\frac{d\Phi}{d\beta}$ reduced significantly for the flexible case as "dihedral effect was much stronger" according to Pilot 2. $\frac{d\xi}{d\beta}$ was more negative for the flexible case, meaning that larger ailerons deflection was needed to counteract the sideslip. This does not surprise knowing that the wing was highly deformed and thus the ailerons were less efficient for controlling the bank angle as the flexible aircraft exhibited "very strong lateral stability". The same conclusion could be drawn from the rudder data - less rudder deflection was needed to create the same sideslip in the flexible aircraft case, which was also noted by Pilot 2 as "much rudder authority". It is interesting to notice the asymmetry in the case of flexible aircraft, i.e. zero line crossing points of $\Phi(\beta)$, $\xi(\beta)$ and $\zeta(\beta)$ shifted to positive β values. This asymmetry also supports observations from both test pilots, who were flying the flexible configuration, that the aircraft seemed to be left wing heavy. However, the reasons for this asymmetry to appear were not revealed and it needs further investigation of the components of SFFA. During the SH(2)R test the pilot noted (see Fig. F.11) that "C_{l_β} was low and C_{n_β} was moderate to low".

The statistical analysis of data and their fitting shows higher dispersion of data points for the flexible wing aircraft configuration. The precision of the measurements is relatively low, with only exception being $\frac{d\zeta}{d\beta}$ measurement for the rigid aircraft configuration. This lack of precision is an outcome of previously discussed simulator related issues that deteriorate pilots' capabilities of precise aircraft handling. Although this set of data is of low fidelity, it still provides useful insights into differences between rigid and flexible aircraft dynamics.

As this test was highly biased by deficiencies of the simulator hardware, i.e. inceptors for the lateral/directional dynamics, the issues will be discussed in the next section.

Roll mode and roll performance

The roll mode test allowed to evaluate the roll dynamics of the aircraft. The roll performance test was also carried out together with the roll mode test and revealed differences in lateral dynamics between rigid and flexible aircraft. Time histories of the roll mode tests

are provided in Apps. F.5–F.7. The main parameters of the roll mode tests are presented in Table 7.6 and Fig. 7.9.

Table 7.6: Roll mode parameters

Test	Roll	Φ_{datum} [°]	ξ [°]	p_{max} [°/s]	τ_r [s]	$\tau_{\pm 30^\circ}$
RM(1)F	$L \rightarrow R$	-49.5	-10.9	15.9	0.4	9.0
RM(2)R	$L \rightarrow R$	-30.8	-25.0	30.8	0.5	2.4
RM(2)F	$L \rightarrow R$	-34.5	-25.0	23.4	0.6	5.0
RM(1)F	$R \rightarrow L$	32.1	10.9	-29.8	0.5	Nil
RM(2)R	$R \rightarrow L$	32.2	25.0	-32.8	0.5	2.0
RM(2)F	$R \rightarrow L$	27.9	25.0	-29.8	0.5	5.5

The roll mode time constant was around 0.4-0.5 s for both rigid and flexible aircraft. An aircraft that exhibits τ_r of lower than 1.4 s qualifies for Level 1 flying qualities according to MIL-F-8785C [95]. However, this applied only to rigid aircraft case. The roll performance parameter $\tau_{\pm 30^\circ}$, defined by the time needed to roll the aircraft between two bank angles with opposite signs, showed significant differences between flexible and rigid aircraft. $\tau_{\pm 30^\circ}$ times for all test cases were defined between $\pm 30^\circ$ bank angles. Data from test RM(1)F were ignored for the roll performance test due to the reduced aileron angle limit and thus biased the overall results. The comparison of RM(2)R and RM(2)F tests showed a tendency for $\tau_{\pm 30^\circ}$ to increase more than twice for the flexible aircraft, while τ_r change was negligible. The reason for such a change between rigid and flexible aircraft lateral dynamics was the 'wing ratcheting' phenomenon induced by the increased flexibility and, thus, dihedral of the wing. Both test pilots noted that the 'wing ratcheting' introduced the unpredictability of the aircraft response to an aileron input through the "nonlinear roll" (see Fig. F.21) and "roll pause in the process" (see Fig. F.31). Thus, the 'wing ratcheting' is unwanted feature of the aircraft lateral dynamics as it manifests itself as a pause in the developing bank angle Φ (see Fig. 7.9) while the aileron is still deflected and a continuous increase in bank angle is expected. The phenomenon is seen in Fig. 7.9 for RM(1)F and RM(2)F cases as the roll rate p did not stabilise at some particular value, but rather oscillated between zero and maximum values. As the aircraft oscillated around some average value, thus τ_r may be defined. However, the 'wing ratcheting' phenomenon distorted the evaluation of lateral dynamics by the use of classical method and only roll performance analysis allowed to identify the difference between the rigid and flexible aircraft.

The roll mode and performance test showed that τ_r could not properly define the flexible aircraft roll performance as the time constant for both aircraft configurations was very similar. However, $\tau_{\pm 30^\circ}$ showed significant difference between both configurations. Thus, $\tau_{\pm 30^\circ}$ should be considered as a more appropriate parameter to define the roll dynamics of flexible aircraft.

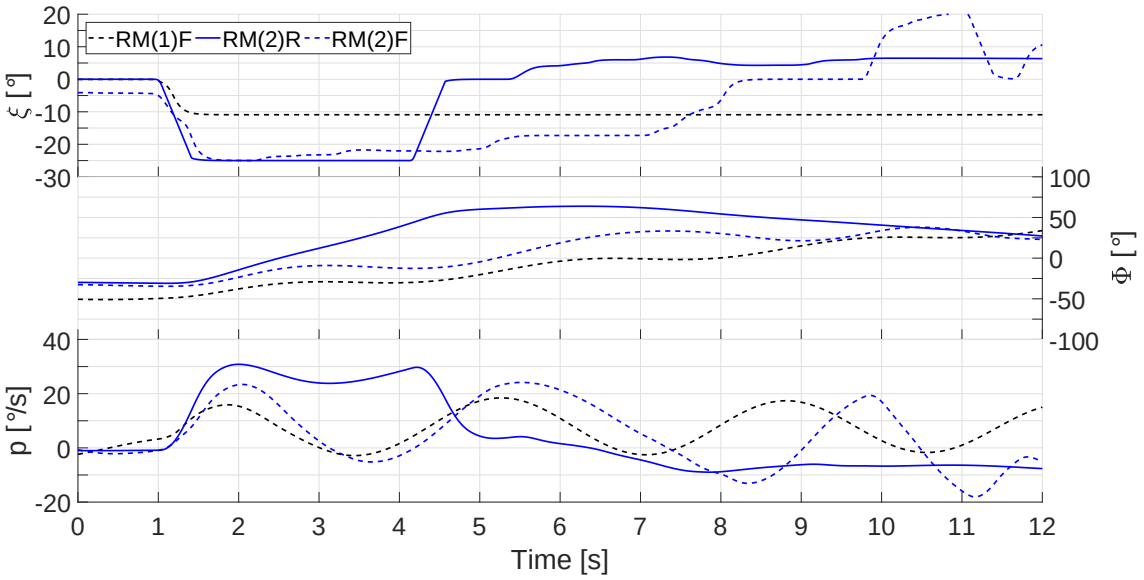

(a) Roll to the right

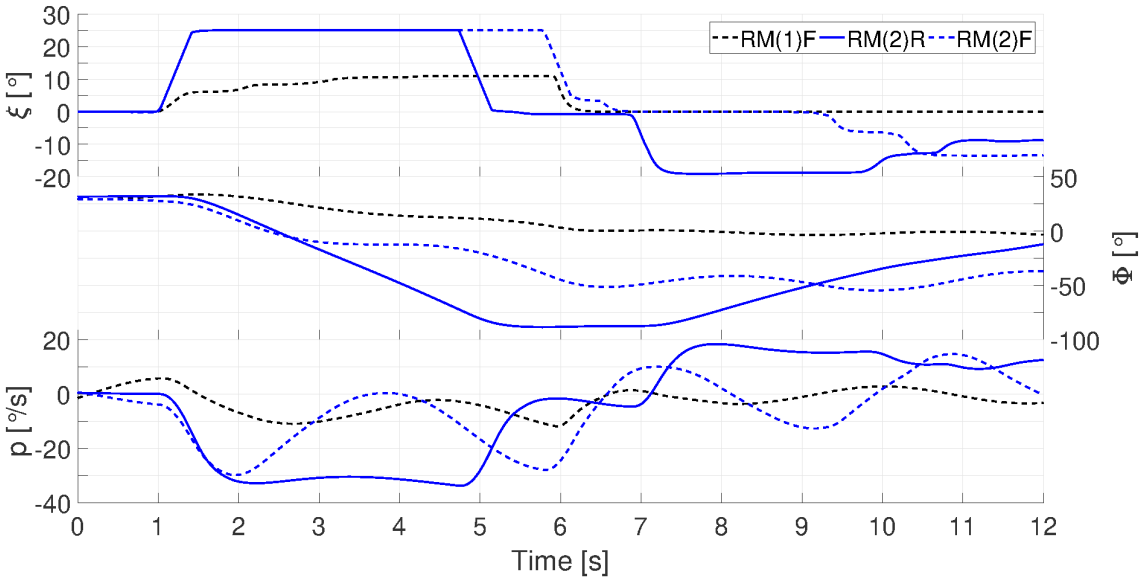

(b) Roll to the left

Figure 7.9: Main parameters for roll mode

From the engineering point of view it is clear from roll tests that the ailerons lose their efficiency due to high wing deformations. Thus, other means of lateral controls should be considered. One of possible solutions for the issue is the use of spoilers rather than ailerons to control the roll - the option that was implemented in Jaguar attack aircraft (according to Pilot 2, who was a test pilot of Jaguars). Hence, this option of lateral controls should also be investigated for very flexible wing aircraft.

Spiral mode

The spiral mode test allowed to evaluate the bank angle stability of the aircraft. Time histories of the spiral mode tests are provided in Apps. F.8–F.10. Main parameters of the spiral mode tests are presented in Table 7.7 and Fig. 7.10.

Table 7.7: Spiral mode parameters

Test	$T_{2_{left}}$ [s]	$T_{2_{right}}$ [s]	Level
SM(1)R	30.1	N/A	1
SM(2)R	32.8	34.4	1
SM(2)F	∞	∞	1

The spiral mode was divergent and its time-to-double amplitude T_2 was between 30 s and 35 s depending on the direction of roll for the rigid aircraft. This value is above 12 s required by MIL-F-8785C [95] to meet Level 1 flying qualities requirements. The spiral mode investigation was initiated at around $\pm 15^\circ$ bank angles. The rigid aircraft reached $\pm 0.6 - 0.8^\circ/s$ roll rate both for left and right spirals. It is interesting to notice that p was higher for the left spiral, thus T_2 was smaller too.

The flexible aircraft exhibited neutral spiral mode stability or the mode was even slightly convergent. However, the time-to-double/half-amplitude parameter was not applicable to this case. As $T_2 \to \infty$ or the mode was convergent Level 1 flying qualities were assigned. Such stability of the spiral mode is a clear evidence of the flexibility effect on wing dihedral, i.e. highly increased wing dihedral transformed the wing into stabilising surface. The roll rate oscillation of around $\pm 1^\circ/s$ seen in Fig. 7.10 showed an average value of $0^\circ/s$.

Slight roll rate oscillation of the rigid aircraft was attributed to the high aspect ratio unswept wing configuration. As seen in Fig. 7.11 the oscillation happened due to coupling between roll rate p and sideslip β. The frequency of both p and β oscillations for rigid and flexible aircraft was around 0.24-0.25 Hz. From Fig. 7.10(b) it is seen that the spiral was entered by the rudder input for the SM(1)R case and by the ailerons input for the SM(2) cases. Comparison of SM(1)R and SM(2)R cases showed higher oscillations of p and β (see Figs. 7.11(a) and 7.11(b)) when the rudder was used to enter the mode. This leads to a concluding remark that C_{l_ζ} is more significant than C_{n_ξ} for the rigid aircraft, which is the influence of a HAR wing. Comparison of rigid and flexible aircraft showed

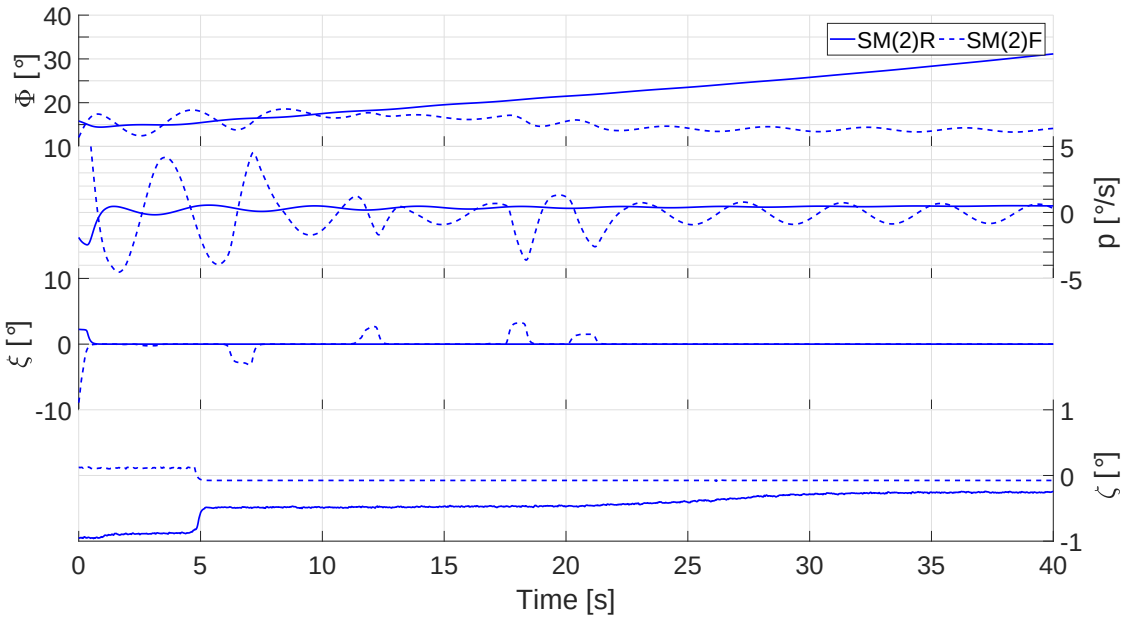

(a) Right spiral

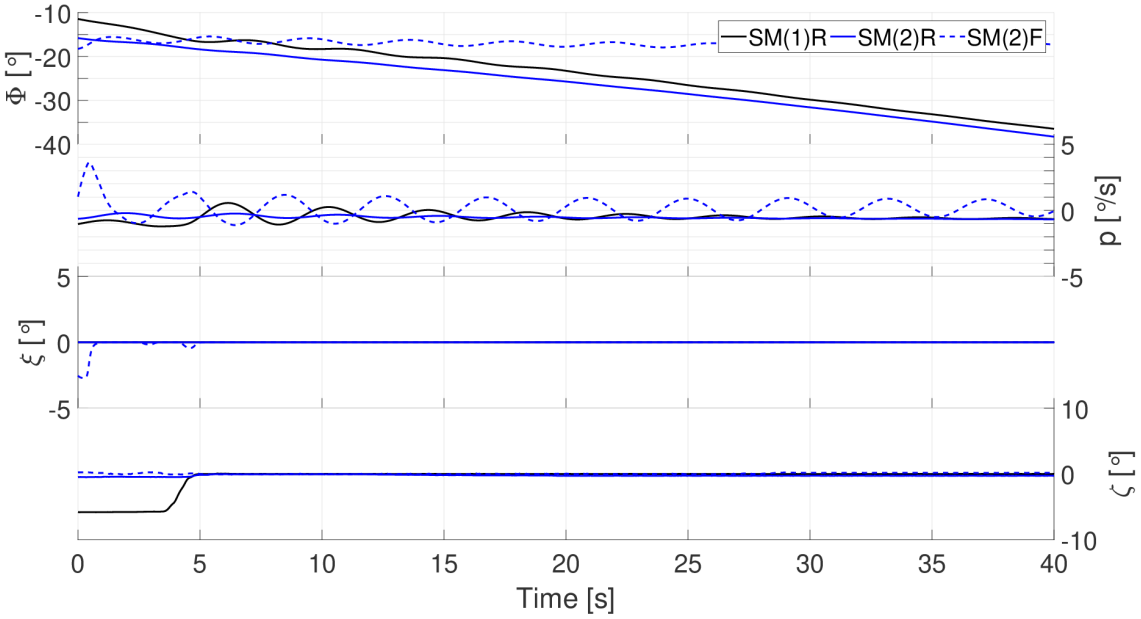

(b) Left spiral

Figure 7.10: Main parameters of the spiral mode

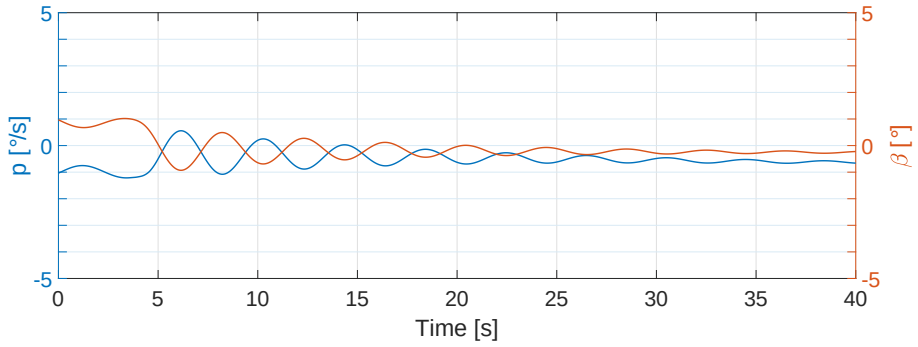

(a) SM(1)R

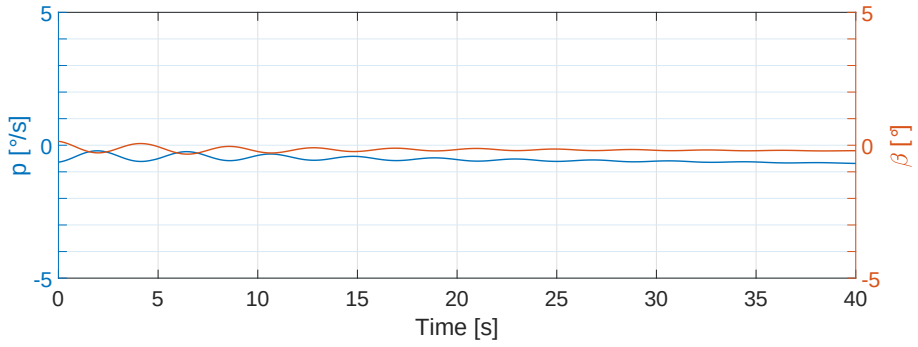

(b) SM(2)R

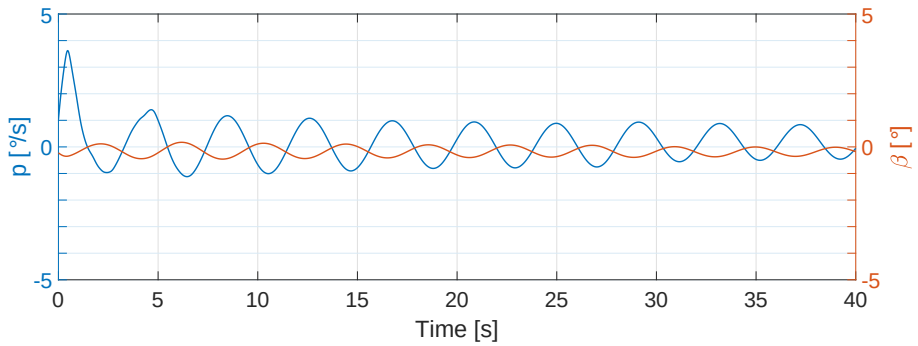

(c) SM(2)F

Figure 7.11: Coupling between the roll rate p and sideslip β

an increase in C_{l_β} for flexible aircraft, which was the effect of increased dihedral due to the wing flexibility.

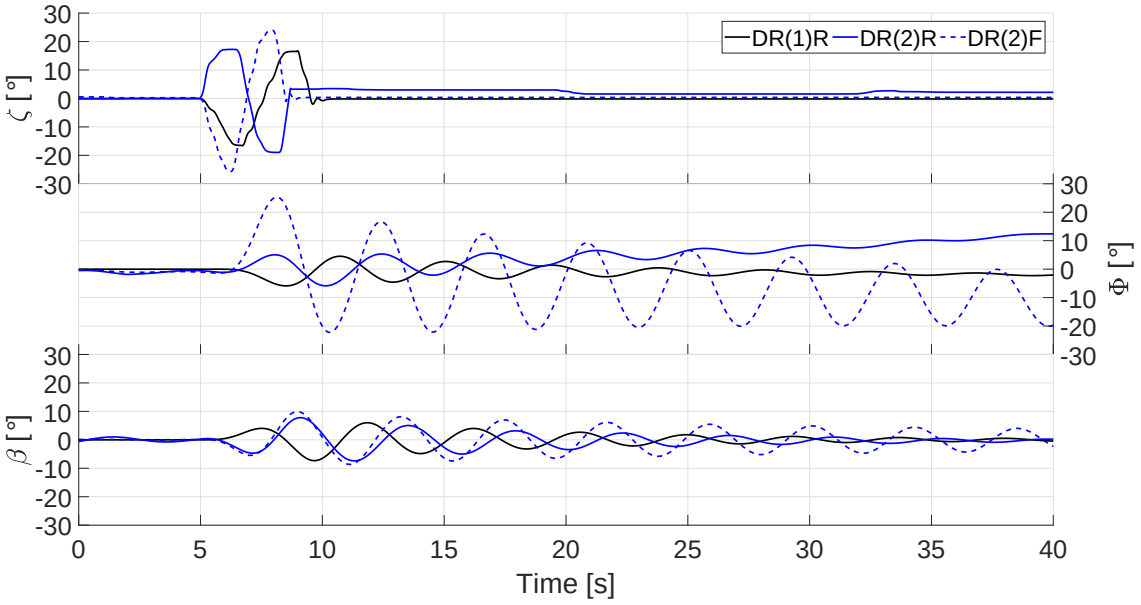

Figure 7.12: Main parameters for Dutch roll mode

Dutch roll mode

The Dutch roll mode test allowed to evaluate the lateral/directional dynamics of the aircraft. Time histories of the Dutch roll mode tests are provided in Apps. F.11–F.13. Main parameters of the Dutch roll mode tests are presented in Table 7.8 and Fig. 7.12.

Table 7.8: Dutch roll parameters

Test	T_{DR} [s]	$\omega_{d_{DR}}$ [Hz]	ζ_{DR} [-]	$\omega_{n_{DR}}$ [Hz]	$\frac{\Delta\Phi}{\Delta\beta}$ [-]
DR(1)R	4.37	0.23	0.06	0.23	2/3
DR(2)R	4.37	0.23	0.06	0.23	2/3
DR(2)F	4.22	0.24	0.02	0.24	9/4

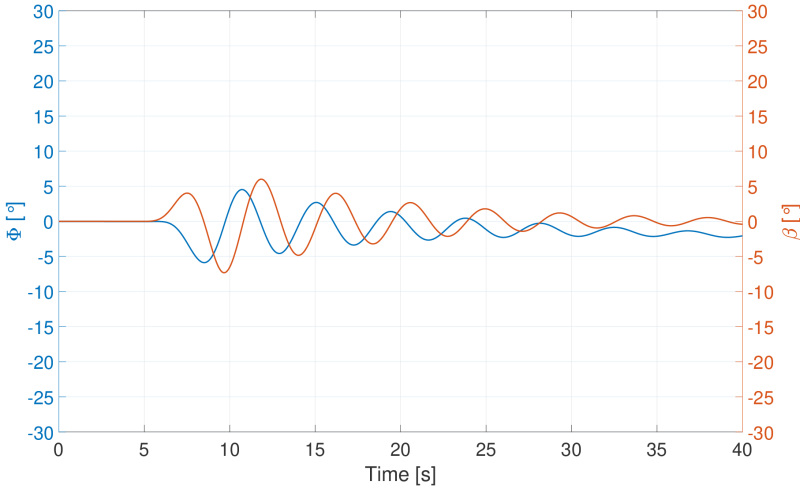

(a) DR(1)R

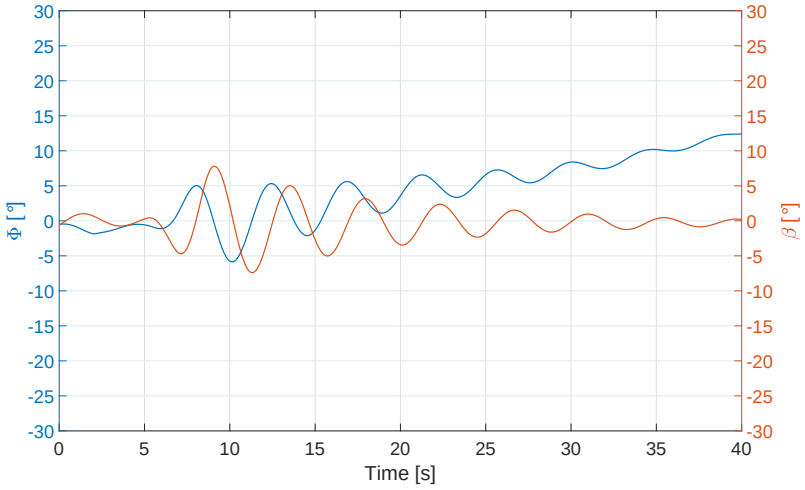

(b) DR(2)R

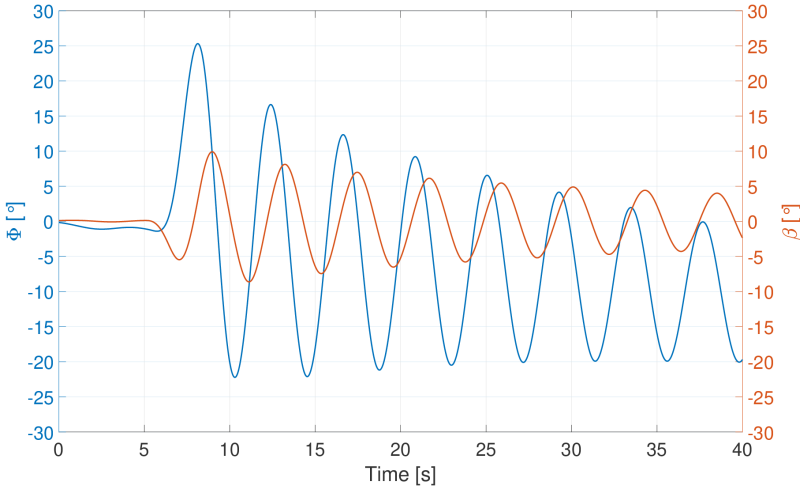

(c) DR(2)F

Figure 7.13: Comparison of Φ and β parameters during Dutch roll mode

The Dutch roll mode was an intrusive dynamic mode in all previous lateral/directional manoeuvres as noted by test pilots. However, this test allowed to quantify the Dutch roll mode in terms of significant parameters, i.e. damping ζ_{DR}, natural frequency $\omega_{n_{DR}}$ and their product $\zeta_{DR}\omega_{n_{DR}}$ according to MIL-F-8785C. Damping of 0.02 for the flexible aircraft and 0.06 for the rigid aircraft put both aircraft configurations under Level 2 requirements. This was also noted by Pilot 1 as a "slightly poorly damped Dutch roll". For the current case to meet Level 1 flying qualities, damping should be higher than 0.19. $\omega_{n_{DR}}$ should be higher than 0.06 Hz for Level 1 - the only requirement that the current aircraft exceeded with 0.23-0.24 Hz natural frequency. $\zeta_{DR}\omega_{n_{DR}}$ values reached 0.014 Hz for the rigid case and 0.005 Hz for the flexible case, which put the rigid aircraft to Level 2 and the flexible aircraft to Level 3. Zero damping is required to meet Level 3 requirements. Data analysis showed that flexibility did not significantly affect the Dutch roll mode frequency.

Figure 7.13 shows another important parameter of the mode - bank angle to sideslip ratio $\frac{\Delta\Phi}{\Delta\beta}$. This parameter allows the pilot to anticipate the behaviour of the aircraft. Usually, the ratio should be 2/3, which would impose the motion of the aircraft nose or wingtip to be of a horizontal ellipse. This, being the classical aircraft response, was also the case for the rigid aircraft. However, for the flexible aircraft 9/4 ratio was recorded, which was not the classical response and, as it was noted by Pilot 2, "a pilot would hate it". This was the case due to increased wing dihedral, which magnified C_{l_β}.

Summary of lateral/directional dynamics

Lateral/directional dynamics of the aircraft were the ones most affected by the increased flexibility of the wing. The roll performance test revealed the 'wing ratcheting' phenomenon that the flexible aircraft experienced. The spiral mode test showed the neutral stability of the flexible aircraft versus the instability for the rigid aircraft, which is the classical aircraft response. The most significant finding, besides the 'wing ratcheting' phenomenon, was a complete change in the Dutch roll dynamics, which altered the motion of the aircraft wingtip from the classical horizontal to the vertical ellipse. All of these changes in dynamics within the flexible aircraft domain were attributed to an increase in the wing dihedral angle.

7.1.4 Slalom task

The slalom test allowed to evaluate the overall dynamic behaviour of the aircraft. Time histories of the slalom tests are provided in Apps. G.1–G.4. CHR scores of the aircraft assigned during the slalom task are presented in Table 7.9.

Table 7.9: CHR scores during the slalom task

Test	SL(2)R	SL(2)F	SL(3)R	SL(3)F
CHR score	long - 2 lat/dir - 5	long - 4 lat/dir - 7	overall - 8	overall - 10

It is vital to discuss the initial pilots' thoughts and insights about the task before beginning more thorough investigation of the slalom test. Pilot 1 refused to fly the task arguing that the deficiencies of SFFA would not allow him to concentrate on assessing the aircraft and thus there was no purpose in flying the task. Pilot 3 assigned overall CHR scores rather than differentiating them between longitudinal and lateral directional. As Pilot 3 had the least experience in handling qualities testing it was an understandable choice by the pilot. Only Pilot 2 agreed both to fly the task and to assign separate CHR scores for longitudinal and lateral/directional handling qualities of the aircraft.

Overall, the rigid aircraft configuration was assigned better CHR scores than the flexible one. Pilot 3 evaluated that the flexible aircraft was not controllable (CHR-10), while the rigid aircraft was controllable, but did not reach adequate performance (8). However, these scores were assigned to overall handling qualities of the aircraft. Assigning CHR scores for longitudinal and lateral/directional handling qualities separately, Pilot 2 evaluated the longitudinal HQs, as seen in Table 7.9, better than the lateral/directional ones. Longitudinal HQs were assessed as desired (2) for the rigid aircraft and adequate (4) for the flexible aircraft. However, lateral/directional HQs were evaluated as only adequate (5) for the rigid case and inadequate (7) for the flexible case. Contrary to Pilot 3 opinion, the controllability of the aircraft was not in question for Pilot 2 as seen from the assigned CHR scores and their definitions from Fig. 2.10. Important to notice here is the fact that Pilot 3 performed exclusively only the slalom task and no other tests, thus the pilot had less structured preparation for the slalom task and less exposure to the deficiencies of the aircraft, which would otherwise be experienced in all previously discussed tests. Such a pilot's exposure to unknown aircraft acted as a surprise factor in the test. Pilot 2 experienced all the deficiencies during the previous tests, thus was more used to the aircraft and it led to higher evaluation of aircraft controllability. Nonetheless, initial assessment of the aircraft as in the case of Pilot 3 is a very important one, as any line pilot from any airline would experience the aircraft with similar preparation as Pilot 3 did without significant initial preparation. According to Pilot 3 assessment of the aircraft HQs, they might cause significant issues for line pilots.

The slalom test revealed most deficiencies of the HARTEN aircraft that were discussed previously. The most significant ones turned out to be the adverse yaw, leading to the Dutch roll, and the 'wing ratcheting', leading to the unpredictability of the roll dynamics. Figure 7.14 shows approximations of the roll rate p and the yaw rate r response to the aileron input during slalom tests, as Ref. [158] states that for the adverse yaw the positive aileron deflection should result in a negative roll and a positive yaw. $p(\xi)$ slopes are negative for both rigid and flexible cases. However, $r(\xi)$ slopes are positive for the

rigid cases, which means that the aircraft tends to turn in opposite direction and is the evidence of the adverse yaw phenomenon. Comparison of the rigid and flexible aircraft configurations revealed that the increased effective dihedral of the wing due to increased flexibility reduced the adverse yaw effect. Also the roll rate reduced more than twice due to reduced aileron efficiency of the deformed wing. According to Pilot 2 the "combination of adverse yaw and Dutch roll" made the "bank angle control most challenging" in the rigid case. Pilot 3 concluded that the "nose was pitching up and down and yawing left and right - it was hard to know what input to make". The flexible aircraft exhibited less adverse yaw, but much of the 'wing rocking', which was experienced and reported by Pilot 3: "A lot of roll oscillations for any lateral control input".

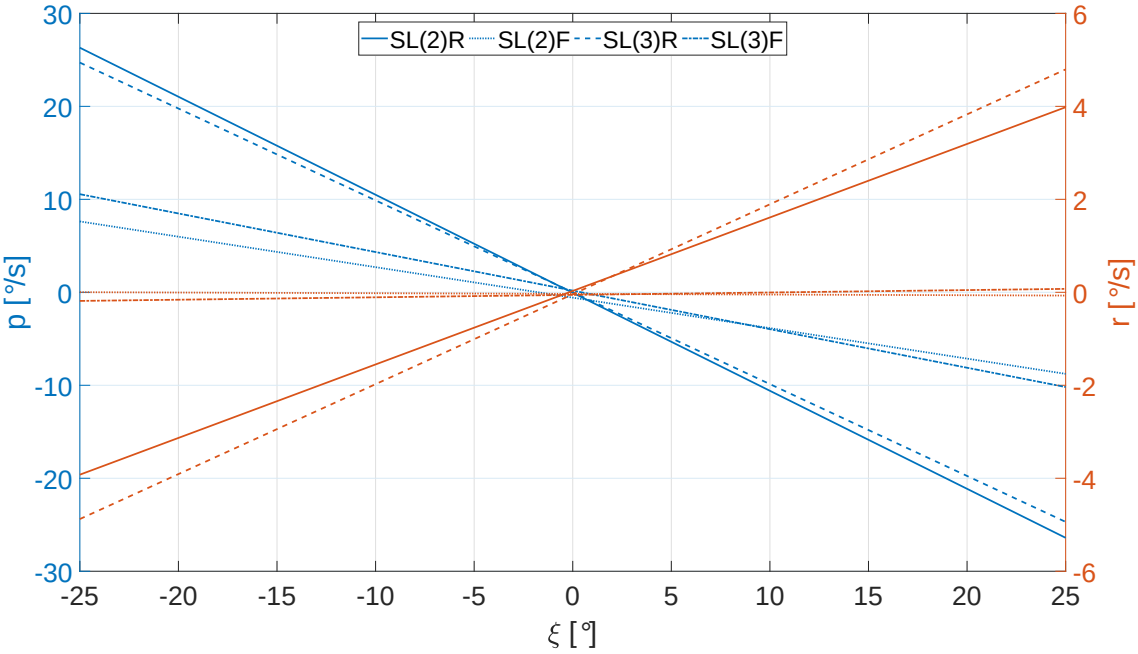

Figure 7.14: Adverse yaw during slalom tests

In summary, the most important outcome from the slalom test is its availability to reveal the dynamics of the tested aircraft. It allowed to expose the pilots along with the aircraft to such flight conditions that the aircraft tendency to phugoid and to Dutch roll was revealed. The 'wing rocking' phenomenon was also noticed along with the poor roll performance due to the 'wing ratcheting'. Moreover, the task also allowed to reveal the deficiencies of the aircraft and the simulator, i.e. too stiff sidestick, lack of friction to throttle inceptor, absence of the slip indicator and motion cues.

7.2 Assessment of SFFA

The testing campaign revealed some deficiencies of the Simulation Framework for Flexible Aircraft. Most of them can only be defined qualitatively rather than quantitatively. These are briefly discussed in this section.

7.2.1 Software

The simulation framework and its limitations were discussed in Ch. 4. However, some of them were signified and new ones were revealed during the testing campaign. The lack of an aerodynamic stall model, no indications of slipping and engine power were the ones noticed during the campaign.

Absence of aerodynamic stall model

The stall test showed one of the most significant limitation of SFFA - the absence of the aerodynamic stall model. Behaviour during the stall must be well understood and investigated for every new configuration of aircraft as the stall is the most critical state of flight and could lead to very dangerous dynamics afterwards. Even more important is the post-stall behaviour of an aircraft. This investigation of the aircraft behaviour cannot be achieved without the proper stall model. Current stall tests showed the rates of descent of 1400-1700 ft/min. Any aerospace engineer would understand that these values are relatively low as the actual RoD values during the stall are much higher, e.g. from 3000 ft/min (Pitts S-2C case) up to 11000 ft/min (AF447 flight case from Ref. [159]). On the other hand, SFFA allows the assessment of the HTP effectiveness and, in case of the elevator limited stall, it allows to assess the sizing of the HTP. Thus, the absence of the stall model in the CA^{2}LM framework prevents it from being used to investigate the pre- and post-stall behaviour of new aircraft configurations, but allows the assessment of the HTP size.

Missing slip indication

The lateral/directional tests revealed the importance of the slip indicator. The most critical test was the steady heading sideslip, where pilots could not estimate whether the sideslip was kept constant or not. Only outside visual references allowed them to assess the trajectory of their flight. Even though the slip indicator does not provide any quantitative data, it allows the pilot to assess the aircraft sidewise response to his/her control input. This understanding of the aircraft dynamics is vital for every pilot as then he/she correlates the control input to aircraft response and the slip indicator acts as a reference.

As shown in Fig. 7.15 the slip indicator is programmed within the primary flight display of the EFS500. However, the required data was not transmitted from the CA^{2}LM framework to the EFS500 and thus there was no indication of slipping on the PFD.

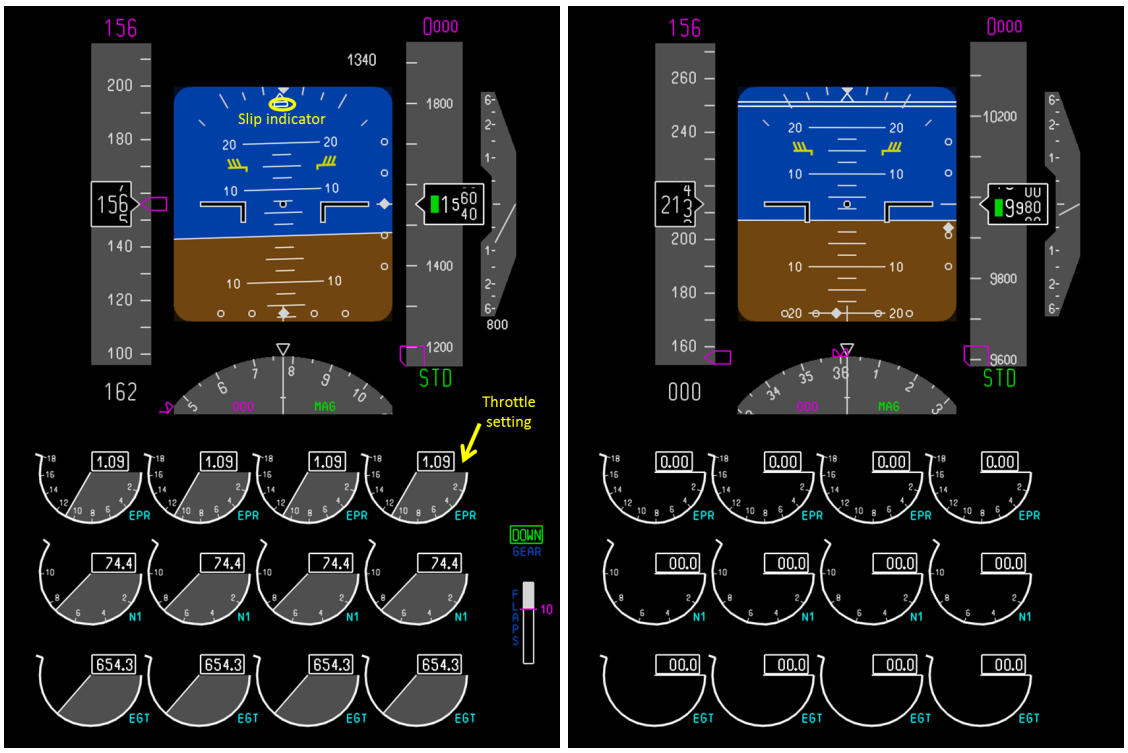

(a) With indications (EFS500 case)

(b) Without indications (SFFA case)

Figure 7.15: Slip and throttle indications on the PFD

Missing engine power indication

The engine power indicators were programmed within the PFD in the EFS500 . However, the engines data flow from the CA^{2}LM framework was not integrated into the SFFA and thus there was no information on engine power settings for the pilots (see Fig. 7.15). This issue along with the lack of friction of the throttle lever made it hard for the pilots to control the thrust and to find the throttle setting for the trim condition.

No longitudinal trimmer

Lack of longitudinal trimmer was a major issue during the flight test campaign. Pilots had to tailor their speed instead of using a longitudinal trimmer. This biased the tests of longitudinal modes as well as made it more difficult to keep the vertical attitude during the lateral/directional tests.

The sidestick that was built into the EFS500 is shown in Fig. 7.16. As seen in the figure the sidestick has no physical trim switch as is the case for all Airbus aircraft. The trim condition is achieved by the auto-trim function and the trim setting of the HTP is

managed by the flight computer in real aircraft and full flight simulators of Airbus aircraft. However, the CA^{2}LM framework does not model the auto-trim function, thus the aircraft can only be trimmed by tailoring the speed. Nonetheless, the trim switch should be installed within the SFFA to relieve the effort of pilots to keep the aircraft in a steady flight. The trim switch would be effortless to implement within the CA^{2}LM framework as the HTP setting angle is one of the trim variables in the trim routine, thus being a direct input to the flight model.

Figure 7.16: The sidestick of the EFS500

7.2.2 Hardware

Sidestick stiffness

The steady heading sideslip test revealed multiple other deficiencies of the SFFA. All pilots reported that sidestick (see Fig. 7.16) was too stiff in lateral motion and pilots were forced to act as almost a “binary system” (according to Pilot 1), i.e. an input was 0 or 1 without possibility to choose intermediate options. The same was noticed by the professional line pilot of Airbus A320/A350, thus supporting the significance of the issue. Too stiff sidestick induced nonlinear behaviour, while the Airbus A320 full flight simulators make use of a linear sidestick loading. This nonlinear behaviour of the sidestick due to too much stiffness prevented the pilots from concentrating on the flying tasks and forced them to give much effort in trying to set some specific sidestick deflection. Pilot 1 described it as “a very uncomfortable condition” as he needed an input of “about 8 pounds right stick to hold it at about 1 mm” deflection to counteract the sideslip. He also noted that “hard gearing combined with high forces on the ailerons made it very hard to balance” the aircraft.

Loose throttle lever

The throttle lever, if not set to its foremost position, would slide aft and thus mislead the pilots. Different thrust setting for the same flight conditions was also the consequence of this issue. As mentioned previously, along with the absence of engine power indication, the pilots did not have any reliable reference for engine settings.

Pedals free play

Pedals' free play was another issue associated with inceptors. It was especially significant for the steady heading sideslip test as only minor rudder inputs were required by pilots. However, test pilots were used to realistic cockpit environments where even small control input produces some aircraft response. It was not the case of the SFFA rudder controls, where small pilot input did not produce any response. This was one of the main issues which prevented the pilots from achieving steady heading sideslip flights, the other one being too large rudder, which was discussed previously.

Central and side sticks

The central stick intervened in the pilot's abilities to choose the inceptor. As the aircraft lateral and longitudinal motions during the test campaign were controlled by sidestick, the presence of the central stick distracted the pilot's attention and sometimes they tried to control the aircraft through the central stick rather than the sidestick.

Motion cues

Another significant deficiency of the simulator is the absence of motion cues. "Feeling no motion cues" resulted in aggressive and unnatural flying according to Pilot 3. This affected the pilot's perception of the aircraft. As mentioned previously the simulator was developed for the engineering and research purposes, thus there was never a goal to implement motion cues.

7.3 Summary of the chapter

7.3.1 Summary of longitudinal and lateral/directional FQs and HQs

The differences between the rigid and flexible aircraft dynamics were investigated during the pilot-in-the-loop flight simulation campaign. Standard flight test techniques were applied to induce longitudinal and lateral/directional dynamics of the aircraft. The stall conditions were assessed at the beginning. The flight controls limited stall was investigated as there was no aerodynamic stall model within the simulation framework. The comparison between rigid and flexible aircraft showed an increase in the stall speed by 4%-9% and in the rate of descent by 6%-14%. An increase in angle of attack was around

7%. The longitudinal dynamics of both configurations were assessed by exciting the short period and the phugoid modes by a pitch doublet input. Both modes were assessed against CS 25 and MIL-F-8785C requirements. The rigid aircraft exhibited higher SPPO mode damping than the flexible one. Thus, the rigid aircraft met Level 1 and the flexible aircraft met Level 2 requirements regarding the damping of SPPO. The frequency criterion did not show any significant difference between the rigid and the flexible configurations, which was also backed up by the pilot's comment that the flexible aircraft was "qualitatively similar to rigid". However, the acceleration sensitivity criterion revealed significant difference between the two configurations, i.e. n/α parameter was around two times larger for the flexible aircraft than for the rigid one. The overall assessment of the SPPO mode showed that the flying qualities tend to degrade from Level 1 for the rigid aircraft to Level 2 for the flexible aircraft. The assessment of the phugoid mode showed that there was an insignificant difference between the periods of the mode. However, the damping showed much higher difference - it increased by more than 20% for the flexible aircraft. The overall damping of both rigid and flexible airframes met Level 2 requirements.

The investigation of the lateral/directional dynamics revealed more significant differences between rigid and flexible aircraft dynamics. The steady heading sideslip test showed reduced lateral/directional stability of the flexible aircraft in terms of the $d\Phi/d\beta$ parameter as the "dihedral effect was much stronger". Larger aileron deflections were needed to counteract the sideslip as the flexible wing was largely deformed and the ailerons lost a significant part of their efficiency as the flexible aircraft exhibited a "very strong lateral stability". On the other hand, less rudder deflection was needed in case of the flexible aircraft to produce the same amount of sideslip as in the rigid aircraft case, thus leading to "much rudder authority". One of the pilots also concluded that "C_{l_β} was low and C_{n_β} was moderate to low". The roll mode test showed the time constant τ_r of approximately 0.4 s for both rigid and flexible aircraft, which met Level 1 requirements. However, the 'wing ratcheting' phenomenon, experienced during the test of the flexible aircraft, was very unpleasant for pilots as it was challenging to anticipate the behaviour of the aircraft as it introduced the "nonlinear roll" response. Thus, the roll performance parameter $\tau_{\pm 30^\circ}$, which considers the time required for the aircraft to bank from -30° to $+30^\circ$, was introduced and revealed significant change due to the increased wing flexibility: while the rigid aircraft required 2-2.5 s to bank, the flexible aircraft required 5-5.5 s. The investigation of the spiral mode revealed the positive side of the increased dihedral effect as the mode, which is usually unstable for classical aircraft, was neutrally stable or even slightly stable for the flexible aircraft. Both rigid and flexible aircraft met Level 1 requirements as the T_2 time constant was 30-35 s for the rigid aircraft and infinite for the flexible aircraft. The Dutch roll mode assessment took into account frequency, damping and their product parameters. Both aircraft configurations met Level 2 requirements when the damping was considered and Level 1 requirements when the frequency was considered. However, the rigid aircraft met Level 2 and the flexible aircraft met only Level 3 requirements, when assessing the aircraft response with respect to the product of the damping and the frequency. One of the most significant findings of the Dutch roll

mode test was the principal change in the dynamics of the mode between the rigid and the flexible aircraft - $\Delta\Phi/\Delta\beta$ for the rigid case was 2/3, while for the flexible case it was 9/4. Thus, the rigid aircraft exhibited a classical horizontal oval motion during the mode, while the flexible aircraft exhibited the vertical oval motion. Such dynamics were evaluated as hard to predict by pilots. However, this opinion was considered to be largely biased by pilots' experience only on classical rigid aircraft. Hence, the lateral/directional tests showed significant changes in the dynamics of the flexible aircraft when high wing deformations are taken into account.

The slalom task was used to assess the difference between the rigid and the flexible aircraft handling qualities and Cooper-Harper Rating scores were assigned during the simulations. Overall, HQs of the flexible aircraft were assessed worse than those of the rigid aircraft and the lateral/directional HQs were assessed worse than the longitudinal. The longitudinal HQs of the rigid aircraft were assessed as good with negligible deficiencies, while of the flexible aircraft were assessed as with minor deficiencies. Lateral/directional HQs were evaluated with moderate deficiencies for the rigid case and with major deficiencies for the flexible case. The 'wing rocking' was present during the simulation of the flexible aircraft along with "a lot of roll oscillations for any lateral control input". The assigned CHR scores highly depended on a pilot's previous flight test experience and the preparation for the flight simulation campaign with the SFFA and the HARTEN aircraft. All the limitations and deficiencies of the SFFA biased the assessment of HQs of aircraft. However, differences between relatively rigid and flexible aircraft, which were identified by pilots previously, could still be identified using the slalom task. Hence, as this simulation campaign was also a first trial of the slalom task, an important conclusion is that the task may be successfully used to reveal deficiencies and assess HQs of new aircraft configurations.

7.3.2 Discussion of SFFA

All of the issues discussed above affected the pilots' perception and abilities to assess the handling qualities. Some of the issues are relatively easy to solve, i.e. data from the CA^{2}LM framework just needs to be transferred to the EFS500 in case of slipping and engine setting indications. Other issues are more complex. Firstly, the aerodynamic stall model should be developed and implemented within the CA^{2}LM framework. It would require additional computational power and thus may slow down the simulation. A thorough analysis of possible stall models and finding the best way to integrate it with the current unsteady aerodynamic model are required to improve the SFFA. Secondly, the current configurations of inceptors caused many issues. The sidestick stiffness, especially in the lateral direction, should be reduced to represent a realistic Airbus cockpit environment. On the other hand the throttle lever friction should be increased to stop the lever from moving by its own from the position set by a pilot. Pedals free play should also be reduced so that every rudder input results in a change of directional equilibrium. It would also allow to reduce the bias, especially when trying to compensate the rudder input by

ailerons. Isolating one of the two control sticks during tests would allow to remove pilot's distraction, which was discussed above. Although it is a minor issue, it would make easier to allocate attention for pilots. Finally, possible options of motion cues should be considered in the future versions of the simulator. It would possibly require redevelopment of the EFS500 architecture, but would allow to bring the simulator to a more realistic environment.

Chapter 8

Conclusions and further work

A review of available literature indicated a knowledge gap in the field of handling qualities of large flexible aircraft. It also indicated a demand for flexible aircraft pilot-in-the-loop simulation and testing capabilities. Thus, an investigation of the structural flexibility impact on the aircraft handling characteristics has been presented in this thesis. The investigation was carried out by simulating the high aspect ratio flexible wing aircraft HARTEN within the Simulation Framework for Flexible Aircraft (SFFA) and performing the pilot-in-the-loop flight simulation campaign with three professional test pilots. Although the SFFA was developed specifically for this simulation campaign, it provides a baseline capability to simulate future conceptual aircraft models. Hence, the flight simulation campaign also allowed a critical assessment of the SFFA and highlighted its main deficiencies. The findings of the simulation campaign and the overall thesis project are summarised in this section. Further research directions are provided at the end of the chapter along with the list of already published articles and papers.

8.1 Conclusions

The investigation of the extended EoM showed notable impact of the additional terms to the dynamics of a flexible aircraft:

- The trim state investigation showed little change between α_{trim} estimated by the classical EoM and the extended EoM. The difference between both EoM cases for the rigid aircraft was around 0.5% and for the flexible aircraft around 1.9%, which suggests that the extended EoM should be used when considering flexible aircraft.

- The lateral/directional dynamics investigation showed significant changes between the classical EoM and the extended EoM, especially when considering the flexible aircraft. The roll acceleration was underpredicted by up to 51.4% by the classical EoM due to higher oscillation damping when the structural motion is not taken into account.

The integration of the extended EoM into the CA^{2}LM framework, its upgrades and further integration with the EFS500 flight simulator led to the development of the Simulation Framework for Flexible Aircraft SFFA:

- A detailed review of the CA^{2}LM framework demonstrated its capability to simulate any flexible or rigid aircraft. The absence of the aerodynamic stall model and the nonlinear structural dynamics model were indicated as the main limiting factors of the framework.

- The development of the SFFA required an integration of the CA^{2}LM framework with the EFS500 flight simulator. The algebraic loops, present in the CA^{2}LM framework, were overcome by using the 'unit delay' blocks in order to accomplish the integration. The Speedgoat real-time machine was also incorporated into the loop to allow the CA^{2}LM framework to run in real time.

Two versions of the HARTEN aircraft, i.e. the rigid and the flexible, were then programmed into the SFFA and a brief investigation of the aircraft was performed:

- The HARTEN aircraft exhibited unusually aft neutral point position of 90%-95% for the rigid configuration and 103%-111% for the flexible configuration. The analysis showed that the potential reason for such a case was the oversize of the HTP, which was also confirmed by comparing its volume ratio to the classical values.

- The oversize of the HTP and the VTP also potentially led to the oversize of the corresponding control surfaces, i.e. the elevator and the rudder. Both points indicate potential deficiencies in the design procedure, used to size the empennage, which also lead to mass penalties.

The HARTEN aircraft was then presented to three professional test pilots, who performed the pilot-in-the-loop assessment of the aircraft, the comparison between FQs and HQs of its rigid and flexible configurations. The most significant findings of this simulation campaign are:

- The stall speed is higher for the flexible aircraft as the loss of the lift due to the wing bending must be compensated by the higher flight velocity. It was shown that V_S increased by around 4%-9%.

- The damping of the longitudinal dynamic modes decreased for the flexible aircraft due to increased structural motion, which degraded FQs and HQs. However, the frequency of the longitudinal modes was not affected by the increased wing flexibility as the fuselage was kept rigid.

- The longitudinal/directional modes were significantly affected by the highly increased wing dihedral angle for the more flexible wing. The roll mode investigation provided evidence of the roll time constant τ_r inapplicability for the flexible

wing aircraft assessment as the aircraft was subject to the 'wing ratcheting' phenomenon. Hence, the other time constant $\tau_{\pm 30^\circ}$, which defines the time needed to bank an aircraft from -30° to $+30^\circ$, was proposed as a potential solution for flexible configurations. The spiral mode, unstable for the rigid aircraft, exhibited neutral stability in case of the flexible aircraft. The Dutch roll mode showed the classical yaw dominated motion for the rigid aircraft. However, the roll dominated motion of the mode appeared for the flexible aircraft, which is a significant change of aircraft dynamics. The flexible aircraft also exhibited significantly decreased damping of the Dutch roll oscillation.

- The slalom task revealed the degradation of the flexible aircraft HQs compared to the rigid aircraft.

The slalom task also provided evidence of being a potentially more efficient way to assess the handling qualities as it revealed both the 'wing ratcheting' and the 'wing rocking' phenomena. The SFFA was also assessed during the simulation campaign:

- The simulation campaign provided evidence of the SFFA capability to assess the FQs and HQs of new aircraft configurations. The SFFA was evaluated positively by the pilots as a baseline capability for the potential use for assessing future aircraft concepts.
- The absence of the aerodynamic stall model prevented a realistic aircraft behaviour at high angles of attack and full assessment of its stall characteristics.
- The absence of the slip and the engine power indications made it hard for the pilots to define the setting of the aircraft configuration.
- The aircraft control settings were also significantly affected by too stiff sidestick, too loose throttle lever and too large pedals free play.
- The absence of the motion cues resulted in potentially more aggressive and unnatural flying.

8.2 Further work

8.2.1 Handling qualities of flexible aircraft

The research of the large wing deformations on handling qualities of aircraft was initiated in this thesis. However, mainly due to the previously discussed limitations of the CA^{2}LM framework, only qualitative rather than quantitative assessment could be made. Moreover, pilots' opinion on HQs was biased by the deficiencies of the EFS500 flight simulator. Thus, after the improvements to SFFA, the investigation of HQs of flexible aircraft could be expanded.

Firstly, appropriate flight dynamic parameters should be identified to quantify the lateral/directional dynamics. As it was noticed, the roll time constant τ_r showed acceptable values for the flexible case. However, due to the 'wing ratcheting' phenomenon, the pilots assessed the roll dynamics as hardly predictable. Thus, the need for new parameters of roll and yaw dynamics assessment is clear.

Secondly, the correlation of pilots' opinion with the flight dynamic parameters should be made for the lateral/directional dynamics. The Gibson Dropback criterion along with the boundaries from the flight tests provided by Mooij, correlates pilots' opinion and flight dynamic parameters for the longitudinal dynamics. Similar correlation should be done for both lateral and directional dynamics as they are highly affected by the aircraft wing flexibility.

EBMM, discussed in the literature review, showed its applicability to quantify the longitudinal dynamics. The investigation of its applicability for the lateral/directional dynamics should be carried out. It could be used as a potential parameter to define the lateral/directional dynamics of a flexible aircraft.

Finally, the application boundaries of the slalom task should be defined, as the task looks promising HQs evaluation technique. It was successfully tested during the flight simulation campaign. However, its suitability for small/medium/large aircraft should be investigated along with proposing the guidance on choosing the sizing parameters of the task elements.

8.2.2 Simulation Framework for Flexible Aircraft

As discussed in this thesis, limitations and deficiencies of the SFFA limit pilots' capabilities to assess HQs of tested aircraft. In order to have the framework that would allow simulating flexible aircraft and their dynamics the following upgrades should be done for SFFA.

Firstly, the nonlinear structural dynamics model should be implemented in the CA^{2}LM framework. The absence of it prevents the framework of being used to quantify any kind of aircraft dynamics arising due to its structural flexibility. It was discussed in the literature review that the linear structural model, currently implemented in the CA^{2}LM framework, cannot capture the same dynamics as the nonlinear model. Thus, as the extended EoM take into account structural deformations directly, flight dynamic effects due to structural flexibility cannot be captured too. Hence, the implementation of the nonlinear structural model is the vital task in order to carry out the research of the flexible aircraft in the future. Although the application of the nonlinear structural dynamics model is of the highest significance, the higher order interpolation schemes for transferring forces and moments between aerodynamic and structural frames should be also considered. Their influence on the resultant aeroelastic behaviour should also be evaluated.

Secondly, the aerodynamic stall model should be developed for the CA^{2}LM framework. Absence of it prevents an aircraft to be tested at the flight envelope part of low velocities. However, this part of the flight envelope is vital as many of critical velocities

are defined according to it. Hence, the implementation of the aerodynamic stall model should be among the highest priority tasks.

Another issue of the CA^{2}LM framework is its inability to rapidly change aerofoils. Usually the implementation of new aircraft configurations means implementation of new aerofoils. However, considering the complexity of the aerodynamic model and amount of data required for it, the tool to generate all the required aerodynamic data for aerofoils should be developed within the CA^{2}LM framework. It is not the highest priority task, but it is required in order to increase the versatility of the framework.

Another component of the SFFA - the EFS500 flight simulator - needs many improvements too. However, they are related more to pilots' convenience to fly rather than aircraft dynamics modelling and are not as significant as improvements discussed above. Many of them are already programmed in the flight simulator and only need changes of the CA^{2}LM-EFS500 interface file. Hence, the slip and thrust data should be transferred from the CA^{2}LM framework to the EFS500 system and displayed on the EFIS screen.

The discussion of the flight simulation campaign revealed many deficiencies of the EFS500 hardware. The throttle lever friction should be increased, so that the inceptor would maintain its set position and a pilot would not need to concentrate on keeping the thrust setting by hand. Secondly, the sidestick should be relaxed, as it was noted during the campaign that it was very stiff and effectively forced the pilot to operate as a binary system. Finally, the free play of pedals should be reduced so that the rudder could be controlled more precisely.

8.3 Contribution to knowledge

This thesis contributed to knowledge in the following aspects:

1. The assessment of flying and handling qualities of the flexible aircraft by carrying out the pilot-in-the-loop simulations for the rigid and flexible aircraft. The comparison between the two revealed significant differences in the lateral/directional dynamics.

2. The development of the Simulation Framework for Flexible Aircraft. It is a new element of the initial aircraft design process that allows pilot-in-the-loop testing of new rigid/flexible aircraft configurations. Changes made to the CA^{2}LM framework also allow rapid implementation of any fixed-wing aircraft configuration.

3. The derivation and investigation of the extended flight dynamic equations of motion for flexible aircraft. It was shown that significant differences in the lateral/directional aircraft dynamics appear when the structural flexibility is taken into consideration within the extended EoM. It showed an increasing importance of the extended EoM for modelling higher flexibility aircraft.

4. A study of the SFFA framework. The pilot-in-the-loop simulation campaign and comments from pilots revealed many software and hardware deficiencies and limitations. They also provided insights into their impact on pilots' capabilities to assess simulated aircraft. Knowing these deficiencies and limitations allows to improve the SFFA.

5. The development of the slalom task. The new task allows an efficient rapid longitudinal and lateral/directional handling qualities testing.

8.4 Dissemination of results

8.4.1 Technical presentations

Modelling framework for flight dynamics of flexible aircraft
Airbus DiPaRT 2016 Meeting
The Centre for Modelling & Simulation (CFMS), Bristol, November 2016

Development and analysis of equations of motion for a flexible aircraft
XIII conference "Aviation 2017"
Antanas Gustaitis' Aviation Institute, Vilnius, Lithuania, April 2017

Pilot-in-the-loop simulation of flexible aircraft in MATLAB/Simulink: implementation & coding peculiarities
Airbus DiPaRT 2017 Meeting
The Centre for Modelling & Simulation (CFMS), Bristol, November 2017

8.4.2 Conference papers

Modelling framework for handling qualities analysis of flexible aircraft
AIAA Modeling and Simulation Technologies Conference, January 2017
Accurate prediction of interactions between aeroelasticity effects, flight control and flight dynamics are critical for the evaluation of handling qualities for future aircraft concepts. A simulation framework for such analyses, known as CA^{2}LM, is presented in this paper together with the modelling techniques and methods used to develop the framework. Aerodynamic surfaces were modelled using the Modified Strip Theory (MST) approach and a state-space representation of the Leishman-Beddoes unsteady aerodynamics model. A modal approach allows the analysis of structural flexibility and each mode's influence on structural deflections. The derivation of equations of motion that provide a new approach to modelling flexible aircraft is presented. This takes into account the variations in mass and inertia properties due to structural deformations. The AX-1 generic large transport aircraft model is analysed as an example of the CA^{2}LM framework capabilities. Results show that according to the Gibson Dropback Criterion longitudinal handling

qualities of the AX-1 with no flight control system are unsatisfactory. The analysis of the structural stiffness influence shows that increasing flexibility of an aircraft structure deteriorates the longitudinal handling qualities. The short-period damping ratio is within Level 2 acceptability requirements. In contrast, the short-period frequency and acceleration sensitivity graph shows that the AX-1 model handling qualities are within Level 1 acceptability requirements. Finally, steps towards the future development of the CA^{2}LM framework are listed.

Pilot-in-the-loop simulation of flexible aircraft in MATLAB/Simulink: implementation and coding peculiarities
AIAA Modeling and Simulation Technologies Conference, January 2018
Integration of flight dynamic models, developed in the MATLAB/Simulink environment, with an engineering flight simulation platform allows rapid pilot-in-the-loop evaluation of new aircraft concepts at early stages of design. This paper aims to provide an overview of the integration activities needed to develop an engineering flight simulator capable of providing means to assess future concept aircraft, such as high aspect ratio wing configurations, where aeroelastic effects have a significant impact on rigid body flight dynamics. Details of the approach used to integrate an aeroelastic simulation framework with an engineering flight simulator are presented. The challenges of obtaining a real-time simulation capability and coding peculiarities of this approach are discussed. The paper expands on the discussion of integration and coding, and provides an example that demonstrates capabilities of such a framework for handling qualities assessment of a high aspect ratio wing aircraft.

Co-authored conference papers

Comparison of reduced order aerodynamic models and RANS simulations for whole aircraft aerodynamics
AIAA Atmospheric Flight Mechanics Conference, January 2018

Method to assess lateral handling qualities of aircraft with wingtip morphing
AIAA Atmospheric Flight Mechanics Conference, January 2018

8.4.3 Journal articles

Modelling framework for flight dynamics of flexible aircraft
Aviation, October 2016
The flight dynamics and handling qualities of any flexible aircraft can be analysed within the Cranfield Aircraft Accelerated Loads Model (CA^{2}LM) framework. The modelling techniques and methods used to develop the framework are presented. The aerodynamic surfaces were modelled using the Modified Strip Theory (MST) and a state-space repre-

sentation to model unsteady aerodynamics. With a modal approach, the structural flexibility and each mode's influence on the structure deflections are analysed. To supplement the general overview of the framework equations of motion, models of atmosphere, gravity, fuselage and engines are introduced. The AX-1 general transport aircraft model is analysed as an example of the CA^{2}LM framework capabilities. The results showed that, according to the Gibson Dropback criterion, the aircraft with no control system lacks the stability and its longitudinal handling qualities are unsatisfactory. Finally, the steps for future developments of the CA^{2}LM framework are listed within conclusions.

Co-authored journal article

Verification of a reduced order aeroservoelastic framework through RANS simulations (submitted on 17 April 2018)
CEAS Aeronautical Journal

References

[1] Anonymous. Aviation: Benefits beyond borders. Technical report, Air Transport Action Group, Geneva, Switzerland, July 2016.

[2] Anonymous. Aviation benefits. Technical report, Industry High Level Group, Montreal, Canada, 2017.

[3] Anonymous. IATA technology roadmap. Technical report, International Air Transport Association, Montreal, Canada, June 2013.

[4] Jeff Tollefson. UN agency proposes greenhouse-gas standard for aircraft. *Nature*, 530(7590):266–266, February 2016.

[5] Adel Abbas, Javier de Vicente, and Eusebio Valero. Aerodynamic technologies to improve aircraft performance. *Aerospace Science and Technology*, 28(1):100–132, July 2013.

[6] Daniel P. Raymer. *Aircraft Design: A Conceptual Approach*. American Institute of Aeronautics and Astronautics, Reston, VA, 4th edition, 2006.

[7] Leland M. Nicolai and Grant Carichner. Static stability and control. In *Fundamentals of Aircraft and Airship Design*, pages 575–600. American Institute of Aeronautics and Astronautics, Reston, VA, 2010.

[8] Demetrios Kellari, Edward F. Crawley, and Bruce G. Cameron. Architectural decisions in commercial aircraft from the DC-3 to the 787. *Journal of Aircraft*, 55(2):792–804, March 2018.

[9] Martin R. Waszak and David K. Schmidt. Flight dynamics of aeroelastic vehicles. *Journal of Aircraft*, 25(6):563–571, June 1988.

[10] Edmund J. Field and Ken F. Rossitto. Approach and landing longitudinal flying qualities for large transports based on in-flight results. In *24th Atmospheric Flight Mechanics Conference*, Portland, OR, August 1999. American Institute of Aeronautics and Astronautics.

[11] Herman J. Damveld. *A Cybernetic Approach to Assess the Longitudinal Handling Qualities of Aeroelastic Aircraft*. PhD thesis, Delft University of Technology, Delft, Netherlands, May 2009.

[12] Stuart P. Andrews. *Modelling and Simulation of Flexible Aircraft: Handling Qualities with Active Load Control*. PhD thesis, Cranfield University, Cranfield, UK, March 2011.

[13] Martin R. Waszak, John B. Davidson, and David K. Schmidt. A simulation study of the flight dynamics of elastic aircraft. Technical Report NASA CR-4102, NASA Langley Research Center, Hampton, VA, December 1987.

[14] Thomas E. Noll, John M. Brown, Marla E. Perez-Davis, Stephen D. Ishmael, Geary C. Tiffany, and Matthew Gaier. Helios mishap investigation report. Technical report, NASA, January 2004.

[15] Jonathan E. Cooper, Mark H. Lowenberg, Mohammad M. Lone, Kevin Garry, Alastair K. Cooke, and Etienne Coetzee. High Aspect Ratio Technology Enablers - HARTEn. Research proposal, Airbus, University of Bristol, Cranfield University, February 2014.

[16] Ludwig Prandtl. Tragflügeltheorie. I. Mitteilung. *Nachrichten von der Gesellschaft der Wissenschaften zu Göttingen – Mathematisch-Physikalische Klasse*, pages 451–477, 1918.

[17] Mark D. Maughmer. The evolution of sailplane wing design. In *AIAA International Air and Space Symposium and Exposition: The Next 100 Years*, Dayton, OH, July 2003. American Institute of Aeronautics and Astronautics.

[18] V. K. Jakubov. Influence of elastic wing-twisting on certain characteristics of longitudinal stability and controllability of a glider. In *10th OSTIV Congress*, South Cerney, UK, June 1965. OSTIV Publications.

[19] Fred Thomas. *Fundamentals of Sailplane Design*. College Park Press, College Park, MD, 3rd edition, 1999.

[20] Piero Morelli. On the dynamic longitudinal stability of sailplanes with fixed and free controls. In *8th OSTIV Congress*, Cologne, Germany, June 1960. OSTIV Publications.

[21] Joosung J. Lee. Historical and future trends in aircraft performance, cost, and emissions. Master's thesis, Massachusetts Institute of Technology, Cambridge, MA, September 2000.

[22] Ger J. J. Ruijgrok. *Elements of Airplane Performance*. VSSD, Delft, Netherlands, 2nd edition, 2009.

[23] Tom Dodt. Introducing the 787. In *ISASI 2011*, Salt Lake City, UT, September 2011. International Society of Air Safety Investigators.

[24] Marty K. Bradley, Christopher K. Droney, and Timothy J. Allen. Subsonic Ultra Green Aircraft Research phase II: Volume I – truss braced wing design exploration. Technical Report NASA/CR-2015-218704/Volume I, NASA, Washington, DC, January 2015.

[25] Robert F. Stengel. *Flight Dynamics*. Princeton University Press, Princeton, NJ, 2004.

[26] Michael V. Cook. *Flight Dynamics Principles: A Linear Systems Approach to Aircraft Stability and Control*. Butterworth-Heinemann, Amsterdam, Netherlands, 3rd edition, 2013.

[27] William S. Hemp. Note on the dynamics of a slightly deformable body. Technical Report 5, College of Aeronautics, Cranfield, UK, February 1947.

[28] Ronald D. Milne. Dynamics of the deformable aeroplane. Technical Report R. & M. No. 3345, Aeronautical Research Council, London, UK, 1964.

[29] B. Fraeijs De Veubeke. The dynamics of flexible bodies. *International Journal of Engineering Science*, 14(10):895–913, January 1976.

[30] Patrick Hamill. *A Student's Guide to Lagrangians and Hamiltonians*. Cambridge University Press, Cambridge, UK, 2014.

[31] Joseph R. Canavin and Peter W. Likins. Floating reference frames for flexible spacecraft. *Journal of Spacecraft and Rockets*, 14(12):724–732, December 1977.

[32] Firdaus E. Udwadia and Robert E. Kalaba. A new perspective on constrained motion. *Proceedings: Mathematical and Physical Sciences*, 439(1906):407–410, November 1992.

[33] Firdaus E. Udwadia and Robert E. Kalaba. On the foundations of analytical dynamics. *International Journal of Non-Linear Mechanics*, 37(6):1079–1090, September 2002.

[34] Firdaus E. Udwadia and Phailaung Phohomsiri. Explicit equations of motion for constrained mechanical systems with singular mass matrices and applications to multi-body dynamics. *Proceedings of the Royal Society A: Mathematical, Physical and Engineering Sciences*, 462(2071):2097–2117, July 2006.

[35] Firdaus E. Udwadia and Robert E. Kalaba. *Analytical Dynamics: A New Approach*. Cambridge University Press, Cambridge, UK, 2008.

[36] Firdaus E. Udwadia and Aaron D. Schutte. Equations of motion for general constrained systems in Lagrangian mechanics. *Acta Mechanica*, 213(1-2):111–129, August 2010.

[37] Leonard Meirovitch and Ilhan Tuzcu. The lure of the mean axes. *Journal of Applied Mechanics*, 74(3):497–504, 2007.

[38] David K. Schmidt. Discussion: "The Lure of the Mean Axes" (Meirovitch, L., and Tuzcu, I., ASME J. Appl. Mech., 74(3), pp. 497–504). *Journal of Applied Mechanics*, 82(12):125501, October 2015.

[39] Sally A. Keyes, Peter J. Seiler, and David K. Schmidt. A Newtonian development of the mean-axis equations of motion for flexible aircraft. In *AIAA Atmospheric Flight Mechanics Conference*, Grapevine, TX, January 2017. American Institute of Aeronautics and Astronautics.

[40] Gregory D. Howe. Non-centroidal equations of motion for flight simulation. In *AIAA Atmospheric Flight Mechanics Conference*, Grapevine, TX, January 2017. American Institute of Aeronautics and Astronautics.

[41] David K. Schmidt and David L. Raney. Modeling and simulation of flexible flight vehicles. *Journal of Guidance, Control, and Dynamics*, 24(3):539–546, May 2001.

[42] Marthinus C. Van Schoor and Andreas H. Von Flotow. Aeroelastic characteristics of a highly flexible aircraft. *Journal of Aircraft*, 27(10):901–908, October 1990.

[43] Mark Drela. Integrated simulation model for preliminary aerodynamic, structural, and control-law design of aircraft. In *40th Structures, Structural Dynamics, and Materials Conference*, St. Louis, MO, April 1999. American Institute of Aeronautics and Astronautics.

[44] Mayuresh J. Patil, Dewey H. Hodges, and Carlos E. S. Cesnik. Nonlinear aeroelastic analysis of aircraft with high-aspect-ratio wings. In *39th AIAA/ASME/ASCE/AHS/ASC Structures, Structural Dynamics, and Materials Conference*, Long Beach, CA, April 1998. American Institute of Aeronautics and Astronautics.

[45] Mayuresh J. Patil and Dewey H. Hodges. On the importance of aerodynamic and structural geometrical nonlinearities in aeroelastic behavior of high-aspect-ratio wings. *Journal of Fluids and Structures*, 19(7):905–915, August 2004.

[46] Mayuresh J. Patil and Dewey H. Hodges. Flight dynamics of highly flexible flying wings. *Journal of Aircraft*, 43(6):1790–1799, November 2006.

[47] Mayuresh J. Patil, Dewey H. Hodges, and Carlos E. S. Cesnik. Nonlinear aeroelasticity and flight dynamics of high-altitude long-endurance aircraft. *Journal of Aircraft*, 38(1):88–94, January 2001.

[48] Mayuresh J. Patil, Dewey H. Hodges, and Carlos E. S. Cesnik. Nonlinear aeroelastic analysis of complete aircraft in subsonic flow. *Journal of Aircraft*, 37(5):753–760, September 2000.

[49] Mayuresh J. Patil, Dewey H. Hodges, and Carlos E. S. Cesnik. Limit cycle oscillations in high-aspect-ratio wings. *Journal of Fluids and Structures*, 15(1):107–132, January 2001.

[50] Christopher M. Shearer and Carlos E. S. Cesnik. Nonlinear flight dynamics of very flexible aircraft. *Journal of Aircraft*, 44(5):1528–1545, September 2007.

[51] Rafael Palacios and Carlos E. S. Cesnik. Low-speed aeroelastic modeling of very flexible slender wings with deformable airfoils. In *49th AIAA/ASME/ASCE/AHS/ASC Structures, Structural Dynamics, and Materials Conference*, Schaumburg, IL, April 2008. American Institute of Aeronautics and Astronautics.

[52] Joseba Murua, Rafael Palacios, and J. Michael R. Graham. Modeling of nonlinear flexible aircraft dynamics including free-wake effects. In *AIAA Atmospheric Flight Mechanics Conference*, Toronto, Canada, August 2010. American Institute of Aeronautics and Astronautics.

[53] Rafael Palacios, Joseba Murua, and Robert Cook. Structural and aerodynamic models in nonlinear flight dynamics of very flexible aircraft. *AIAA Journal*, 48(11):2648–2659, November 2010.

[54] Joseba Murua, Rafael Palacios, and J. Michael R. Graham. Applications of the unsteady vortex-lattice method in aircraft aeroelasticity and flight dynamics. *Progress in Aerospace Sciences*, 55:46–72, November 2012.

[55] Salvatore Maraniello and Rafael Palacios. Optimal rolling maneuvers with very flexible wings. *AIAA Journal*, 55(9):2964–2979, September 2017.

[56] Marcelo Santiago Sousa, Pedro Paglione, Roberto Gil Annes Silva, Flavio Luiz Cardoso-Ribeiro, and Sebastiao Simoes Cunha. Mathematical model of one flexible transport category aircraft. *Aircraft Engineering and Aerospace Technology*, 89(3):384–396, May 2017.

[57] Anonymous. Certification specifications and acceptable means of compliance for large aeroplanes. Certification Specifications CS-25, European Aviation Safety Agency, Cologne, Germany, August 2017.

[58] Hartley A. Soule. Flight measurements of the dynamic longitudinal stability of several airplanes and a correlation of the measurements with pilots' observations of handling characteristics. Technical Report NACA-TR-578, NACA Langley Aeronautical Laboratory, Langley Field, VA, January 1937.

[59] Ben O. Howard. Desirable qualities of transport airplanes from the pilot's point of view. *Journal of the Aeronautical Sciences*, 6(1):15–19, November 1938.

[60] Melvin N. Gough. Notes on stability from the pilot's standpoint. *Journal of the Aeronautical Sciences*, 6(10):395–398, August 1939.

[61] Geoffrey T. R. Hill. The flying controls of the aeroplane. *Journal of the Royal Aeronautical Society*, 43(342):411–440, June 1939.

[62] Otto C. Koppen. Airplane stability and control from a designer's point of view. *Journal of the Aeronautical Sciences*, 7(4):135–140, February 1940.

[63] Robert R. Gilruth. Requirements for satisfactory flying qualities of airplanes. Technical Report NACA-TR-755, NACA Langley Aeronautical Laboratory, Langley Field, VA, January 1943.

[64] Arthur R. Collar. The expanding domain of aeroelasticity. *Journal of the Royal Aeronautical Society*, 50(428):613–636, August 1946.

[65] Richard B Skoog. An analysis of the effects of aeroelasticity on static longitudinal stability and control of a swept-wing airplane. Technical Report NACA-TR-1298, NACA Ames Aeronautical Laboratory, Moffett Field, CA, January 1957.

[66] William Bihrle. A handling qualities theory for precise flight path control. Technical Report AFFDL-TR-65-198, Air Force Flight Dynamics Laboratory, Wright-Patterson AFB, OH, June 1966.

[67] David A. Kivioja. Comparison of the control anticipation parameter and the bandwidth criterion during the landing task. Master's thesis, Air Force Institute of Technology, Wright-Patterson AFB, OH, March 1996.

[68] David A. Kivioja, Christopher C. McCann, Mark R. Schaible, James C. McEachen, David N. Larson, and Justin D. Paines. A limited evaluation of predicting pilot opinion of aircraft handling qualities in the landing phase of flight using the control anticipation parameter and bandwidth criteria (HAVE CAP). Technical Report AFFTC-TR-95-78, Air Force Flight Test Center, Wright-Patterson AFB, OH, January 1996.

[69] John C. Gibson. *The Definition, Understanding and Design of Aircraft Handling Qualities*. Delft University of Technology, Delft, Netherlands, 1995.

[70] James E. Gautrey and Michael V. Cook. A generic control anticipation parameter for aircraft handling qualities evaluation. *The Aeronautical Journal*, 102(1013):151–160, March 1998.

[71] Edmund J. Field. *Flying Qualities of Transport Aircraft : Precognitive or Compensatory?* PhD thesis, Cranfield University, Cranfield, UK, June 1995.

[72] Edmund J. Field. The application of a C* flight control law to large civil transport aircraft. Technical Report 9303, Cranfield Institute of Technology, Cranfield, UK, March 1993.

[73] Gregg F. Bartley. Boeing B-777: Fly-by-wire flight controls. In Cary R. Spitzer, editor, *The Avionics Handbook*. CRC Press, Boca Raton, FL, 1st edition, 2001.

[74] Harold N. Tobie, Eiden M. Elliot, and Lawrence G. Malcom. A new longitudinal handling qualities criterion. In *18th Annual National Aerospace Electronics Conference*, Dayton, OH, 1966. Institute of Electrical and Electronics Engineers.

[75] Herman A. Mooij. Criteria for low-speed longitudinal handling qualities. Master's thesis, TU Delft, Dordrecht, Netherlands, December 1984.

[76] Kioumars Najmabadi, Monte R. Evans, Edward E. Coleman, Robert J. Bleeg, Richard S. Breuhaus, Dorr Marshall Anderson, and Timothy A. Nelson. Aircraft pitch-axis stability and command augmentation system. Patent US 6,325,333 B1, The Boeing Company, Seattle, WA, December 2001.

[77] Dominik Niedermeier and Anthony A. Lambregts. Fly-by-wire augmented manual control - basic design considerations. In *28th Congress of the International Council of the Aeronautical Sciences*, Brisbane, Australia, September 2012. International Council of the Aeronautical Sciences.

[78] T. Peter Neal and Rogers E. Smith. An in-flight investigation to develop control system design criteria for fighter airplanes. Technical Report AFFDL-TR-70-74, Air Force Flight Dynamics Laboratory, Wright-Patterson AFB, OH, December 1970.

[79] John C. Gibson. Piloted handling qualities design criteria for high order flight control systems. In *Criteria for Handling Qualities of Military Aircraft*, Fort Worth, TX, April 1982. NATO Advisory Group for Research and Development.

[80] John Hodgkinson. *Aircraft Handling Qualities*. Blackwell Science, Oxford, UK, 1999.

[81] Duane T. McRuer, Irving L. Ashkenas, and Dunstan Graham. *Aircraft Dynamics and Automatic Control*. Princeton University Press, Princeton, NJ, 1973.

[82] Roger H. Hoh, Thomas T. Myers, Irving L. Ashkenas, Robert F. Ringland, and Samuel J. Craig. Development of handling quality criteria for aircraft with independent control of six degrees of freedom. Technical Report AFWAL-TR-81-3027, Air Force Flight Dynamics Laboratory, Wright-Patterson AFB, OH, April 1981.

[83] Roger H. Hoh. Advances in flying qualities: Concepts and criteria for a mission oriented flying qualities specification. Technical report, Systems Technology, Inc., Hawthorne, CA, May 1988.

[84] T. Peter Neal and Rogers E. Smith. A flying qualities criterion for the design of fighter flight-control systems. *Journal of Aircraft*, 8(10):803–809, October 1971.

[85] Duane T. McRuer and Ezra S. Krendel. Mathematical models of human pilot behavior. Technical Report AD-775 905, NATO Advisory Group for Research and Development, Paris, France, January 1974.

[86] Duane T. McRuer. *Aviation Safety and Pilot Control: Understanding and Preventing Unfavorable Pilot-Vehicle Interactions*. National Academies Press, Washington, DC, 1997.

[87] George E. Cooper and Robert P. Harper. The use of pilot rating in the evaluation of aircraft handling qualities. Technical Report NASA-TN-D-5153, NASA Ames Research Center, Moffett Field, CA, April 1969.

[88] Donald Harris, James E. Gautrey, Katy H. Payne, and Roger Bailey. The Cranfield aircraft handling qualities rating scale: A multidimensional approach to the assessment of aircraft handling qualities. *The Aeronautical Journal*, 104(1034):191–198, April 2000.

[89] William R. Gray. Handling qualities evaluation at the USAF Test Pilot School. In *AIAA Atmospheric Flight Mechanics Conference*, Chicago, IL, August 2009. American Institute of Aeronautics and Astronautics.

[90] David J. Wilson and David R. Riley. Cooper-Harper pilot rating variability. In *AIAA Atmospheric Flight Mechanics Conference*, Boston, MA, August 1989. American Institute of Aeronautics and Astronautics.

[91] David R. Riley and David J. Wilson. More on Cooper-Harper pilot rating variability. In *AIAA Atmospheric Flight Mechanics Conference*, Portland, OR, August 1990. American Institute of Aeronautics and Astronautics.

[92] Sandra G. Hart and Lowell E. Staveland. Development of NASA-TLX (Task Load Index): Results of empirical and theoretical research. In Peter A. Hancock and Najmedin Meshkati, editors, *Advances in Psychology*, volume 52, pages 139–183. Elsevier, Amsterdam, Netherlands, 1988.

[93] David J. Wilson, David K. Riley, and Kevin D. Citurs. Aircraft maneuvers for the evaluation of flying qualities and agility, vol II: Maneuver descriptions and selection guide. Technical Report WL-TR-93-3082, Wright Laboratory, Wright-Patterson AFB, OH, August 1993.

[94] Thomas R. Twisdale and David L. Franklin. Tracking test techniques for handling qualities evaluation. Technical Report AF-FTC-TD-75-1, Air Force Flight Test Center, Edwards AFB, CA, April 1975.

[95] David J. Moorhouse and Robert J. Woodcock. Background information and user guide for MIL-F-8785C, military specification - flying qualities of piloted airplanes. Technical Report AFWAL-TR-81-3109, USAF Wright Aeronautical Laboratories, Wright-Patterson AFB, OH, September 1981.

[96] Laurence R. Young. Some effects of motion cues on manual tracking. *Journal of Spacecraft and Rockets*, 4(10):1300–1303, October 1967.

[97] Richard S. Shirley and Laurence R. Young. Motion cues in man-vehicle control. *IEEE Transactions on Man-Machine Systems*, 9(4):121–128, December 1968.

[98] Jay Loftus and Peter R. Grant. Motion simulation of flexible aircraft. In *AIAA Modeling and Simulation Technologies Conference*, Hilton Head, SC, August 2007. American Institute of Aeronautics and Astronautics.

[99] Peter M. T. Zaal, Jeffery A. Schroeder, and William W. Chung. Objective motion cueing criteria for commercial transport simulators. In *AIAA Modeling and Simulation Technologies Conference*, Atlanta, GA, June 2018. American Institute of Aeronautics and Astronautics.

[100] Eric Groen, Wietse Ledegang, Joris Field, Hafid Smaili, Manfred Roza, Lars Fucke, Suzanne Nooij, Mikhail Goman, Michael Mayrhofer, Larisa Zaichik, Maxim Grigoryev, and Vladimir Biryukov. SUPRA - enhanced upset recovery simulation. In *AIAA Modeling and Simulation Technologies Conference*, Minneapolis, MN, August 2012. American Institute of Aeronautics and Astronautics.

[101] D. Stewart. A platform with six degrees of freedom. *Proceedings of the Institution of Mechanical Engineers*, 180(1):371–386, June 1965.

[102] Eric L. Groen, Mario S. V. Valenti Clari, and Ruud J. A. W. Hosman. Evaluation of perceived motion during a simulated takeoff run. *Journal of Aircraft*, 38(4):600–606, July 2001.

[103] Thomas W. Showalter and Benton L. Parris. The effects of motion and g-seat cues on pilot simulator performance of three piloting tasks. Technical Report NASA-TP-1601, NASA Ames Research Center, Moffett Field, CA, January 1980.

[104] Eric L. Groen, Ian P. Howard, and Bob S. K. Cheung. Influence of body roll on visually induced sensations of self-tilt and rotation. *Perception*, 28(3):287–297, March 1999.

[105] Eric L. Groen, Ruud J. A. W. Hosman, and Jacco W. Dominicus. Motion fidelity during a simulated takeoff. In *AIAA Modeling and Simulation Technologies Conference*, Austin, TX, August 2003. American Institute of Aeronautics and Astronautics.

[106] Jeffery A. Schroeder. Helicopter flight simulation motion platform requirements. Technical Report NASA/TP-1999-208766, NASA Ames Research Center, Moffett Field, CA, July 1999.

[107] Judith Bürki-Cohen and Tiauw H. Go. The effect of simulator motion cues on initial training of airline pilots. In *AIAA Modeling and Simulation Technologies Conference*, San Francisco, CA, August 2005. American Institute of Aeronautics and Astronautics.

[108] Peter R. Grant, Bonnie Yam, Ruud J. A. W. Hosman, and Jeffery A. Schroeder. Effect of simulator motion on pilot behavior and perception. *Journal of Aircraft*, 43(6):1914–1924, November 2006.

[109] Eric L. Groen, Hafid Smaili, and Ruud J. A. W. Hosman. Perception model analysis of flight simulator motion for a decrab maneuver. *Journal of Aircraft*, 44(2):427–435, March 2007.

[110] Dae-Kwan Kim, Jun-Seong Lee, Jin-Young Lee, and Jae-Hung Han. An aeroelastic analysis of a flexible flapping wing using modified strip theory. In *Active and Passive Smart Structures and Integrated Systems 2008*, volume 6928, San Diego, CA, March 2008. International Society for Optics and Photonics.

[111] Stuart P. Andrews and Alastair K. Cooke. An aeroelastic flexible wing model for aircraft simulation. In *48th AIAA Aerospace Sciences Meeting*, Orlando, FL, January 2010. American Institute of Aeronautics and Astronautics.

[112] J. Gordon Leishman. Validation of approximate indicial aerodynamic functions for two-dimensional subsonic flow. *Journal of Aircraft*, 25(10):914–922, October 1988.

[113] J. Gordon Leishman. Indicial lift approximations for two-dimensional subsonic flow as obtained from oscillatory measurements. *Journal of Aircraft*, 30(3):340–351, May 1993.

[114] J. Gordon Leishman. Unsteady lift of a flapped airfoil by indicial concepts. *Journal of Aircraft*, 31(2):288–297, March 1994.

[115] J. Gordon Leishman and K. Q. Nguyen. State-space representation of unsteady airfoil behavior. *AIAA Journal*, 28(5):836–844, May 1990.

[116] Mohammad M. Lone. *Pilot Modelling for Airframe Loads Analysis*. PhD thesis, Cranfield University, Cranfield, UK, January 2013.

[117] Theodore Theodorsen. General theory of aerodynamic instability and the mechanism of flutter. Technical Report NACA-TR-496, NACA Langley Aeronautical Laboratory, Langley Field, VA, January 1949.

[118] Herbert Wagner. Uber die entstehung des dynamischen auftriebs von tragflun. *Zeitschrift fur Angewandte Mathematic and Mechanic*, 5(1):17–35, 1925.

[119] Hans G. Kussner. Zusammenfassender bericht uber den instationaren auftrieb von flugeln. *Luftfahrtforschung*, 13(12):410–424, 1936.

[120] J. Gordon Leishman. Subsonic unsteady aerodynamics caused by gusts using the indicial method. *Journal of Aircraft*, 33(5):869–879, September 1996.

[121] Johannes Weissinger. The lift distribution of swept-back wings. Technical Report NACA-TM-1120, NACA Langley Aeronautical Laboratory, Langley Field, VA, March 1947.

[122] John DeYoung and Charles W. Harper. Theoretical symmetric span loading at subsonic speeds for wings having arbitrary plan form. Technical Report NACA-TR-921, NACA Ames Aeronautical Laboratory, Moffett Field, CA, January 1948.

[123] James D. DeLaurier. An aerodynamic model for flapping-wing flight. *The Aeronautical Journal*, 97(964):125–130, April 1993.

[124] John D. Anderson. *Modern Compressible Flow: With Historical Perspective*. McGraw-Hill, Boston, MA, 3rd edition, 2003.

[125] Hermann Glauert. The effect of compressibility on the lift of an aerofoil. *Proceedings of the Royal Society of London A: Containing Papers of a Mathematical and Physical Character*, 118(779):113–119, March 1928.

[126] Mark Drela and Michael B. Giles. Viscous-inviscid analysis of transonic and low Reynolds number airfoils. *AIAA Journal*, 25(10):1347–1355, October 1987.

[127] Mark Drela. XFOIL: An analysis and design system for low Reynolds number airfoils. In Thomas J. Mueller, editor, *Low Reynolds Number Aerodynamics*, volume 54, pages 1–12. Springer, Berlin, Germany, 1989.

[128] Anonymous. Aerodynamic centre of wing-fuselage-nacelle combinations: Effect of wing-pylon mounted nacelles. Technical Report ESDU 77012, ESDU International, London, UK, November 2013.

[129] Anonymous. Normal force and pitching moment of conical boat-tails. Technical Report ESDU 87033, ESDU International, London, UK, July 1992.

[130] Anonymous. Normal-force-curve and pitching-moment-curve slopes of forebody-cylinder combinations at zero angle of attack for Mach numbers up to 5. Technical Report ESDU 89008, ESDU International, London, UK, December 1990.

[131] Anonymous. Normal force, pitching moment and side force of forebody-cylinder combinations for angles of attack up to 90 degrees and Mach numbers up to 5. Technical Report ESDU 89014, ESDU International, London, UK, September 2004.

[132] Anonymous. Geometrical characteristics of typical bodies. Technical Report ESDU 77028, ESDU International, London, UK, July 1990.

[133] Anonymous. World Geodetic System 1984. Technical Report TR8350.2, National Imagery and Mapping Agency, St. Louis, MO, January 2000.

[134] Anonymous. Properties of a standard atmosphere. Technical Report ESDU 77021, ESDU International, London, UK, March 2005.

[135] Vilius Portapas, Sezsy Y. Yusuf, Mohammad M. Lone, and Etienne Coetzee. Modelling framework for handling qualities analysis of flexible aircraft. In *AIAA Modeling and Simulation Technologies Conference*, Grapevine, TX, January 2017. American Institute of Aeronautics and Astronautics.

[136] Vilius Portapas, Alastair K. Cooke, and Mohammad M. Lone. Modelling framework for flight dynamics of flexible aircraft. *Aviation*, 20(4):173–182, October 2016.

[137] David J. Allerton. EFS500. Teaching guide, Aerosoft, Southampton, UK, March 2016.

[138] David J. Allerton. EFS500. User guide, Aerosoft, Southampton, UK, March 2016.

[139] Paul Jackson. *Jane's All the World's Aircraft: In Service 2014-2015*. IHS Jane's, Coulsdon, UK, 2014.

[140] Anonymous. Type-certificate data sheet for Airbus A318-A319-A320-A321. Technical Report EASA.A.064, European Aviation Safety Agency, Cologne, Germany, December 2017.

[141] Anonymous. Type-certificate data sheet for Boeing 737. Technical Report EASA.IM.A.120, European Aviation Safety Agency, Cologne, Germany, July 2017.

[142] Anonymous. Harten configuration update & FAME-W assumptions. Technical report, Airbus, Bristol, UK, November 2017.

[143] Anonymous. MSC Nastran 2014.1. Quick reference guide, MSC Software Corporation, Newport Beach, CA, June 2015.

[144] Thomas R. Yechout and Steven L. Morris. *Introduction to Aircraft Flight Mechanics: Performance, Static Stability, Dynamic Stability, and Classical Feedback Control*. American Institute of Aeronautics and Astronautics, Reston, VA, 2003.

[145] Michael F. Ashby. *Materials Selection in Mechanical Design*. Butterworth-Heinemann, Burlington, MA, 4th edition, 2011.

[146] Richard M. Hueschen. Development of the Transport Class Model (TCM) aircraft simulation from a sub-scale Generic Transport Model (GTM) simulation. Technical Report NASA/TM-2011-217169, NASA Langley Research Center, Hampton, VA, August 2011.

[147] Anonymous. CAP 696 CAA JAR-FCL examinations. Mass and balance manual (aeroplanes). Manual, CAA Safety Regulation Group, Gatwick Airport South, UK, July 2006.

[148] Darrol Stinton. *Flying Qualities and Flight Testing of the Aeroplane*. Blackwell Science, Oxford, UK, 1996.

[149] Donald T. Ward and Thomas W. Strganac. *Introduction to Flight Test Engineering*. Kendall/Hunt Publishing Company, Dubuque, IA, 2nd edition, 2001.

[150] Ralph D. Kimberlin. *Flight Testing of Fixed-Wing Aircraft*. American Institute of Aeronautics and Astronautics, Reston, VA, 2003.

[151] Jared A. Grauer and Borja Martos. Evaluation of piloted inputs for onboard frequency response estimation. In *AIAA Atmospheric Flight Mechanics Conference*, Boston, MA, August 2013. American Institute of Aeronautics and Astronautics.

[152] Malcolm J Abzug and E. Eugene Larrabee. *Airplane Stability and Control a History of the Technologies That Made Aviation Possible*. Cambridge University Press, Cambridge, UK, 2nd edition, 2002.

[153] Brian P. Lee. Recent experience in flight testing for pilot induced oscillations (PIO) on transport aircraft. *The Aeronautical Journal*, 104(1038):391–395, August 2000.

[154] Chung-Hao Hsu and C. Edward Lan. Theory of wing rock. *Journal of Aircraft*, 22(10):920–924, October 1985.

[155] Joseph Katz. Wing/vortex interactions and wing rock. *Progress in Aerospace Sciences*, 35(7):727–750, October 1999.

[156] Ralph E. Blake. Basic vibration theory. In Allan G. Piersol and Thomas L. Paez, editors, *Harris' Shock and Vibration Handbook*, pages 2.1–2.32. McGraw-Hill, New York, NY, 6th edition, 2010.

[157] Robert K. Heffley and Wayne F. Jewell. Aircraft handling qualities data. Technical Report NASA CR-2144, Systems Technology, Inc., Hawthorne, CA, December 1972.

[158] Wayne Durham. *Aircraft Flight Dynamics and Control*. Wiley, Chichester, UK, 2013.

[159] Anonymous. On the accident on 1st June 2009 to the Airbus A330-203 registered F-GZCP operated by Air France flight AF 447 Rio de Janeiro - Paris. Technical report, Bureau d'Enquêtes et d'Analyses pour la sécurité de l'aviation civile, Le Bourget, France, July 2012.

Appendix A

Data of SUGAR, eta sailplane and Lilienthal hang glider

A.1 The Subsonic Ultra Green Aircraft Research, or SUGAR, Freeze design concept

The Subsonic Ultra Green Aircraft Research, or SUGAR, Freeze design concept picture was taken from the following web page accessed on 21/06/2018.

Figure A.1: NASA/Boeing SUGAR concept aircraft
(Source: https://www1.grc.nasa.gov/wp-content/uploads/SUGAR-Final2-1.jpg)

A.2 Lilienthal hang glider

The Lilienthal hang glider picture was taken from the following web page accessed on 12/10/2018.

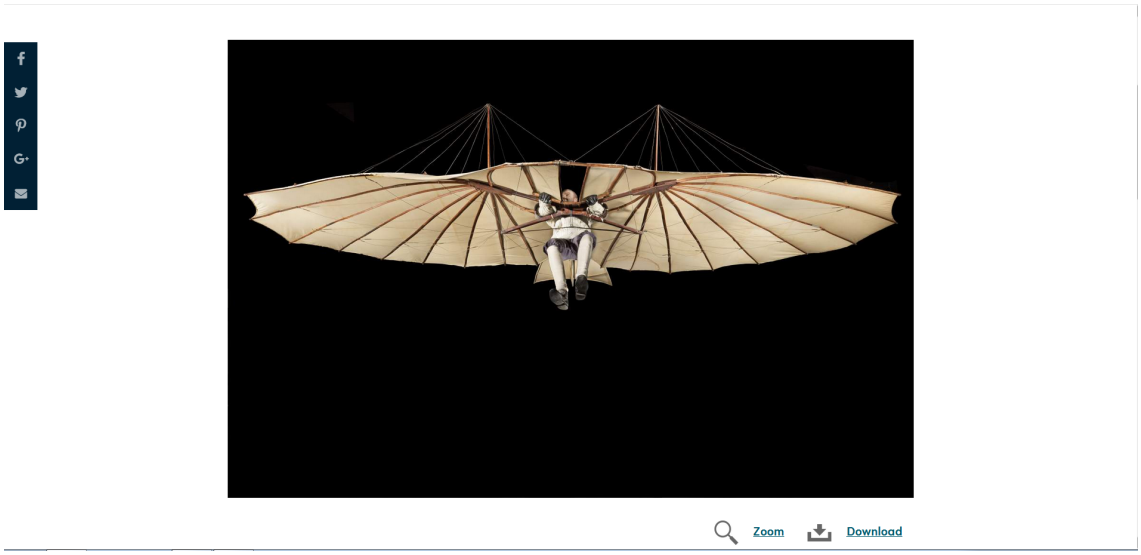

Figure A.2: Lilienthal hang glider
(Source: https://airandspace.si.edu/multimedia-gallery/lilienthal-gliderjpg)

A.3 eta sailplane on final

The eta sailplane picture showing high wing deformation was taken from the following web page accessed on 12/10/2018.

Figure A.3: eta sailplane on final
(Source: https://www.leichtwerk.de/fileadmin/media/archiv/eta-aircraft/eta/...
...images/galerie/marzinzik10.jpg)

A.4 Aspect ratio of eta sailplane

The aspect ratio data of the eta sailplane was taken from the following web page accessed on 12/10/2018.

eta AIRCRAFT

- Das Projekt eta
- Die Philosophie
- Der Projektstand
- Technische Daten
- Technologie
- Werknummer 2
- Flugerprobung
- Verkauf
- Galerie

- Sitemap
- Kontakt
- Copyright

DAS PROJEKT eta

PROJEKTDATEN

Der griechische Buchstabe η (eta) steht in der Welt der Technik für den Wirkungsgrad. Der Wirkungsgrad ist ein Maß für die Effizienz bei der Ausnutzung von Energie. Für ein Segelflugzeug ist ein hohes Maß an Effizienz von besonderer Bedeutung, um schwache Aufwinde in Höhengewinn und eine einmal gewonnene Höhe in eine möglichst weite Flugstrecke umsetzen zu können. Im Projekt **eta** sollten alle technischen Möglichkeiten zur Steigerung des Wirkungsgrades ausgeschöpft werden.

Als Name für ein Segelflugzeug steht **eta** dabei für den kompromisslosen Einsatz modernster Entwurfsverfahren, Werkstoffe und Fertigungstechniken, um einen möglichst großen Leistungssprung zu erreichen.

Neben der Steigerung der Flugleistungen wurde großes Augenmerk auf möglichst einfache und ausgewogene Flugeigenschaften gelegt. Hierfür wurde sogar auf das letzte Quentchen Steigerung der Flugleistung im Geradeausflug verzichtet, da gute Flugeigenschaften ebenfalls zu einer Verbesserung der Gesamtleistung führen, die der Pilot mit einem Flugzeug erzielen kann. **eta** soll auch keinesfalls nur von sehr erfahrenen Segelfliegern beherrscht werden können, sondern mit den Fähigkeiten eines durchschnittlich trainierten Piloten zu hervorragenden überlandflugerlebnissen führen.

Im Auftrag der weltbekannten Wettbewerbs- und Rekordsegelflieger Erwin Müller, Hans-Werner Große, Hartmut Lodes, Dr. Jan Krüger, Bruno Gantenbrink und Umberto Mantica entwickelt und konstruiert das Ingenieurbüro Flugtechnik & Leichtbau unter Leitung von Dr. Reiner Kickert am Forschungsflughafen Braunschweig ein Segelflugzeug mit extremen Daten:

- Spannweite: 30.90 m
- Streckung: 51.33
- max. Masse: Zulassung 850 kg, Auslegung 950 kg
- doppelsitzig
- eigenstartfähig

Die Fertigung der Flugzeuge erfolgt durch renommierte luftfahrttechnische Betriebe:

- Rumpfbau, Holmgurte für den Flügel, Endmontage:
  Walter Binder Flugmotorenbau
- Flügelbau:

Figure A.4: Aspect ratio of eta sailplane
(Source: https://www.leichtwerk.de/fileadmin/media/archiv/eta-aircraft/eta/...
...de/projekt_eta/index.html)

A.5 Aerodynamic efficiency of eta sailplane

The aerodynamic efficiency data of the eta sailplane was taken from the following web page accessed on 12/10/2018.

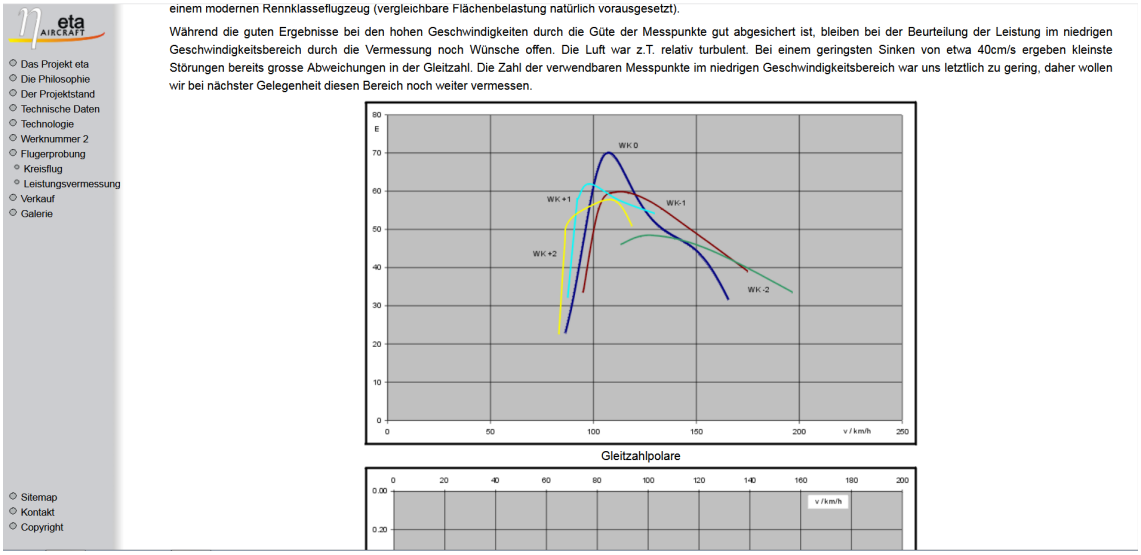

Figure A.5: Aerodynamic efficiency of eta sailplane
(Source: https://www.leichtwerk.de/fileadmin/media/archiv/eta-aircraft/eta/...
...de/flugerprobung/leistung.html)

Appendix A

Unsteady aerodynamic state-space model matrices

The state matrix A is represented as:

$$A = \begin{bmatrix}
\frac{-2V\beta^2 b_1}{c_{aero}} & 0 & 0 & 0 & 0 & 0 & 0 & 0 & 0 & 0 & 0 & 0 & 0 & 0 & 0 \\
0 & \frac{-2V\beta^2 b_2}{c_{aero}} & 0 & 0 & 0 & 0 & 0 & 0 & 0 & 0 & 0 & 0 & 0 & 0 & 0 \\
0 & 0 & \frac{-1}{T_\alpha} & 0 & 0 & 0 & 0 & 0 & 0 & 0 & 0 & 0 & 0 & 0 & 0 \\
0 & 0 & 0 & \frac{-1}{T_q} & 0 & 0 & 0 & 0 & 0 & 0 & 0 & 0 & 0 & 0 & 0 \\
0 & 0 & 0 & 0 & \frac{-1}{T\alpha_M b_3} & 0 & 0 & 0 & 0 & 0 & 0 & 0 & 0 & 0 & 0 \\
0 & 0 & 0 & 0 & 0 & \frac{-1}{T\alpha_M b_4} & 0 & 0 & 0 & 0 & 0 & 0 & 0 & 0 & 0 \\
0 & 0 & 0 & 0 & 0 & 0 & \frac{-2V\beta^2 b_5}{c_{aero}} & 0 & 0 & 0 & 0 & 0 & 0 & 0 & 0 \\
0 & 0 & 0 & 0 & 0 & 0 & 0 & \frac{-1}{T q_M} & 0 & 0 & 0 & 0 & 0 & 0 & 0 \\
0 & 0 & 0 & 0 & 0 & 0 & 0 & 0 & 0 & 1 & 0 & 0 & 0 & 0 & 0 \\
0 & 0 & 0 & 0 & 0 & 0 & 0 & 0 & -\left(\frac{2V}{c_{aero}}\right)^2 \beta^4 b_1 b_2 & \frac{-2V(b_1+b_2)\beta^2}{c_{aero}} & 0 & 0 & 0 & 0 & 0 \\
0 & 0 & 0 & 0 & 0 & 0 & 0 & 0 & 0 & 0 & \frac{-1}{T_\xi} & 0 & 0 & 0 & 0 \\
0 & 0 & 0 & 0 & 0 & 0 & 0 & 0 & 0 & 0 & 0 & \frac{-1}{T_{\dot{\xi}}} & 0 & 0 & 0 \\
0 & 0 & 0 & 0 & 0 & 0 & 0 & 0 & 0 & 0 & 0 & 0 & \frac{-2V\beta^2 b_3}{c_{aero}} & 0 & 0 \\
0 & 0 & 0 & 0 & 0 & 0 & 0 & 0 & 0 & 0 & 0 & 0 & 0 & \frac{-1}{T_{\xi_M}} & 0 \\
0 & 0 & 0 & 0 & 0 & 0 & 0 & 0 & 0 & 0 & 0 & 0 & 0 & 0 & \frac{-1}{T_{\dot{\xi}_M}}
\end{bmatrix}$$

The output matrix C is represented as:

$$C = \begin{bmatrix}
\frac{2V\beta^2 A_1 b_1}{c_{aero}} & \frac{2V\beta^2 A_2 b_2}{c_{aero}} & 0 & 0 & 0 & 0 & 0 & 0 & \left(\frac{2V}{c_{aero}}\right)^2 \beta^4 b_1 b_2 & \frac{2V\beta^2(A_1 b_1 + A_2 b_2)}{c_{aero}} & 0 & 0 & 0 & 0 & 0 \\
0 & 0 & 0 & 0 & 0 & 0 & -\frac{2V\beta^2 b_5}{16 c_{aero}} & 0 & 0 & 0 & 0 & 0 & \frac{V\beta^2 b_6}{c_{aero}} & 0 & 0 \\
0 & 0 & -\frac{4}{T\alpha M} & 0 & 0 & 0 & 0 & 0 & 0 & 0 & -\frac{2(1-x_e)}{T_{\xi_M}} & 0 & 0 & 0 & 0 \\
0 & 0 & 0 & 0 & \frac{A_3}{b_3 T\alpha_M M} & \frac{A_4}{b_4 T\alpha_M M} & 0 & 0 & 0 & 0 & 0 & 0 & 0 & \frac{(1-x_e)(2+x_e)}{2T_{\xi_M} M} & 0
\end{bmatrix}$$

Non-circulatory time constants [113] in A and C matrices are:

$$T_\alpha = \frac{c_{aero}k_1}{a(1-M+\pi\beta M^2(A_1b_1+A_2b_2))}$$

$$T_q = \frac{2c_{aero}k_2}{a(1-M+2\pi\beta M^2(A_1b_1+A_2b_2))}$$

$$T_{\alpha_M} = \frac{c_{aero}(A_3b_4+A_4b_3)}{ab_3b_4(1-M)}$$

$$T_{q_M} = \frac{7c_{aero}}{a(15(1-M)+3\pi\beta M^2b_5)}$$

$$T_\xi = \frac{c_{aero}(1-x_e)}{a((1-M)+\frac{F_{10}}{\beta}M^2(A_1b_1+A_2b_2))}$$

$$T_{\dot{\xi}} = \frac{c_{aero}(1-x_e)^2}{2a((1-M)(1-x_e)+\frac{F_{11}}{\pi}\beta^2M^2(A_1b_1+A_2b_2))}$$

$$T_{\xi_M} = \frac{c_{aero}(1-x_e)(2+x_e)}{a(3(1-M)+2b_3M^2\beta(F_4+F_{10}))}$$

$$T_{\dot{\xi}_M} = \frac{c_{aero}((1+x_e)^3+4-12x_e-\frac{3}{2}(1-x_e)^2)}{a(9(1-M)(1-x_e)+6b_3M^2\beta(F_1-F_8-F_4(\frac{1}{2}+x_e)+\frac{F_{11}}{2}))}$$

The input matrix B and the feedthrough matrix D are represented as:

$$B = \begin{bmatrix} 1 & \frac{c_{aero}}{2V} & 0 & 0 \\ 1 & \frac{c_{aero}}{2V} & 0 & 0 \\ 1 & 0 & 0 & 0 \\ 0 & 1 & 0 & 0 \\ 1 & 0 & 0 & 0 \\ 1 & 0 & 0 & 0 \\ 0 & \frac{c_{aero}}{V} & 0 & 0 \\ 0 & \frac{c_{aero}}{V} & 0 & 0 \\ 0 & 0 & 0 & 0 \\ 0 & 0 & \frac{F_{10}}{\pi} & 0 \\ 0 & 0 & 1 & 0 \\ 0 & 0 & 0 & \frac{c_{aero}\exp^{1-x_e}}{2V} \\ 0 & 0 & -\frac{F_4+F_{10}}{2\pi\beta} & \frac{c_{aero}(2F_1-2F_8+F_{11}-F_4(1+2x_e))}{8V\pi\beta} \\ 0 & 0 & 1 & 0 \\ 0 & 0 & 0 & 1 \end{bmatrix} \quad D = \begin{bmatrix} 0 & 0 & 0 & 0 \\ 0 & 0 & 0 & 0 \\ \frac{4}{M} & 0 & \frac{2(1-x_e)}{M} & 0 \\ -\frac{1}{M} & 0 & -\frac{(1-x_e)(2+x_e)}{2M} & 0 \end{bmatrix}$$

Appendix B

Time histories for Gibson Dropback criterion

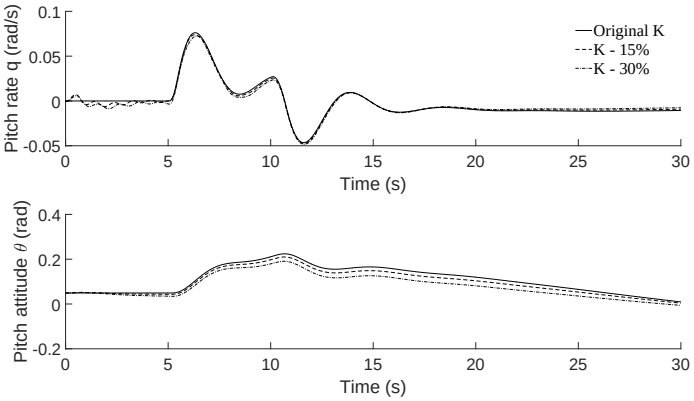

(a) 150 m/s

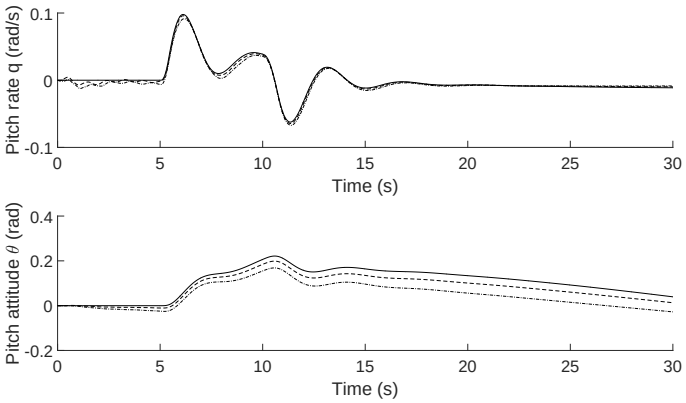

(b) 190 m/s

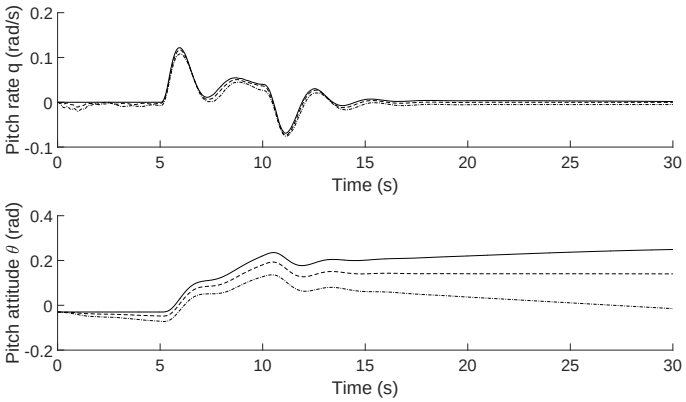

(c) 240 m/s

Figure B.1: Time histories of pitch rate q and pitch angle θ for minimum, maximum and inflection points of Fig. 4.8

Appendix C

Data for the static margin definition of HARTEN

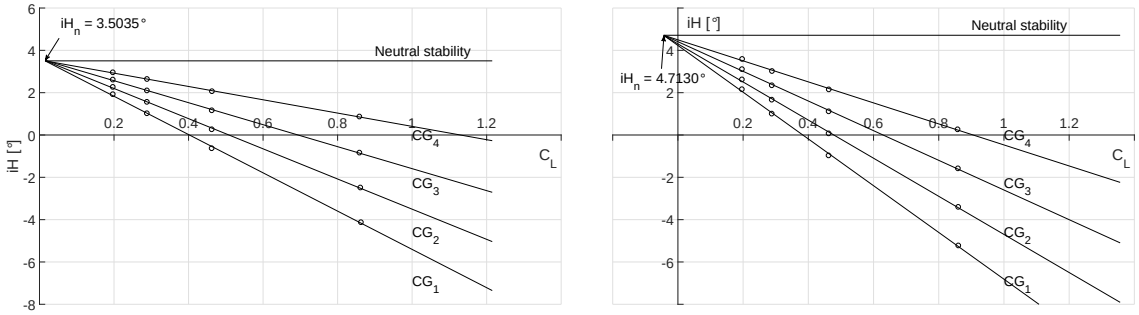

(a) Rigid

(b) Flexible

Figure C.1: $iH(C_L)$ variability with CG change at 5000 ft

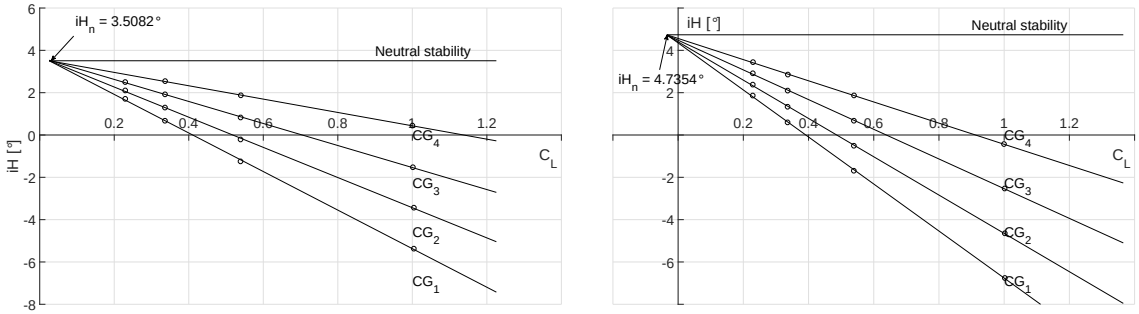

(a) Rigid (b) Flexible

Figure C.2: $iH(C_L)$ variability with CG change at 10000 ft

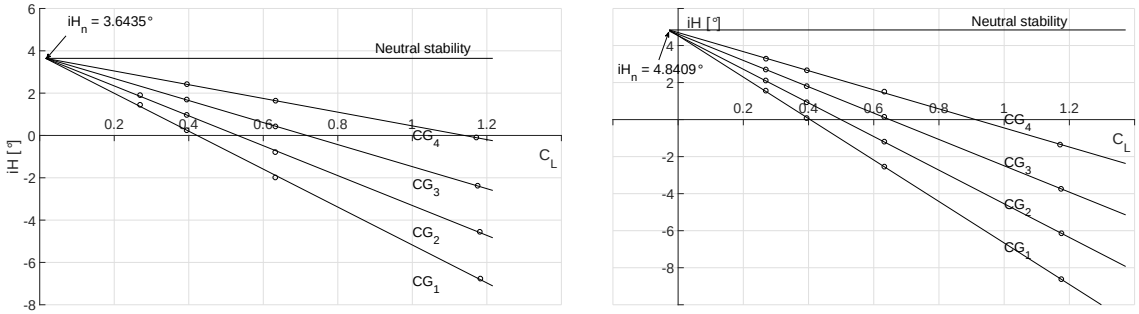

(a) Rigid (b) Flexible

Figure C.3: $iH(C_L)$ variability with CG change at 15000 ft

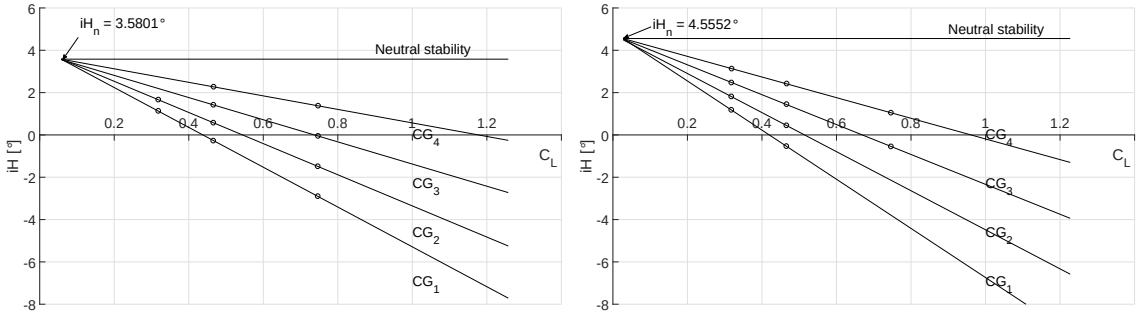

(a) Rigid (b) Flexible

Figure C.4: $iH(C_L)$ variability with CG change at 20000ft

Appendix D

Stall simulation data

D.1 Stall conditions test, pilot 1, rigid A/C – ST(1)R

Date: 24/01/2018 **Time start:** **Time stop:** 16:00

Test No:	ST(1)R	**Test hardware:**	EFS500 + Speedgoat
Test pilot:	(1)	**Model version:**	HARTEN_v1 (R)

Task:	Stall test (ST)
Manoeuvre:	Pitch up

Instrumentation:	
Relevant files:	{D_SIM/D_STRUCT}.DAT @ 24/01/2018 16:00; DSCN9509.MOV; GOPR4015.MP4

Flight velocity: 110 m/s **Flight altitude:** 10000 ft

Aircraft weight: 79 t **Aircraft CG:** 20% MAC

V (EAS)	Observations
157 kt	STALL EVIDENCED BY FULL BACK STICK, A/C FULLY CONTROLLABLE OTHERWISE IN ALL AXES.
1 kt/sec	VERY SLIGHT ROLLING EXCURSIONS.
	A/C RESPONDED EASILY TO STANDARD STALL RECOVERY ACTIONS.
	ALTHOUGH LARGE PITCHING MOTION WITH POWER REQUIRED FURTHER PITCH INPUTS TO
	COMPENSATE.

Notes:

Nil

Notes (from audio recording):

“Fairly stable mush”

“Low speed phugoid”

Figure D.1: Test card (ST(1)R)

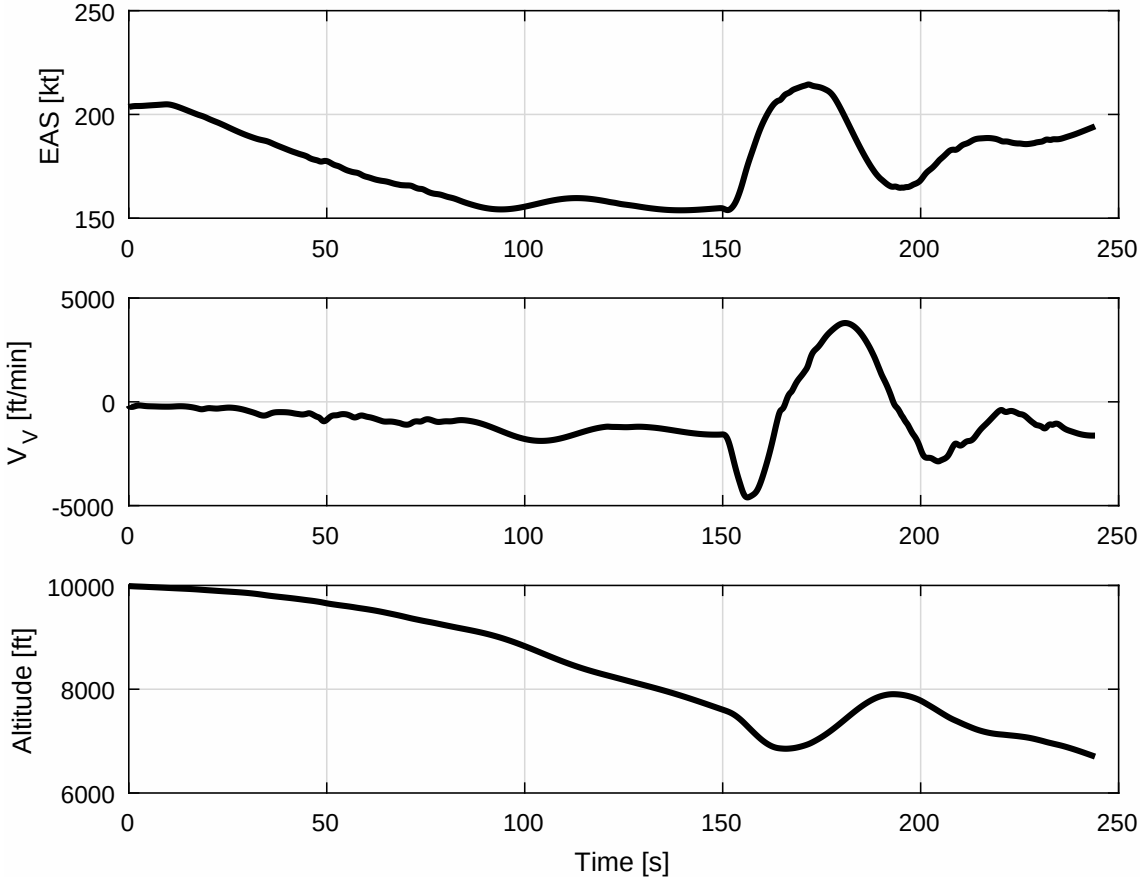

Figure D.2: Time histories of altitude and velocities

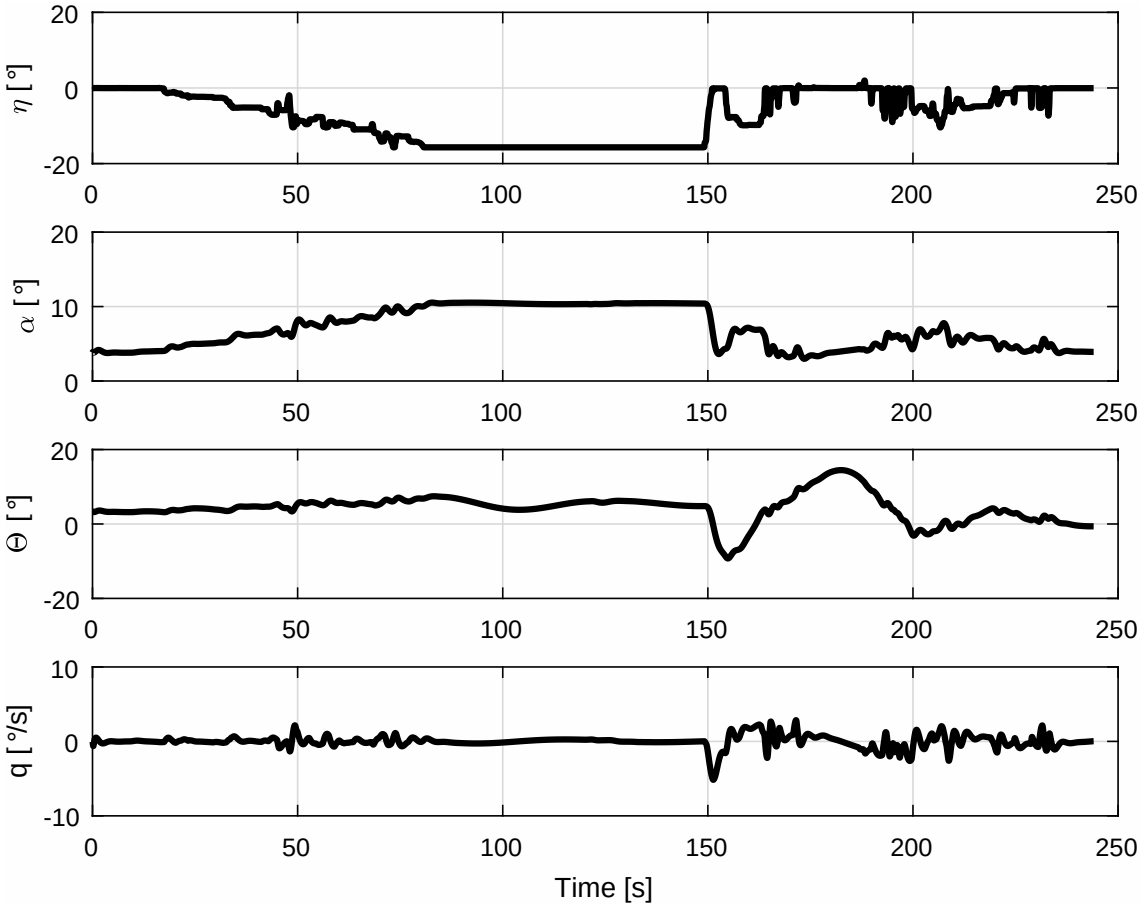

Figure D.3: Time histories of longitudinal parameters

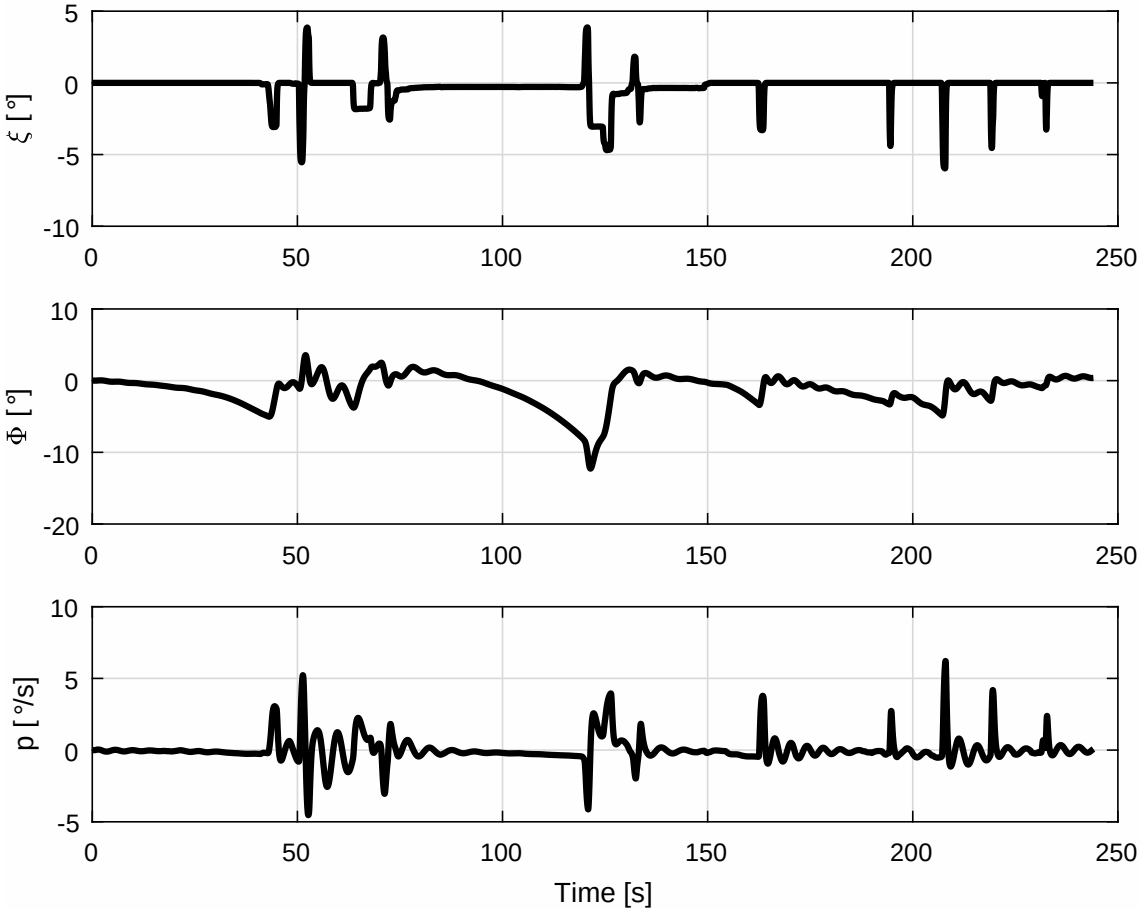

Figure D.4: Time histories of lateral parameters

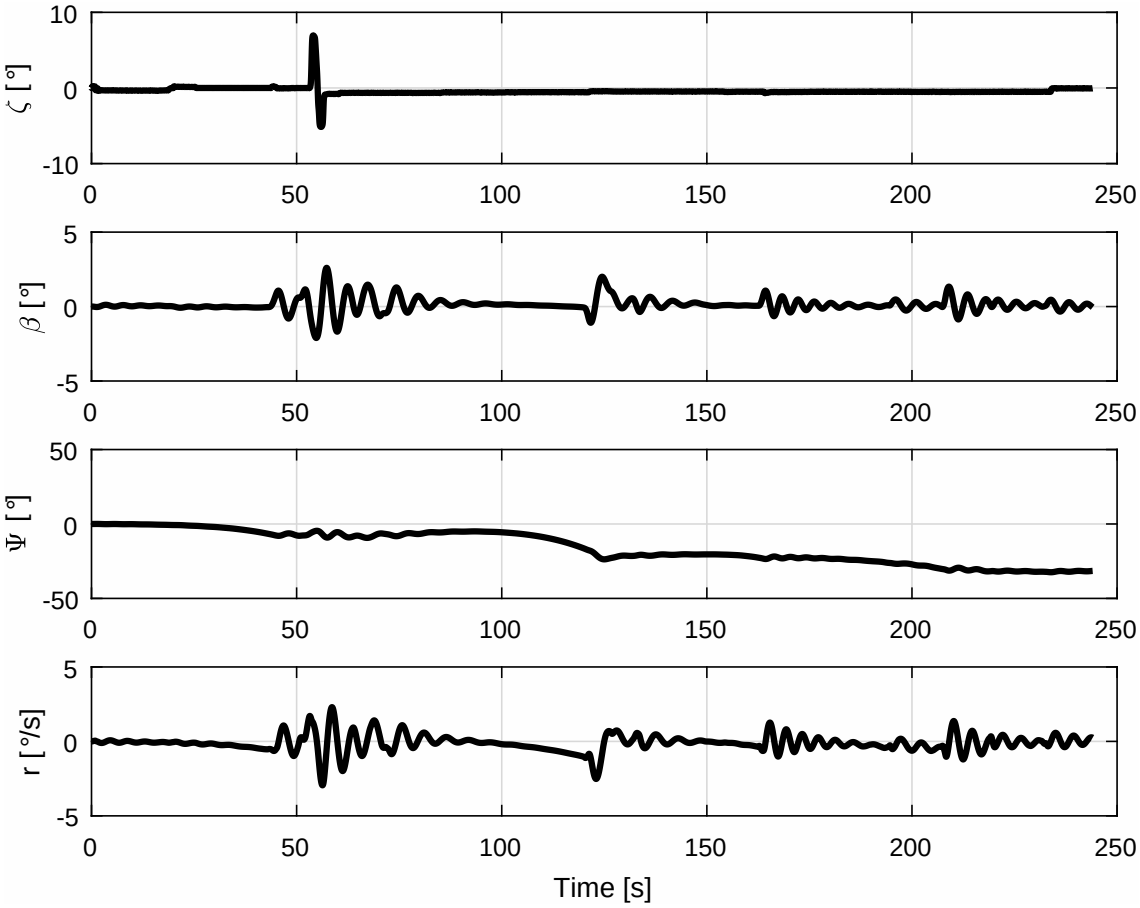

Figure D.5: Time histories of directional parameters

D.2 Stall conditions test, pilot 1, flexible A/C – ST(1)F

Date: 24/01/2018 **Time start:** **Time stop:** 17:13

Test No:	ST(1)F	**Test hardware:**	EFS500 + Speedgoat
Test pilot:	(1)	**Model version:**	HARTEN_v1 (F)

Task:	Stall test (ST)
Manoeuvre:	Pitch up

Instrumentation:	
Relevant files:	{D_SIM/D_STRUCT}.DAT @ 24/01/2018 17:13; DSCN9518.MOV; GOPR4024.MP4

Flight velocity: 110 m/s **Flight altitude:** 10000 ft

Aircraft weight: 79 t **Aircraft CG:** 20% MAC

V (EAS)	Observations
165 kt	STALL EVIDENCED BY FULL BACK STICK.
1 kt/sec	IMMEDIATE RESPONSE TO RELAXATION OF BACK STICK PRESSURE,
Idle power	BUT THEN ENTERED PHUGOID.
	SUBSEQUENTLY ENTERED SOME UNDEMANDED MOTION DOCUMENTED ON VIDEO.

Notes:

$T_{wing\ rocking}$ = 5 sec

Notes (from audio recording):

"It's Dutch rolling on its own"

"Wing rocking superimposed on the phugoid"

Figure D.6: Test card (ST(1)F)

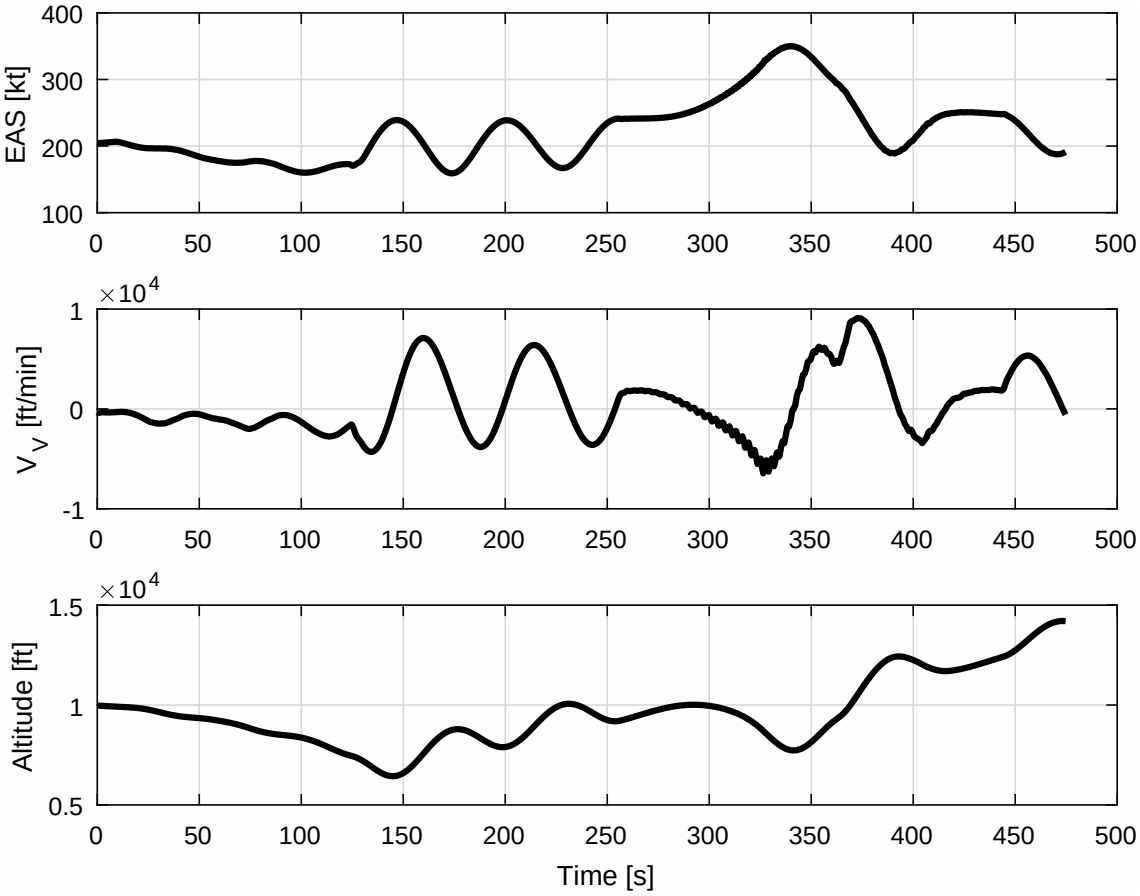

Figure D.7: Time histories of altitude and velocities

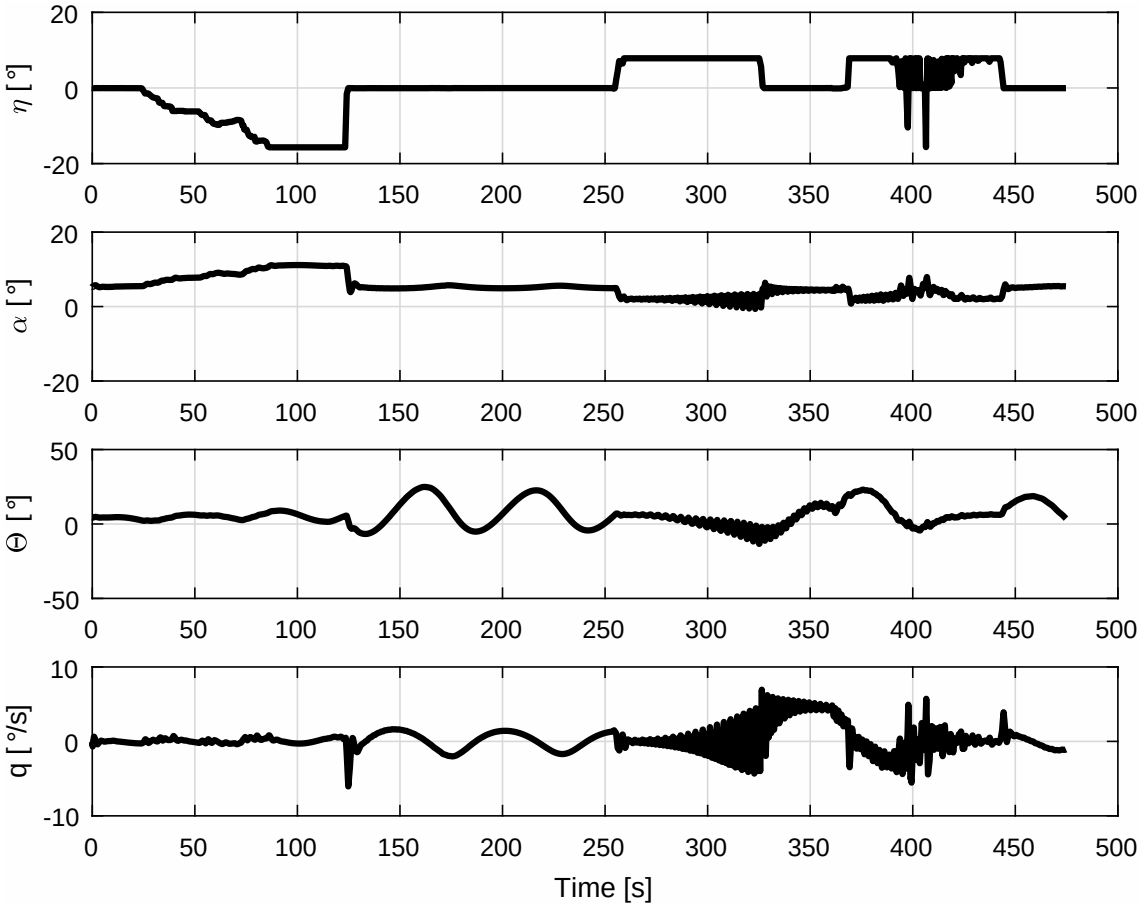

Figure D.8: Time histories of longitudinal parameters

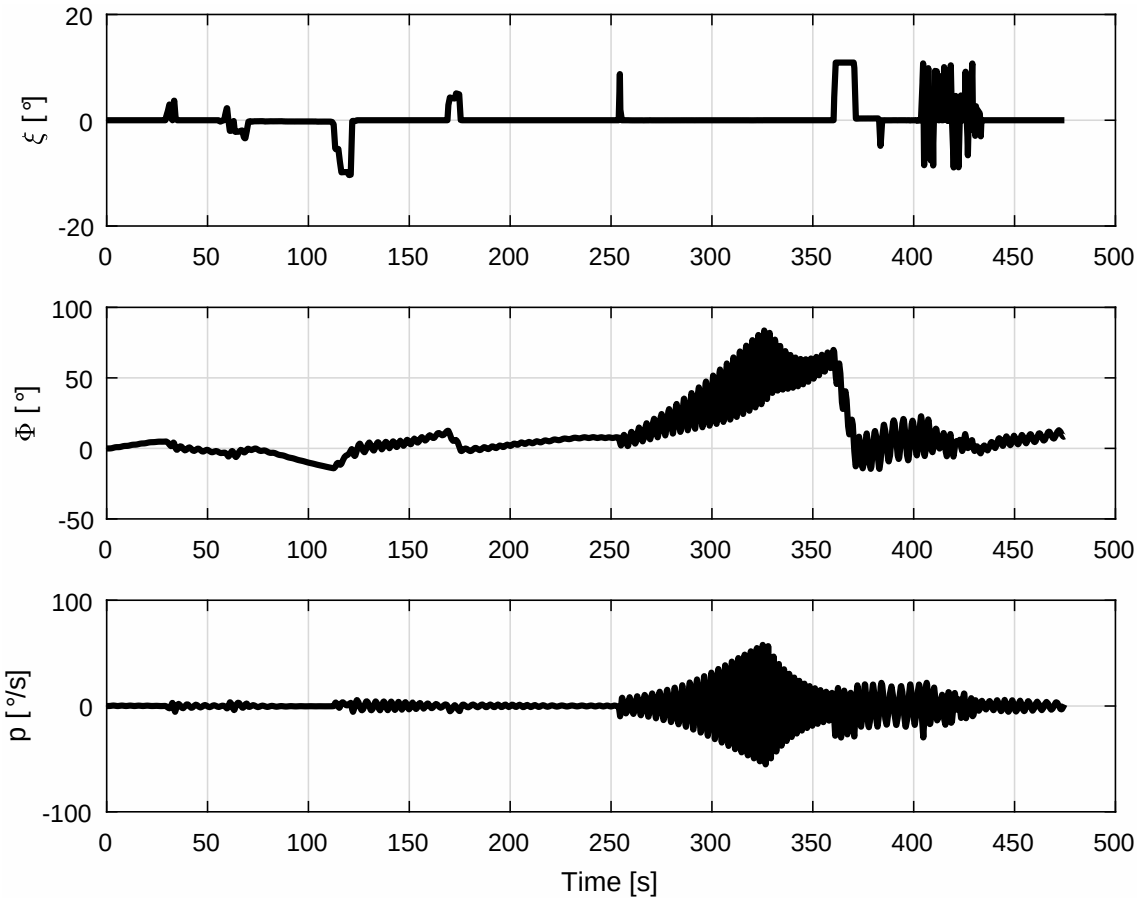

Figure D.9: Time histories of lateral parameters

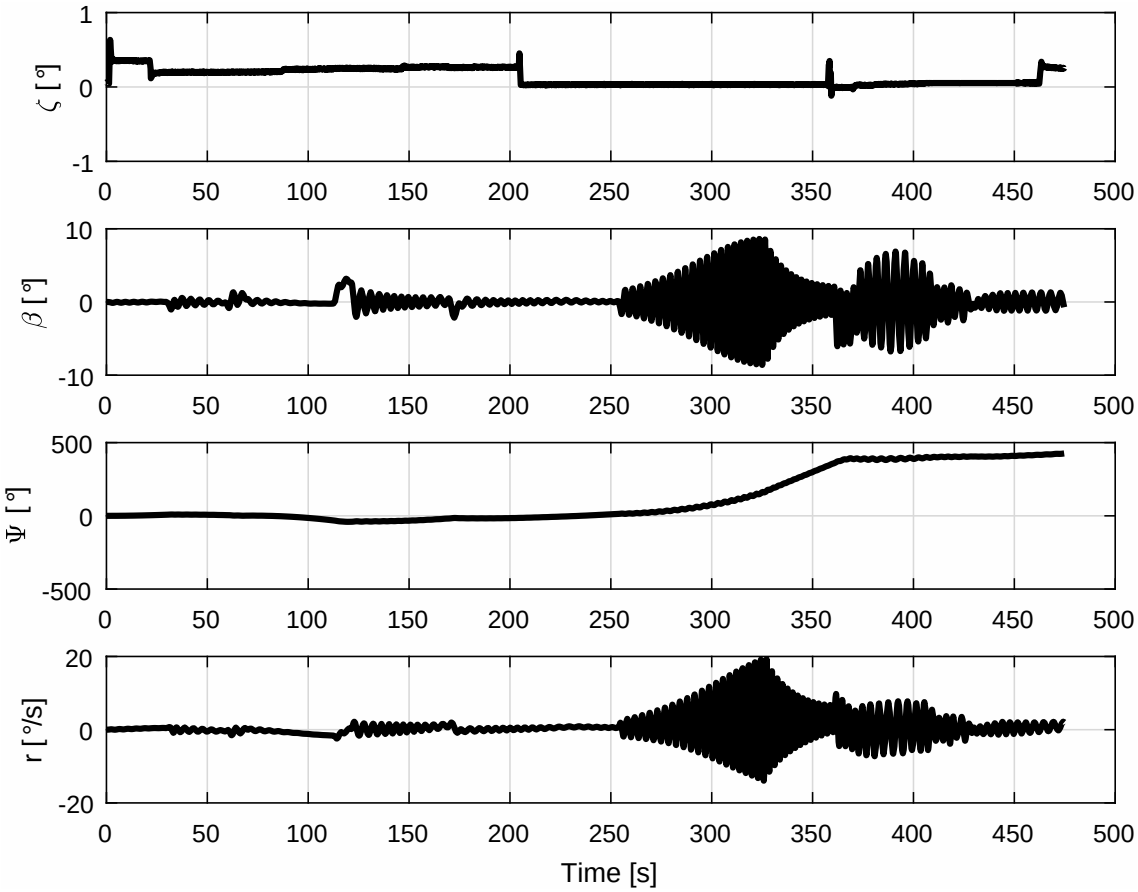

Figure D.10: Time histories of directional parameters

D.3 Stall conditions test, pilot 2, rigid A/C – ST(2)R

Date: 09/02/2018 **Time start:** **Time stop:** 10:19

Test No:	ST(2)R	**Test hardware:**	EFS500 + Speedgoat
Test pilot:	(2)	**Model version:**	HARTEN_v1 (R)

Task:	Stall test (ST)
Manoeuvre:	Pitch up

Instrumentation:	
Relevant files:	{D_LOADS/D_SIM/D_STRUCT}.DAT @ 09/02/2018 10:19; DSCN9578.MOV

Flight velocity: 110 m/s **Flight altitude:** 10000 ft

Aircraft weight: 79 t **Aircraft CG:** 20% MAC

V (EAS)	Observations
134 kt	Idle thrust – easy to maintain wings level during slowdown. At 1 kt/sec. Pull force required.
	Full back control at 134 kt. Not stalled – normal roll response with full back control.
	1800 ft/min descent
	Too loose throttle

Notes:

Nil

Notes (from audio recording):

“Looks left wing heavy”

“Stabilised at about 8 deg pitch attitude and 135 kt”

Figure D.11: Test card (ST(2)R)

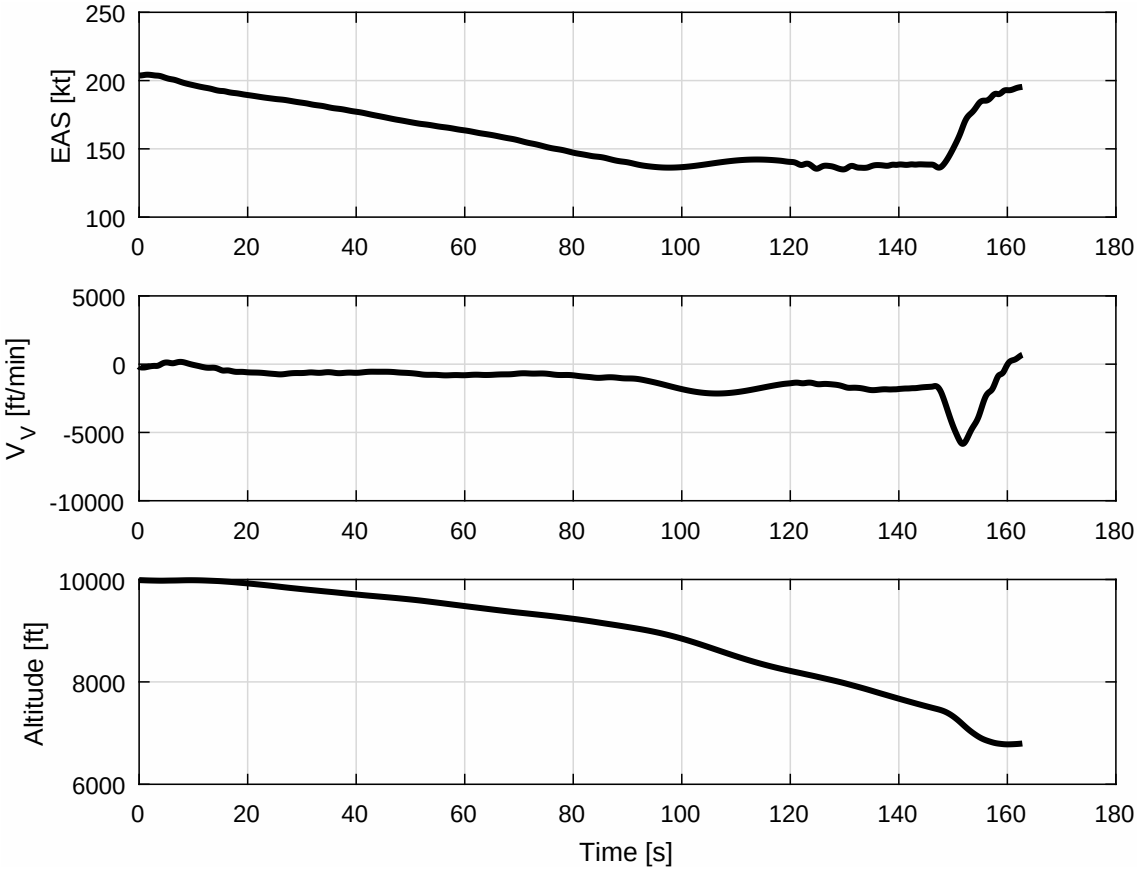

Figure D.12: Time histories of altitude and velocities

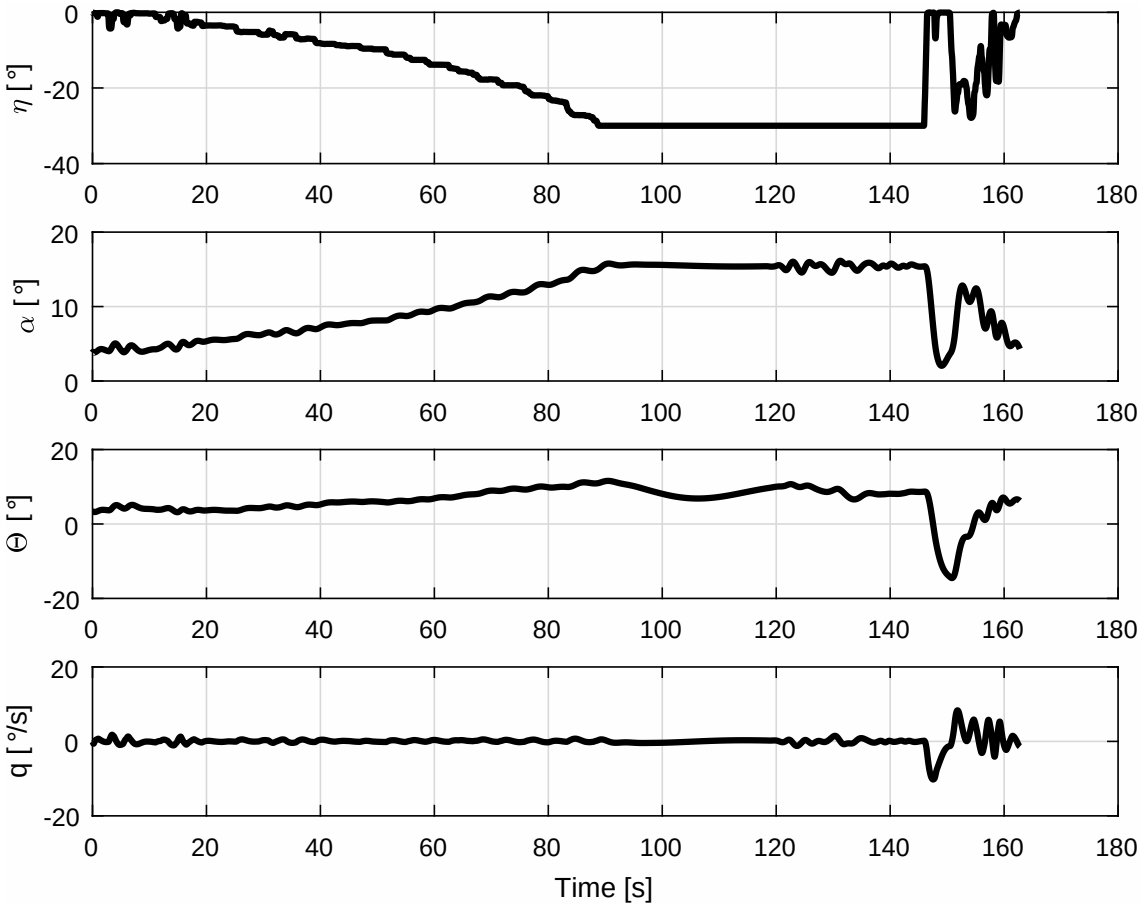

Figure D.13: Time histories of longitudinal parameters

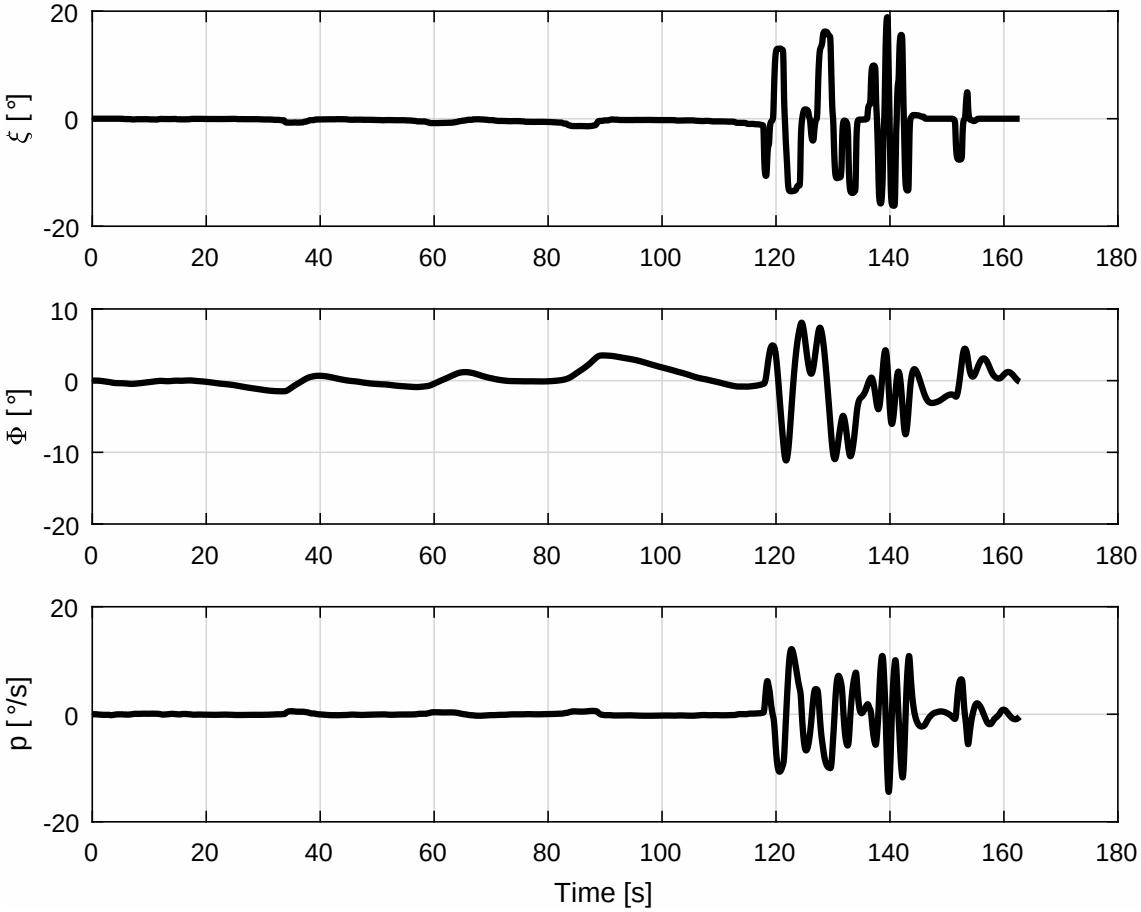

Figure D.14: Time histories of lateral parameters

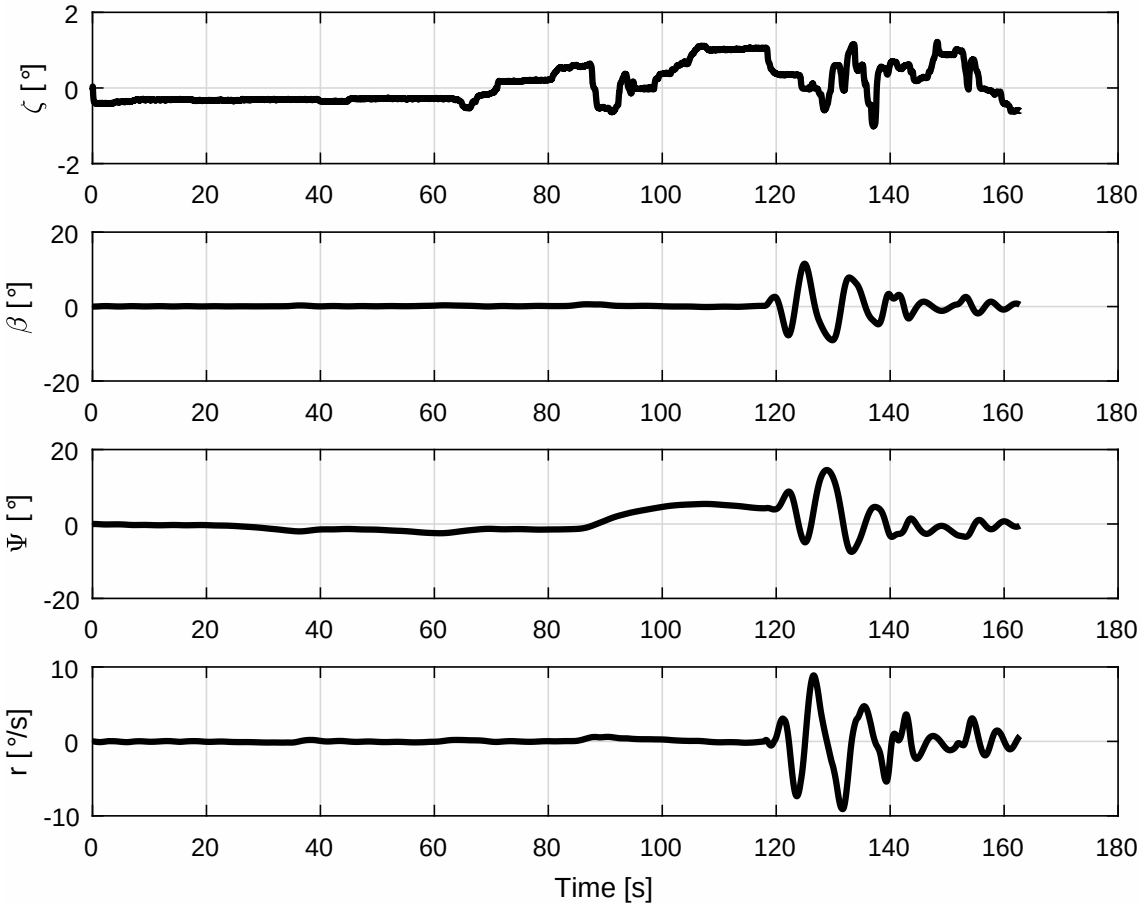

Figure D.15: Time histories of directional parameters

D.4 Stall conditions test, pilot 2, flexible A/C – ST(2)F

Date: 09/02/2018 **Time start:** **Time stop:** 14:02

Test No:	ST(2)F	**Test hardware:**	EFS500 + Speedgoat
Test pilot:	(2)	**Model version:**	HARTEN_v1 (F)

Task:	Stall test (ST)
Manoeuvre:	Pitch up

Instrumentation:	
Relevant files:	{D_LOADS/D_SIM/D_STRUCT}.DAT @ 09/02/2018 14:02; DSCN9590.MOV

Flight velocity: 110 m/s **Flight altitude:** 10000 ft

Aircraft weight: 79 t **Aircraft CG:** 20% MAC

V (EAS)	**Observations**
145 kt	FULL BACK STICK – CONTROL LIMITED
	NO STALL – 1600 FT/MIN DESCENT
	LEFT WING 'HEAVY'
	SLIGHT RIGHT STICK DEFLECTION
	SMALL LATERAL STICK INPUTS EXCITE DUTCH ROLL LIKE BEHAVIOUR

Notes:

Nil

Notes (from audio recording):

Nil

Figure D.16: Test card (ST(2)F)

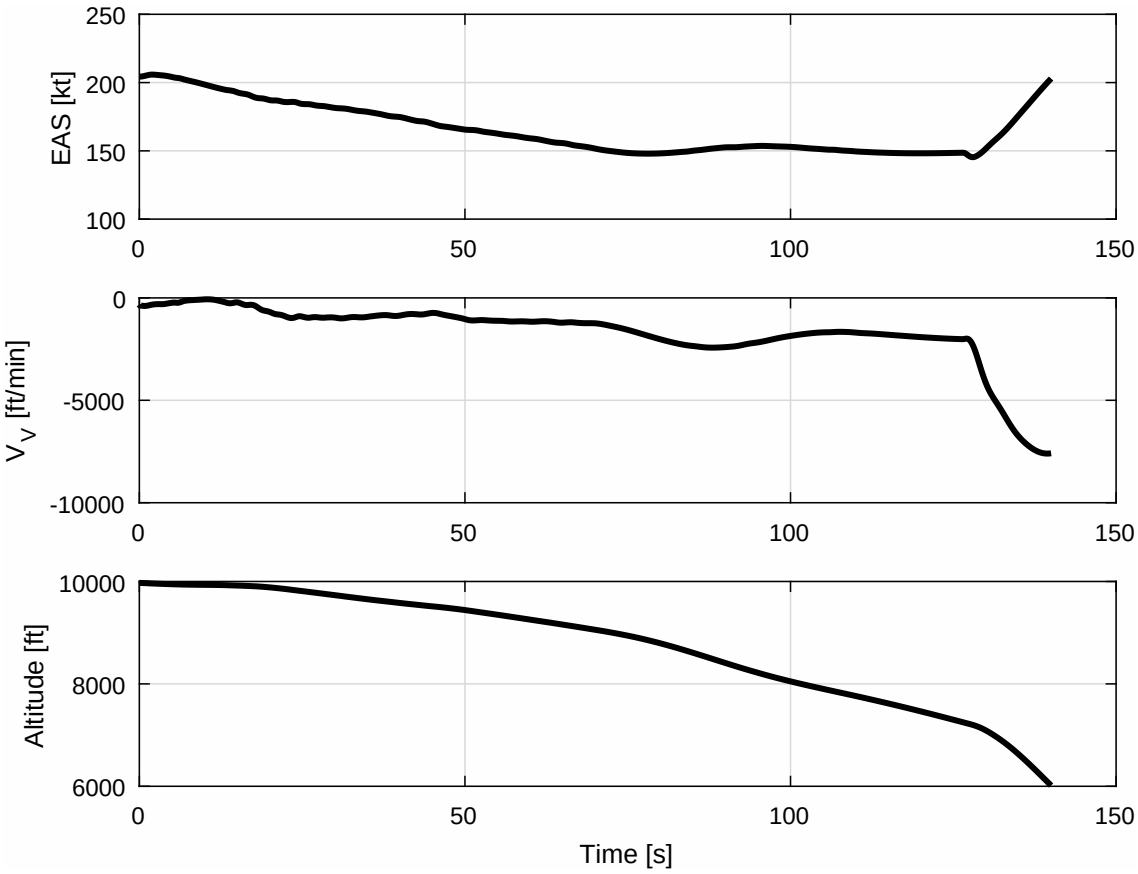

Figure D.17: Time histories of altitude and velocities

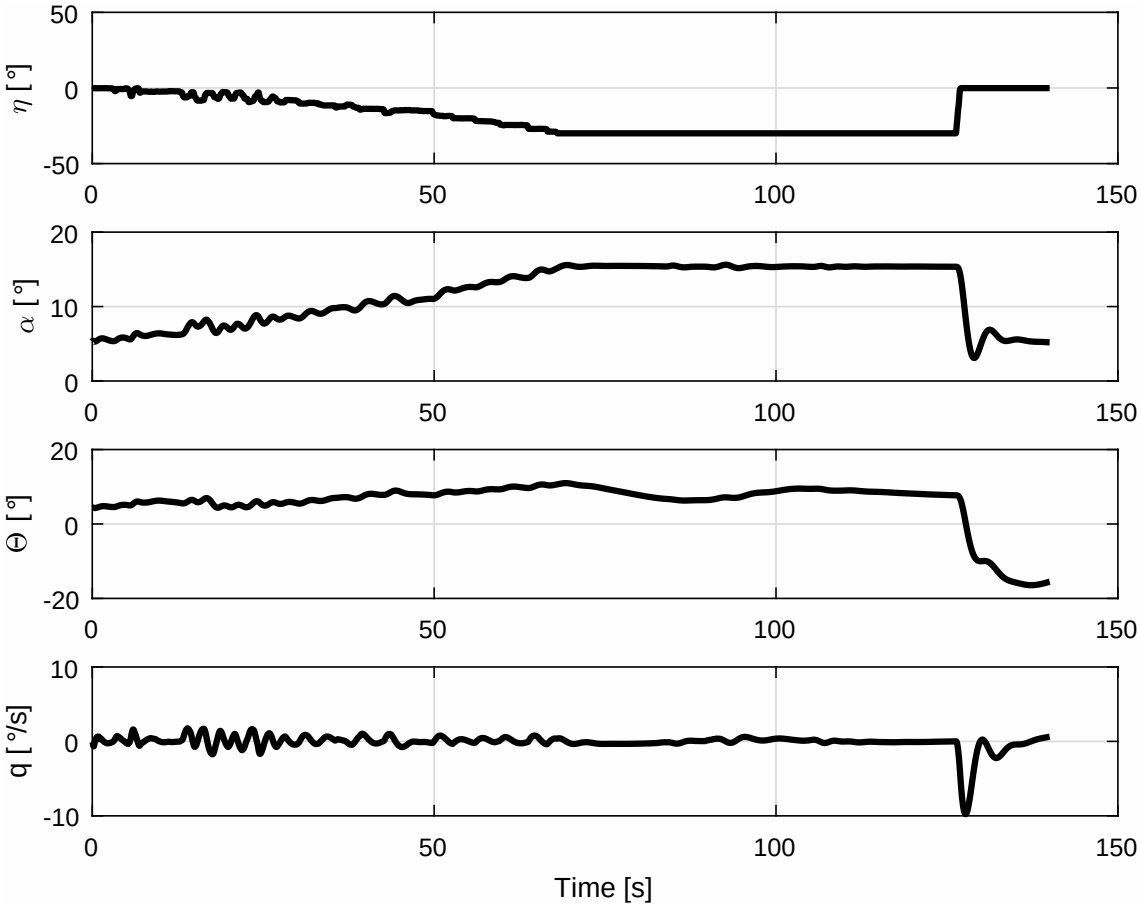

Figure D.18: Time histories of longitudinal parameters

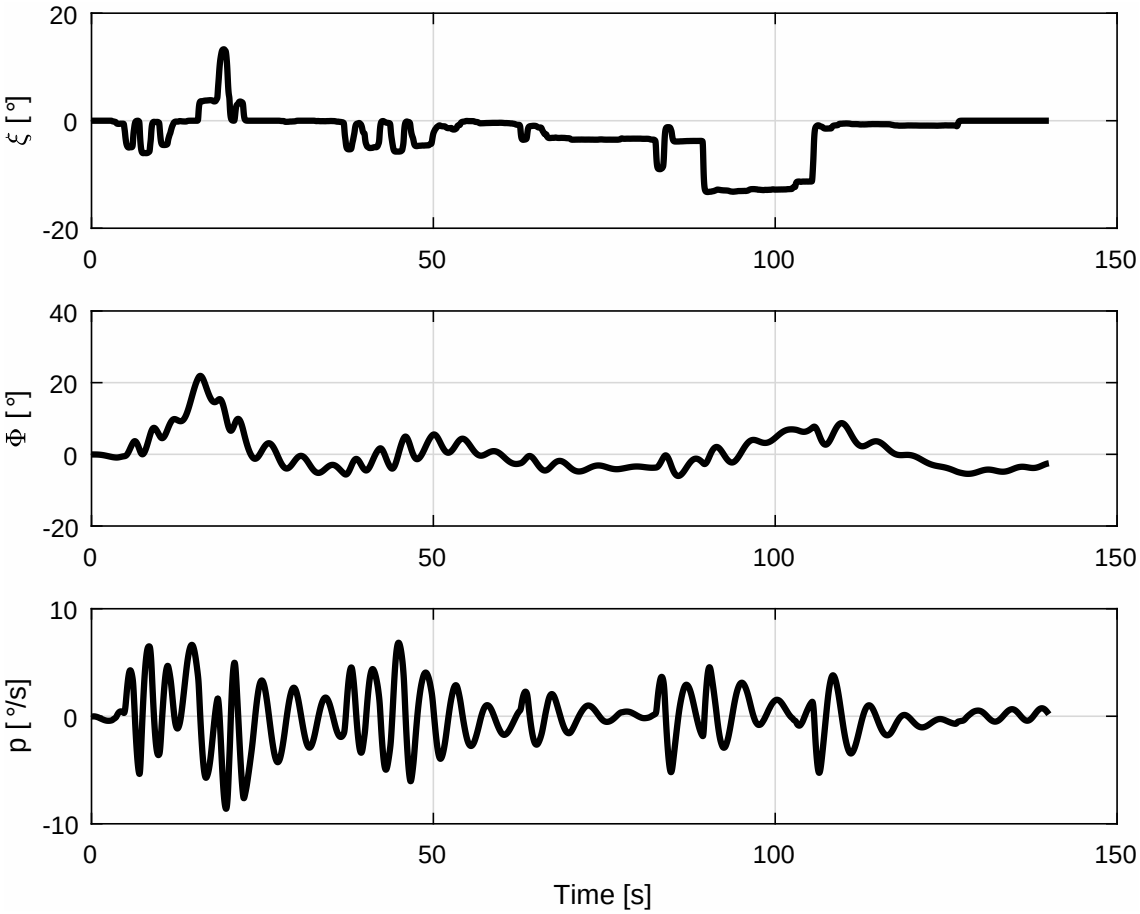

Figure D.19: Time histories of lateral parameters

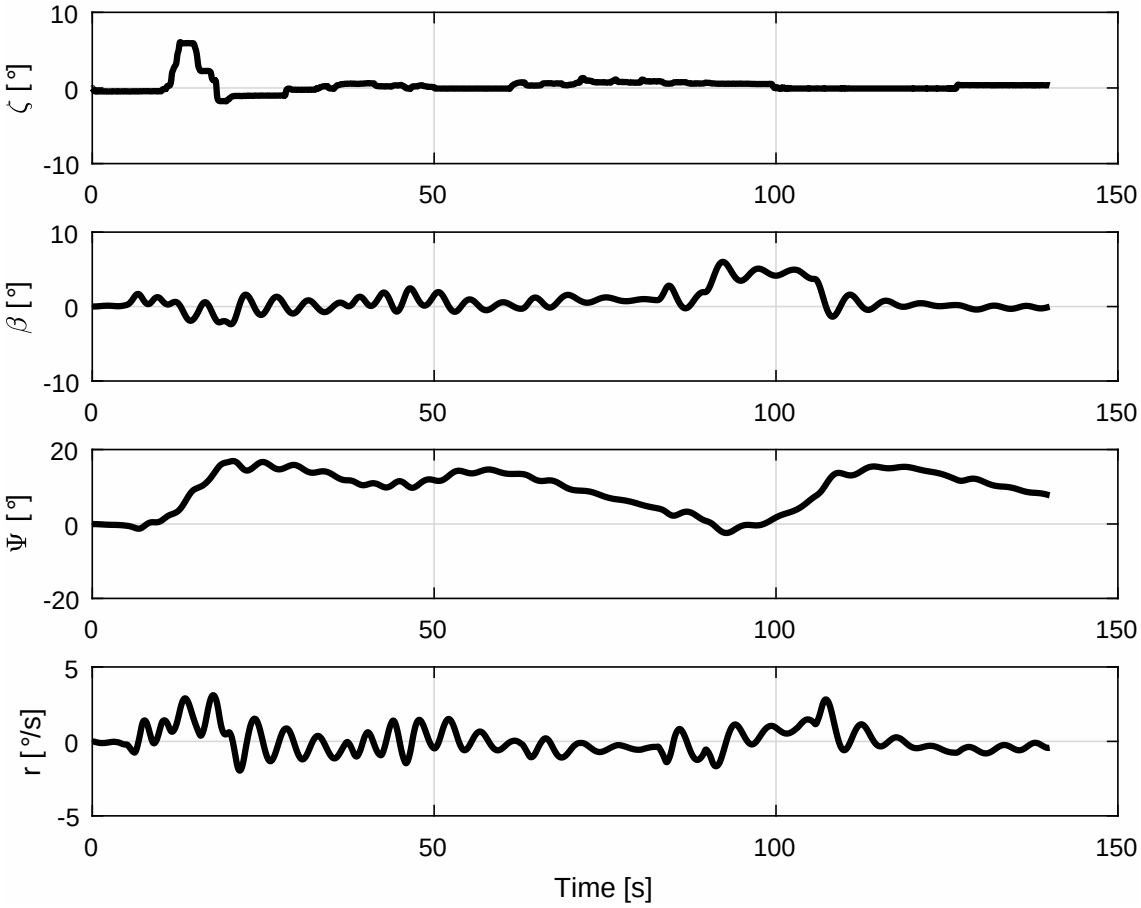

Figure D.20: Time histories of directional parameters

Appendix E

Longitudinal modes simulation data

E.1 SPPO mode, pilot 1, rigid A/C – SP(1)R

Date: 24/01/2018 **Time start:** **Time stop:** 16:10

Test No:	SP(1)R	**Test hardware:**	EFS500 + Speedgoat
Test pilot:	(1)	**Model version:**	HARTEN_v1 (R)

Task:	Longitudinal dynamic modes (SP)
Manoeuvre:	Pitch doublet

Instrumentation:	
Relevant files:	{D_SIM/D_STRUCT}.DAT @ 24/01/2018 16:10; DSCN9510.MOV; GOPR4016.MP4

Flight velocity: 110 m/s **Flight altitude:** 10000 ft

Aircraft weight: 79 t **Aircraft CG:** 20% MAC

SPPO / Pitch doublet

Stick movement:

N_{damp}: 1.5 T_{damp}: 7 sec

Notes:

Freq sweep period = 2 sec; heavily damped

Notes (from audio recording):

Nil

Figure E.1: Test card (SP(1)R)

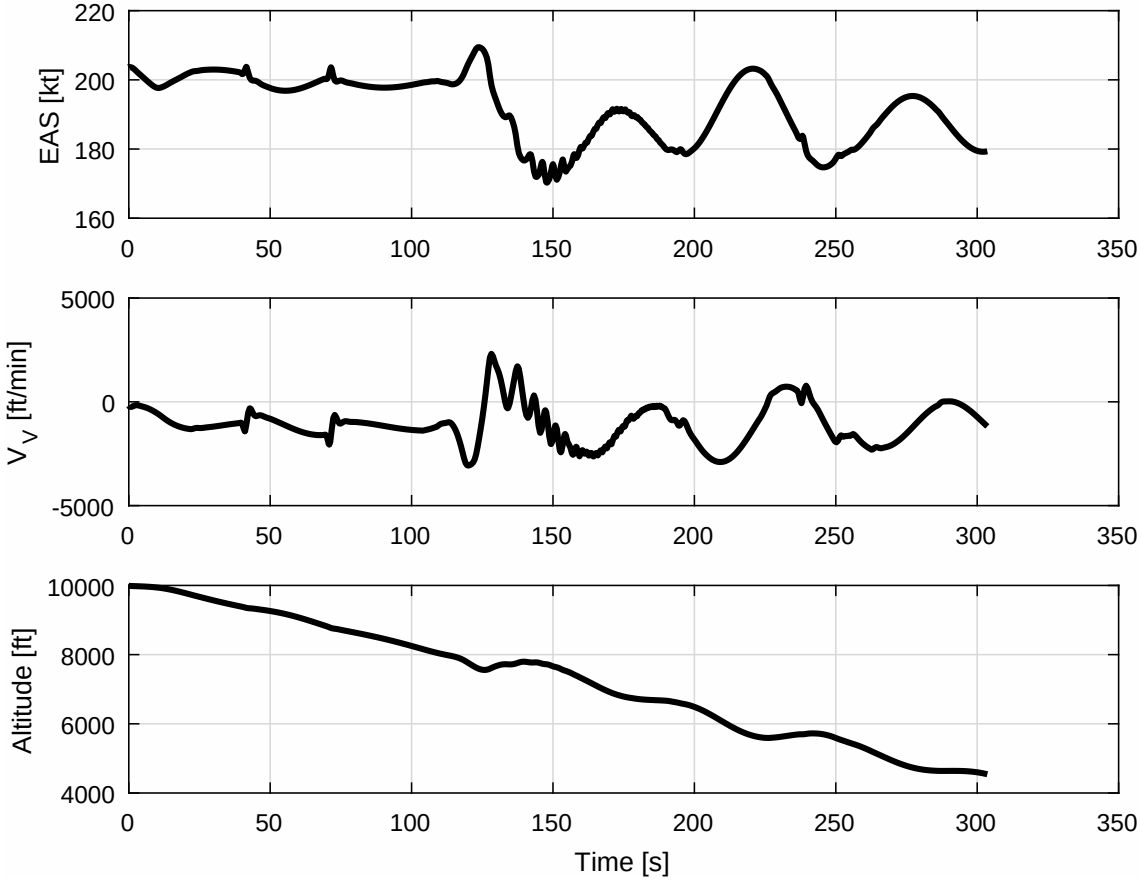

Figure E.2: Time histories of altitude and velocities

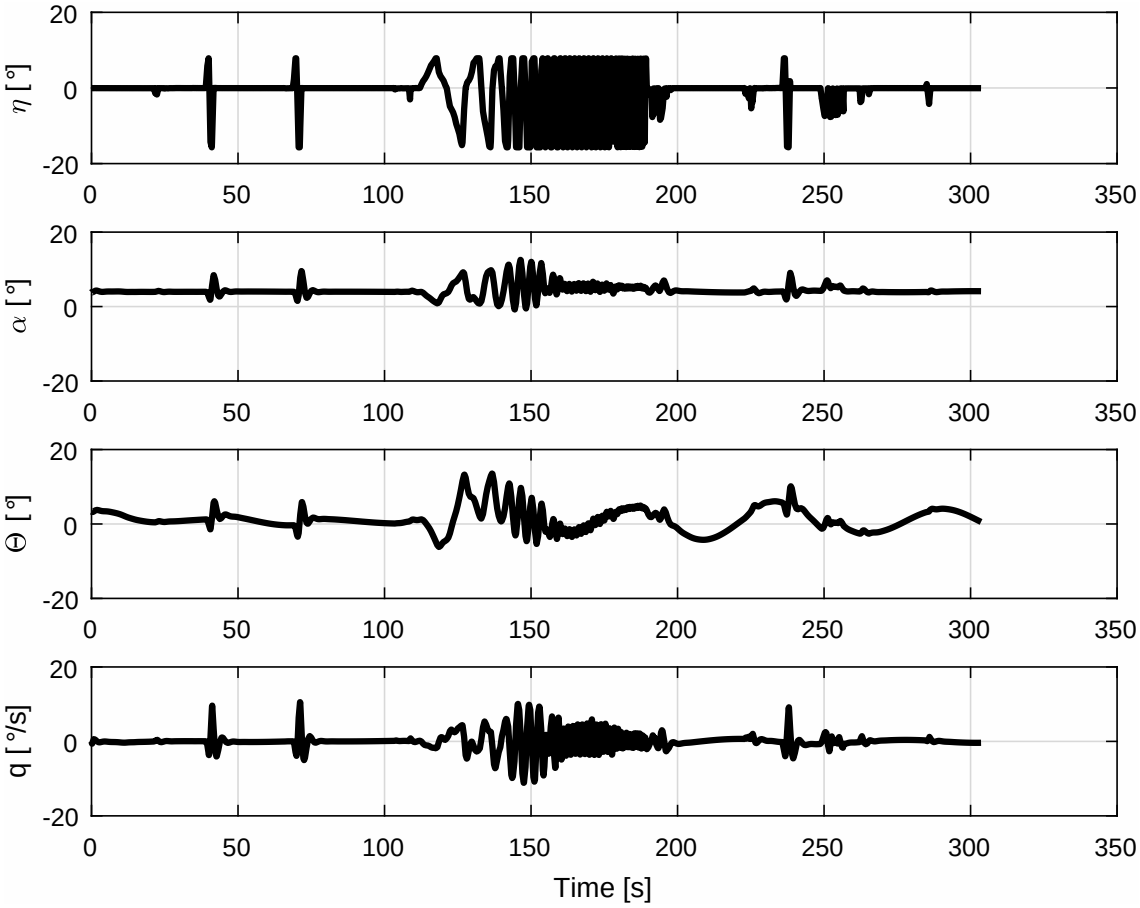

Figure E.3: Time histories of longitudinal parameters

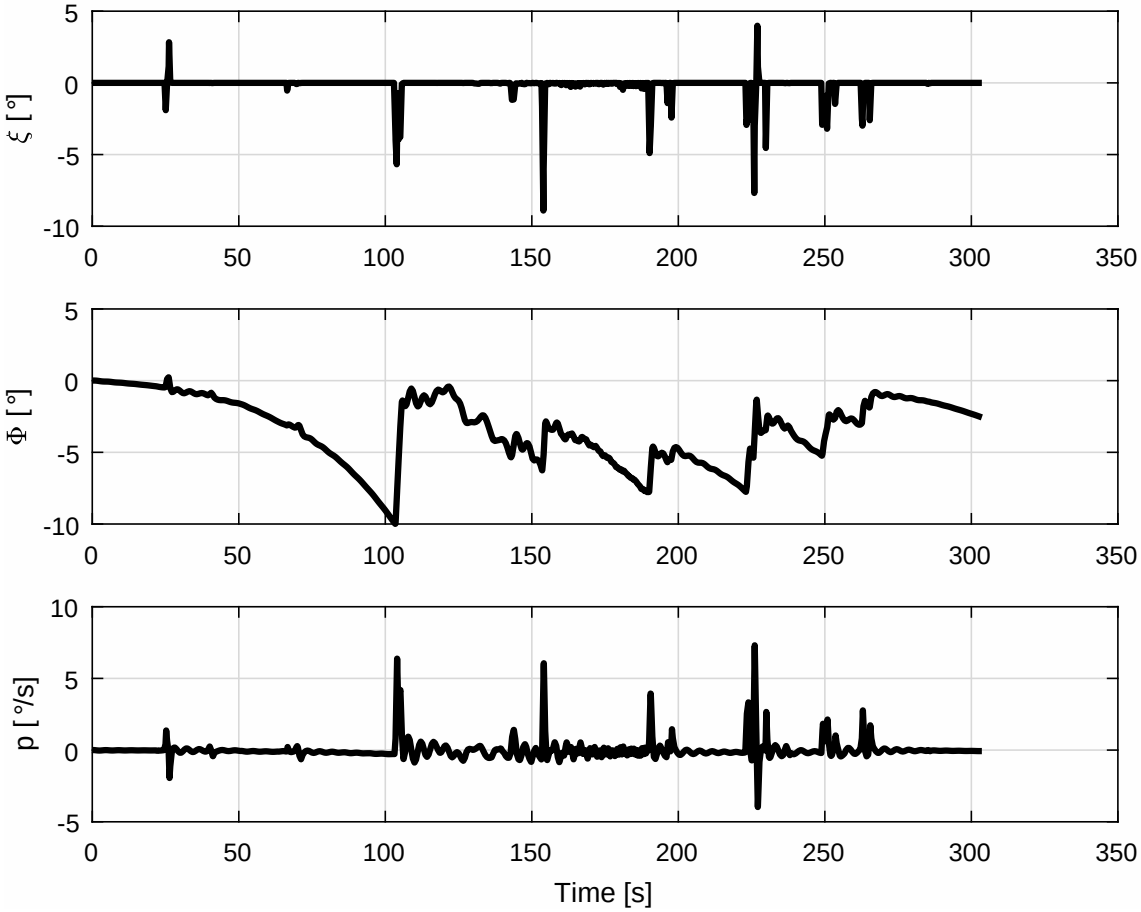

Figure E.4: Time histories of lateral parameters

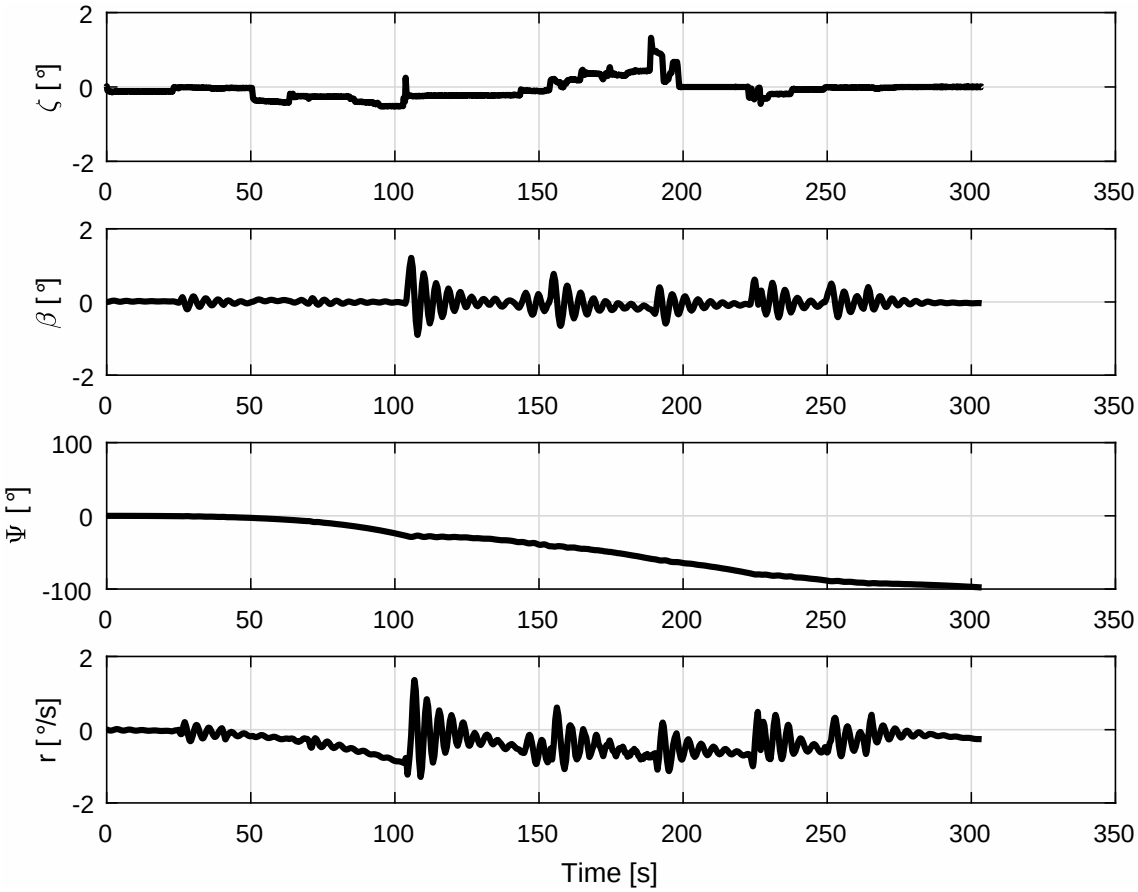

Figure E.5: Time histories of directional parameters

E.2 SPPO mode, pilot 1, flexible A/C – SP(1)F

Date: 24/01/2018 **Time start:** **Time stop:** 17:17

Test No:	SP(1)F	**Test hardware:**	EFS500 + Speedgoat
Test pilot:	(1)	**Model version:**	HARTEN_v1 (F)

Task:	Longitudinal dynamic modes (SP)
Manoeuvre:	Pitch doublet

Instrumentation:	
Relevant files:	{D_SIM/D_STRUCT}.DAT @ 24/01/2018 17:17; DSCN9519.MOV; GOPR4025.MP4

Flight velocity: 110 m/s **Flight altitude:** 10000 ft

Aircraft weight: 79 t **Aircraft CG:** 20% MAC

SPPO / Pitch doublet

Stick movement:

N_{damp}: 1 T_{damp}: 6 sec

Notes:

Nil

Notes (from audio recording):

"Deadbeat" – about damping

Figure E.6: Test card (SP(1)F)

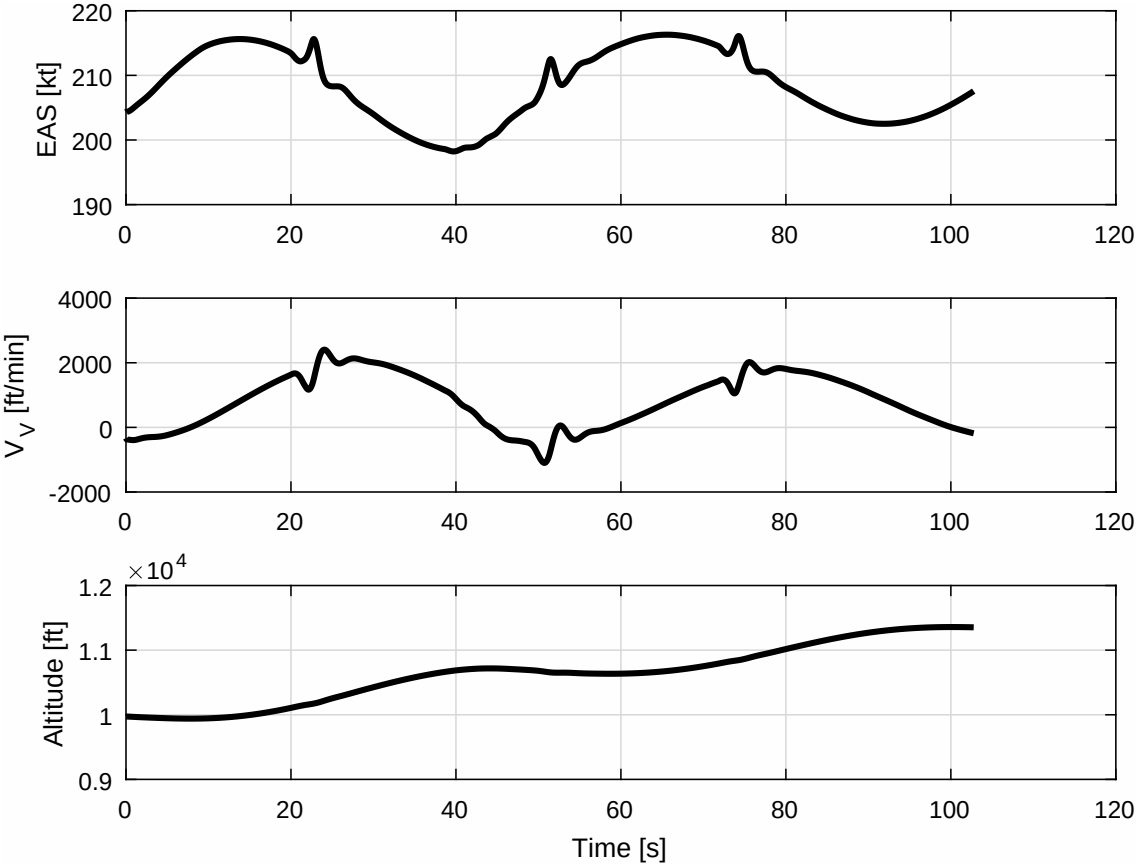

Figure E.7: Time histories of altitude and velocities

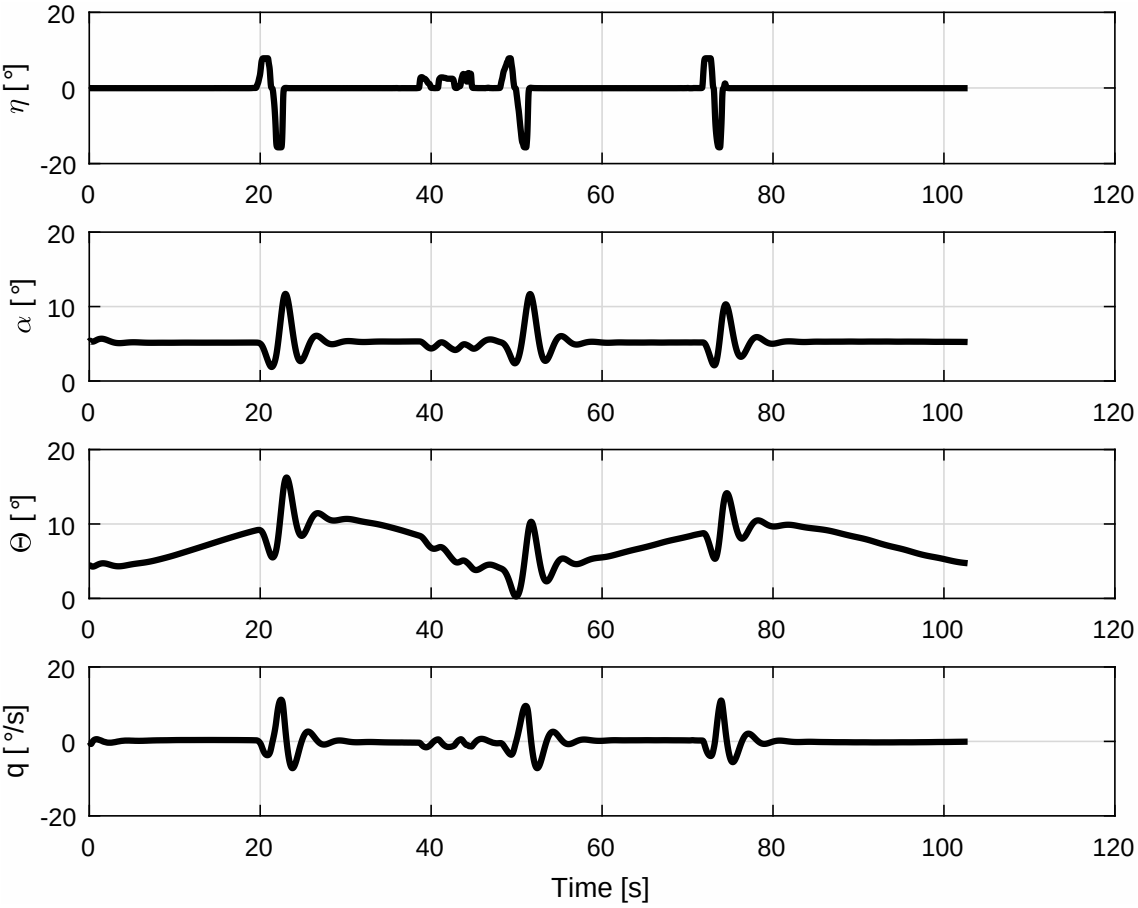

Figure E.8: Time histories of longitudinal parameters

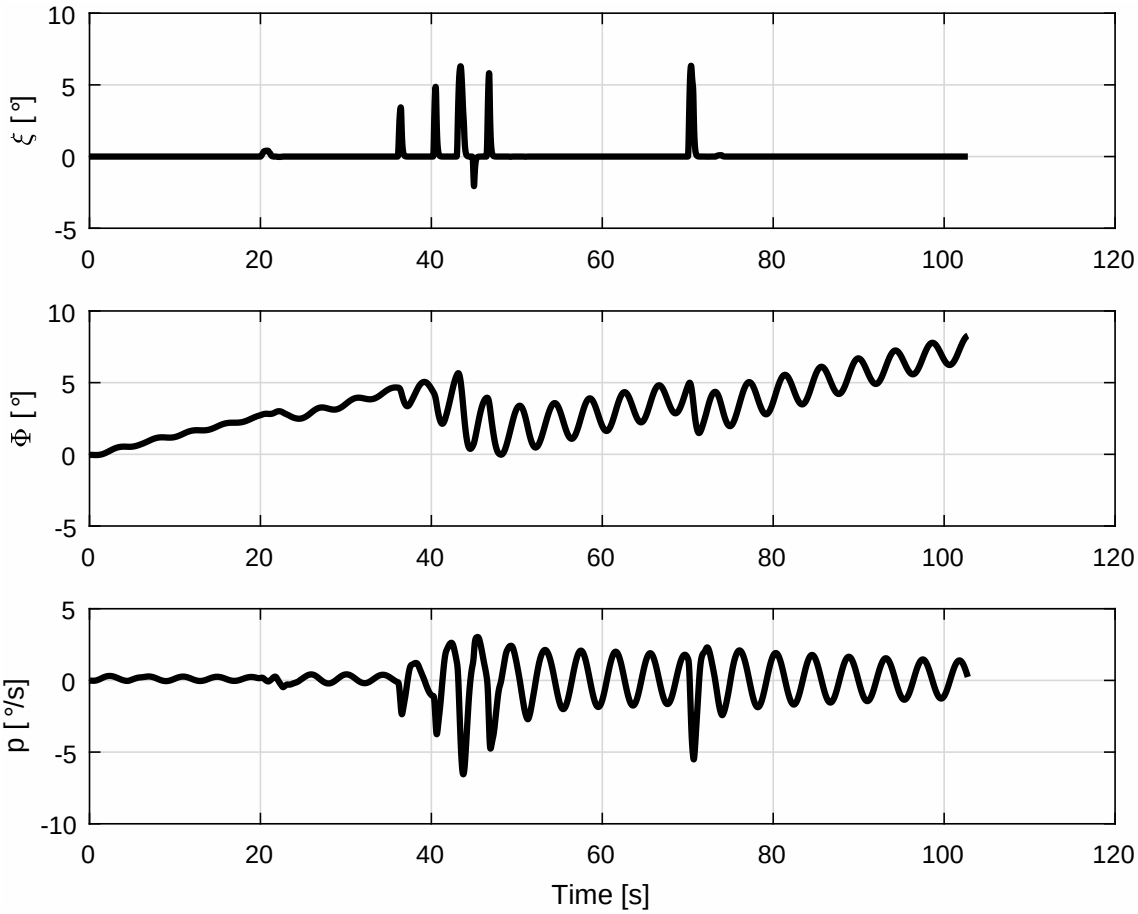

Figure E.9: Time histories of lateral parameters

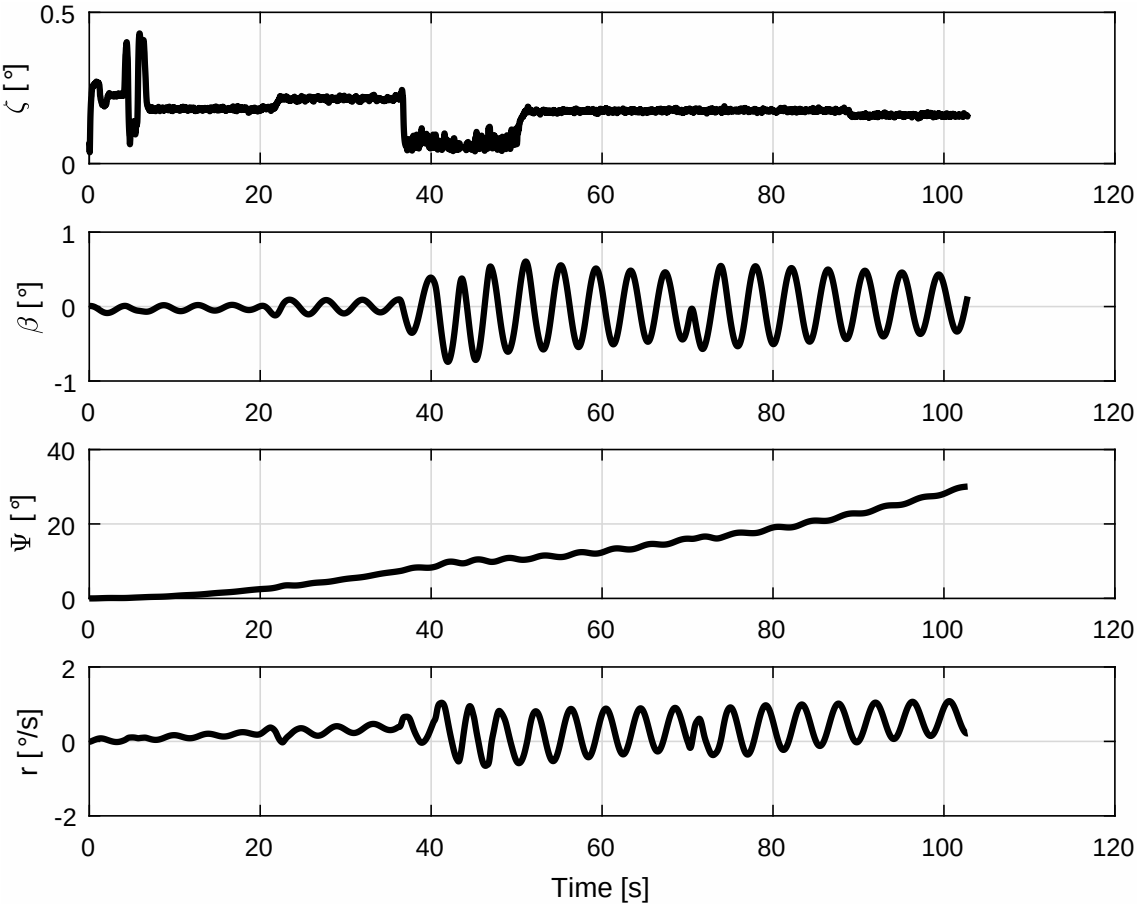

Figure E.10: Time histories of directional parameters

E.3 SPPO mode, pilot 2, rigid A/C – SP(2)R

Date: 09/02/2018 **Time start:** **Time stop:** 10:24

Test No:	SP(2)R	**Test hardware:**	EFS500 + Speedgoat
Test pilot:	(2)	**Model version:**	HARTEN_v1 (R)

Task:	Longitudinal dynamic modes
Manoeuvre:	Pitch doublet + frequency sweep

Instrumentation:	
Relevant files:	{D_LOADS/D_SIM/D_STRUCT}.DAT @ 09/02/2018 10:24; DSCN9579.MOV; DSCN9580.MOV

Flight velocity: 110 m/s **Flight altitude:** 10000 ft

Aircraft weight: 79 t **Aircraft CG:** 20% MAC

SPPO / Pitch doublet

Stick movement:

N_{damp}: 1 deg/sec T_{damp}: 1.5 sec (well damped)

Notes:

Frequency sweep; limited bandwidth; 0 to 1 Hz

Notes (from audio recording):

Nil

Figure E.11: Test card (SP(2)R)

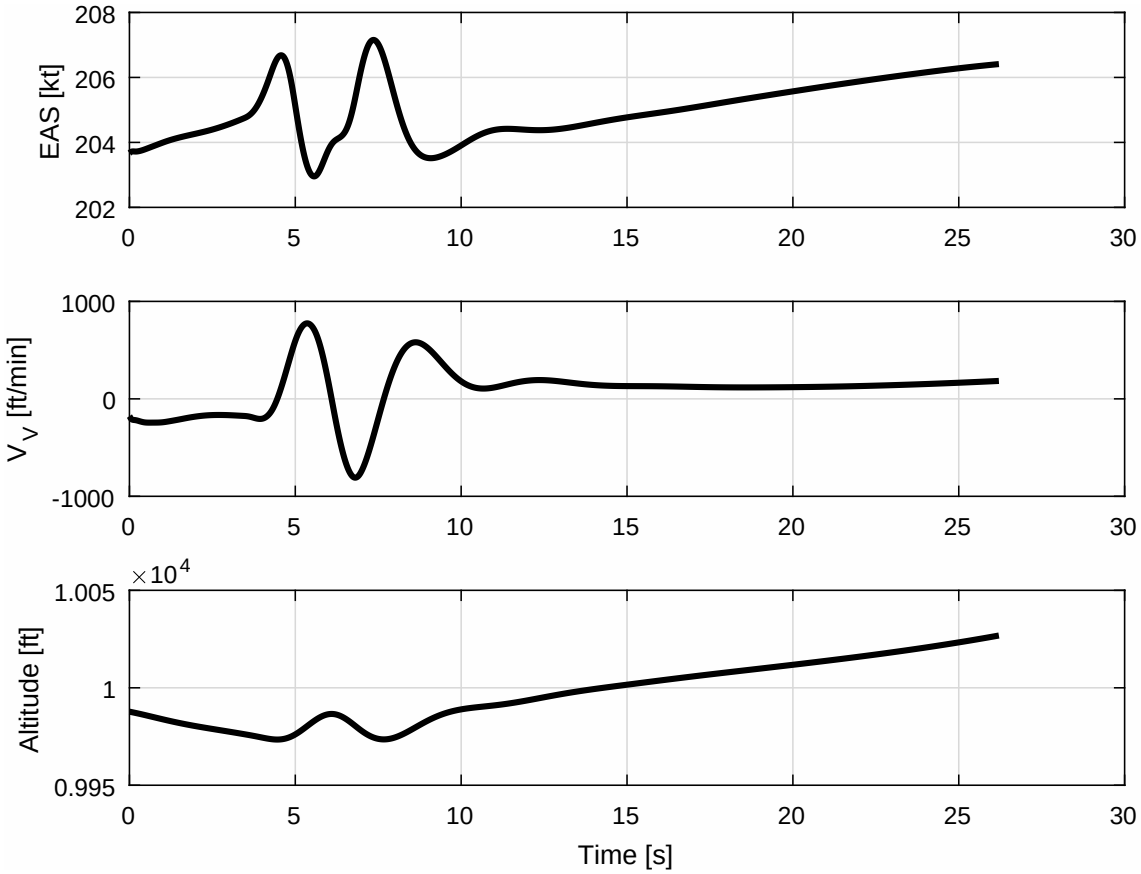

Figure E.12: Time histories of altitude and velocities

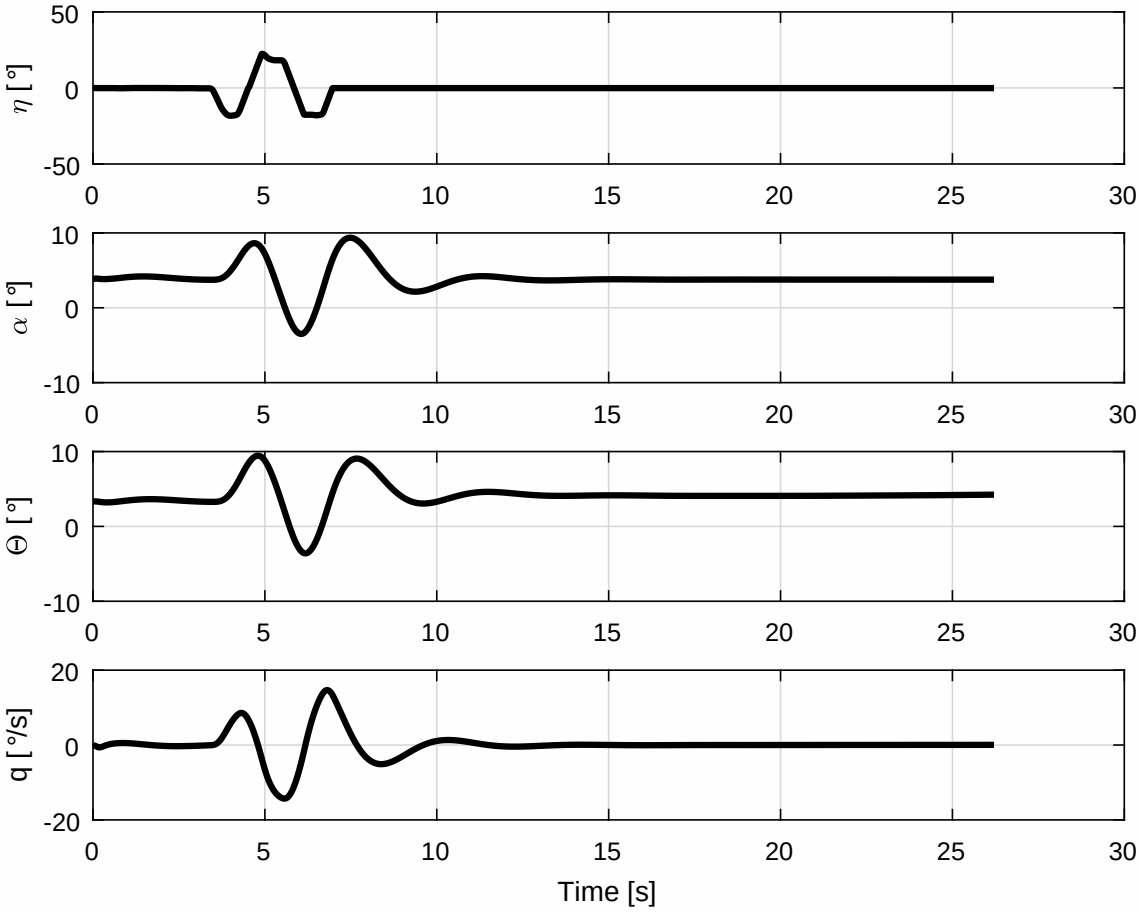

Figure E.13: Time histories of longitudinal parameters

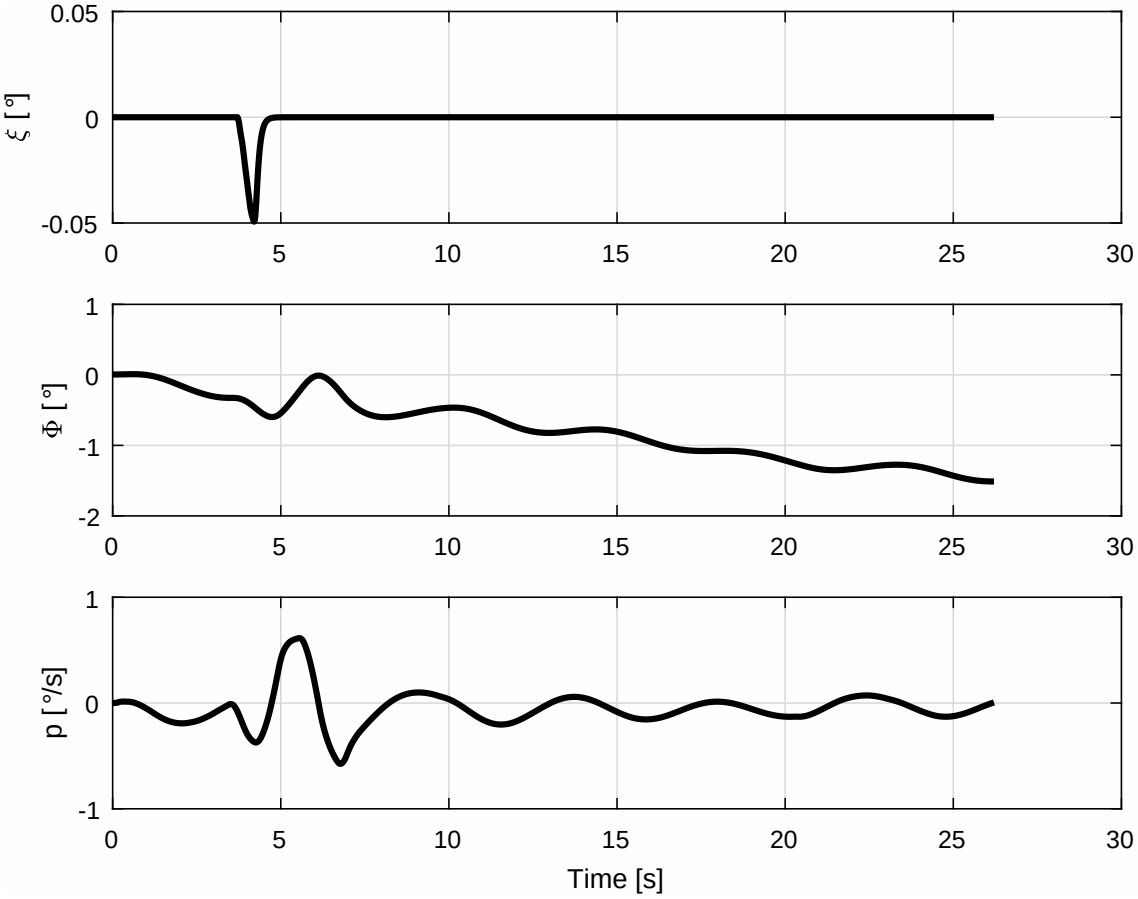

Figure E.14: Time histories of lateral parameters

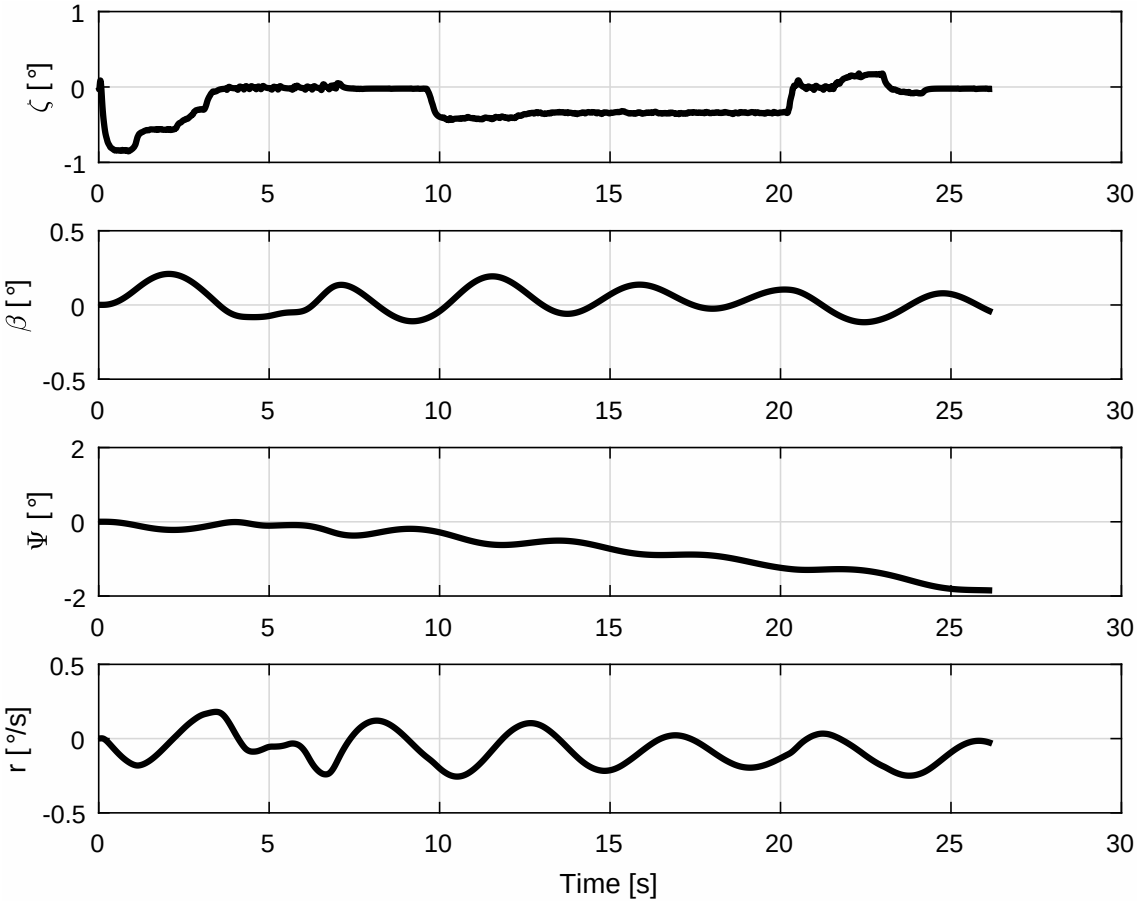

Figure E.15: Time histories of directional parameters

E.4 SPPO mode, pilot 2, flexible A/C, frequency sweep input – SP(2)F-FS

Date: 09/02/2018 **Time start:** **Time stop:** 14:14

Test No:	SP(2)F-FS	**Test hardware:**	EFS500 + Speedgoat
Test pilot:	(2)	**Model version:**	HARTEN_v1 (F)

Task:	Longitudinal dynamic modes SP(2)F
Manoeuvre:	Pitch doublet

Instrumentation:	
Relevant files:	{D_LOADS/D_SIM/D_STRUCT}.DAT @ 09/02/2018 14:14; DSCN9593.MOV

Flight velocity: 110 m/s **Flight altitude:** 10000 ft

Aircraft weight: 79 t **Aircraft CG:** 20% MAC

SPPO / Pitch doublet

Stick movement:

N_{damp}: T_{damp}:

Notes:

Frequency sweep – qualitatively similar to rigid

Notes (from audio recording):

Figure E.16: Test card (SP(2)F-FS)

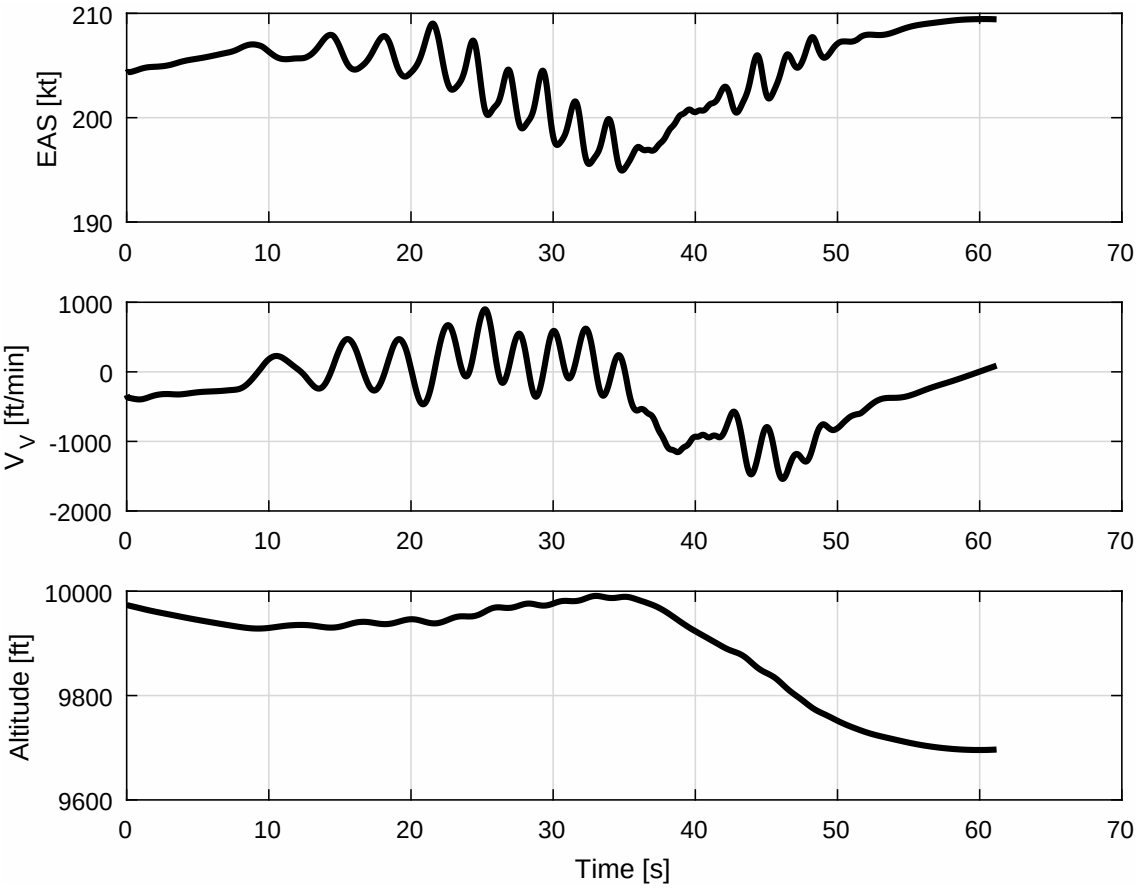

Figure E.17: Time histories of altitude and velocities

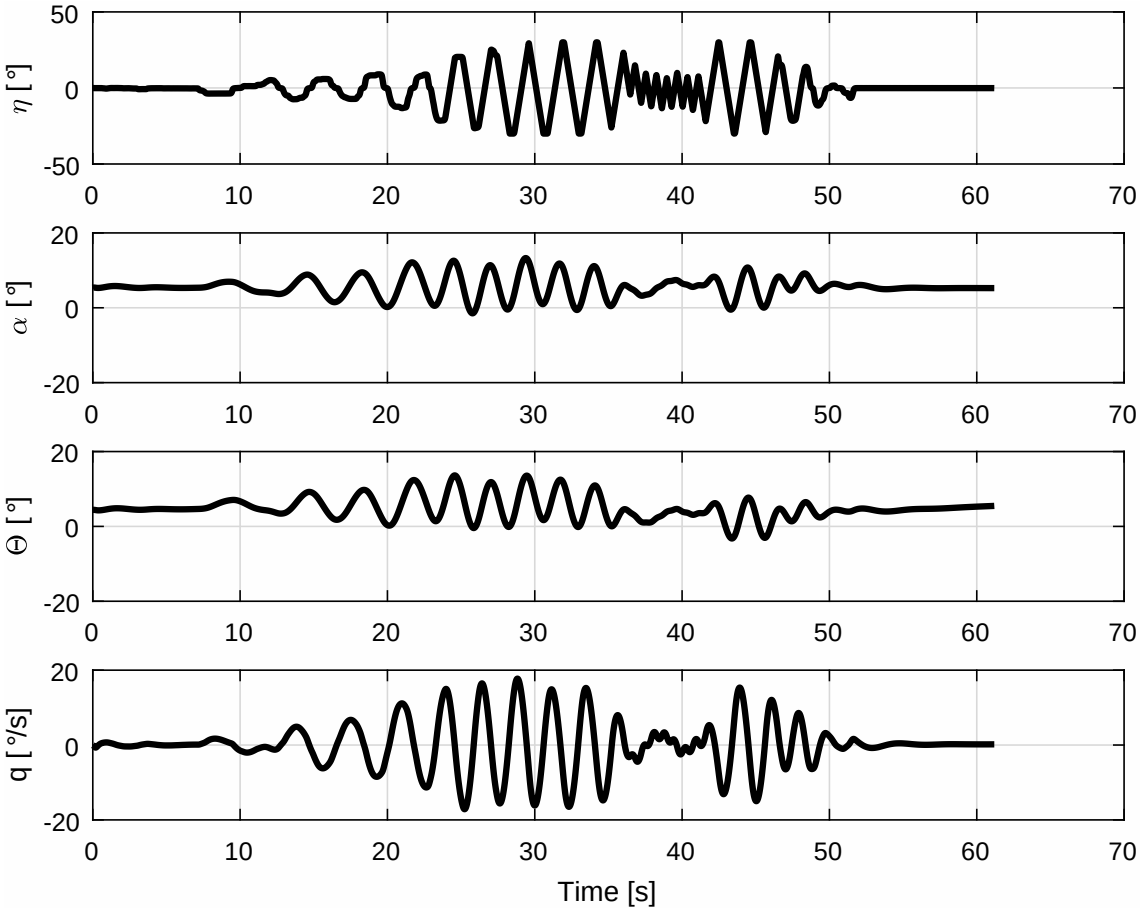

Figure E.18: Time histories of longitudinal parameters

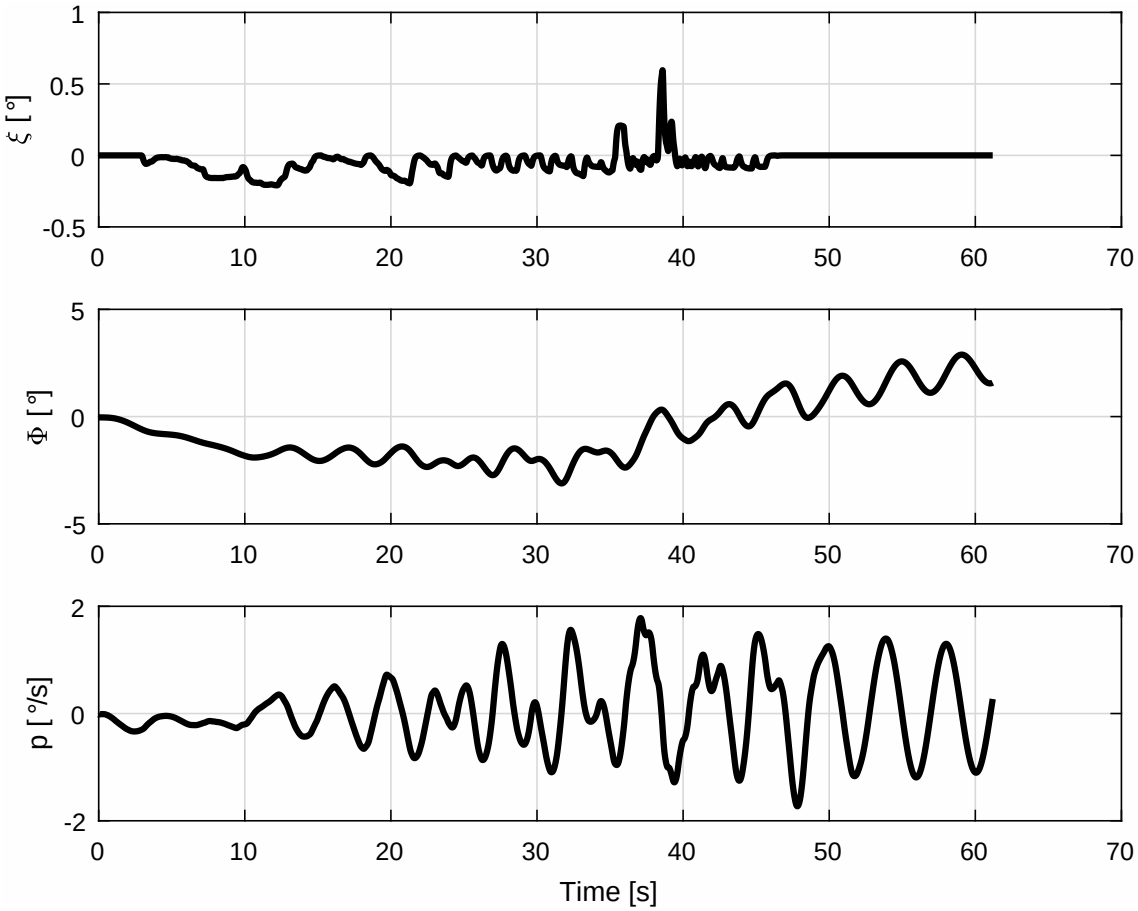

Figure E.19: Time histories of lateral parameters

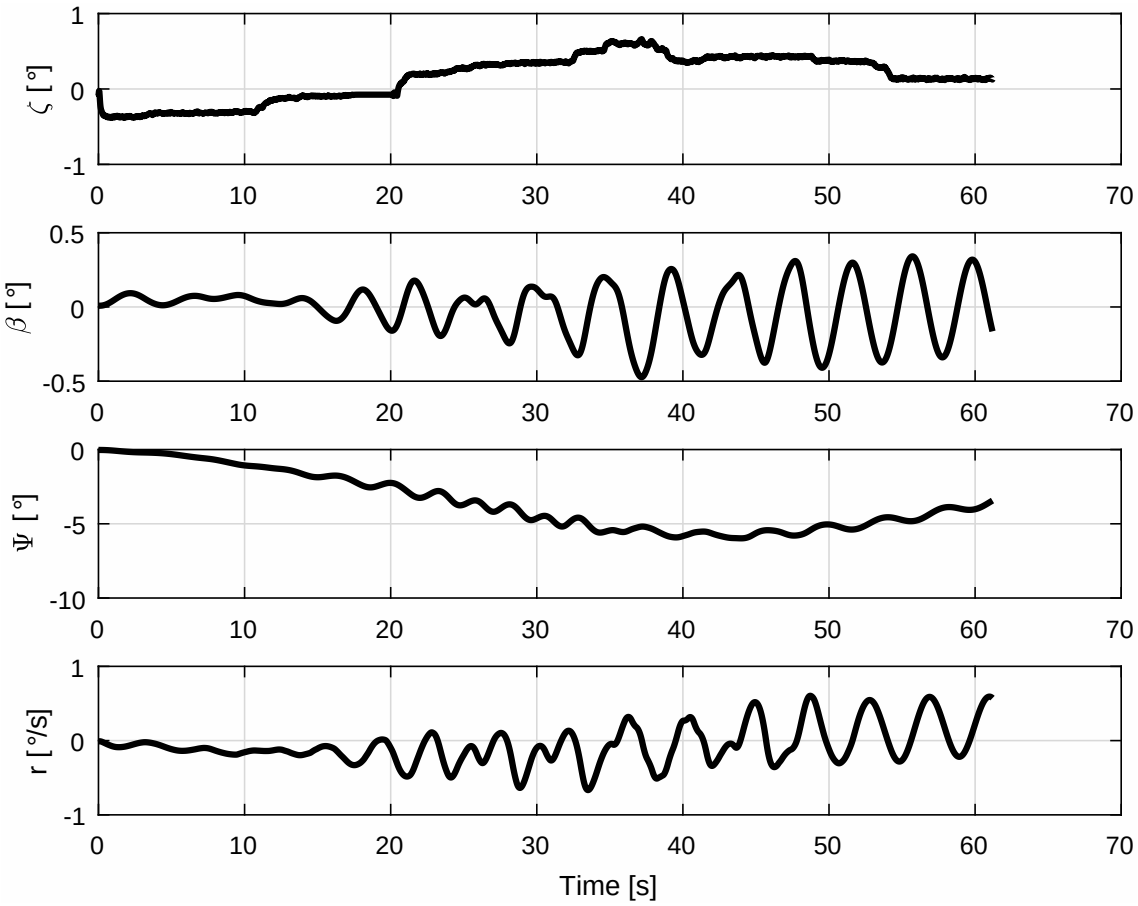

Figure E.20: Time histories of directional parameters

E.5 SPPO mode, pilot 2, flexible A/C, elevator doublet input – SP(2)F-PD

Date: 09/02/2018 **Time start:** **Time stop:** 14:06

Test No:	SP(2)F-PD	**Test hardware:**	EFS500 + Speedgoat
Test pilot:	(2)	**Model version:**	HARTEN_v1 (F)

Task:	Longitudinal dynamic modes SP(2)F
Manoeuvre:	Pitch doublet

Instrumentation:	
Relevant files:	{D_LOADS/D_SIM/D_STRUCT}.DAT @ 09/02/2018 14:06; DSCN9591.MOV

Flight velocity: 110 m/s **Flight altitude:** 10000 ft

Aircraft weight: 79 t **Aircraft CG:** 20% MAC

SPPO / Pitch doublet

Stick movement:

N_{damp}: Slightly slower than rigid T_{damp}: Damping reduced over rigid; 3 or 4 pitch overshoots

Notes:

Nil

Notes (from audio recording):

Nil

Figure E.21: Test card (SP(2)F-PD)

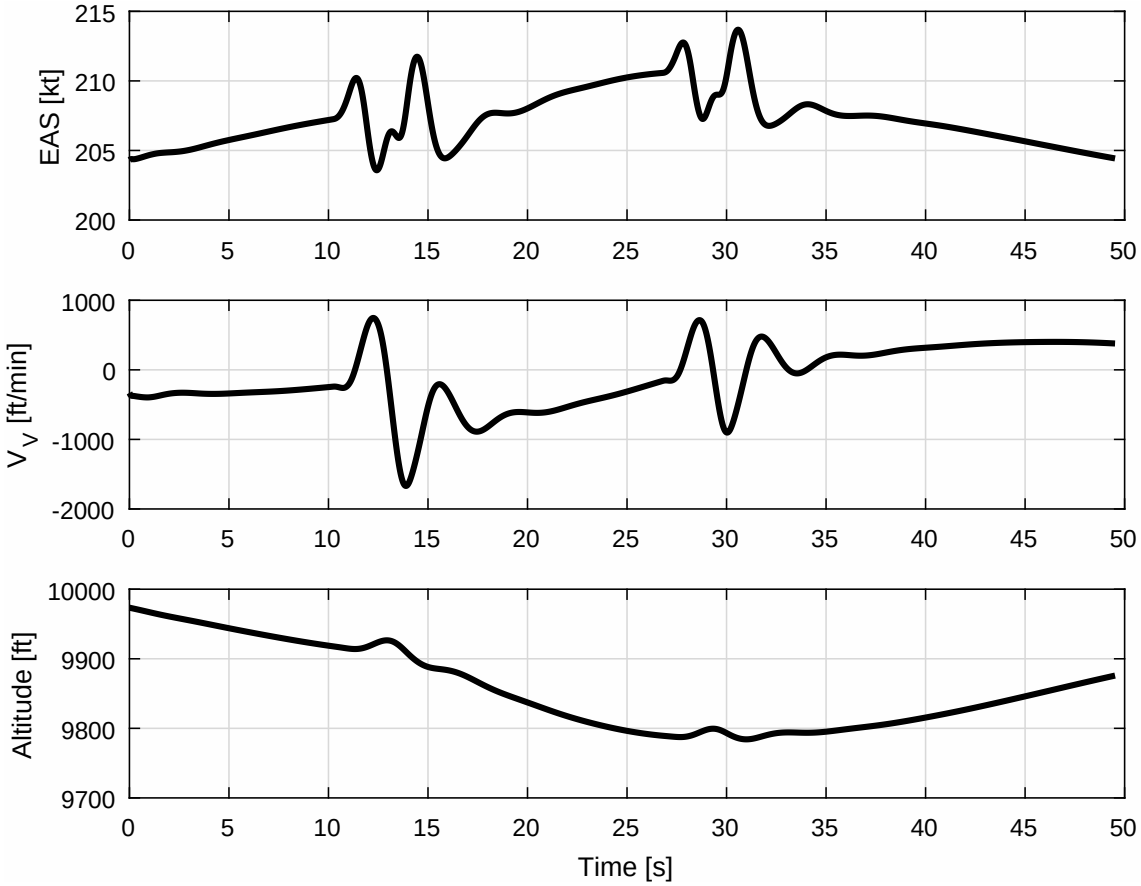

Figure E.22: Time histories of altitude and velocities

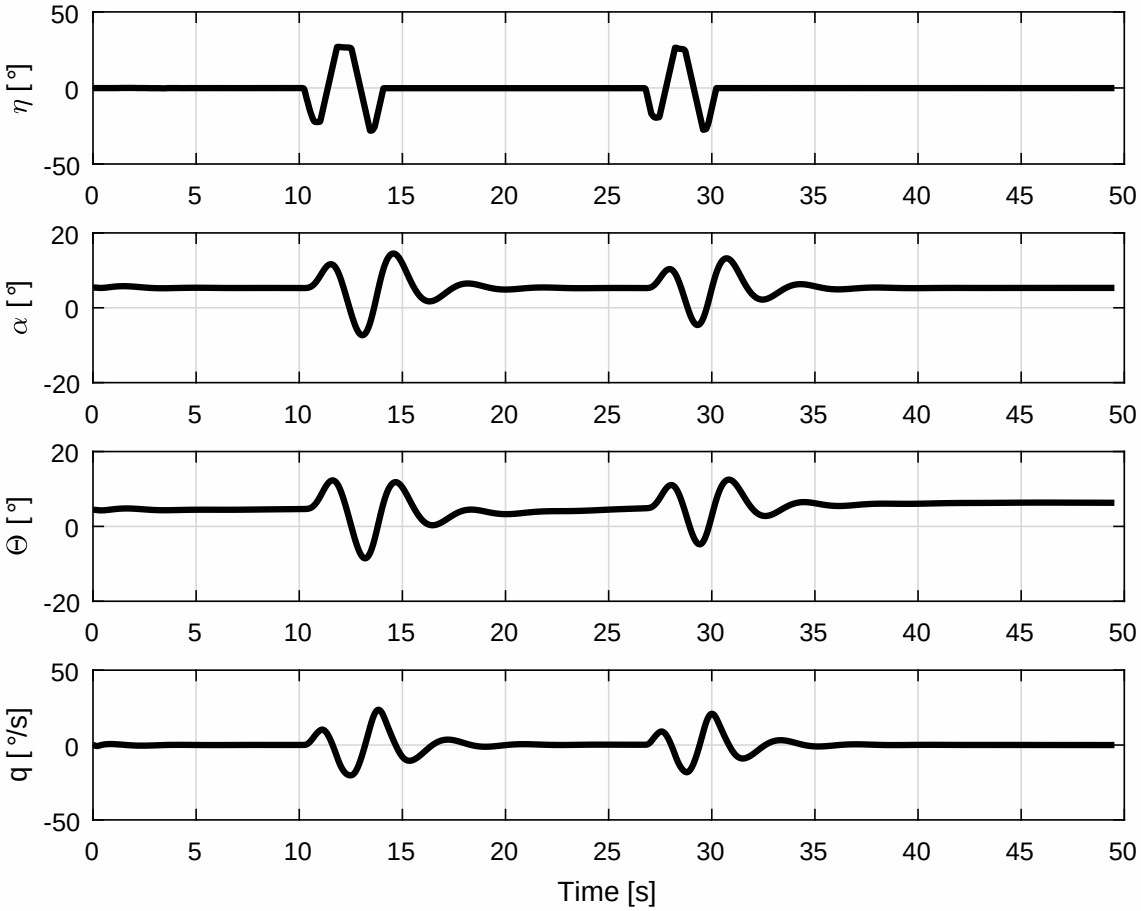

Figure E.23: Time histories of longitudinal parameters

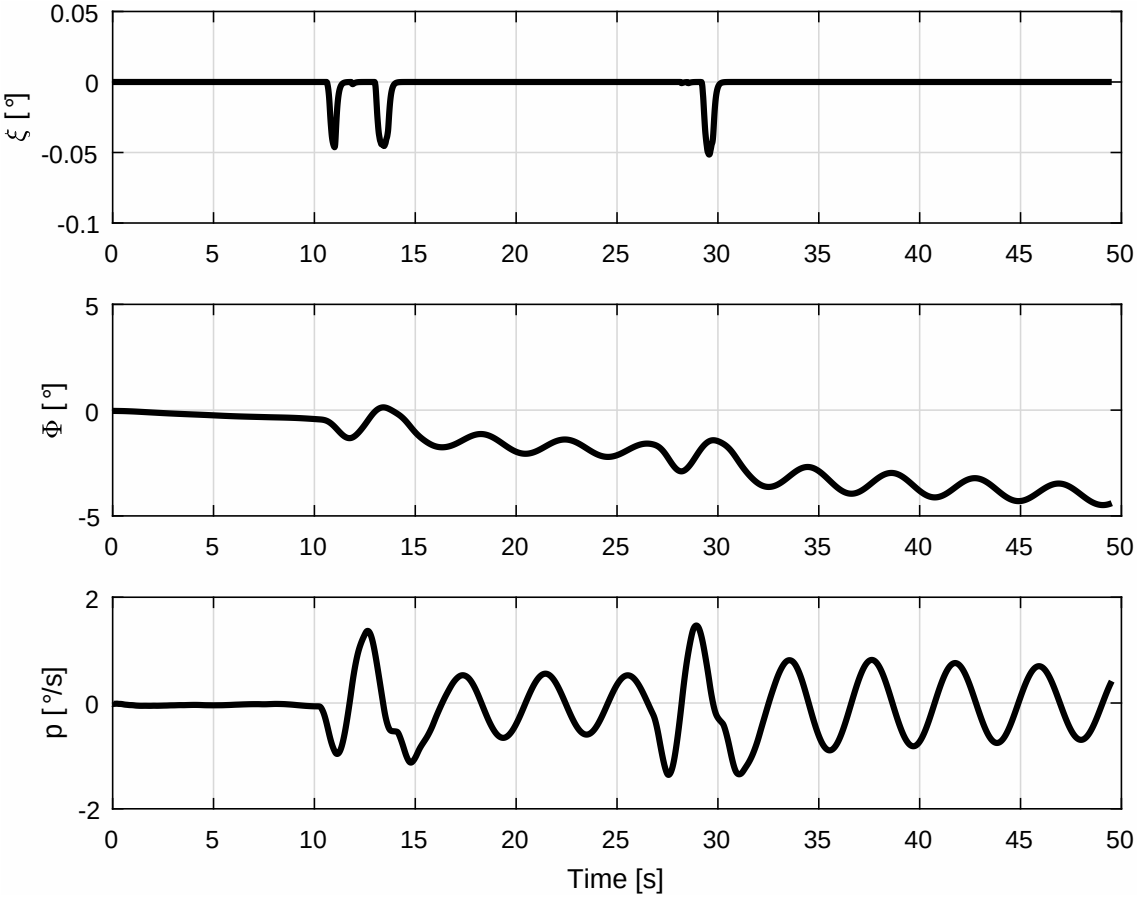

Figure E.24: Time histories of lateral parameters

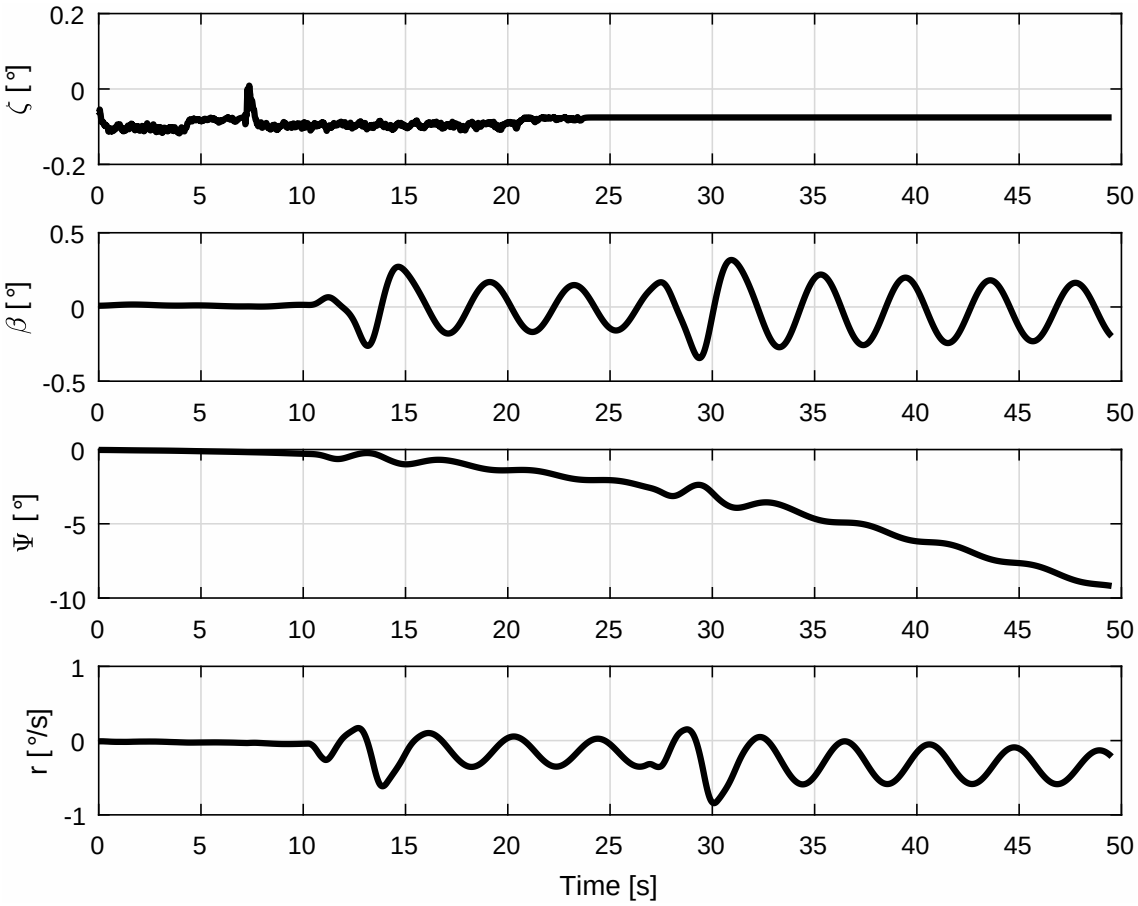

Figure E.25: Time histories of directional parameters

E.6 Phugoid mode, pilot 1, rigid A/C – PH(1)R

Date: 24/01/2018 **Time start:** **Time stop:** 16:19

Test No:	PH(1)R	**Test hardware:**	EFS500 + Speedgoat
Test pilot:	(1)	**Model version:**	HARTEN_v1 (R)

Task:	Longitudinal dynamic modes (PH)
Manoeuvre:	Pitch doublet

Instrumentation:	
Relevant files:	{D_SIM/D_STRUCT}.DAT @ 24/01/2018 16:19; DSCN9511.MOV; GOPR4017.MP4

Flight velocity: 110 m/s **Flight altitude:** 10000 ft

Aircraft weight: 79 t **Aircraft CG:** 20% MAC

Phugoid

T	Alt	V (EAS)	T	Alt	V (EAS)
0		230	100	7200	220
10	8600		110	7180	221
20		194	120	7200	211
30	8900	190			
40	8300	220			
50	7940	224			
60	8000	214			
70	8180	194			
80	8000	199			
90		218			

Notes:

Subsequently entered combined phugoid / spiral dive. This responded initially to standard recovery, but then entered a secondary divergence.

Notes (from audio recording):

“Lack of pitch trimmer”

“It started phugoiding already without me making an input”

Figure E.26: Test card (PH(1)R)

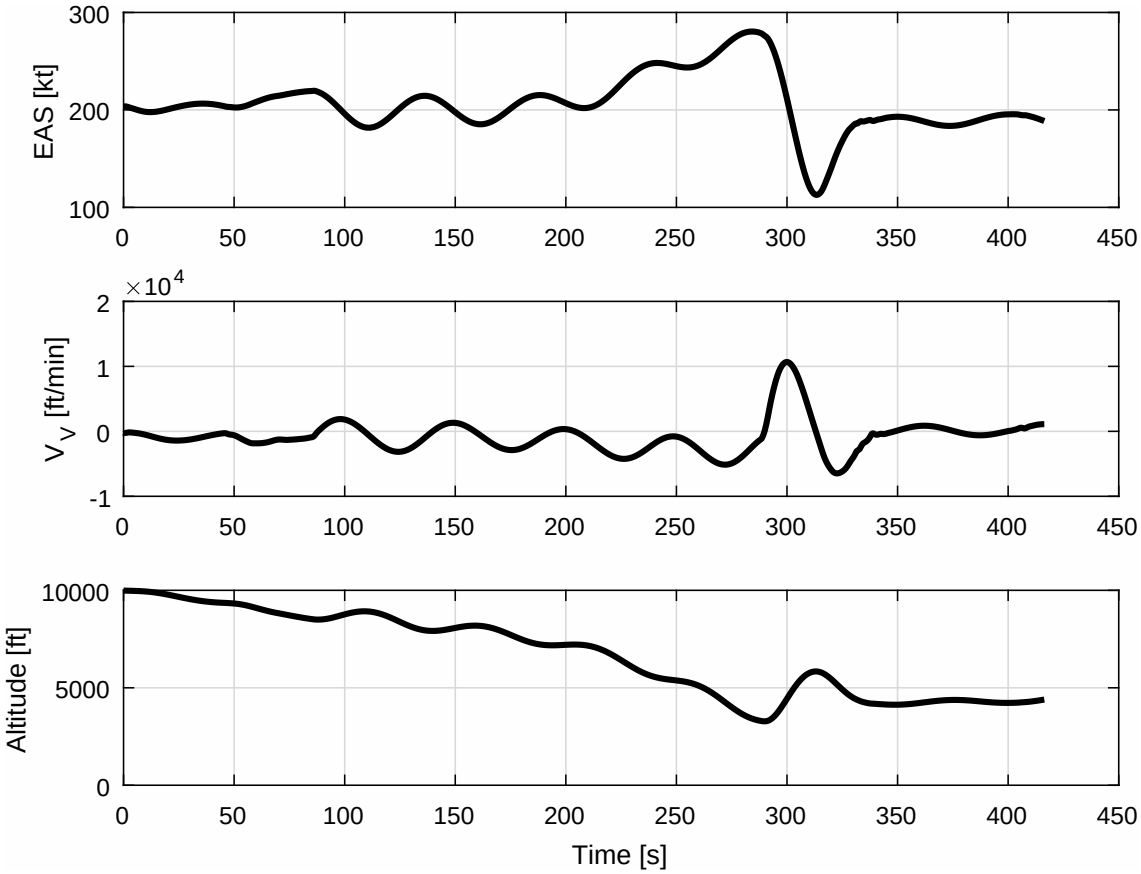

Figure E.27: Time histories of altitude and velocities

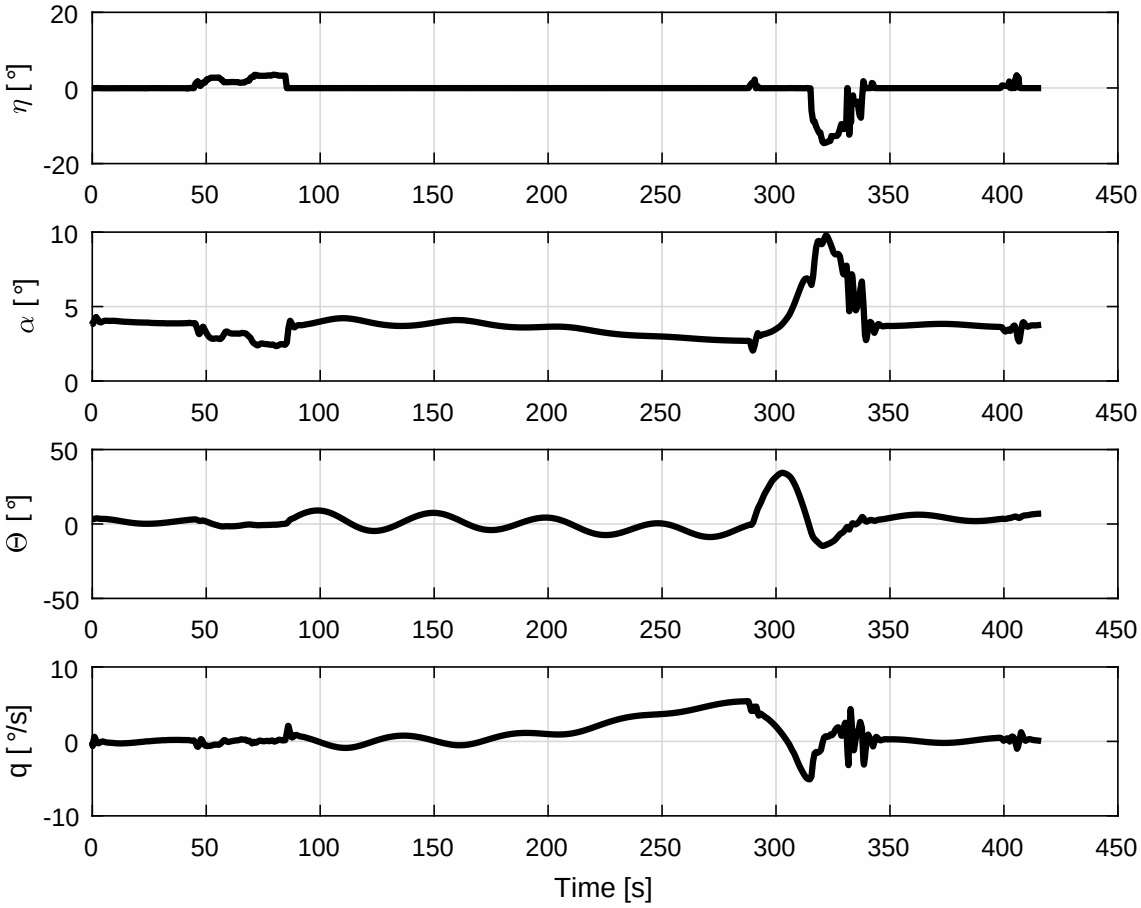

Figure E.28: Time histories of longitudinal parameters

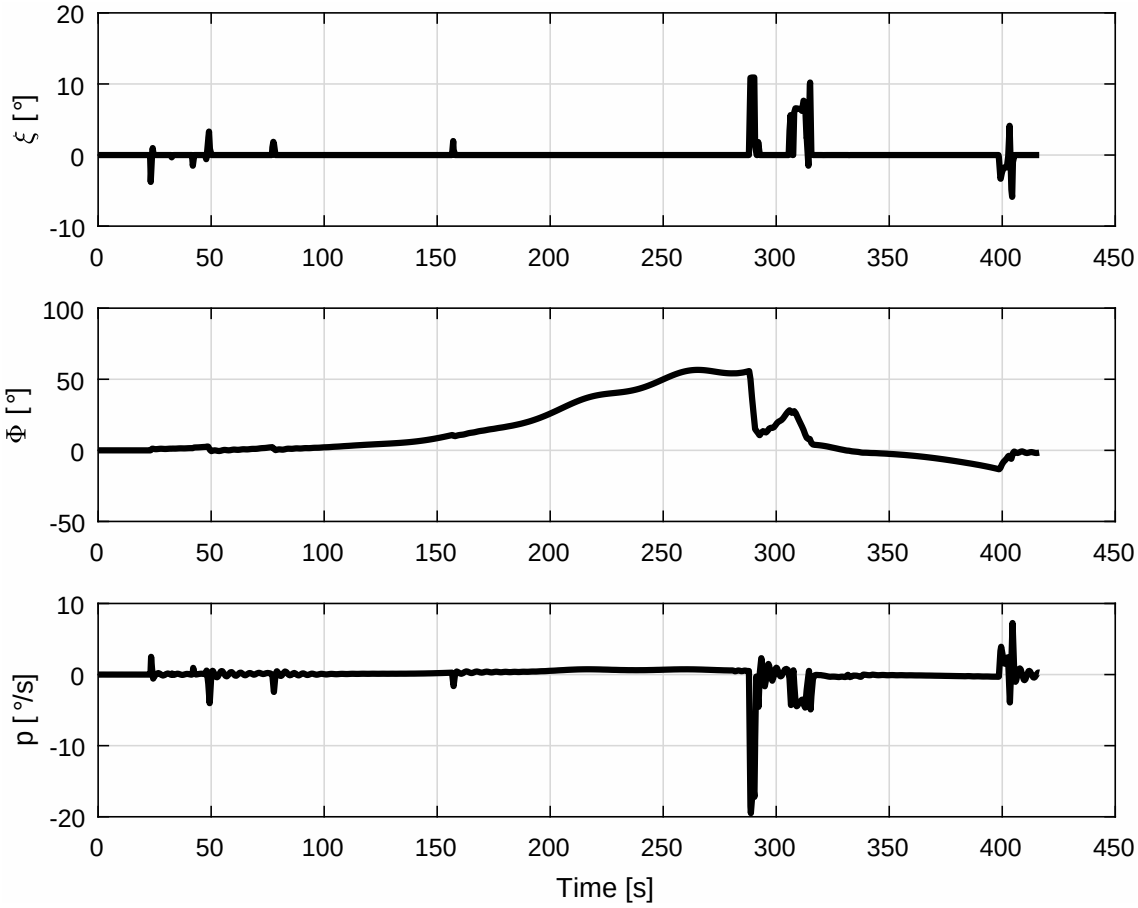

Figure E.29: Time histories of lateral parameters

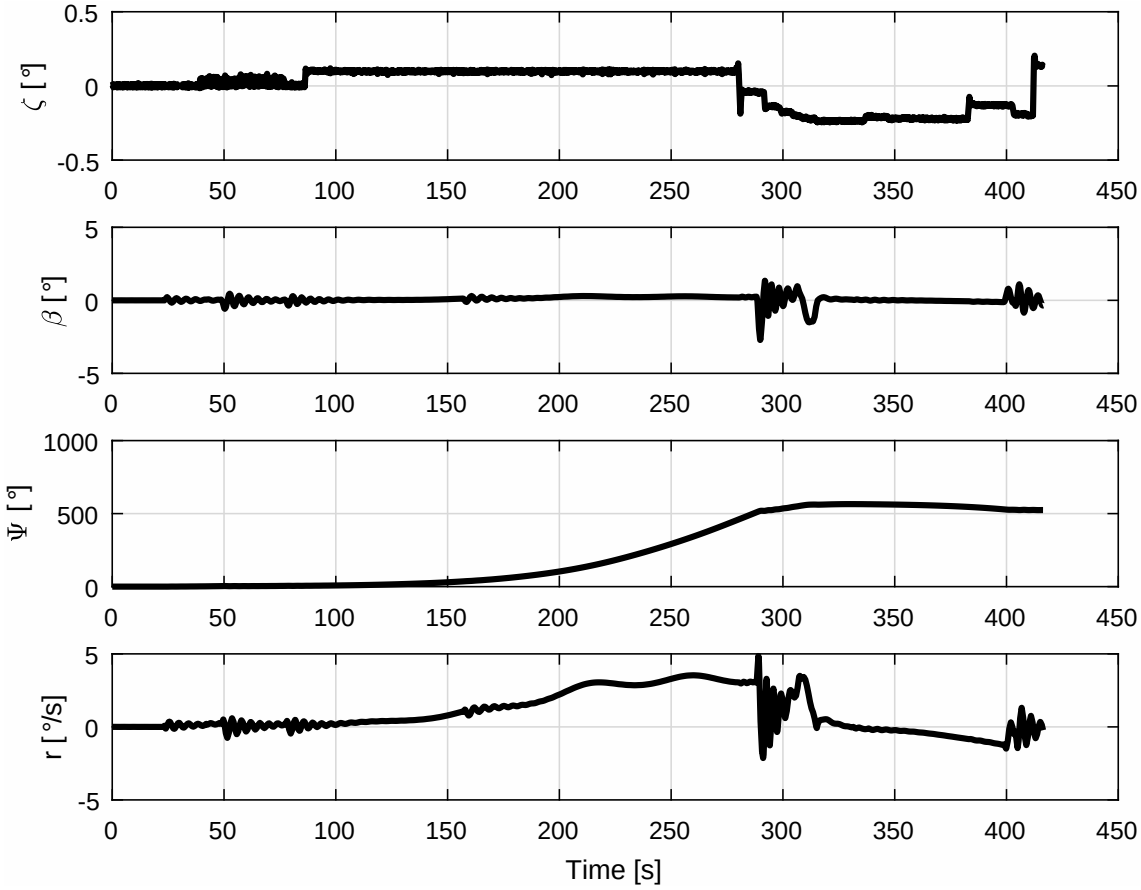

Figure E.30: Time histories of directional parameters

E.7 Phugoid mode, pilot 1, flexible A/C – PH(1)F

Date: 24/01/2018 **Time start:** **Time stop:** 17:22

Test No:	PH(1)F	**Test hardware:**	EFS500 + Speedgoat
Test pilot:	(1)	**Model version:**	HARTEN_v1 (F)

Task:	Longitudinal dynamic modes (PH)
Manoeuvre:	Pitch doublet

Instrumentation:	
Relevant files:	{D_SIM/D_STRUCT}.DAT @ 24/01/2018 17:22; DSCN9520.MOV

Flight velocity: 110 m/s **Flight altitude:** 10000 ft

Aircraft weight: 79 t **Aircraft CG:** 20% MAC

Phugoid

T	Alt	V (EAS)	T	Alt	V (EAS)
0	10700	190			
30	9960	238			
55	10900	196			
1:25	10300	237			
1:50	11080	204	10 right bank		
2:20	10400	241			
2:50	11080	217	20 right bank		

Notes:

Nil

Notes (from audio recording):

Nil

Figure E.31: Test card (PH(1)F)

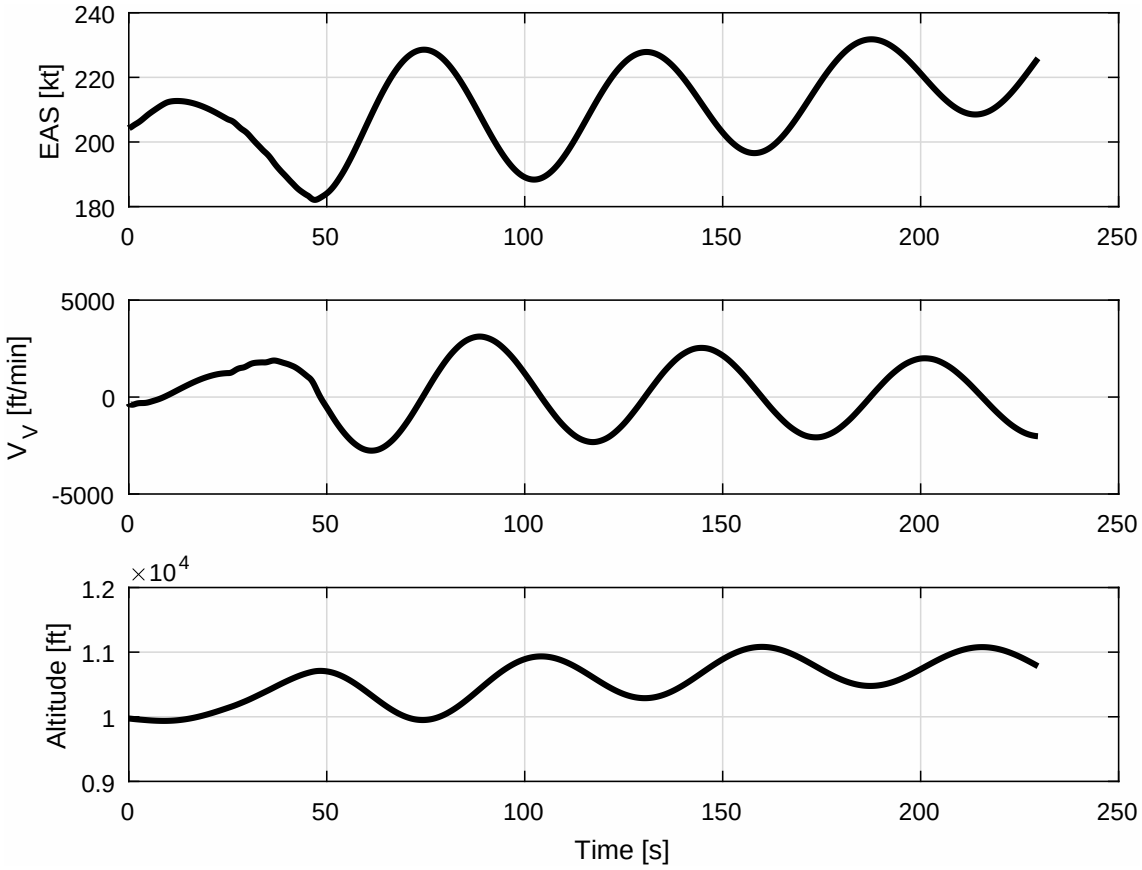

Figure E.32: Time histories of altitude and velocities

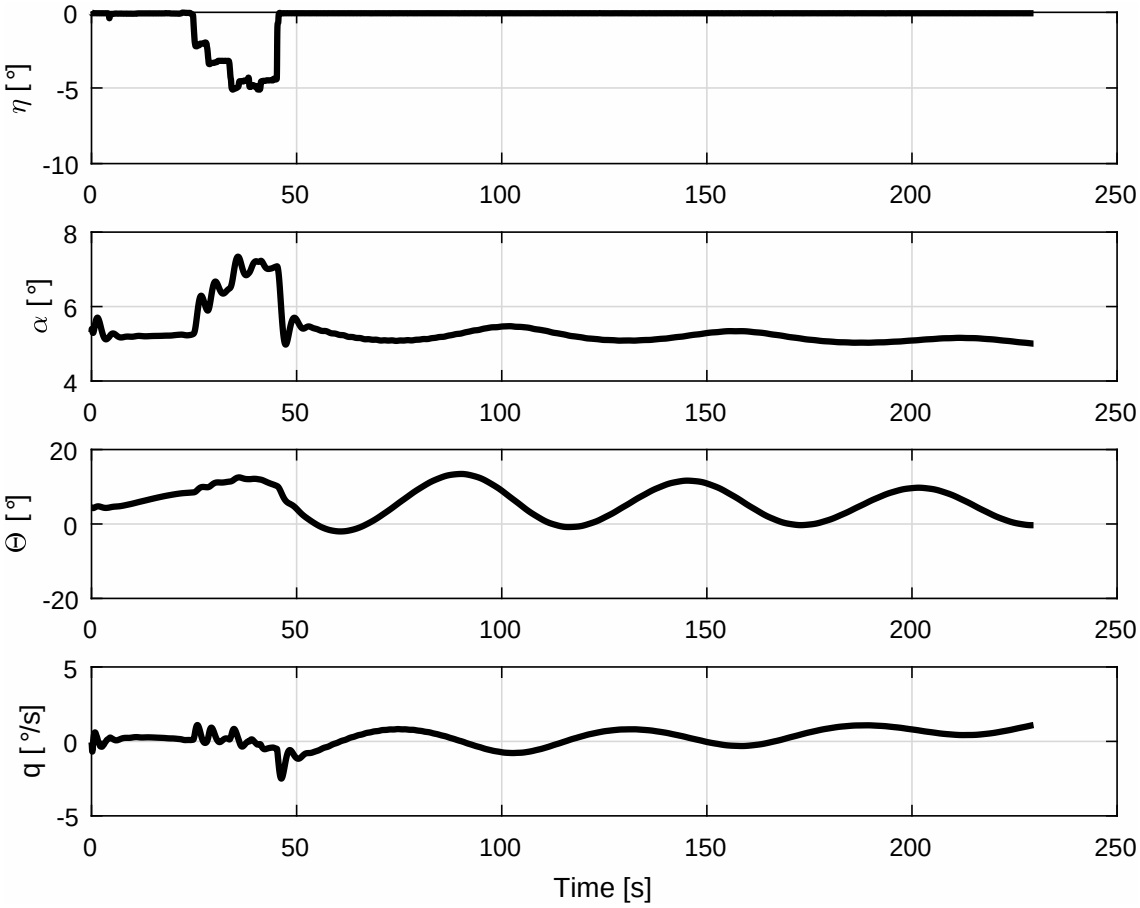

Figure E.33: Time histories of longitudinal parameters

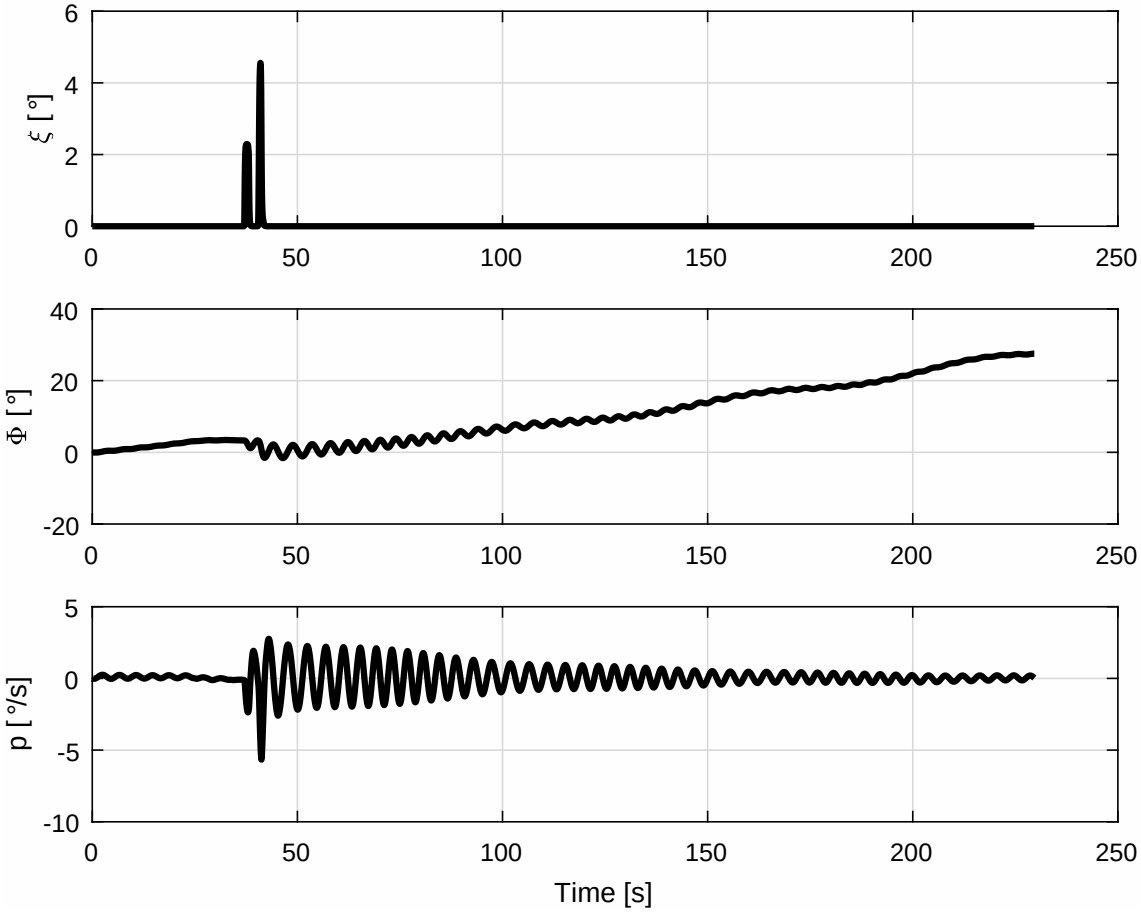

Figure E.34: Time histories of lateral parameters

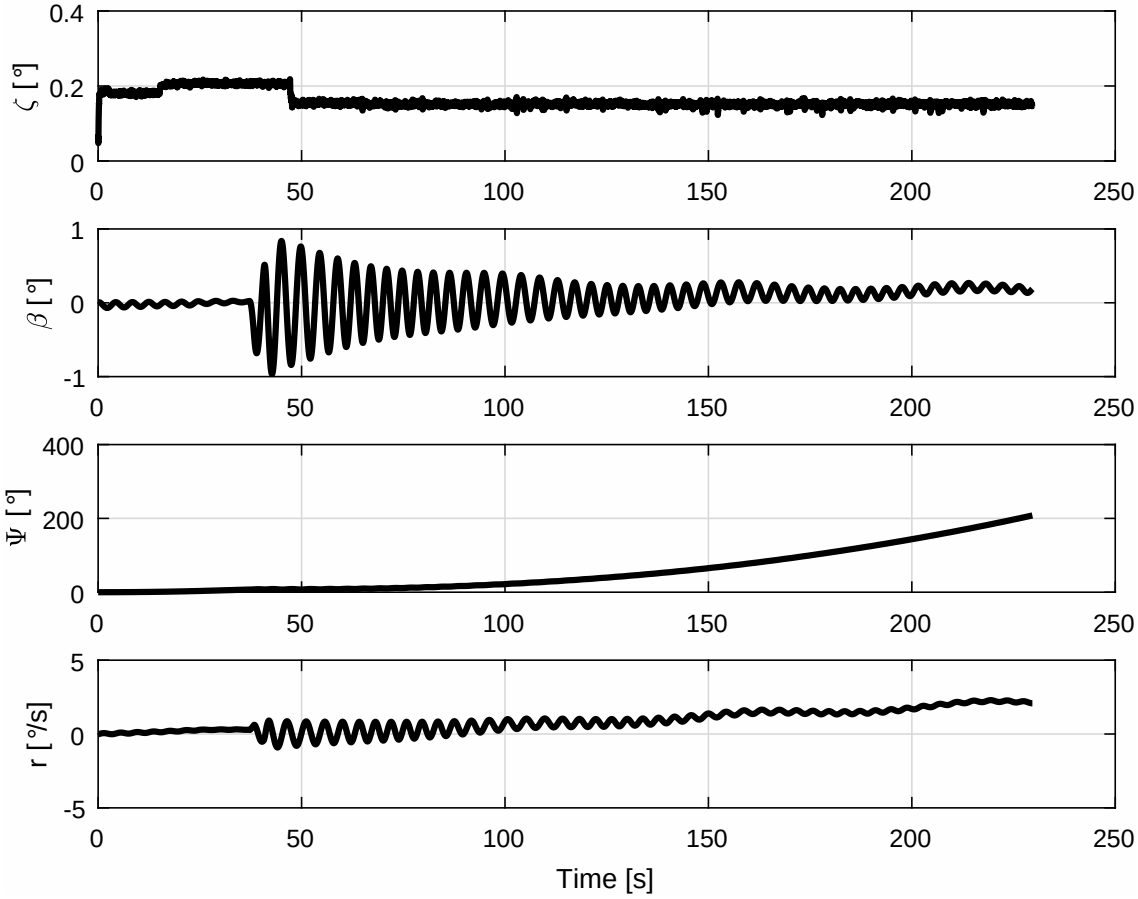

Figure E.35: Time histories of directional parameters

E.8 Phugoid mode, pilot 2, rigid A/C – PH(2)R

Date: 09/02/2018 **Time start:** **Time stop:** 10:37

Test No:	PH(2)R	**Test hardware:**	EFS500 + Speedgoat
Test pilot:	(2)	**Model version:**	HARTEN_v1 (R)

Task:	Longitudinal dynamic modes
Manoeuvre:	Pitch doublet

Instrumentation:	
Relevant files:	{D_LOADS/D_SIM/D_STRUCT}.DAT @ 09/02/2018 10:37; DSCN9581.MOV

Flight velocity: 110 m/s **Flight altitude:** 10000 ft

Aircraft weight: 79 t **Aircraft CG:** 20% MAC

Phugoid

T	Alt	V (EAS)	T	Alt	V (EAS)
		213			
		196			
		231		Moderate LSS	
		199		Near neutral	
		229		Phugoid	Stability
		201		Very slightly	Convergent
		226			
		203	20		
		225			
		205			

Notes:

Nil

Notes (from audio recording):

Nil

Figure E.36: Test card (PH(2)R)

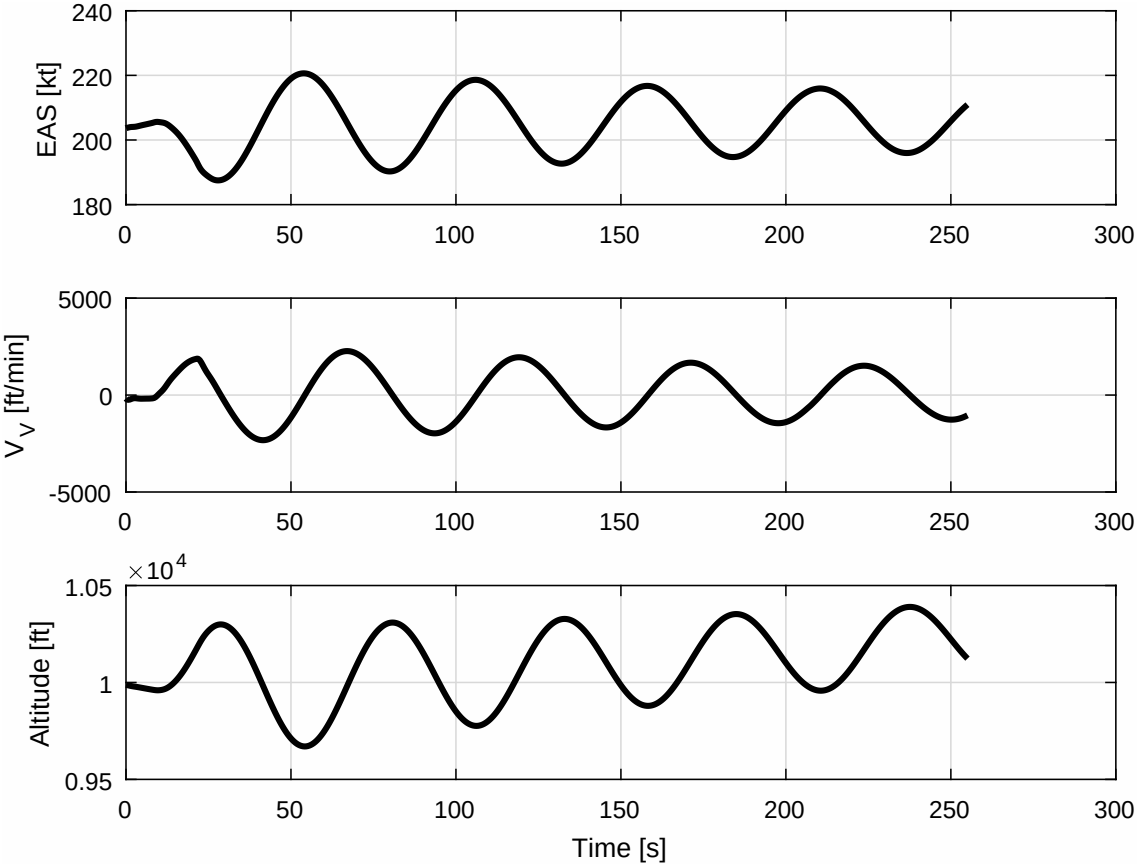

Figure E.37: Time histories of altitude and velocities

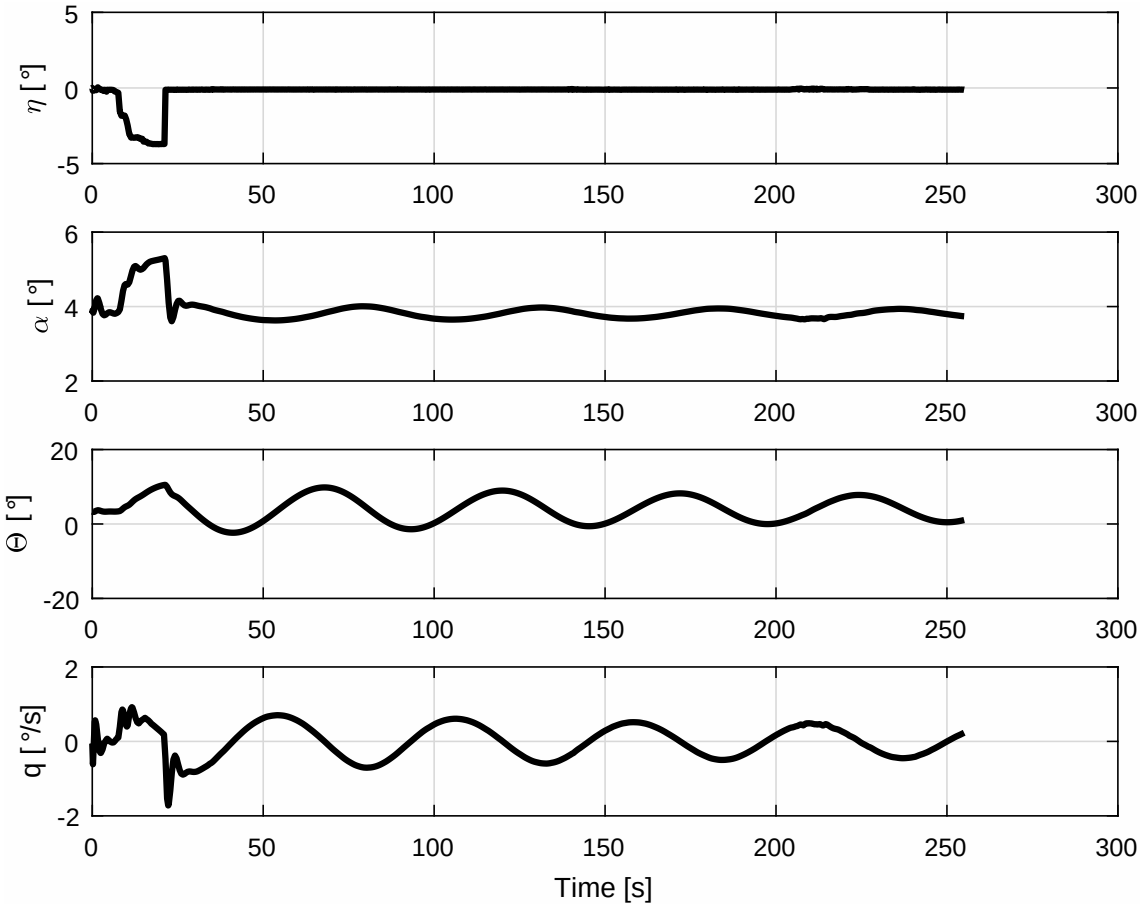

Figure E.38: Time histories of longitudinal parameters

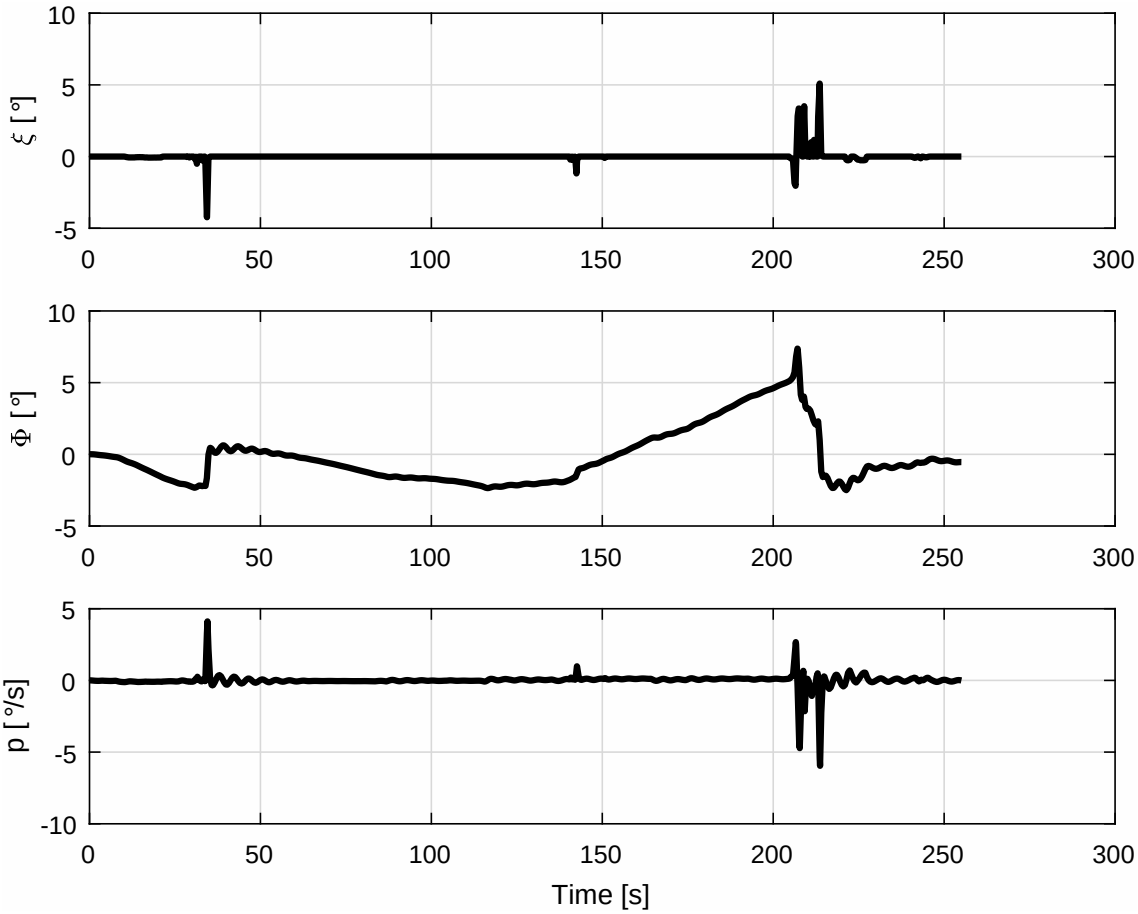

Figure E.39: Time histories of lateral parameters

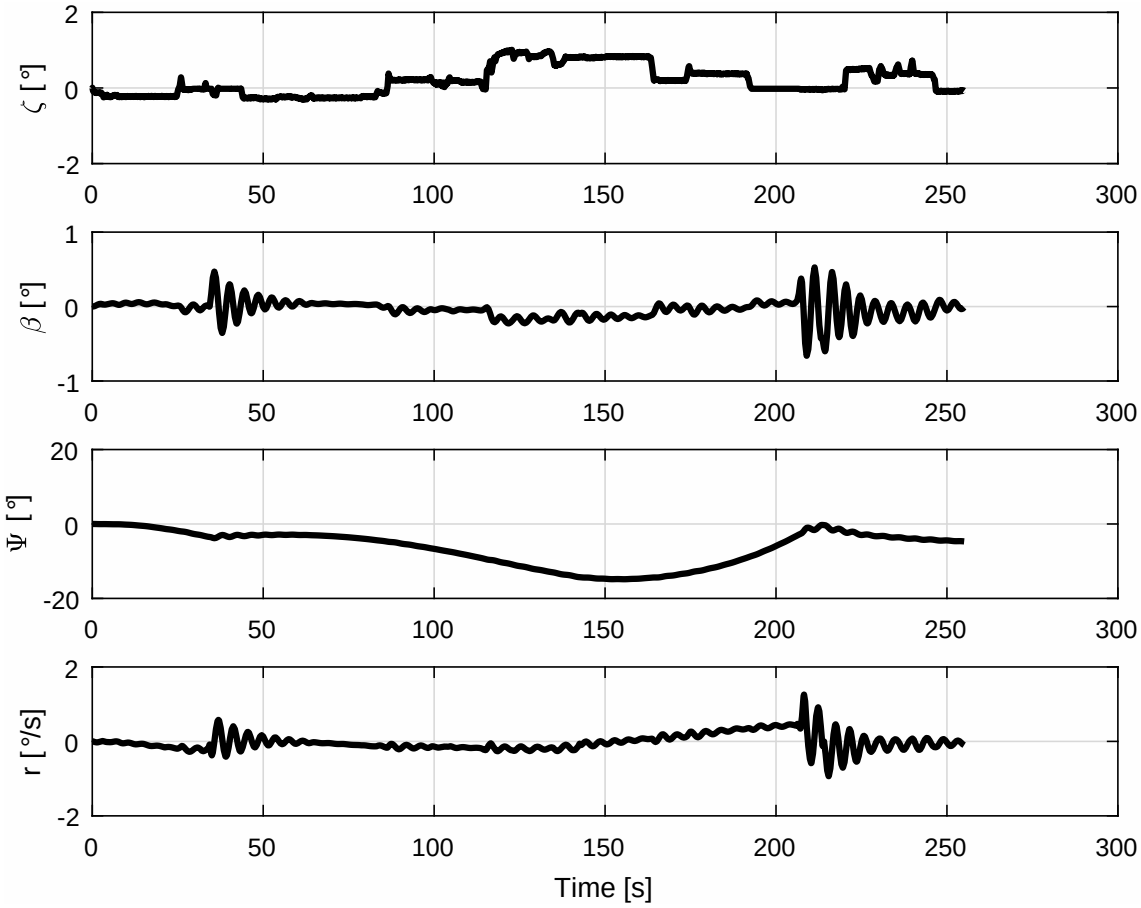

Figure E.40: Time histories of directional parameters

E.9 Phugoid mode, pilot 2, flexible A/C – PH(2)F

Date: 09/02/2018 **Time start:** **Time stop:** 14:18

Test No:	PH(2)F	**Test hardware:**	EFS500 + Speedgoat
Test pilot:	(2)	**Model version:**	HARTEN_v1 (F)

Task:	Longitudinal dynamic modes (PH)
Manoeuvre:	Pitch doublet

Instrumentation:	
Relevant files:	{D_LOADS/D_SIM/D_STRUCT}.DAT @ 09/02/2018 14:18; DSCN9594.MOV

Flight velocity: 110 m/s **Flight altitude:** 10000 ft

Aircraft weight: 79 t **Aircraft CG:** 20% MAC

Phugoid

T	Alt	V (EAS)	T	Alt	V (EAS)
0		200			
28		227			
56		201			
88		226			
115		203			
140		223			

Notes:

Low damping

Notes (from audio recording):

Nil

Figure E.41: Test card (PH(2)F)

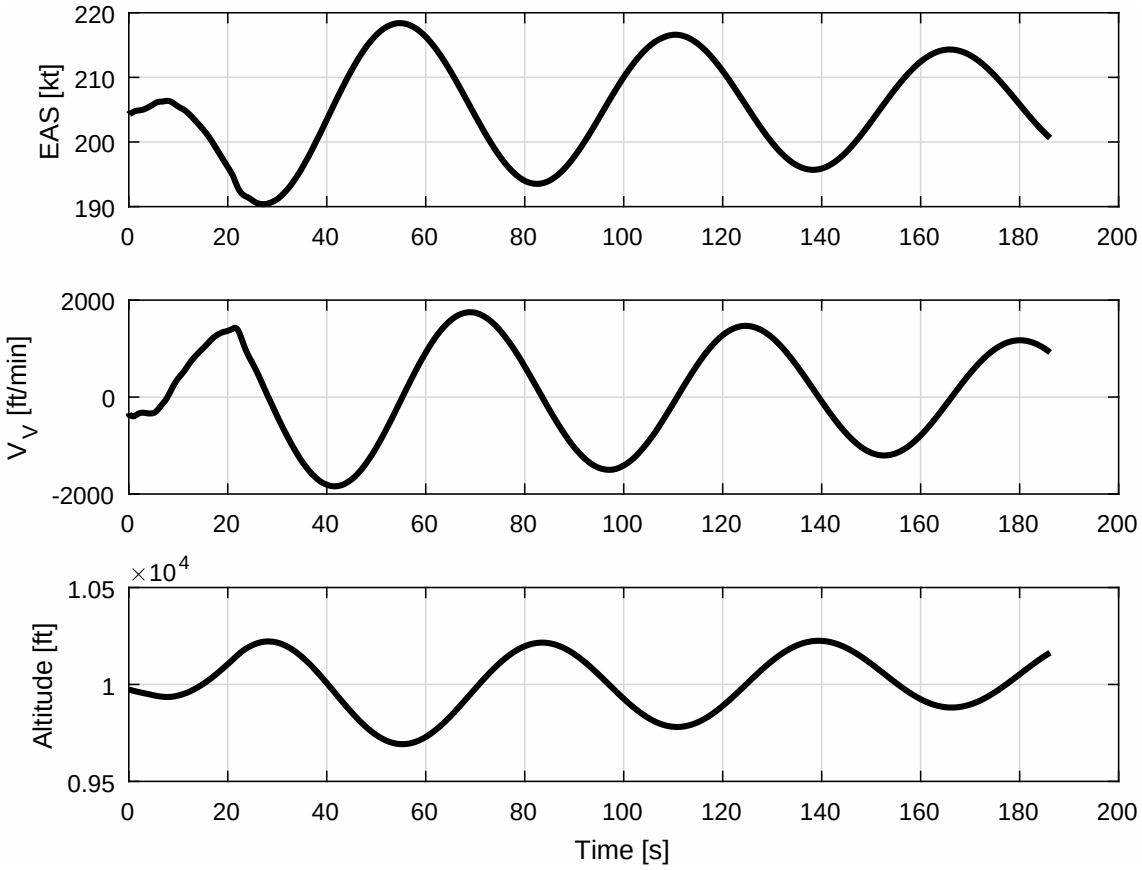

Figure E.42: Time histories of altitude and velocities

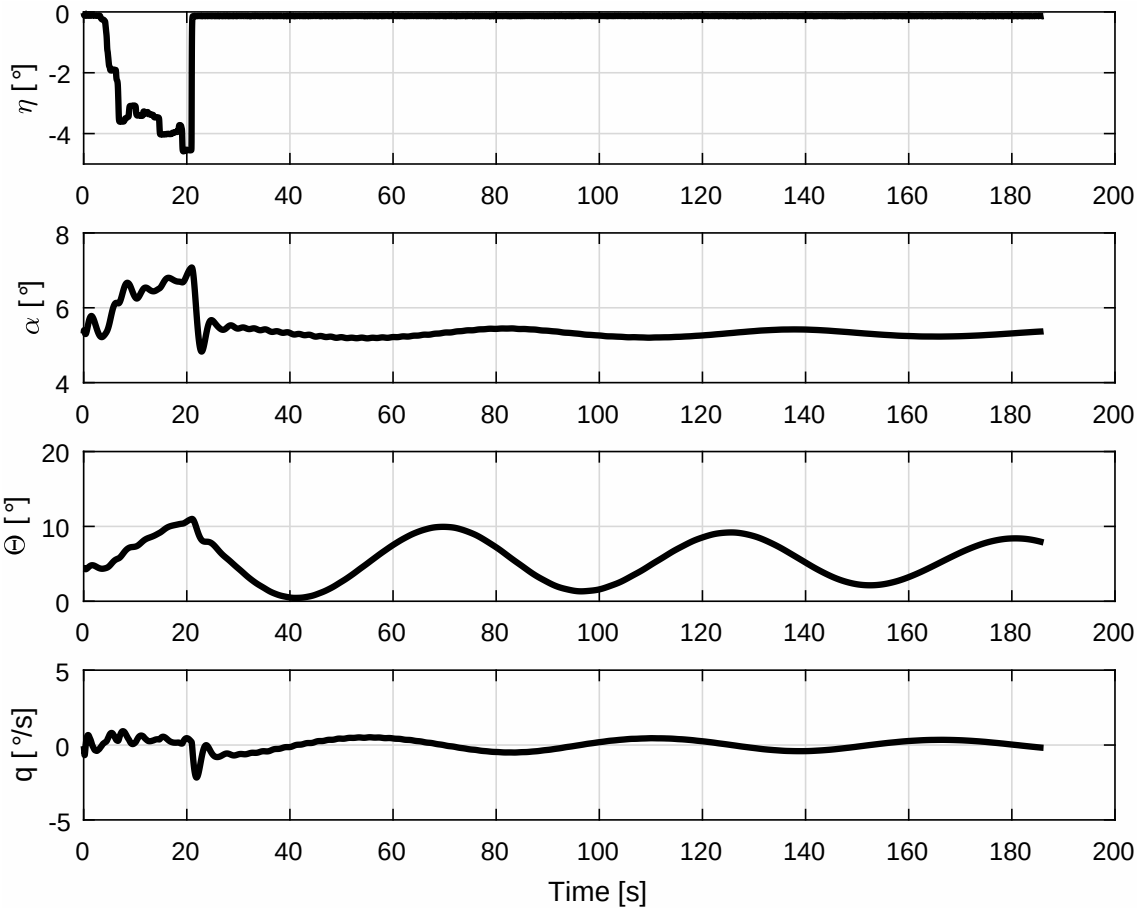

Figure E.43: Time histories of longitudinal parameters

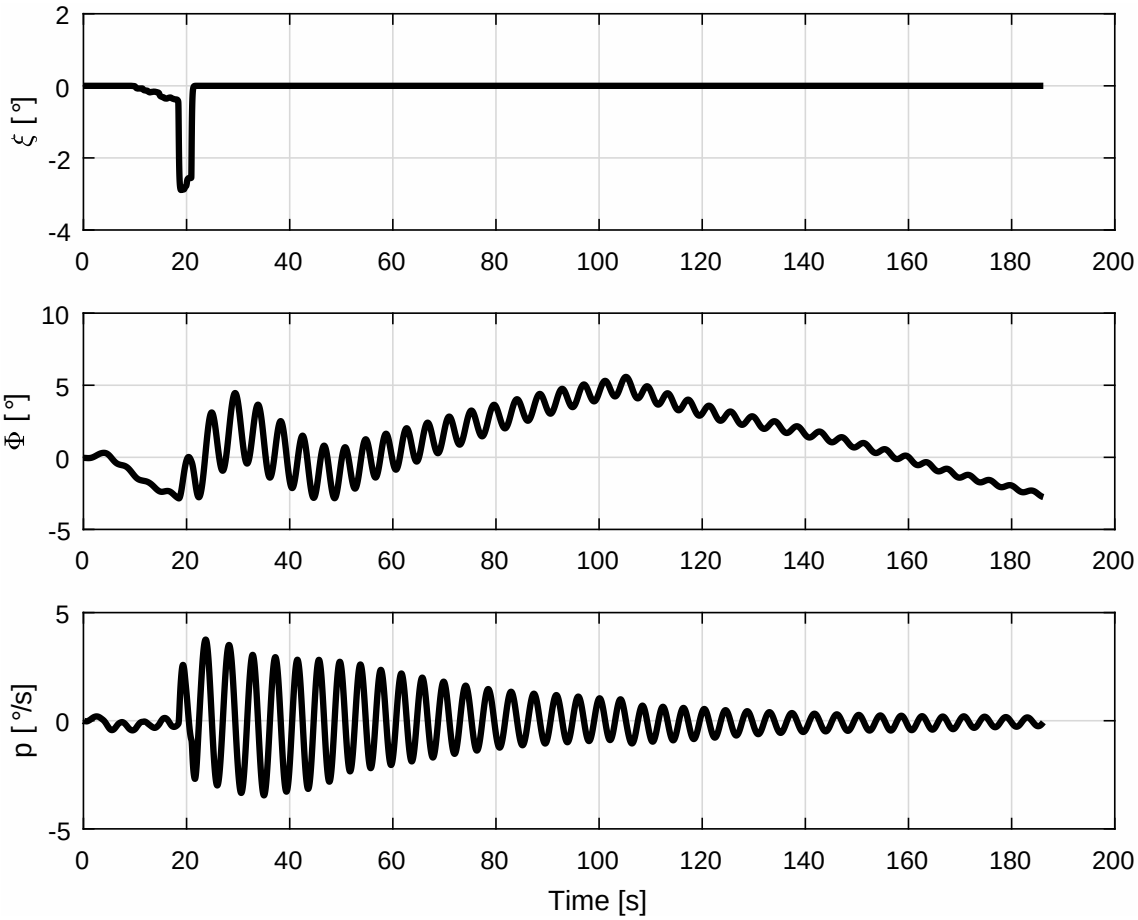

Figure E.44: Time histories of lateral parameters

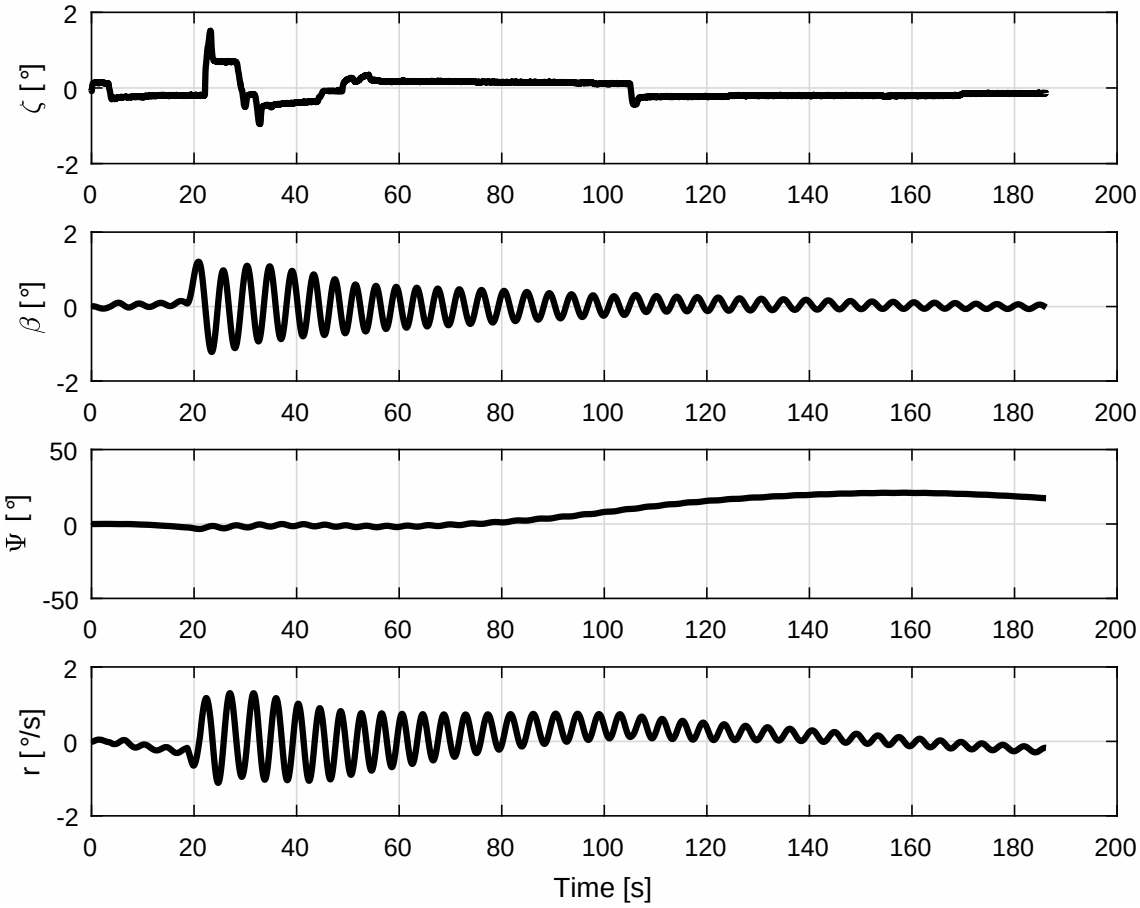

Figure E.45: Time histories of directional parameters

Appendix F

Lateral/directional modes simulation data

F.1 Steady heading sideslip, pilot 1, rigid A/C – SH(1)R

Date: 24/01/2018 **Time start:** **Time stop:** 16:41

Test No:	SH(1)R	**Test hardware:**	EFS500 + Speedgoat
Test pilot:	(1)	**Model version:**	HARTEN_v1 (R)

Task:	Lateral / directional modes (SHSS) (SH)
Manoeuvre:	

Instrumentation:	
Relevant files:	{D_SIM/D_STRUCT}.DAT @ 24/01/2018 16:41; DSCN9514.MOV; GOPR4020.MP4

Flight velocity: 110 m/s **Flight altitude:** 10000 ft

Aircraft weight: 79 t **Aircraft CG:** 20% MAC

SHSS

Unable to fly test due to controls imbalance. Full rudder needed 2-3 mm lateral stick, which in reality was in the free play and could not be held accurately.

Notes:

Nil

Notes (from audio recording):

"This is a very uncomfortable condition to hold as probably about 30 lbs pressure from my left toe and about 8 lbs right stick to hold it at about 1 mm"

Figure F.1: Test card (SH(1)R)

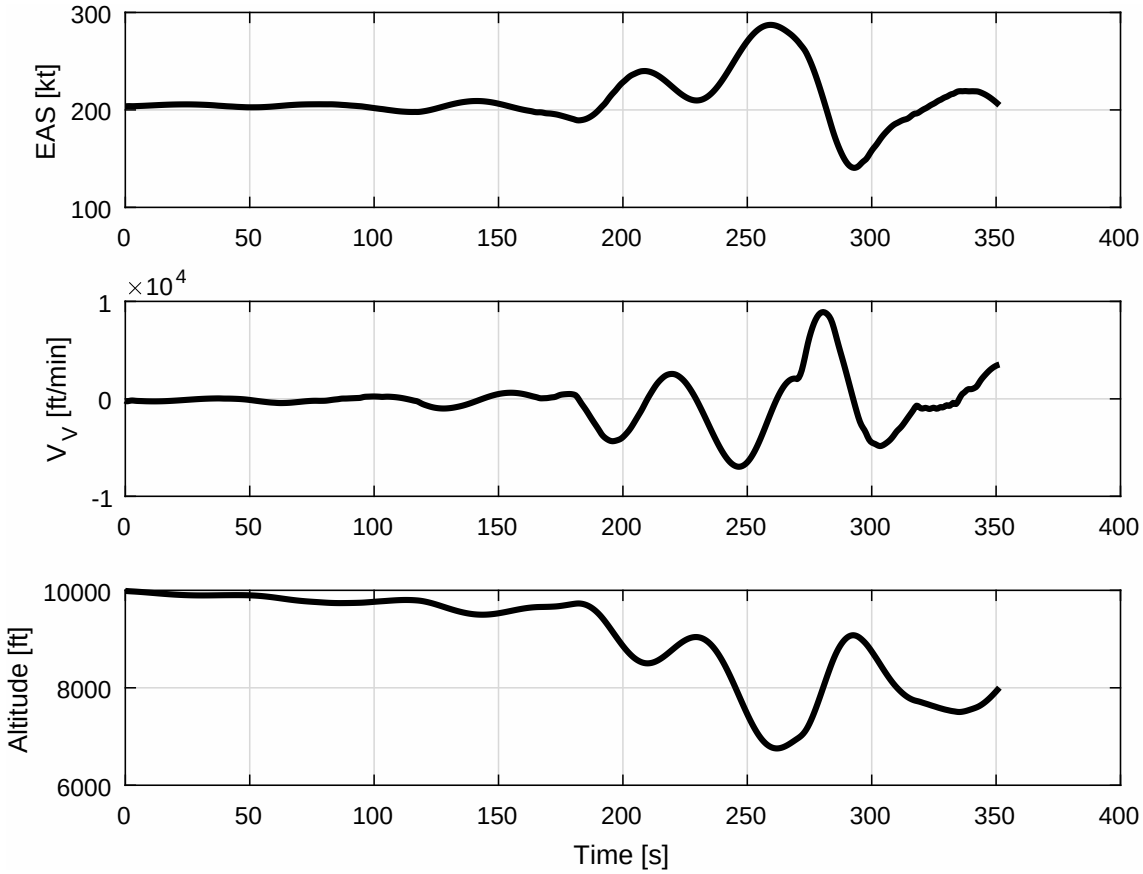

Figure F.2: Time histories of altitude and velocities

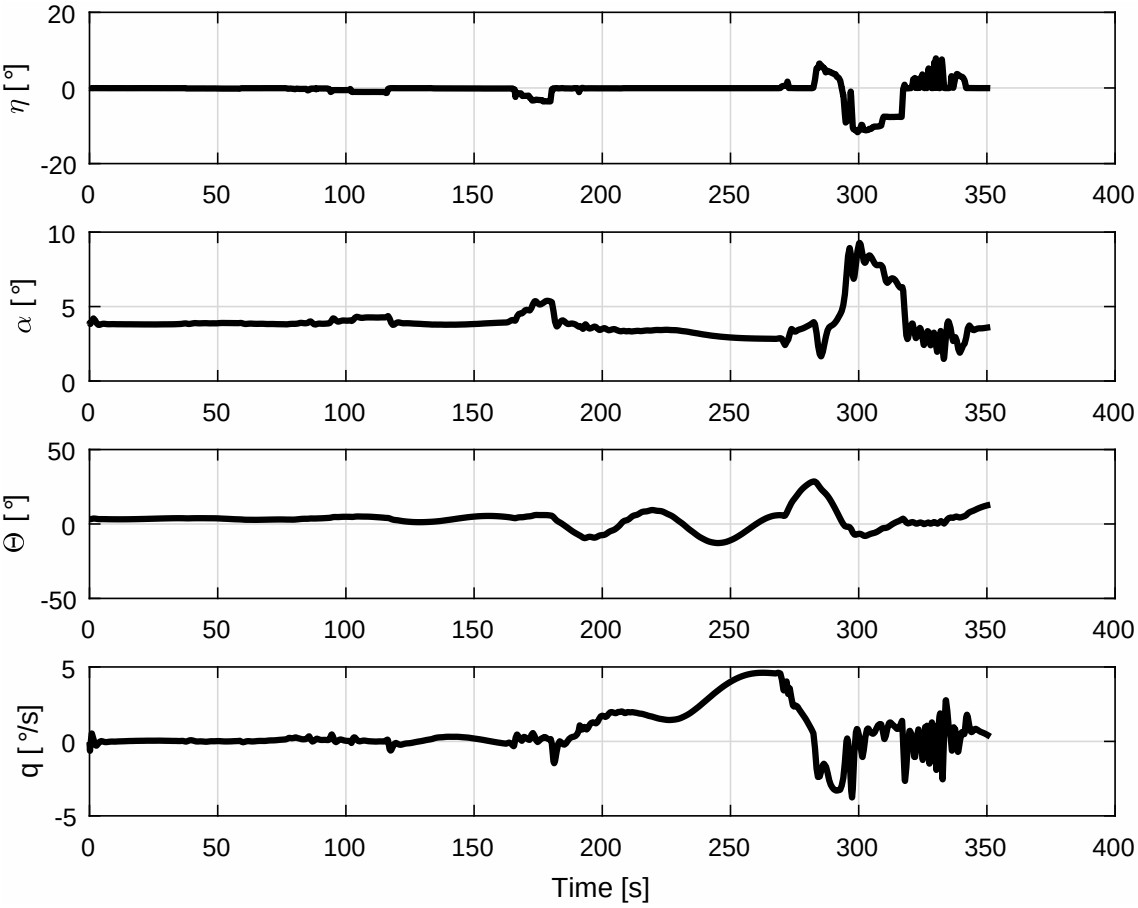

Figure F.3: Time histories of longitudinal parameters

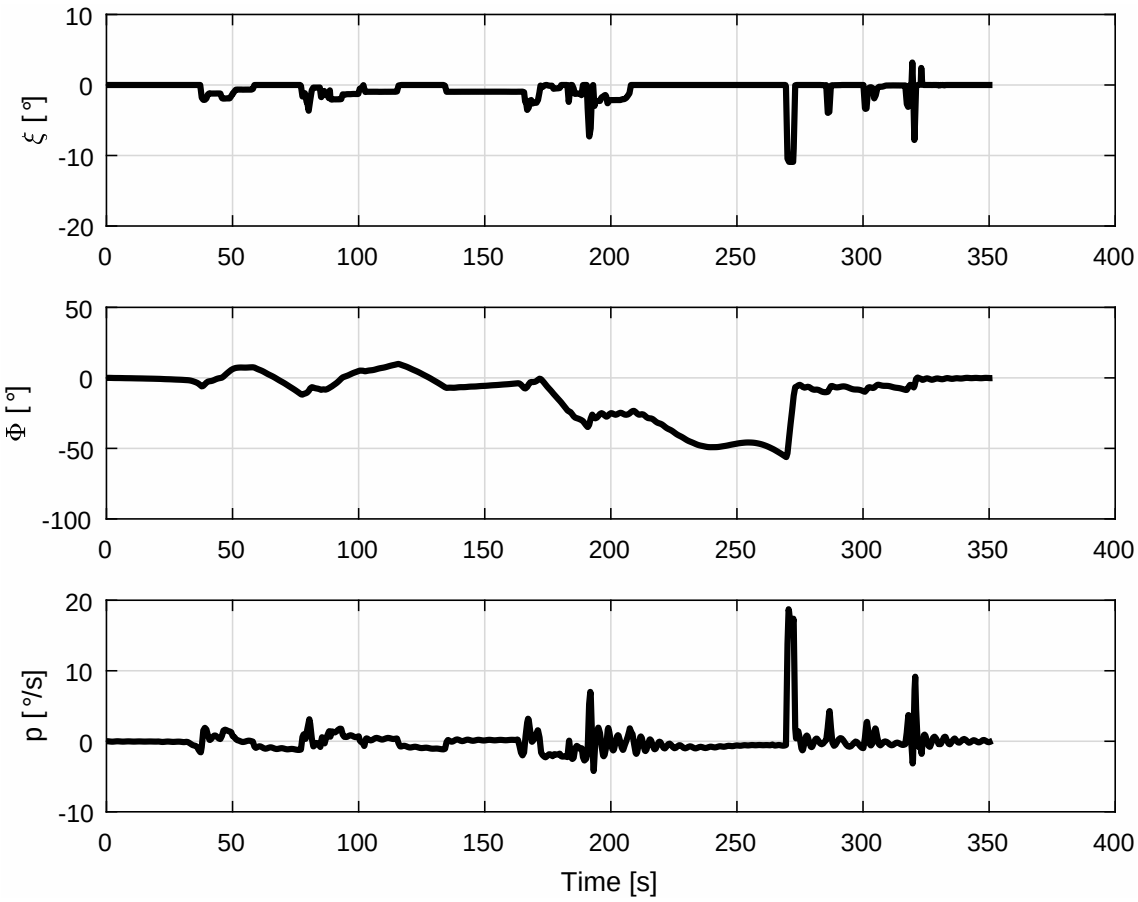

Figure F.4: Time histories of lateral parameters

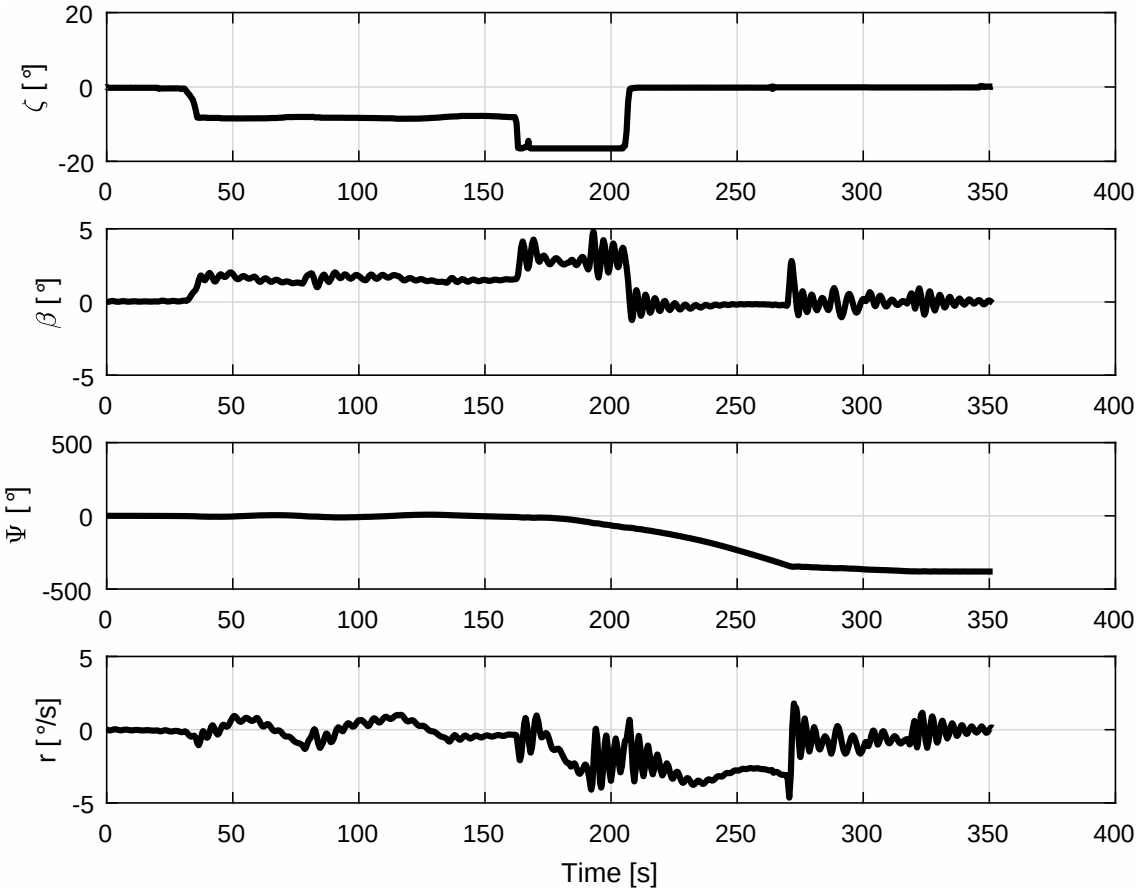

Figure F.5: Time histories of directional parameters

F.2 Steady heading sideslip, pilot 1, flexible A/C – SH(1)F

Date: 24/01/2018 **Time start:** **Time stop:** 17:31

Test No:	SH(1)F	**Test hardware:**	EFS500 + Speedgoat
Test pilot:	(1)	**Model version:**	HARTEN_v1 (F)

Task:	Lateral / directional modes (SHSS) (SH)
Manoeuvre:	

Instrumentation:	
Relevant files:	{D_SIM/D_STRUCT}.DAT @ 24/01/2018 17:31; DSCN9522.MOV

Flight velocity: 110 m/s **Flight altitude:** 10000 ft

Aircraft weight: 79 t **Aircraft CG:** 20% MAC

SHSS

Rudder	Aileron	Pitch	Notes
0			
1/3 left			
2/3 left			
Full left			
Release			
1/3 right			
2/3 right			
Full right			
Release			

Notes:

Nil

Notes (from audio recording):

“Hard of gearing combined with a high forces on the ailerons makes it very hard to balance it”

Figure F.6: Test card (SH(1)F)

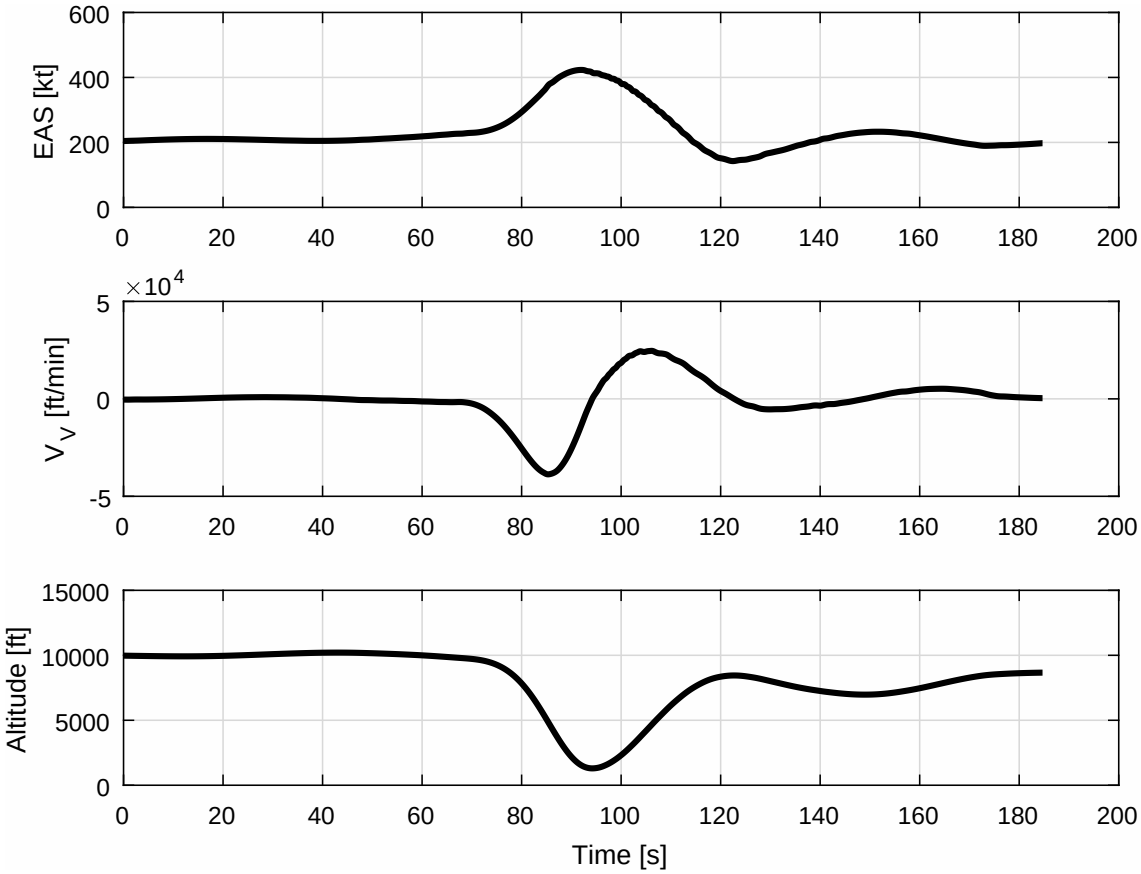

Figure F.7: Time histories of altitude and velocities

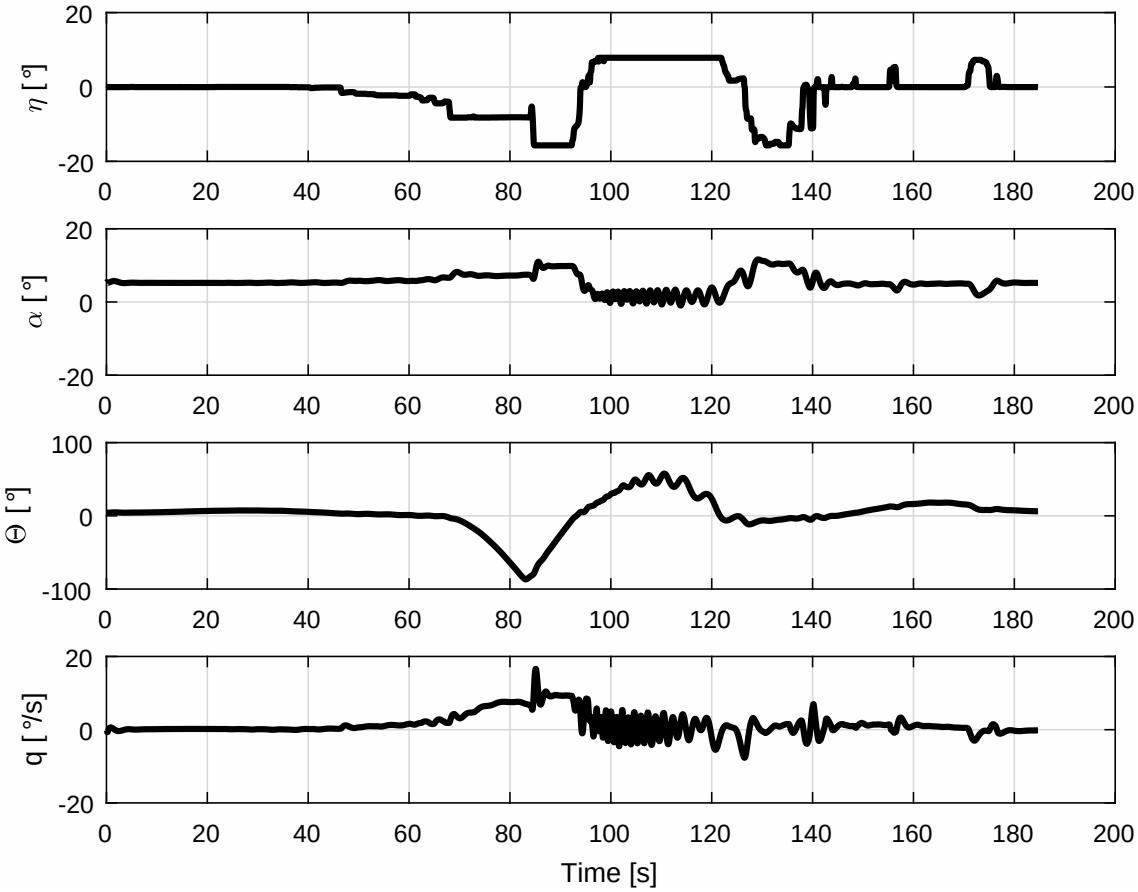

Figure F.8: Time histories of longitudinal parameters

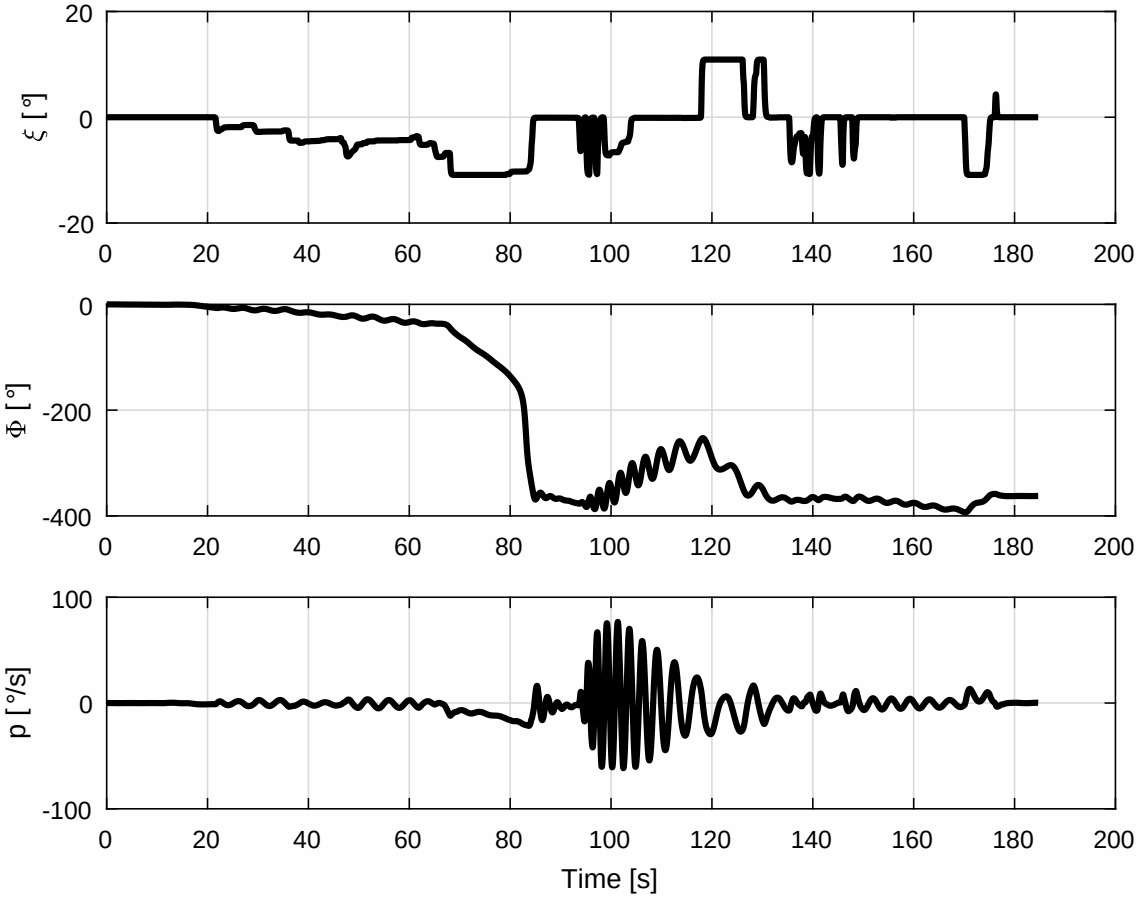

Figure F.9: Time histories of lateral parameters

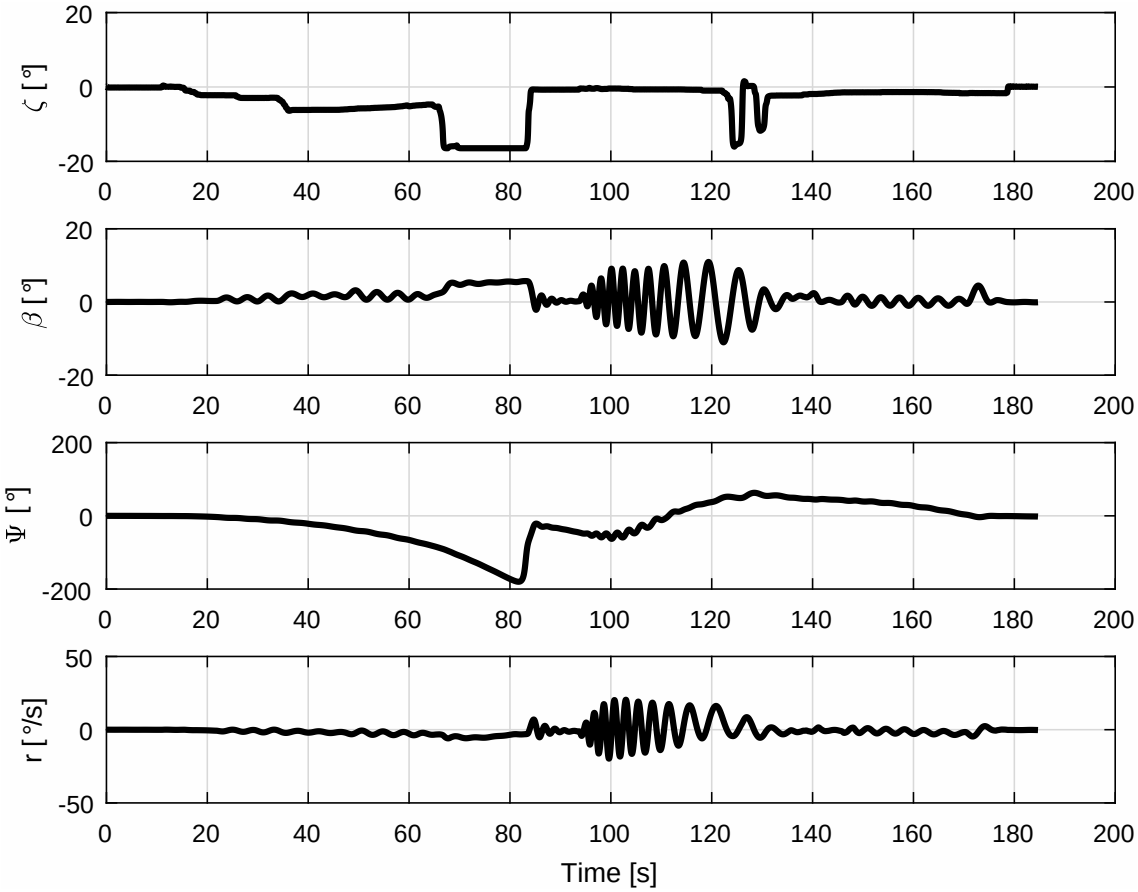

Figure F.10: Time histories of directional parameters

F.3 Steady heading sideslip, pilot 2, rigid A/C – SH(2)R

Date: 09/02/2018 **Time start:** **Time stop:** 10:49

Test No:	SH(2)R	**Test hardware:**	EFS500 + Speedgoat
Test pilot:	(2)	**Model version:**	HARTEN_v1 (R)

Task:	Lateral / directional modes (SHSS, roll mode) (SH)
Manoeuvre:	

Instrumentation:	
Relevant files:	{D_LOADS/D_SIM/D_STRUCT}.DAT @ 09/02/2018 10:49; DSCN9582.MOV

Flight velocity: 110 m/s **Flight altitude:** 10000 ft

Aircraft weight: 79 t **Aircraft CG:** 20% MAC

SHSS

Rudder	Aileron	Pitch	Notes
0	0		
1/3 left	Slight right	N/A	5 lbs left foot and 1 lb stick
2/3 left	Slight right	N/A	
Full left	Slight right	N/A	2-3 deg bank for steady heading
Release			10 deg heading change on release
1/3 right	Slight left	N/A	
2/3 right	Slight left	N/A	
Full right	Slight left	N/A	2-3 deg bank
Release			10 deg heading change on release

Notes:

CLβ low CNβ – moderate-low

Notes (from audio recording):

“phi/beta ratio 1/5” – after releasing left rudder

Figure F.11: Test card (SH(2)R)

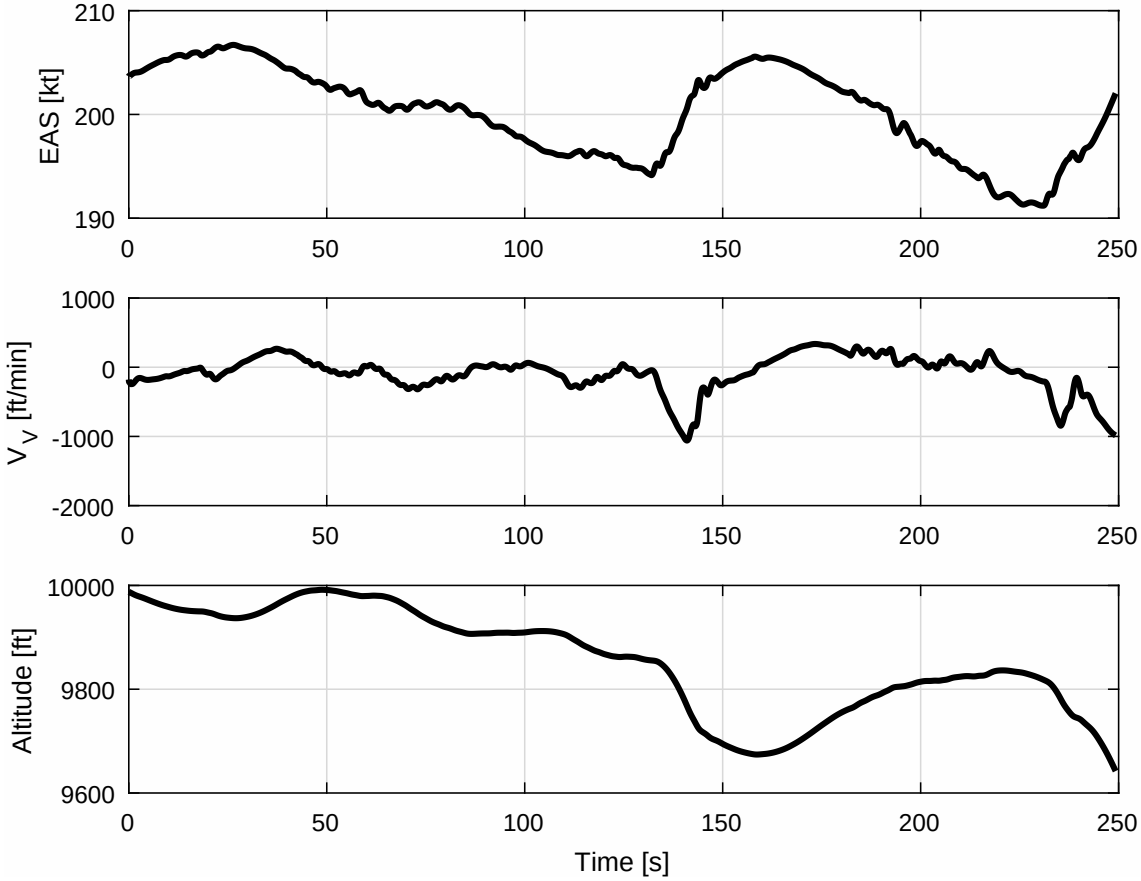

Figure F.12: Time histories of altitude and velocities

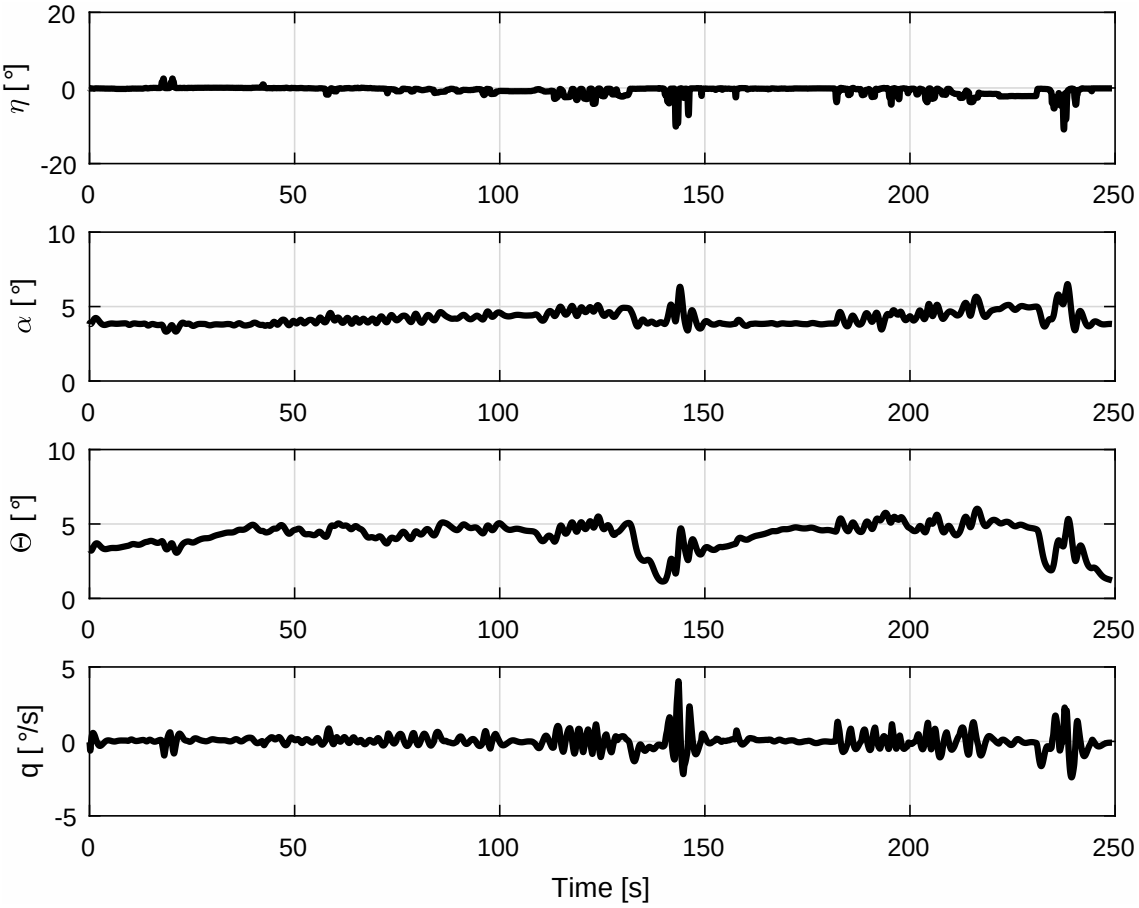

Figure F.13: Time histories of longitudinal parameters

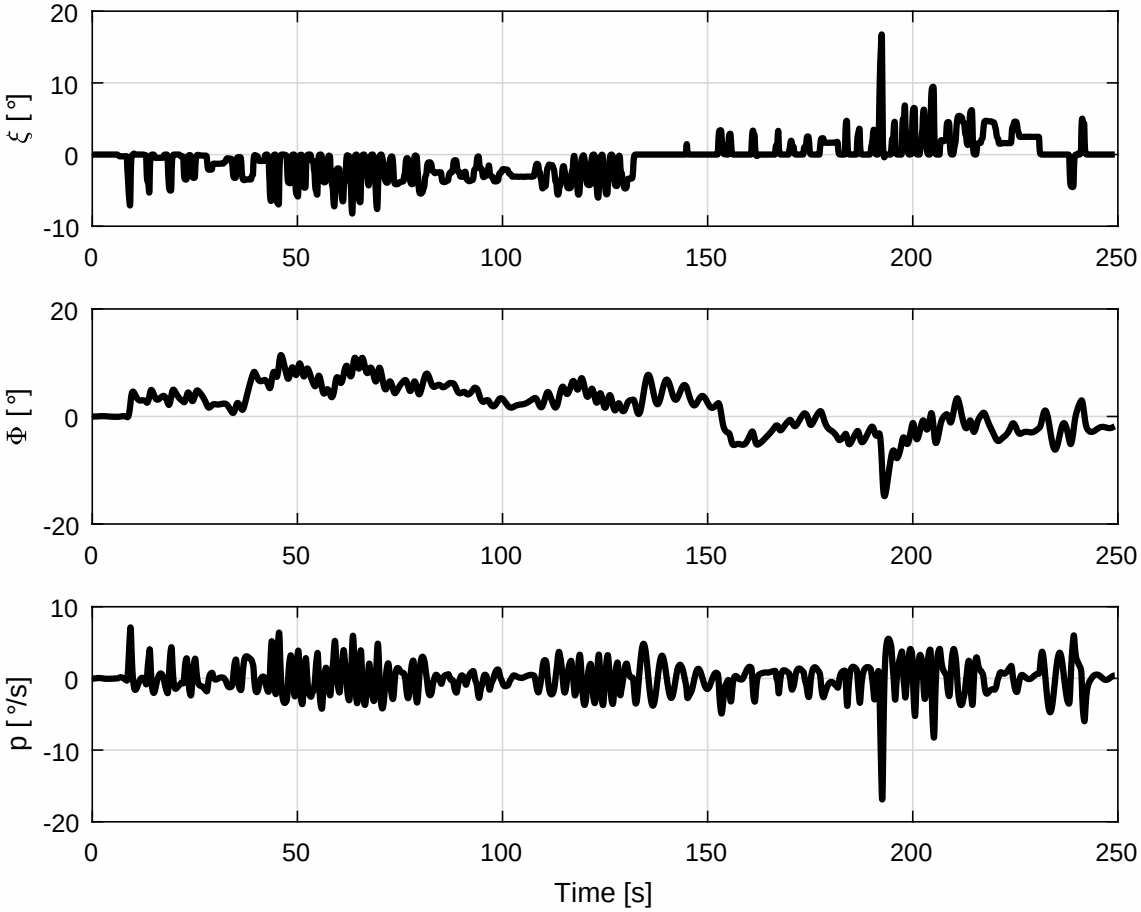

Figure F.14: Time histories of lateral parameters

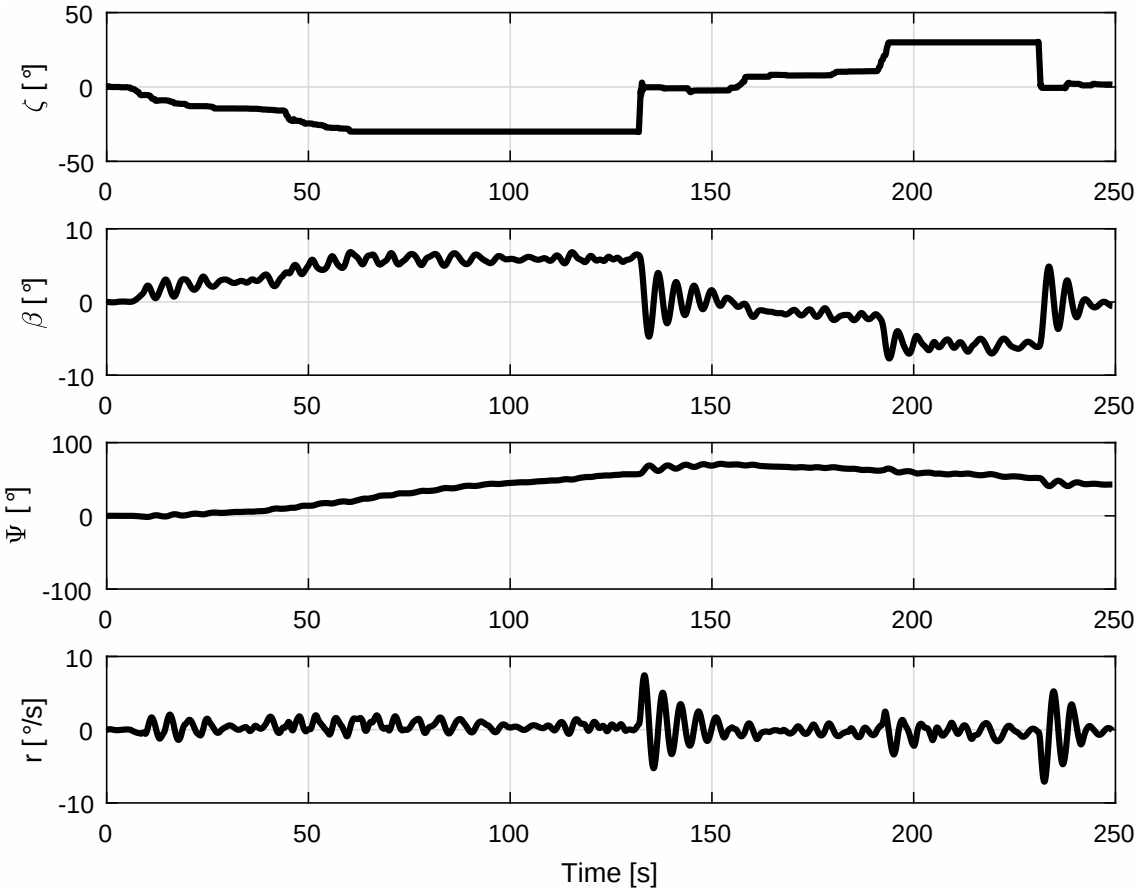

Figure F.15: Time histories of directional parameters

F.4 Steady heading sideslip, pilot 2, flexible A/C – SH(2)F

Date: 09/02/2018 **Time start:** **Time stop:** 14:27

Test No:	SH(2)F	**Test hardware:**	EFS500 + Speedgoat
Test pilot:	(2)	**Model version:**	HARTEN_v1 (F)

Task:	Lateral / directional modes (SHSS) (SH)
Manoeuvre:	

Instrumentation:	
Relevant files:	{D_LOADS/D_SIM/D_STRUCT}.DAT @ 09/02/2018 14:27; DSCN9595.MOV

Flight velocity: 110 m/s **Flight altitude:** 10000 ft

Aircraft weight: 79 t **Aircraft CG:** 20% MAC

SHSS

Rudder	Aileron	Pitch	Notes
0			
1/3 left			
2/3 left			
Full left			
Release			
1/3 right			5 lbs push on foot; 1 lb left stick force
2/3 right			
Full right			Not enough stick
Release			

Notes:

Much rudder authority

Dihedral effect much stronger

Very strong lateral stability

Notes (from audio recording):

Nil

Figure F.16: Test card (SH(2)F)

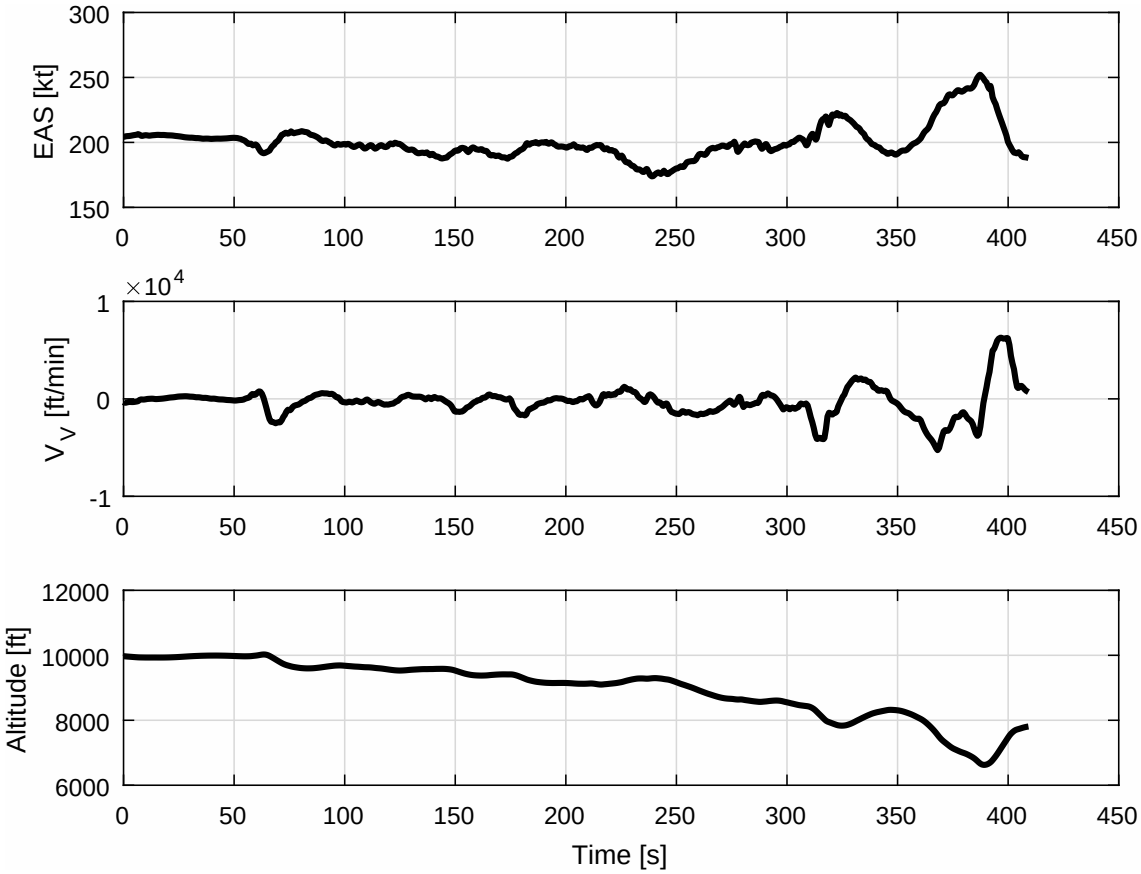

Figure F.17: Time histories of altitude and velocities

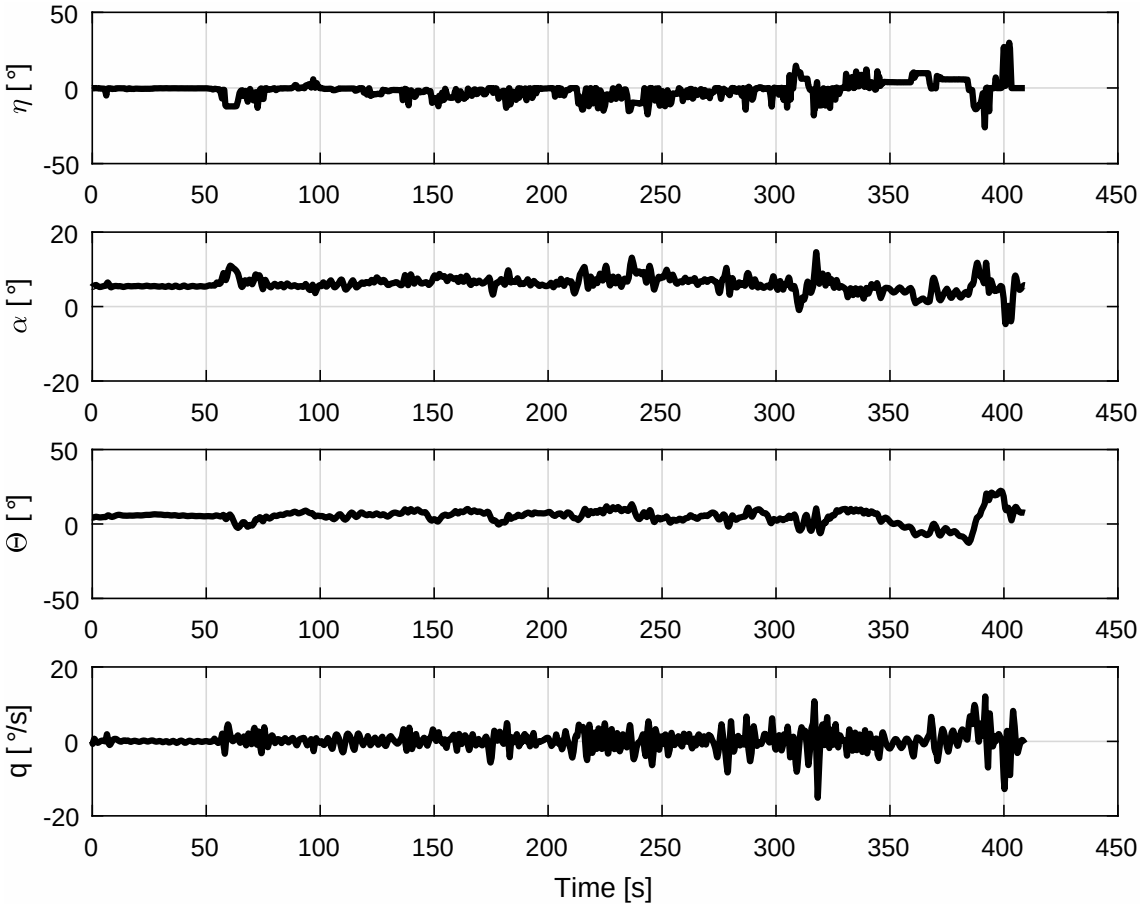

Figure F.18: Time histories of longitudinal parameters

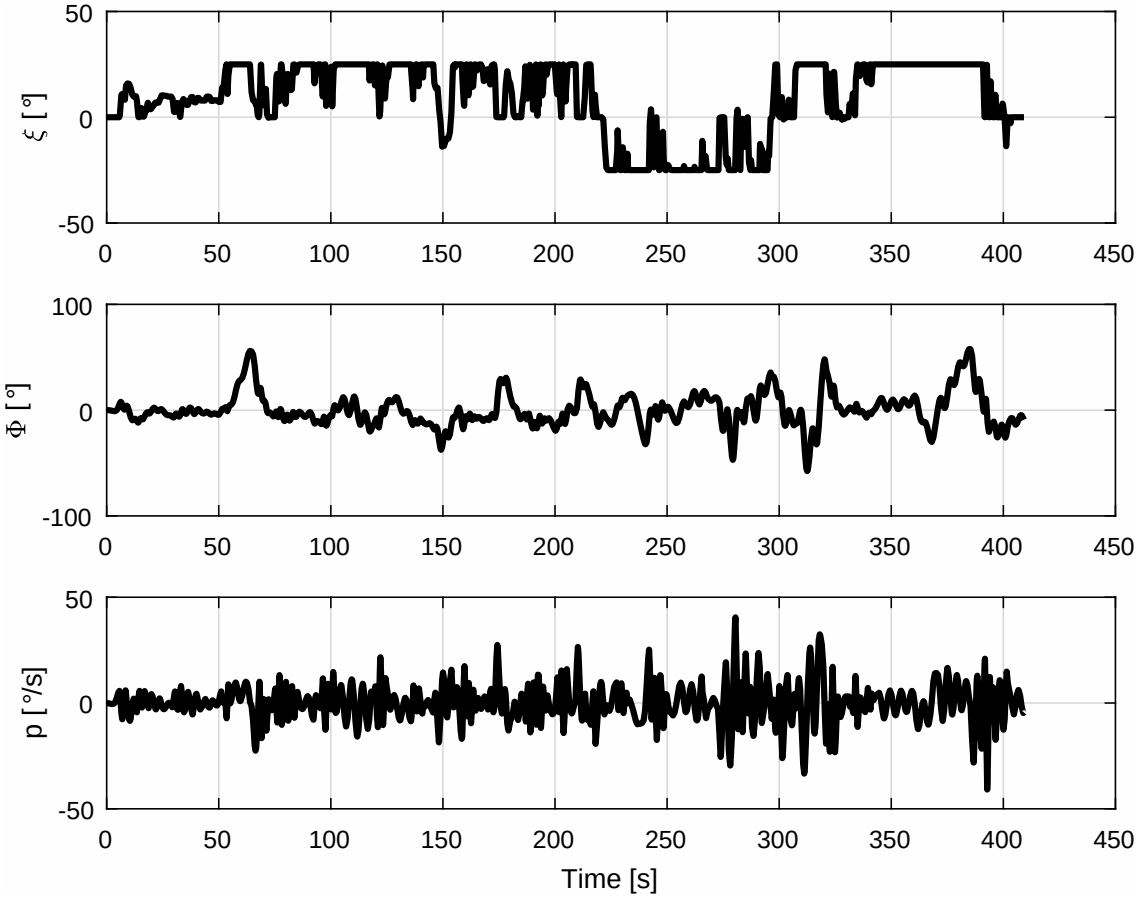

Figure F.19: Time histories of lateral parameters

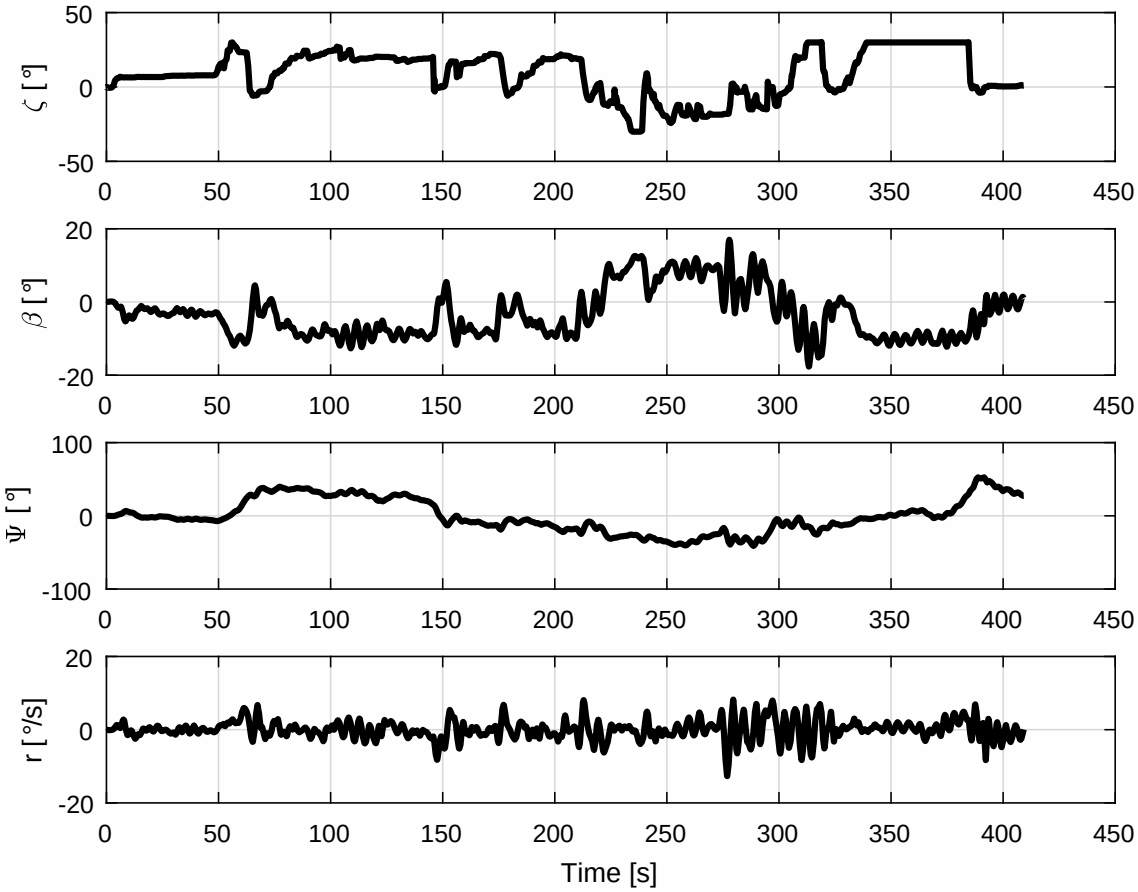

Figure F.20: Time histories of directional parameters

F.5 Roll mode, pilot 1, flexible A/C – RM(1)F

Date: 24/01/2018 **Time start:** **Time stop:** 17:36

Test No:	RM(1)F	**Test hardware:**	EFS500 + Speedgoat
Test pilot:	(1)	**Model version:**	HARTEN_v1 (F)

Task:	Lateral / directional modes (roll mode) (RM)
Manoeuvre:	

Instrumentation:	
Relevant files:	{D_SIM/D_STRUCT}.DAT @ 24/01/2018 17:36; DSCN9523.MOV

Flight velocity: 110 m/s **Flight altitude:** 10000 ft

Aircraft weight: 79 t **Aircraft CG:** 20% MAC

Roll 30 left → 30 right (full aileron)

Time: Time const: Rudder:

Roll 30 right → 30 left (full aileron)

Time: Time const: Rudder:

Notes:

$T_{wing\ rocking}$ = 3.5 sec

Notes (from audio recording):

"Nonlinear roll due to intrusion of wing rocking"

"Undamped roll oscillation"

"The peak roll rate due to this oscillation is slightly greater than the maximum achievable roll rate available from use of the ailerons"

Figure F.21: Test card (RM(1)F)

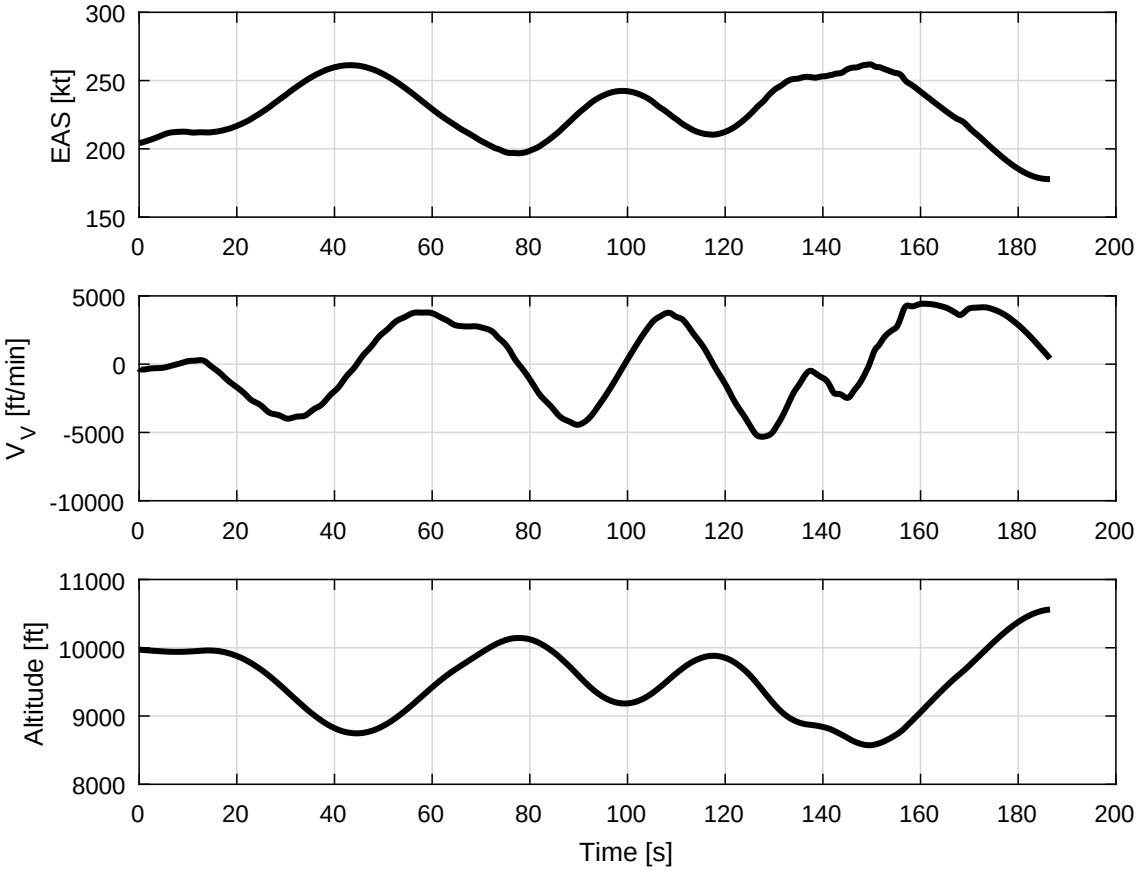

Figure F.22: Time histories of altitude and velocities

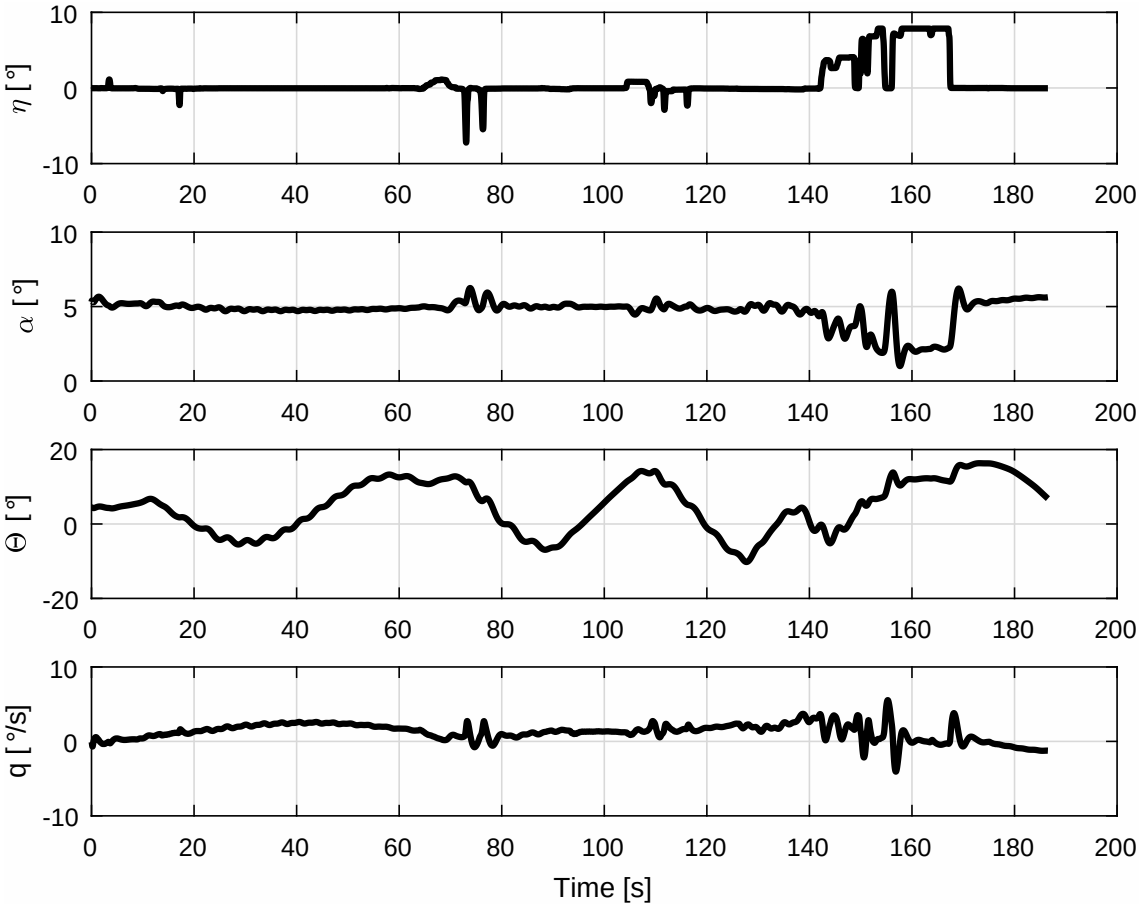

Figure F.23: Time histories of longitudinal parameters

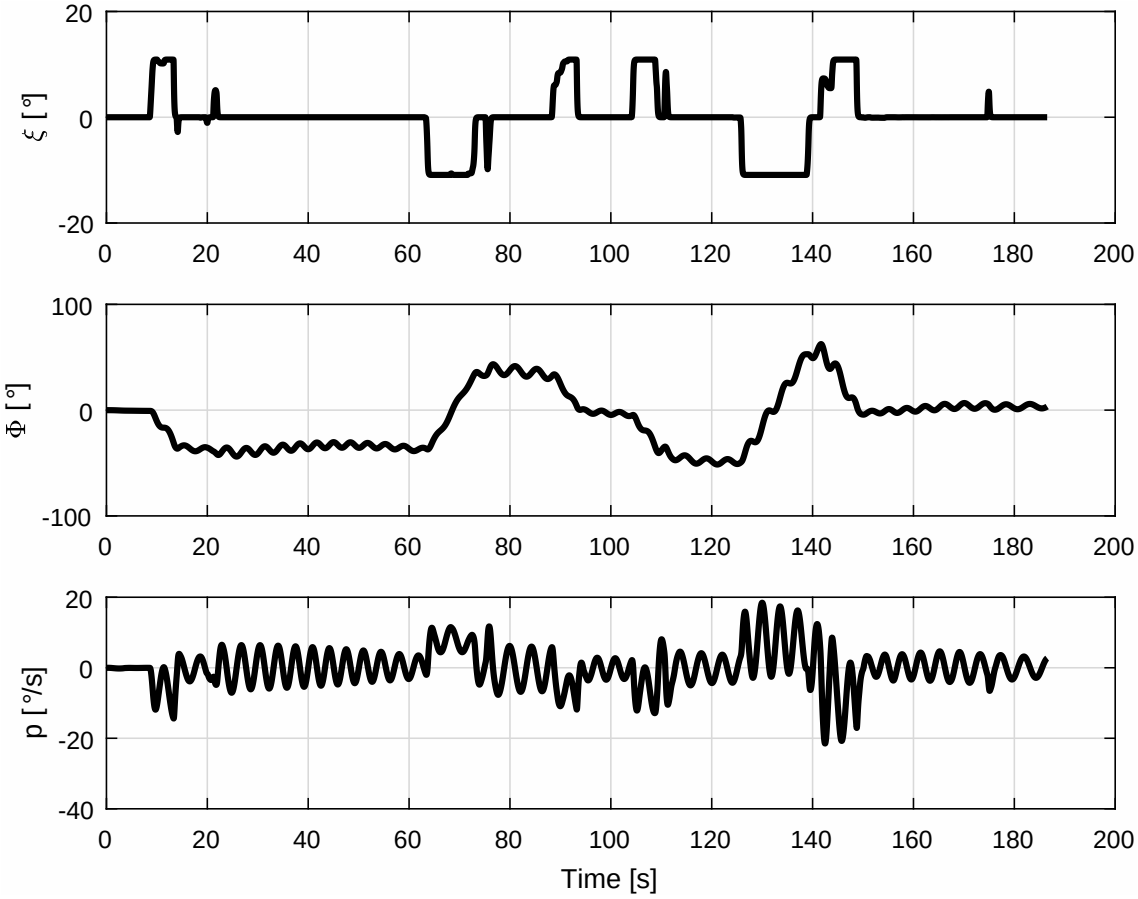

Figure F.24: Time histories of lateral parameters

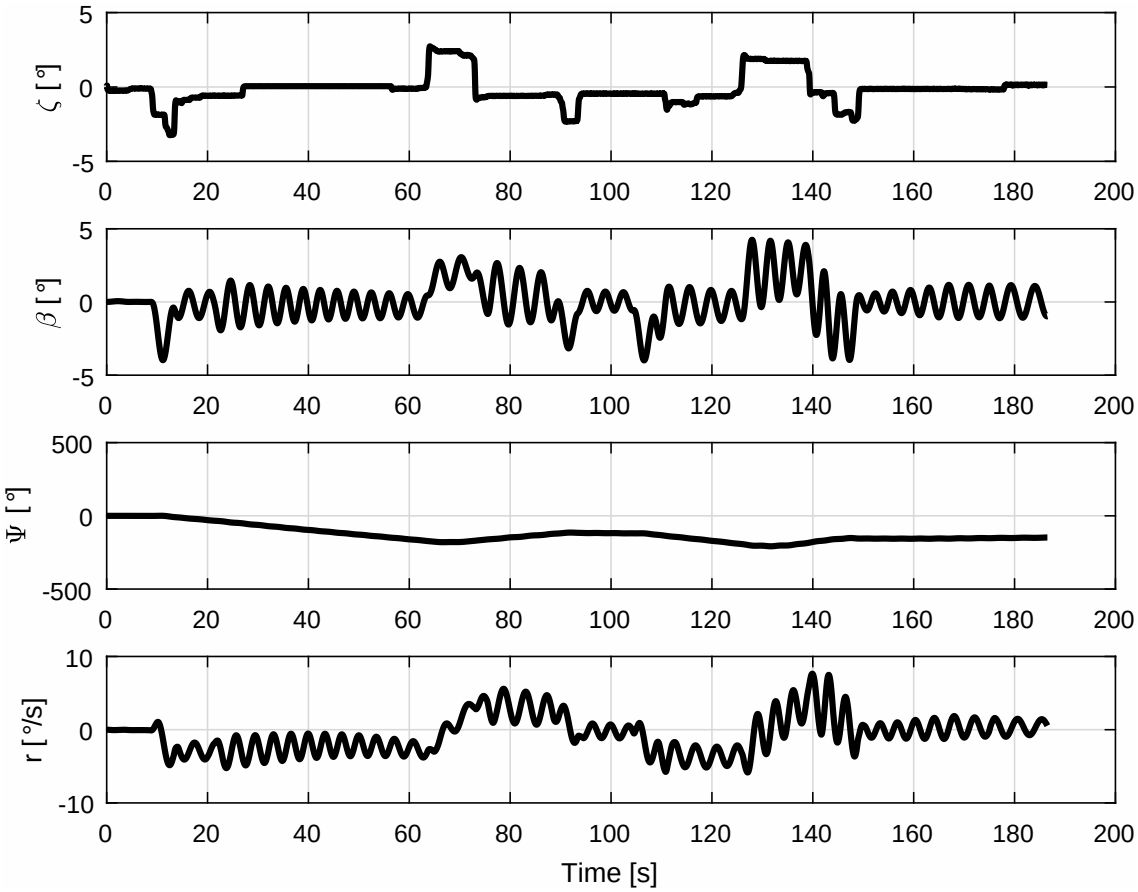

Figure F.25: Time histories of directional parameters

F.6 Roll mode, pilot 2, rigid A/C – RM(2)R

Date: 09/02/2018 **Time start:** **Time stop:** 10:59

Test No:	RM(2)R	**Test hardware:**	EFS500 + Speedgoat
Test pilot:	(2)	**Model version:**	HARTEN_v1 (R)

Task:	Lateral / directional modes (SHSS, roll mode) (SH)
Manoeuvre:	

Instrumentation:	
Relevant files:	{D_LOADS/D_SIM/D_STRUCT}.DAT @ 09/02/2018 10:59; DSCN9584.MOV

Flight velocity: 110 m/s **Flight altitude:** 10000 ft

Aircraft weight: 79 t **Aircraft CG:** 20% MAC

Roll 30 left → 30 right (full aileron)

Time: 2 sec Time const: < 1 sec Rudder: Nil

Roll 30 right → 30 left (full aileron)

Time: 2 sec Time const: < 1 sec Rudder: Nil

Notes:

Very small adverse yaw

Notes (from audio recording):

“Not much Dutch roll”

Figure F.26: Test card (RM(2)R)

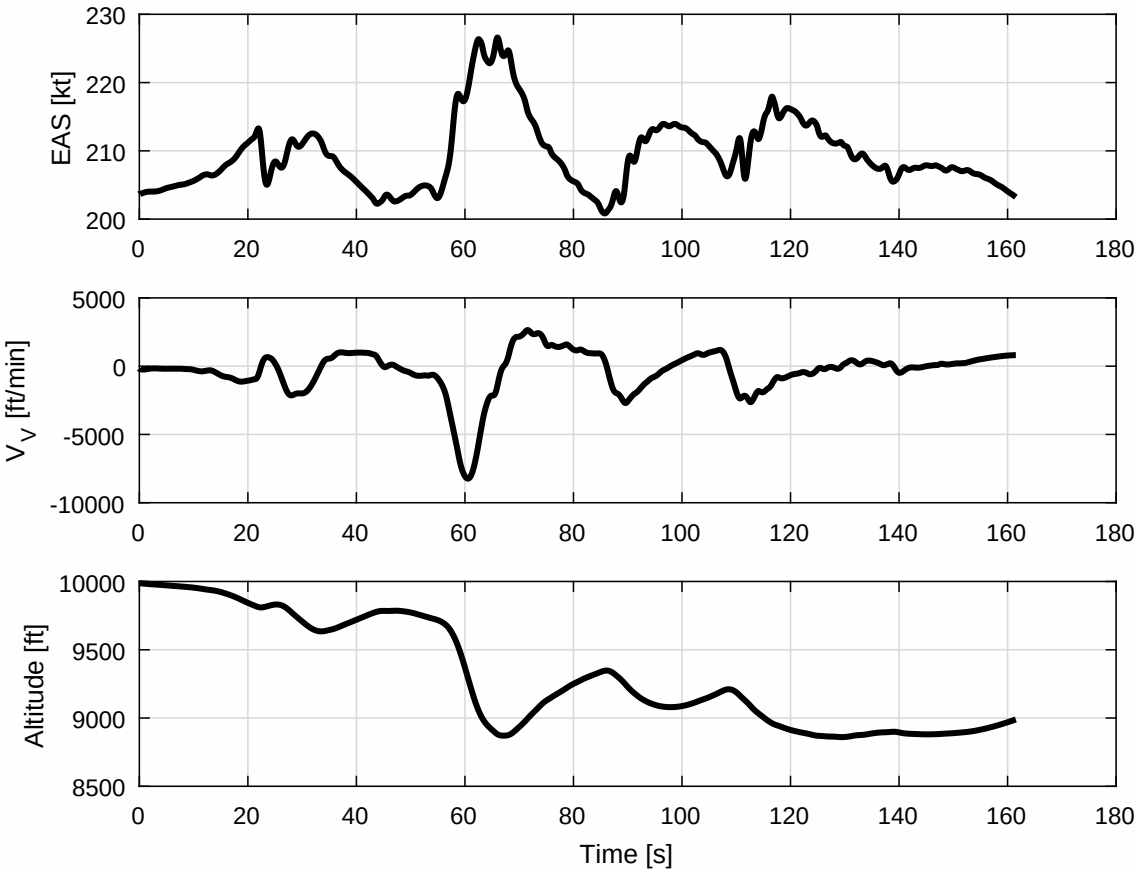

Figure F.27: Time histories of altitude and velocities

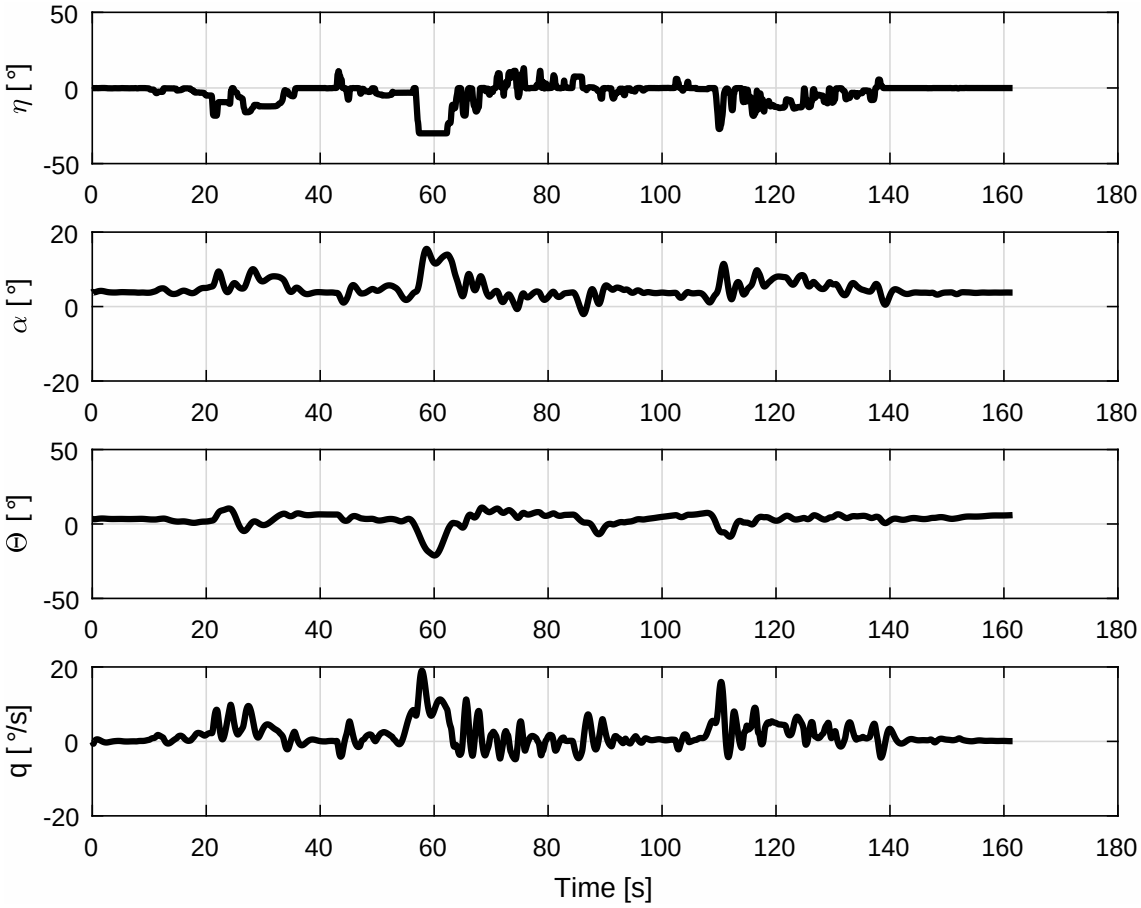

Figure F.28: Time histories of longitudinal parameters

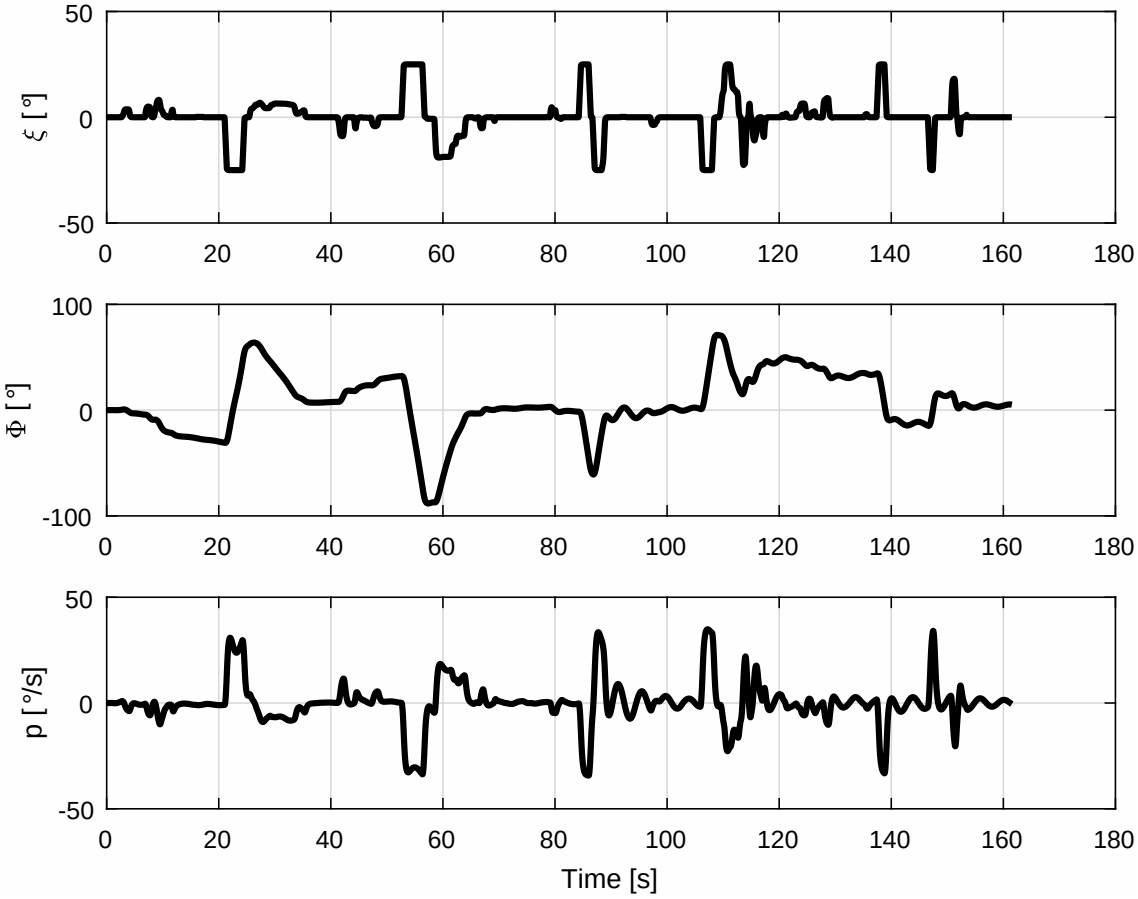

Figure F.29: Time histories of lateral parameters

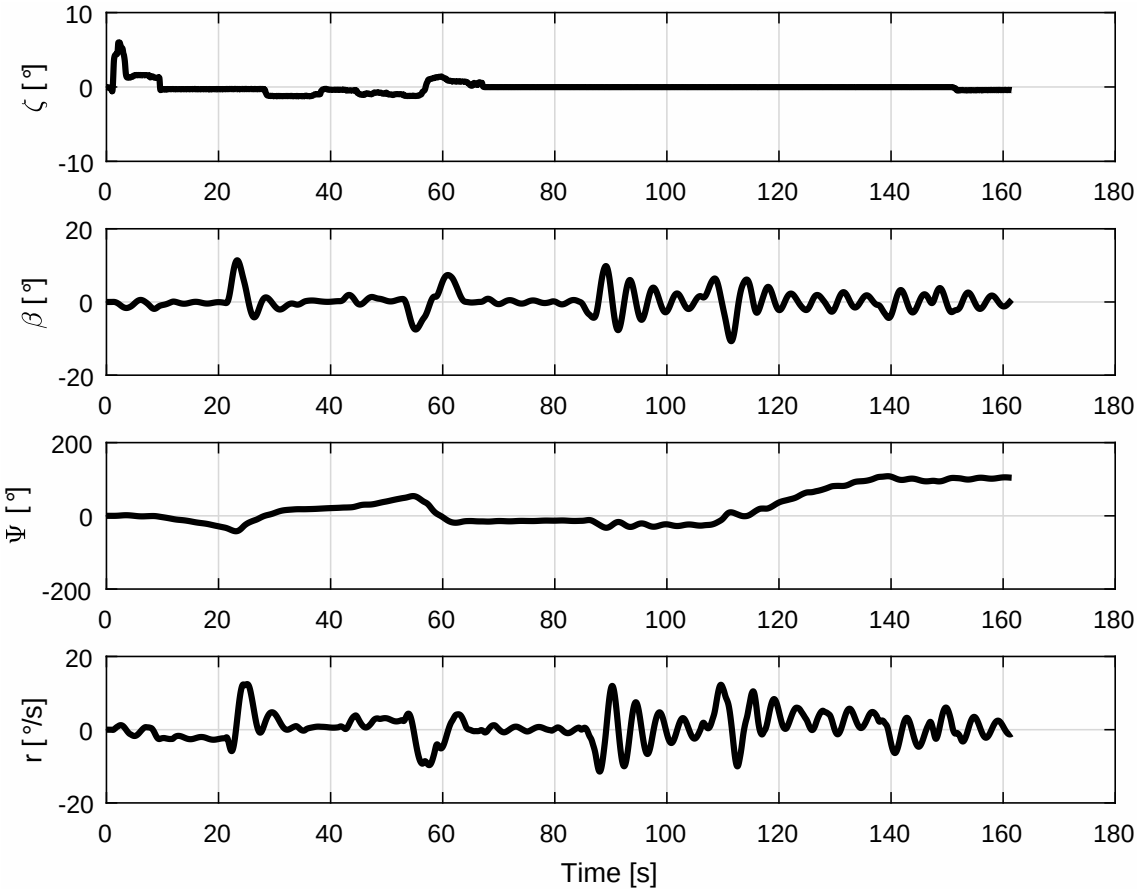

Figure F.30: Time histories of directional parameters

F.7 Roll mode, pilot 2, flexible A/C – RM(2)F

Date: 09/02/2018 **Time start:** **Time stop:** 14:31

Test No:	RM(2)F	**Test hardware:**	EFS500 + Speedgoat
Test pilot:	(2)	**Model version:**	HARTEN_v1 (F)

Task:	Lateral / directional modes (roll mode) (RM)
Manoeuvre:	

Instrumentation:	
Relevant files:	{D_LOADS/D_SIM/D_STRUCT}.DAT @ 09/02/2018 14:31; DSCN9596.MOV

Flight velocity: 110 m/s **Flight altitude:** 10000 ft

Aircraft weight: 79 t **Aircraft CG:** 20% MAC

Roll 30 left → 30 right (full aileron)

Time: 5 sec Time const: Rudder:

Roll 30 right → 30 left (full aileron)

Time: 4 sec Time const: Rudder:

Notes:

Issues due to roll stop; adverse yaw + sideslip;

Spoilers should be considered for roll control

Notes (from audio recording):

“Roll pause in the process”

Figure F.31: Test card (RM(2)F)

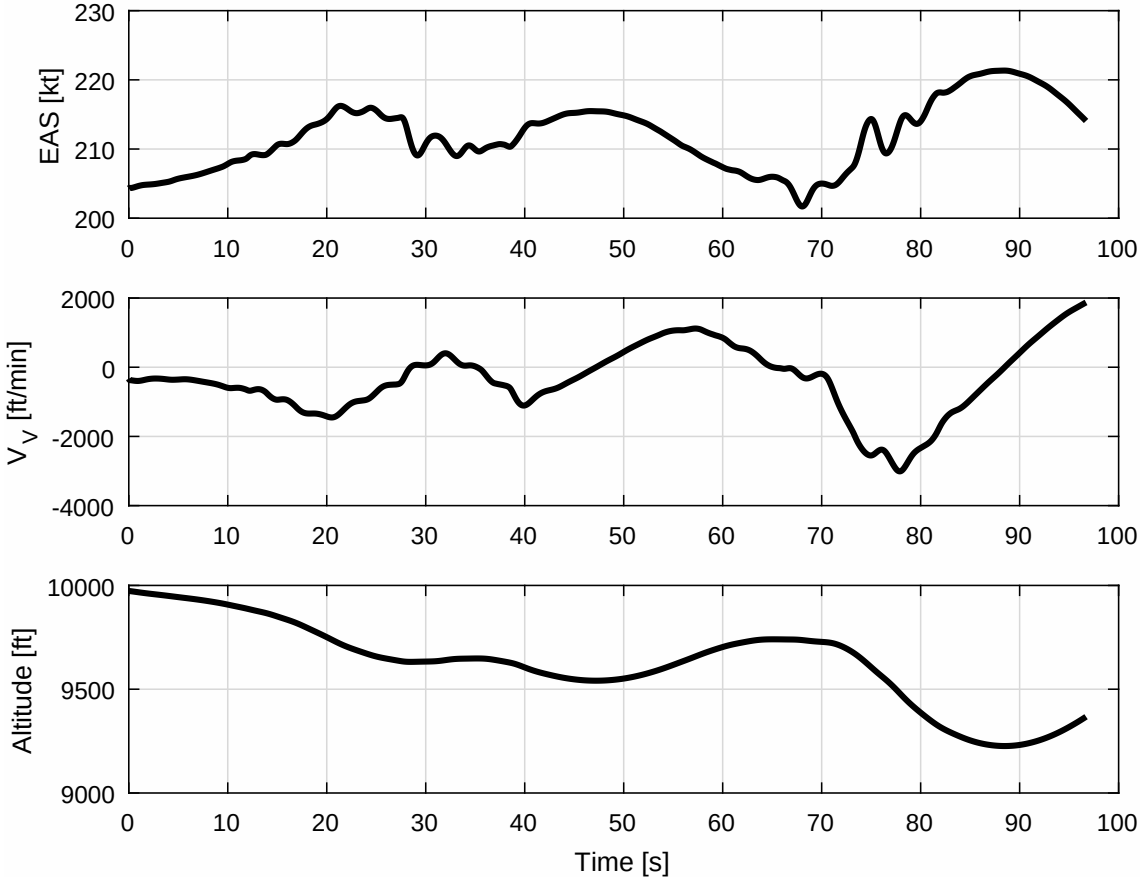

Figure F.32: Time histories of altitude and velocities

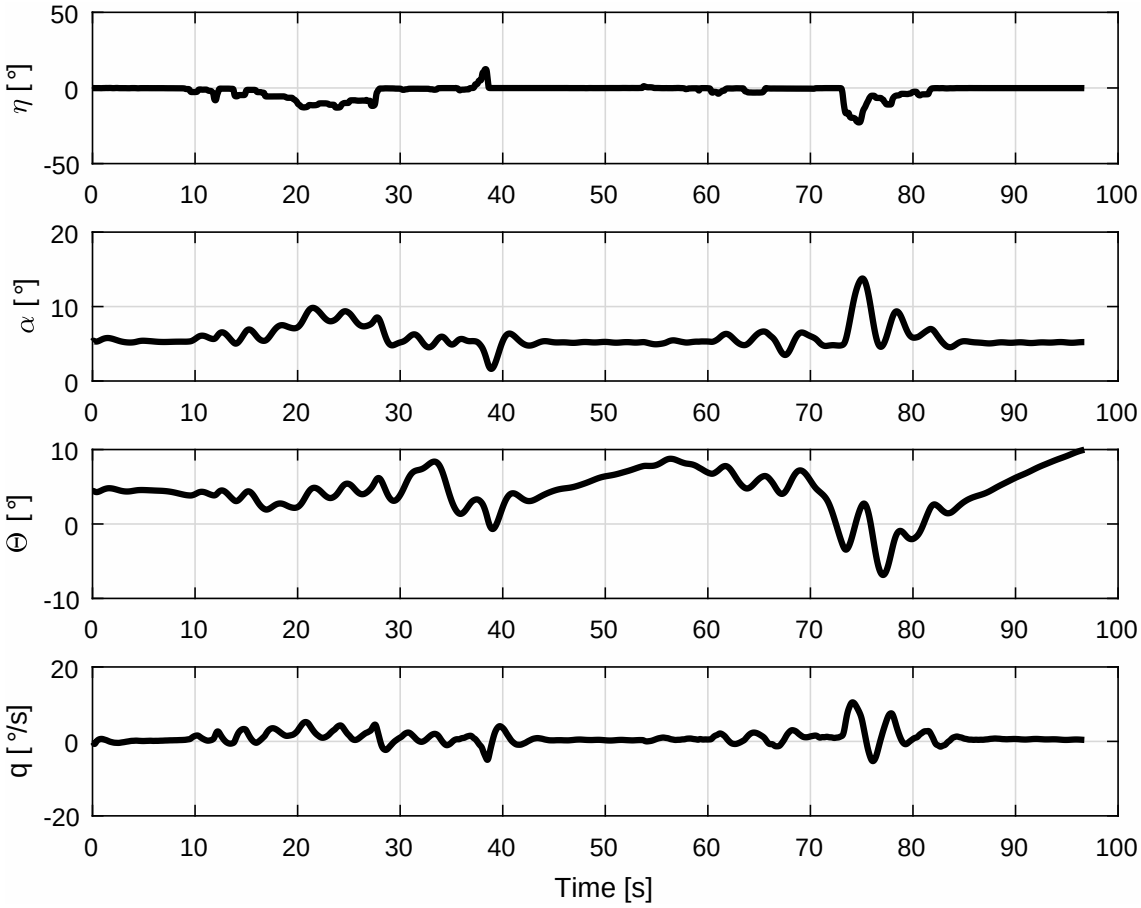

Figure F.33: Time histories of longitudinal parameters

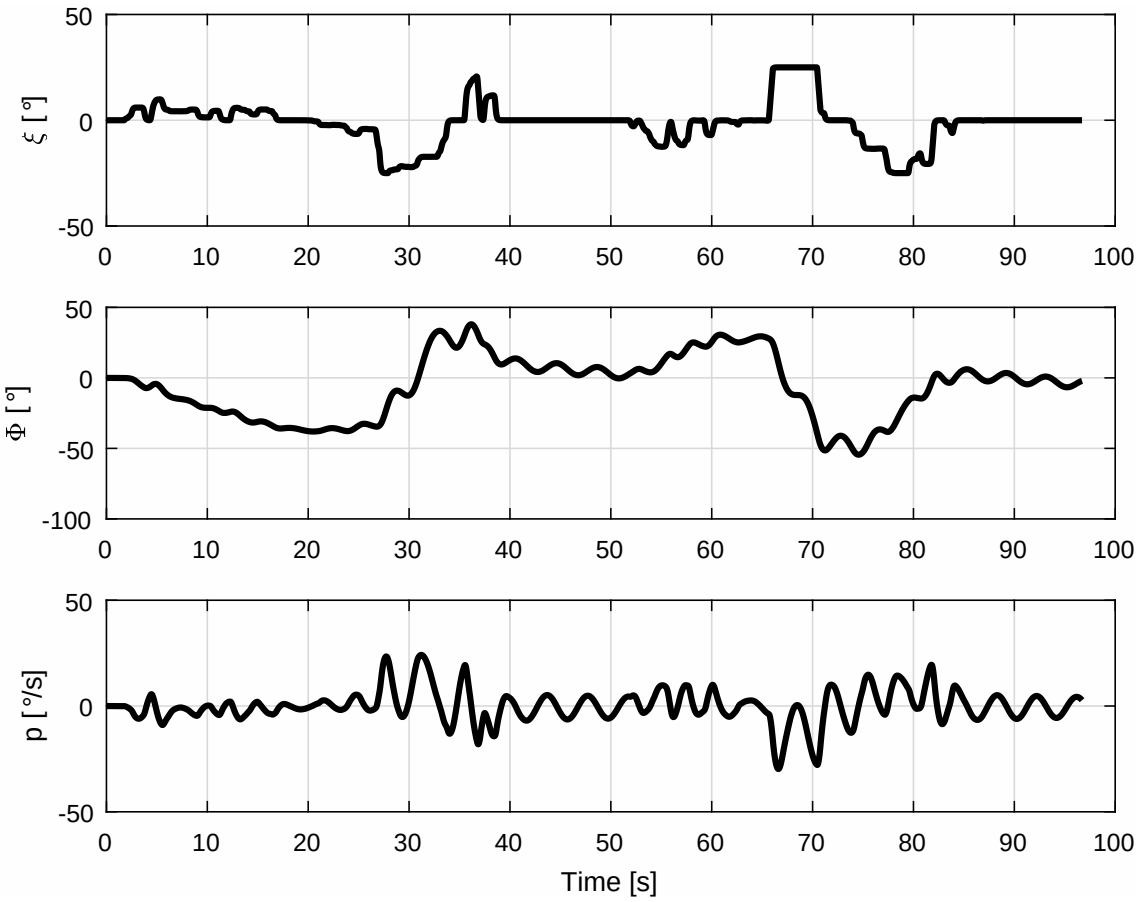

Figure F.34: Time histories of lateral parameters

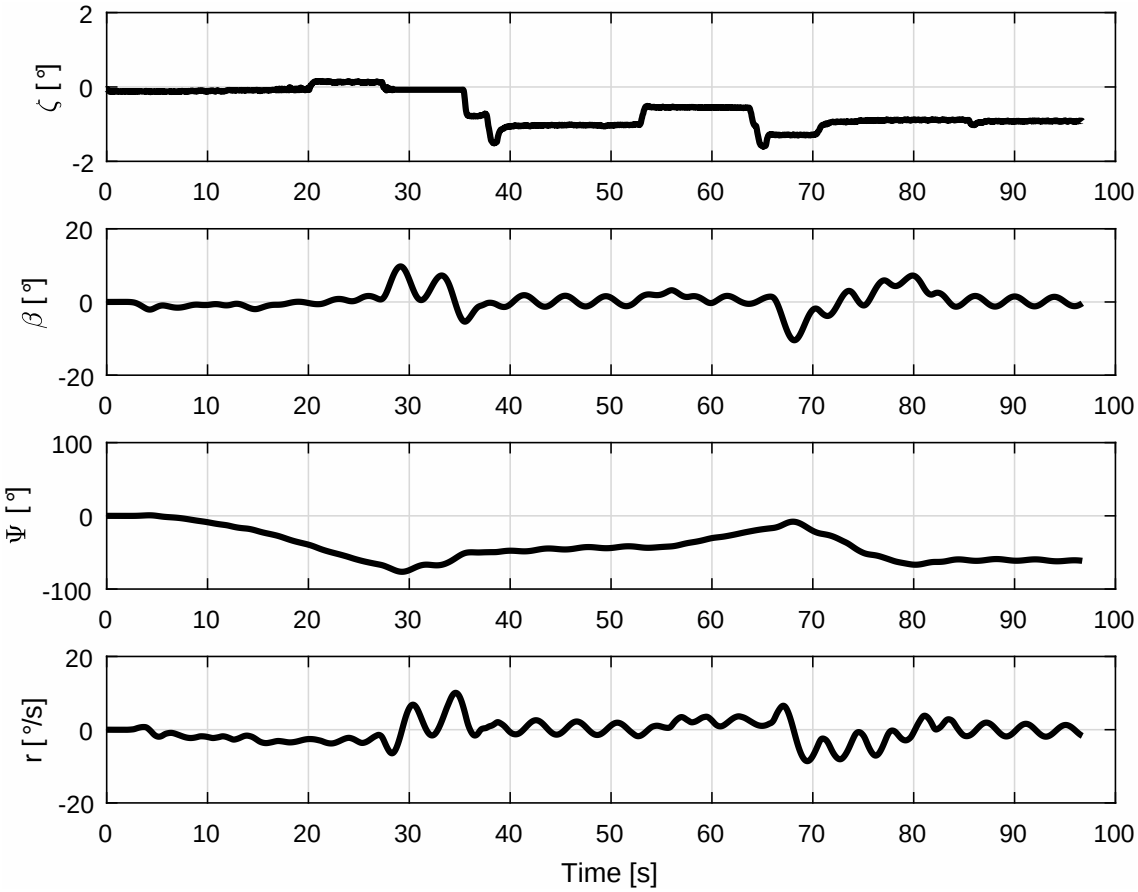

Figure F.35: Time histories of directional parameters

F.8 Spiral mode, pilot 1, rigid A/C – SM(1)R

Date: 24/01/2018 **Time start:** **Time stop:** 16:49

Test No:	SM(1)R	**Test hardware:**	EFS500
Test pilot:	(1)	**Model version:**	HARTEN_v1 (R)

Task:	Lateral / directional modes (spiral mode) (SM)
Manoeuvre:	

Instrumentation:	
Relevant files:	{D_SIM/D_STRUCT}.DAT @ 24/01/2018 16:49; DSCN9515.MOV; GOPR4021.MP4

Flight velocity: 110 m/s **Flight altitude:** 10000 ft

Aircraft weight: 79 t **Aircraft CG:** 20% MAC

Spiral mode

15° left: T_2 = 25 sec;

Notes:

15° right: T_2 = 32 sec;

Notes:

Notes:

A/C from spiral mode continued into spiral dive

Insufficient control after recovery from spiral dive

Notes (from audio recording):

“Insufficient elevator authority” – about recovery from a dive

Figure F.36: Test card (SM(1)R)

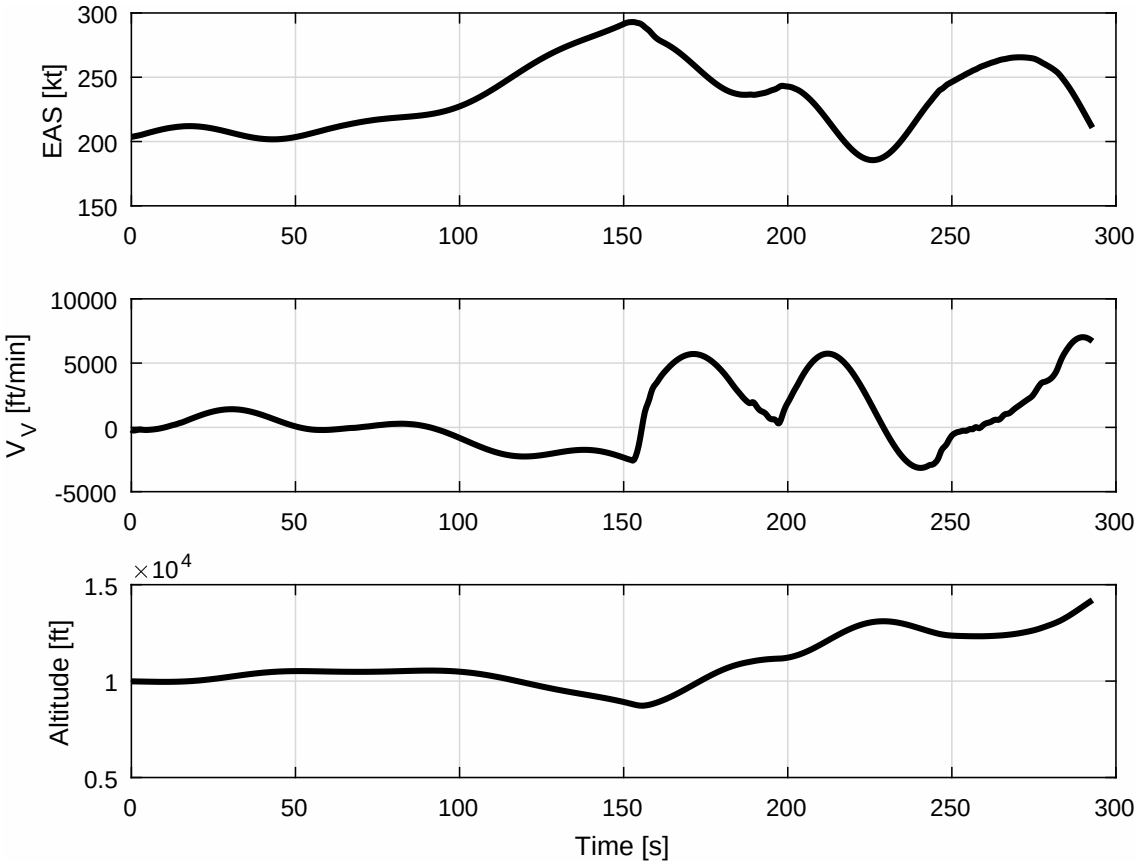

Figure F.37: Time histories of altitude and velocities

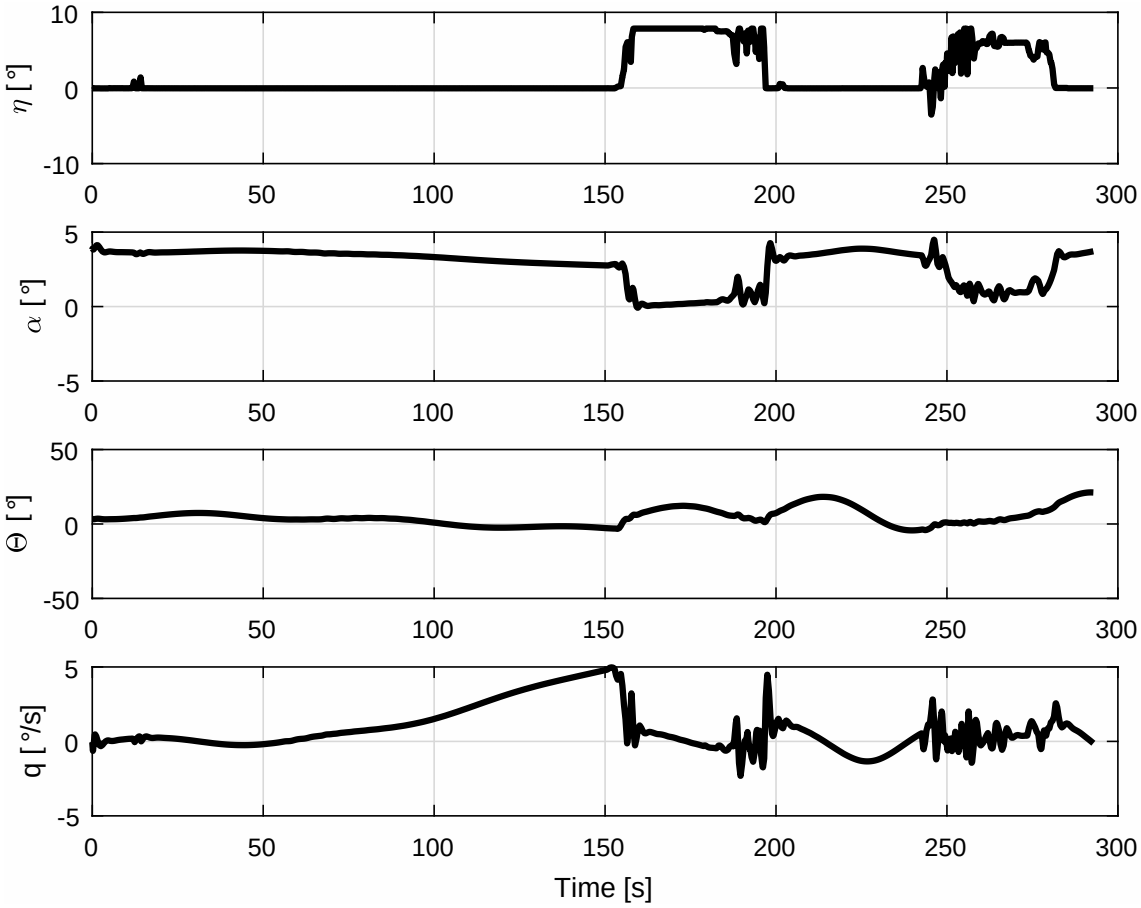

Figure F.38: Time histories of longitudinal parameters

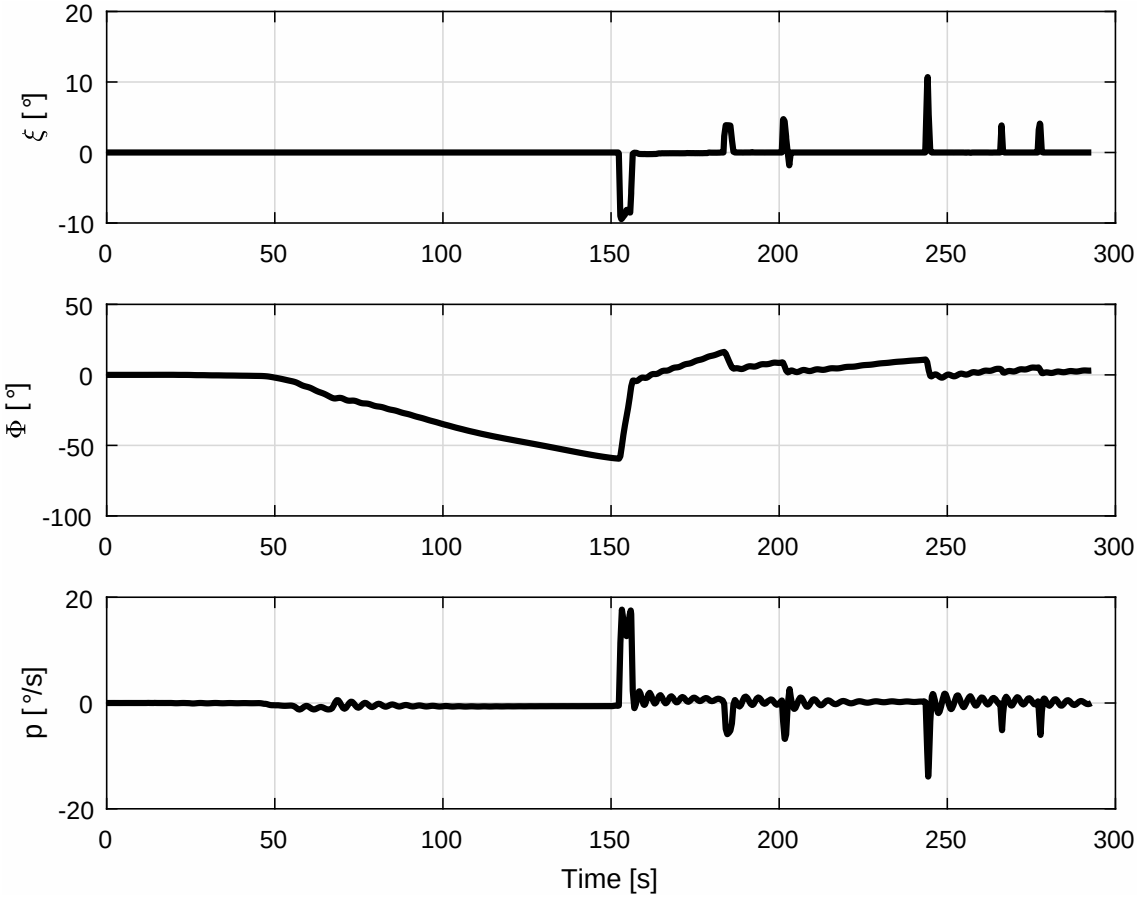

Figure F.39: Time histories of lateral parameters

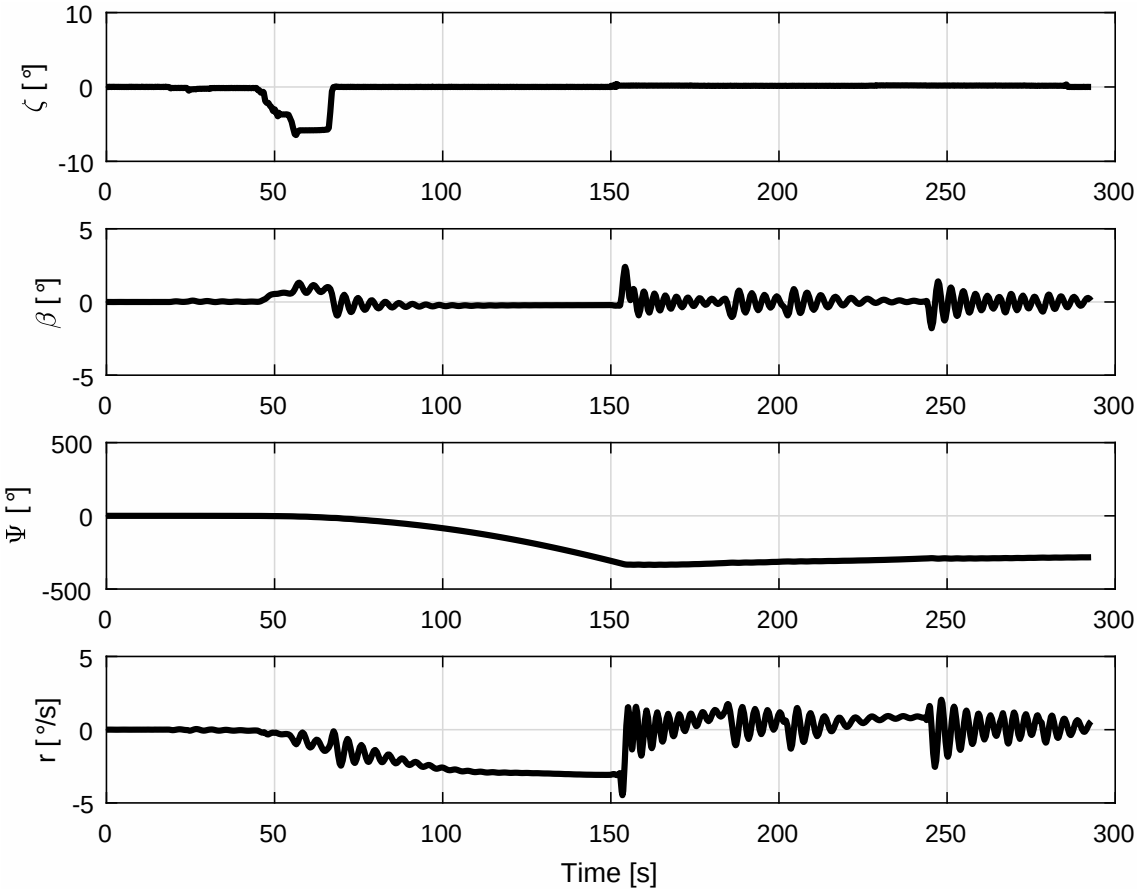

Figure F.40: Time histories of directional parameters

F.9 Spiral mode, pilot 2, rigid A/C – SM(2)R

Date: 09/02/2018 **Time start:** **Time stop:** 11:07

Test No:	SM(2)R	**Test hardware:**	EFS500 + Speedgoat
Test pilot:	(2)	**Model version:**	HARTEN_v1 (R)

Task:	Lateral / directional modes (spiral mode) (SM)
Manoeuvre:	

Instrumentation:	
Relevant files:	{D_LOADS/D_SIM/D_STRUCT}.DAT @ 09/02/2018 11:07; DSCN9585.MOV

Flight velocity: 110 m/s **Flight altitude:** 10000 ft

Aircraft weight: 79 t **Aircraft CG:** 20% MAC

Spiral mode

15° left: T_2 = 30 sec; 22 sec with speed constant

Notes:

15° right: T_2 = 35 sec; 25 sec with speed constant

Notes:

Notes:

Directional stability is higher – confirms SHSS results

Unstable within acceptable tolerance

Notes (from audio recording):

Nil

Figure F.41: Test card (SM(2)R)

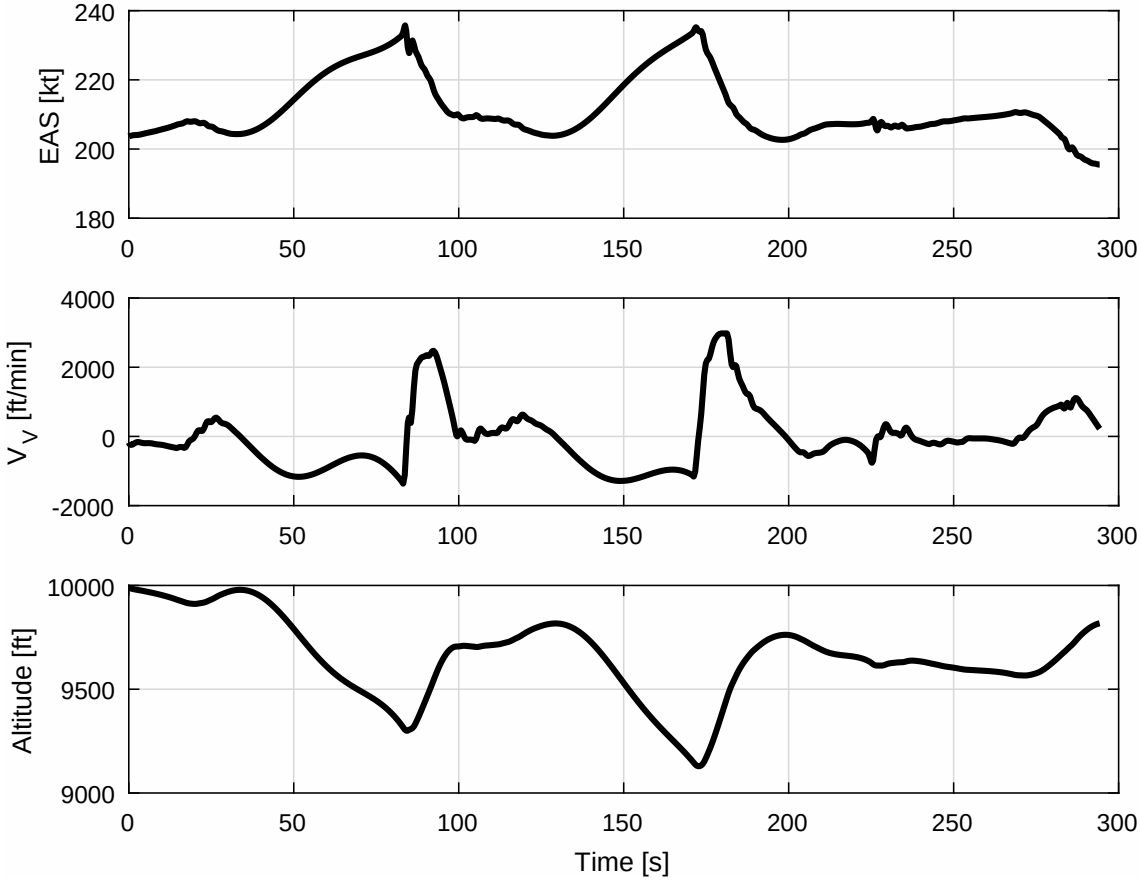

Figure F.42: Time histories of altitude and velocities

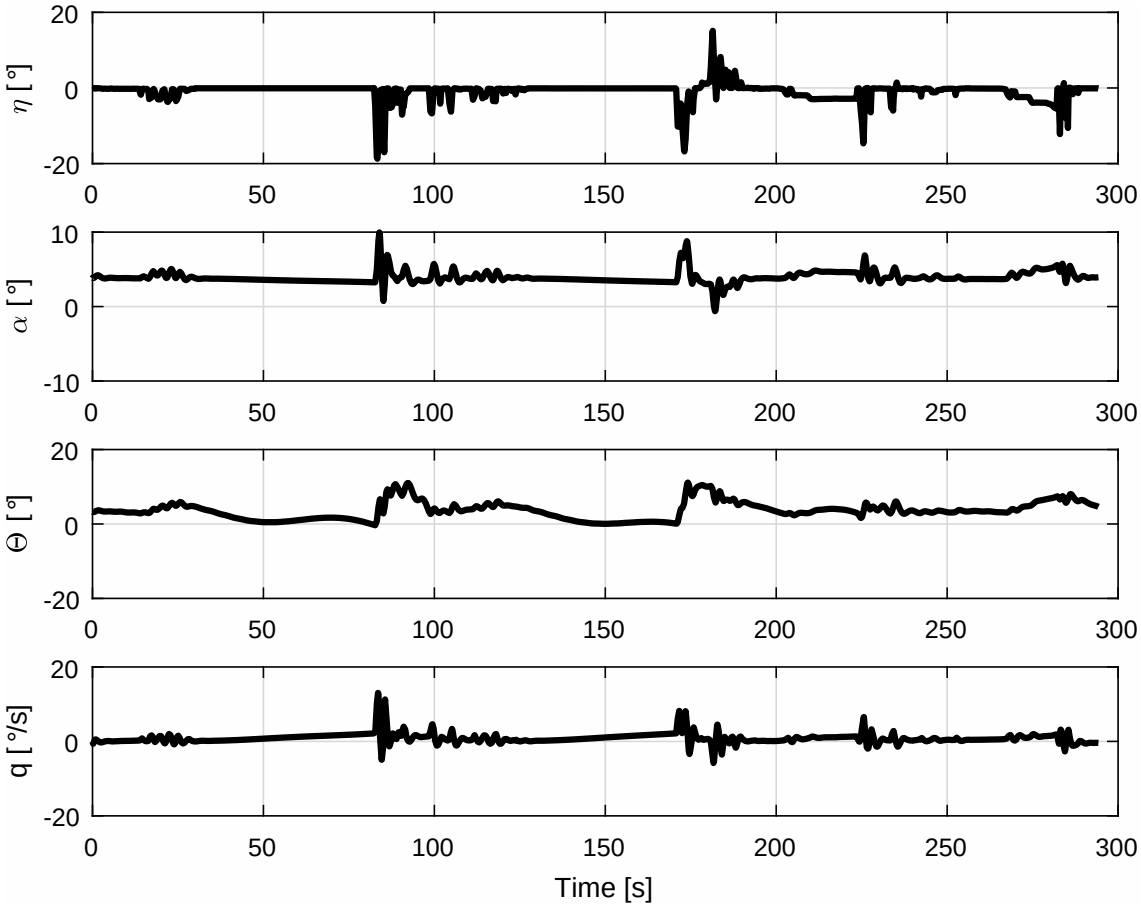

Figure F.43: Time histories of longitudinal parameters

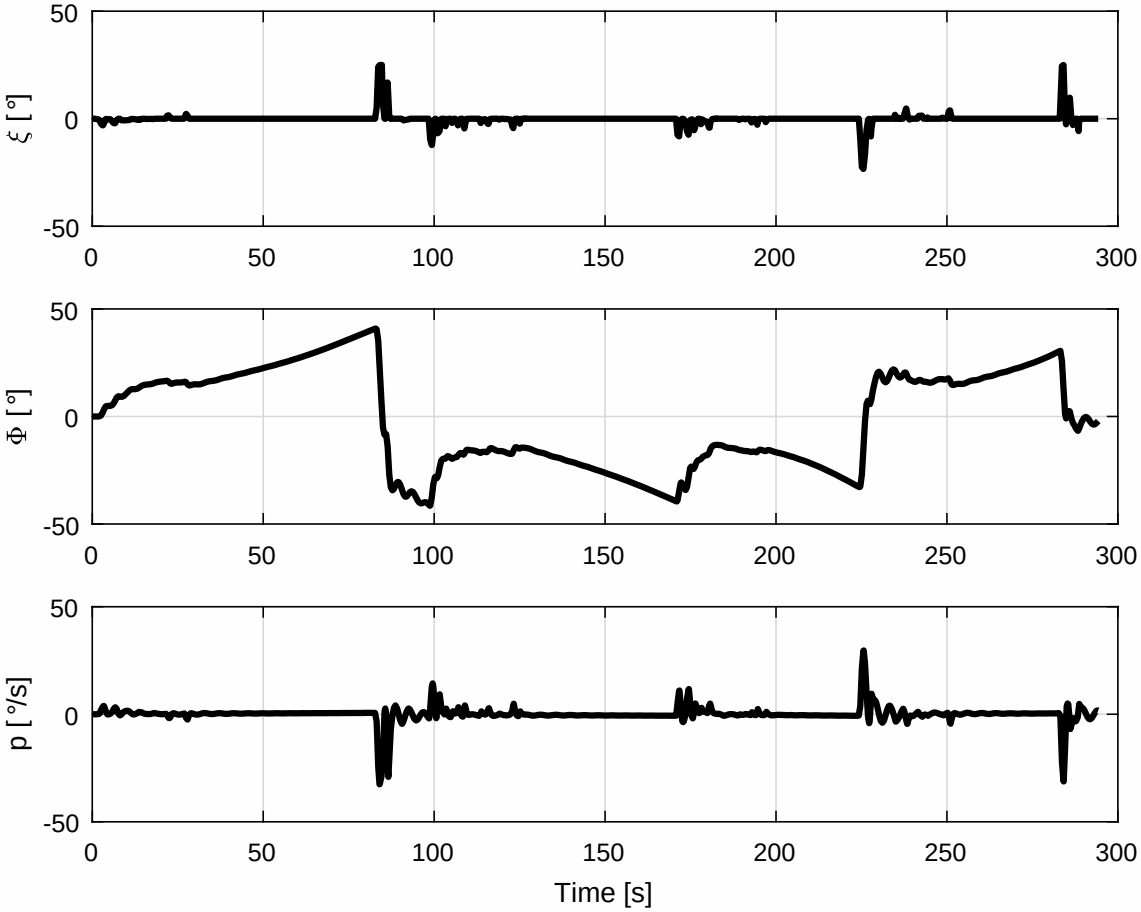

Figure F.44: Time histories of lateral parameters

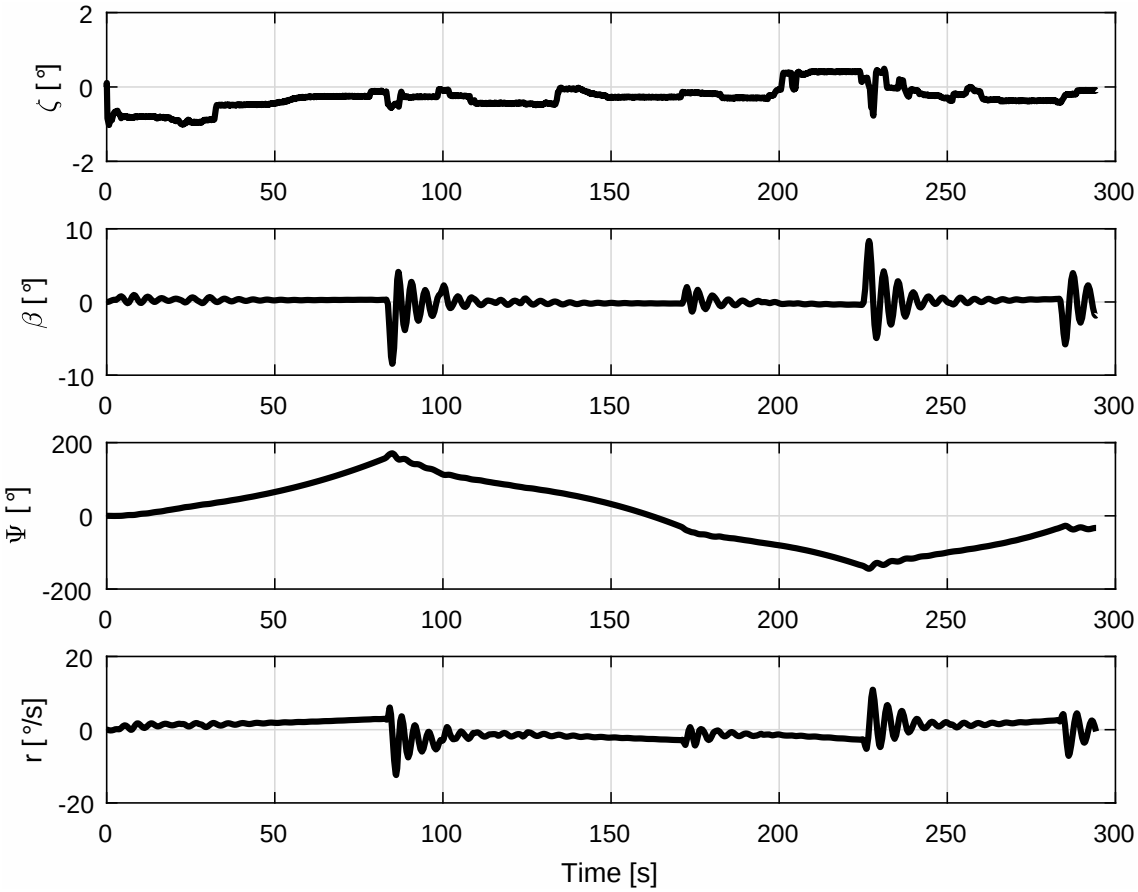

Figure F.45: Time histories of directional parameters

F.10 Spiral mode, pilot 2, flexible A/C – SM(2)F

Date: 09/02/2018 **Time start:** **Time stop:** 14:39

Test No:	SM(2)F	**Test hardware:**	EFS500 + Speedgoat
Test pilot:	(2)	**Model version:**	HARTEN_v1 (F)

Task:	Lateral / directional modes (spiral mode) (SM)
Manoeuvre:	

Instrumentation:	
Relevant files:	{D_LOADS/D_SIM/D_STRUCT}.DAT @ 09/02/2018 14:39; DSCN9597.MOV

Flight velocity: 110 m/s **Flight altitude:** 10000 ft

Aircraft weight: 79 t **Aircraft CG:** 20% MAC

Spiral mode

15° left: NEUTRAL TO SLIGHTLY STABLE

Notes:

15° right: NEUTRAL TO SLIGHTLY STABLE

Notes:

Notes:

Nil

Notes (from audio recording):

“Dutch roll ±1 deg at 18 deg left”

Figure F.46: Test card (SM(2)F)

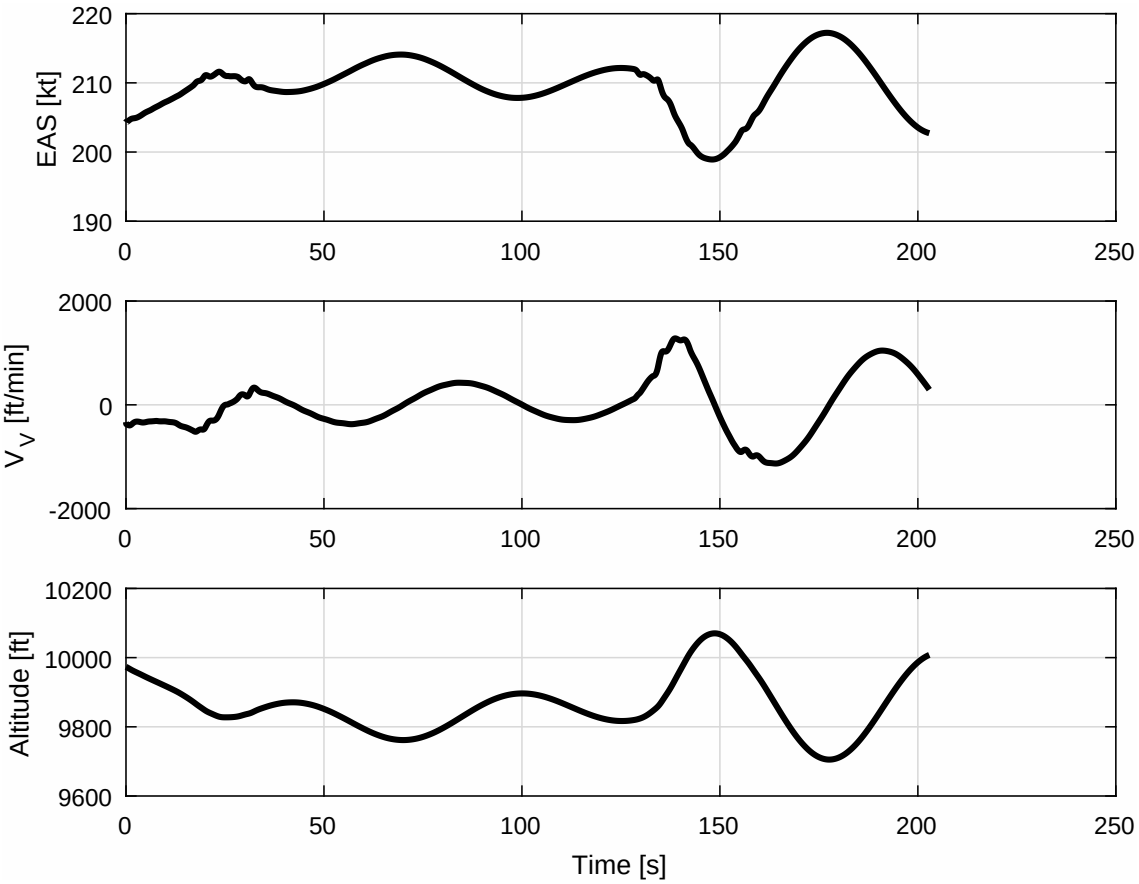

Figure F.47: Time histories of altitude and velocities

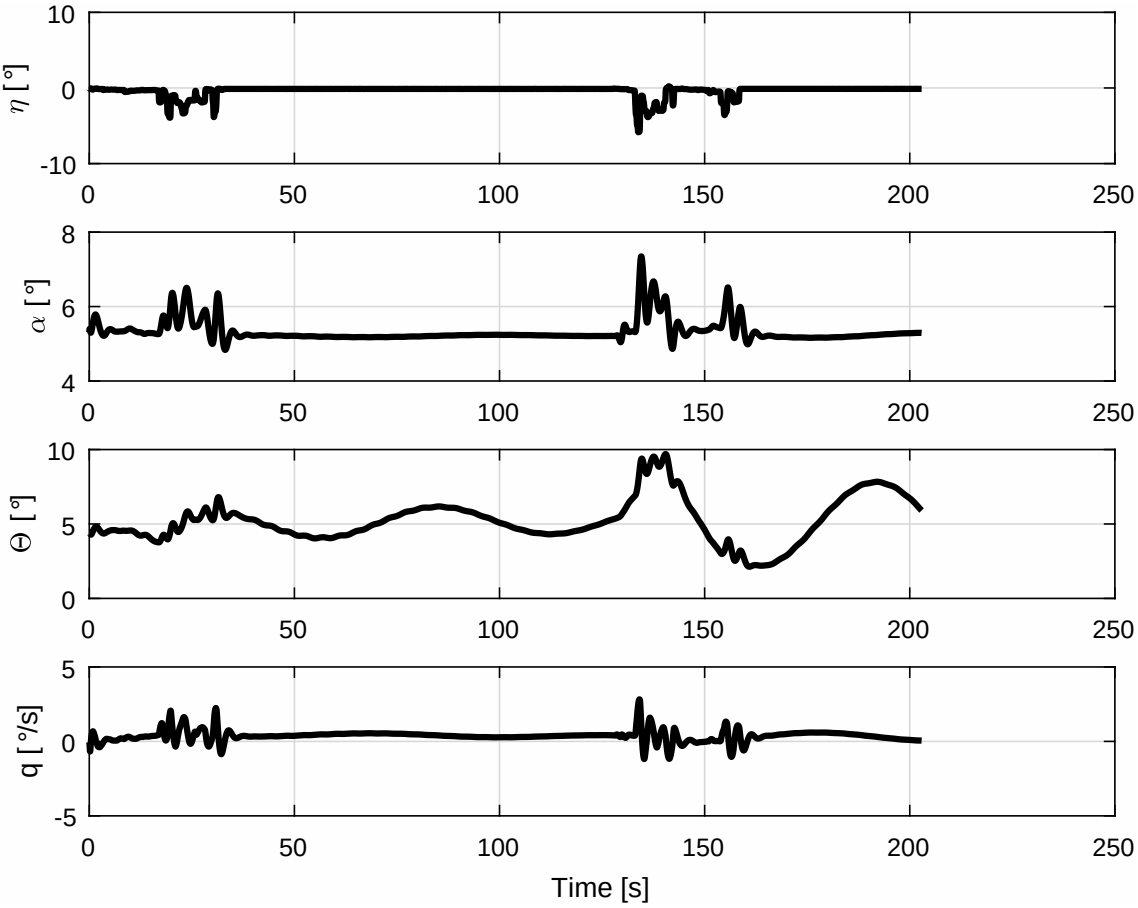

Figure F.48: Time histories of longitudinal parameters

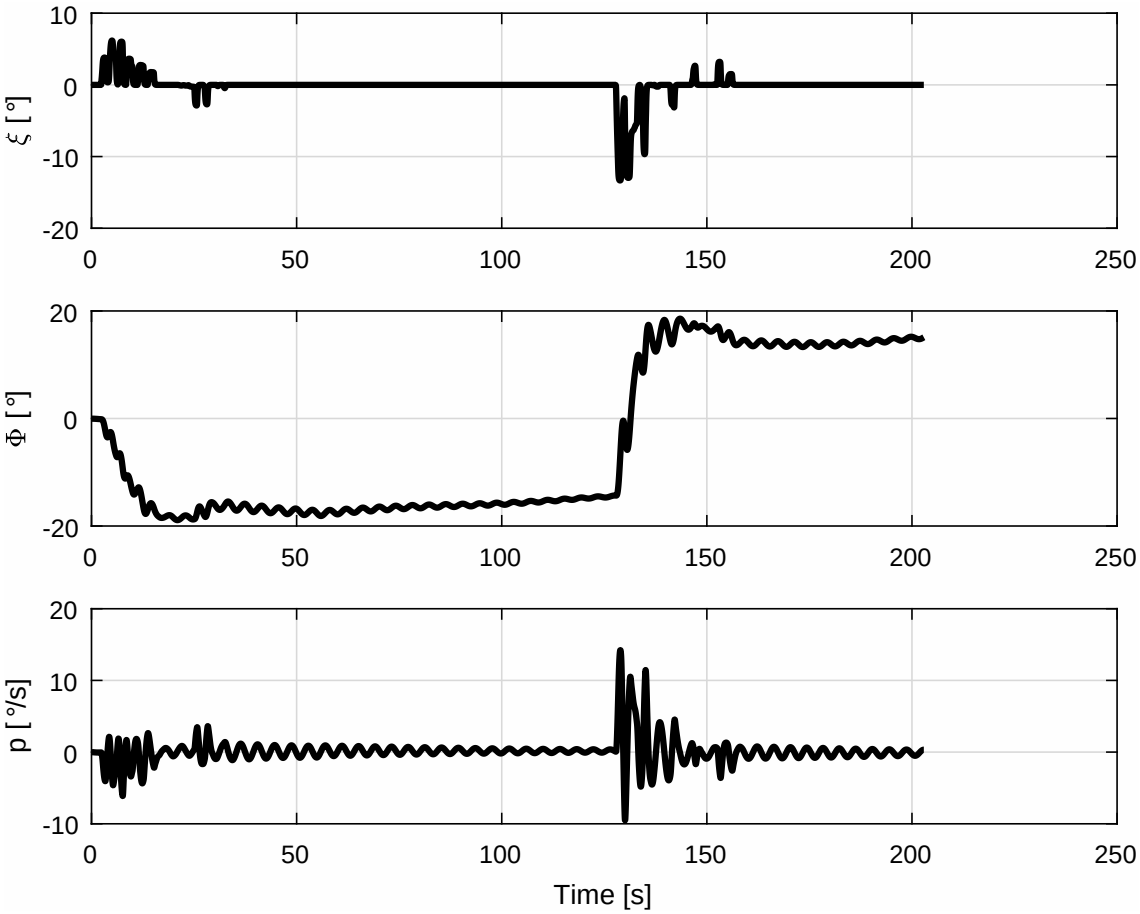

Figure F.49: Time histories of lateral parameters

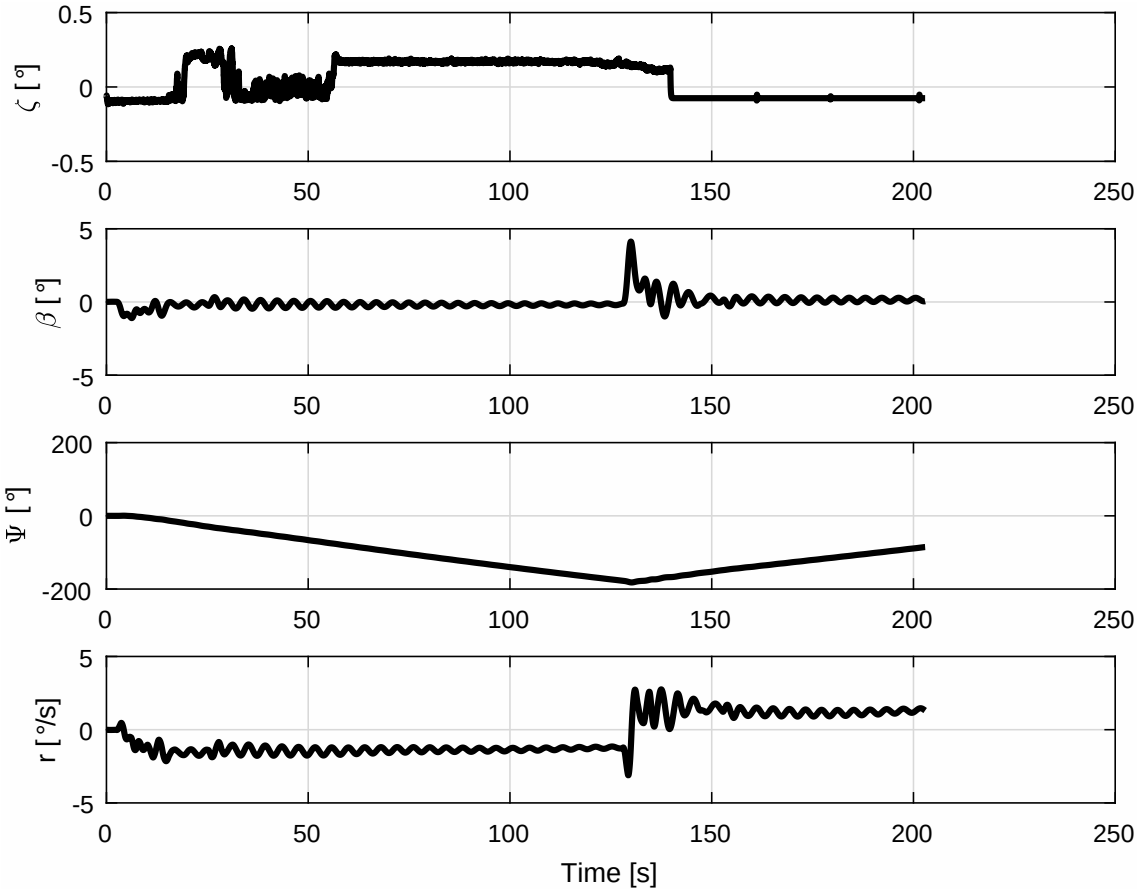

Figure F.50: Time histories of directional parameters

F.11 Dutch roll, pilot 1, rigid A/C – DR(1)R

Date: 24/01/2018 **Time start:** **Time stop:** 17:01

Test No:	DR(1)R	**Test hardware:**	EFS500 + Speedgoat
Test pilot:	(1)	**Model version:**	HARTEN_v1 (R)

Task:	Lateral / directional modes (Dutch roll mode) (DR)
Manoeuvre:	

Instrumentation:	
Relevant files:	{D_SIM/D_STRUCT}.DAT @ 24/01/2018 17:01; DSCN9517.MOV; GOPR4023.MP4

Flight velocity: 110 m/s **Flight altitude:** 10000 ft

Aircraft weight: 79 t **Aircraft CG:** 20% MAC

Rudder doublet

T_{damp}: 28 sec N_{damp}: 7

Notes:

Forced Dutch roll

F:

Shape: 3/1 yaw/roll

Notes:

Characteristics are OK; might be improved by a yaw damper

Notes (from audio recording):

“This stick is a bit like flying badly adjusted F-16”

“That is not actually particularly problematic characteristics… not brilliant, but the Dutch roll is not intruding on anything else”

“Slightly poorly damped Dutch roll”

Figure F.51: Test card (DR(1)R)

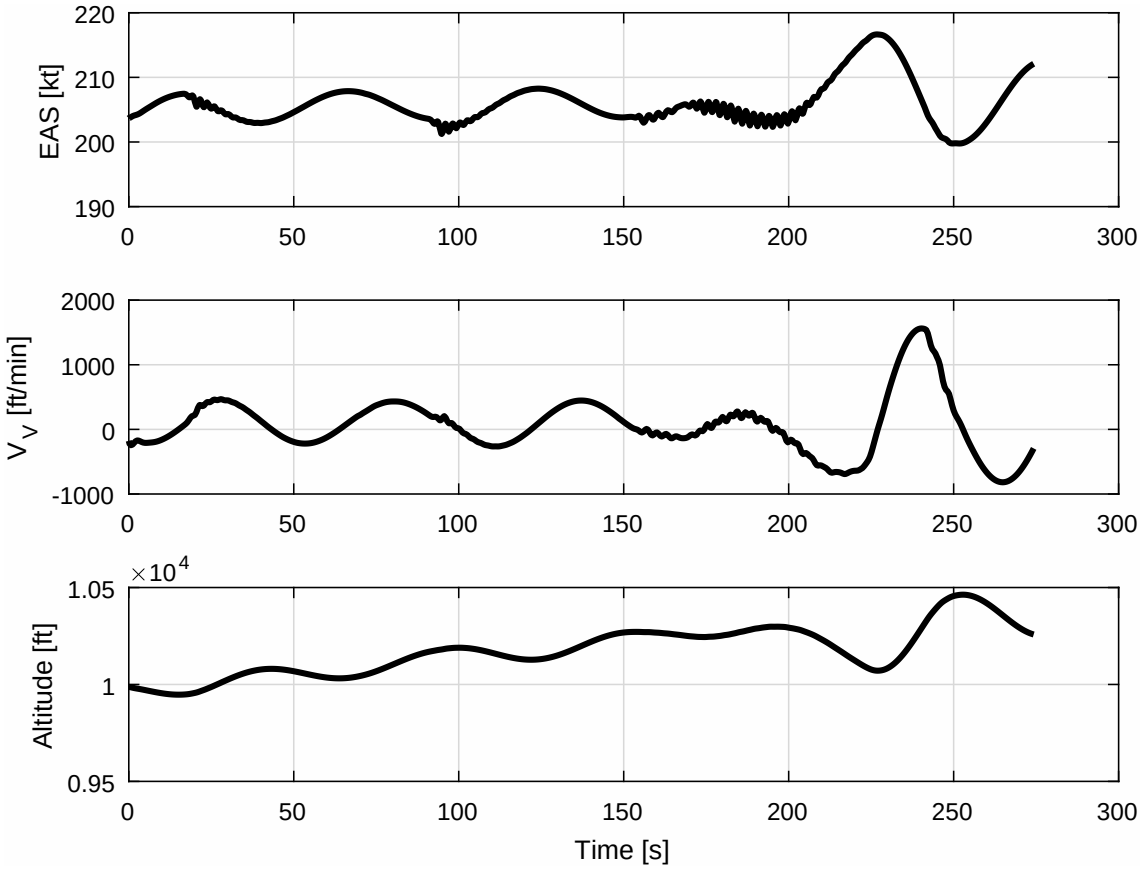

Figure F.52: Time histories of altitude and velocities

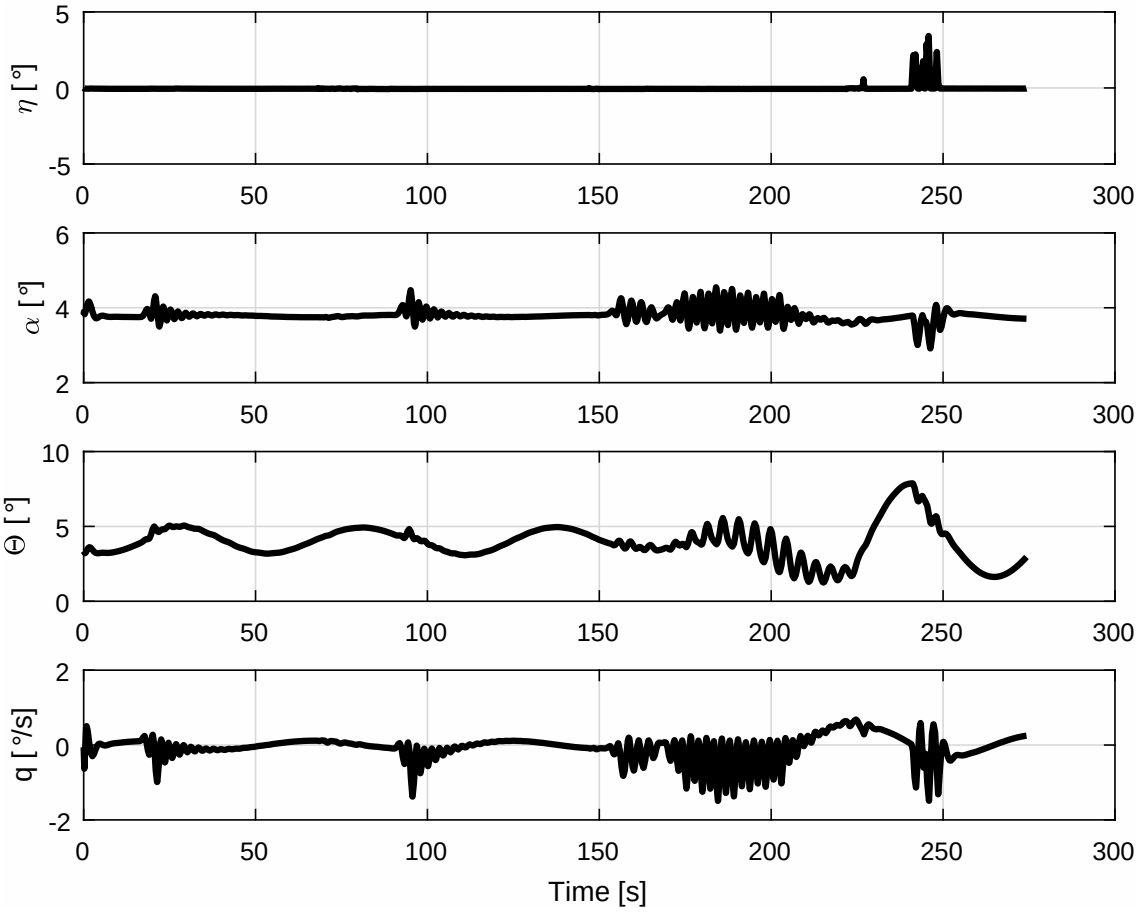

Figure F.53: Time histories of longitudinal parameters

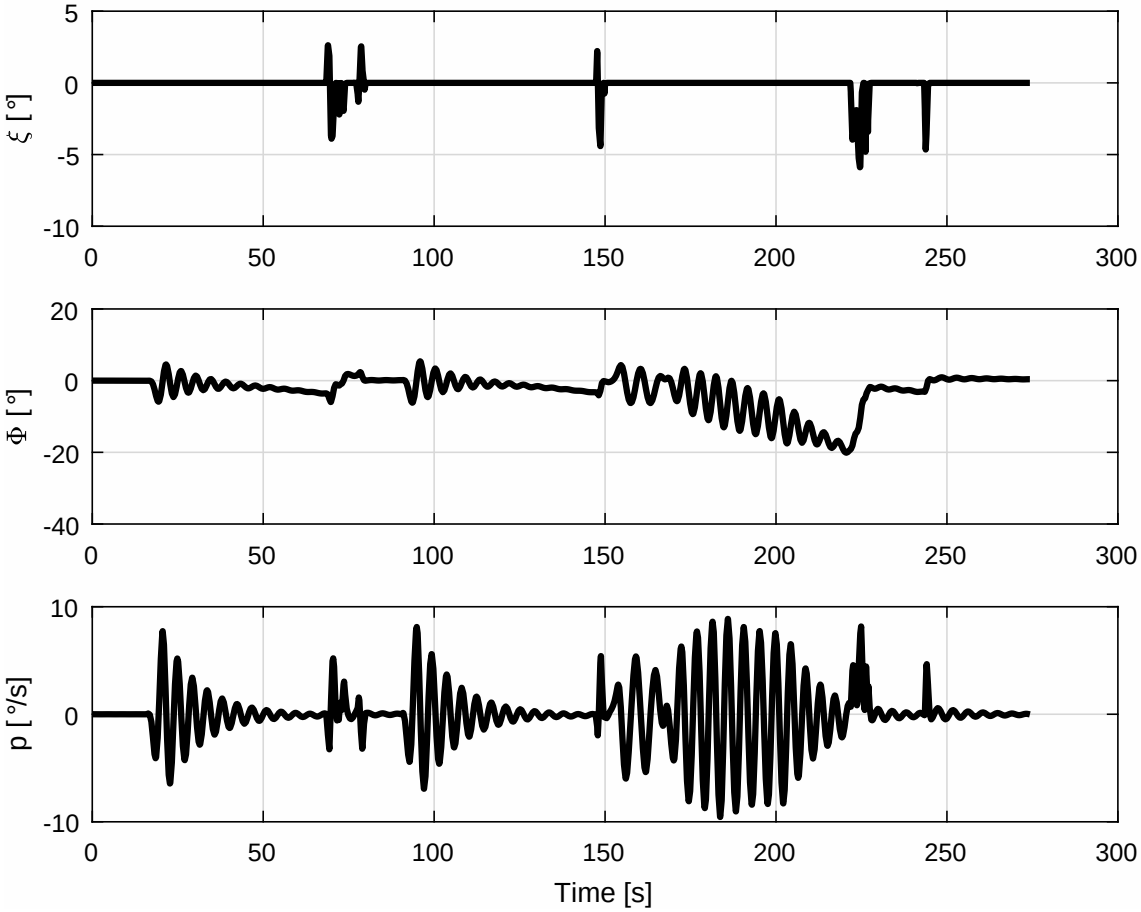

Figure F.54: Time histories of lateral parameters

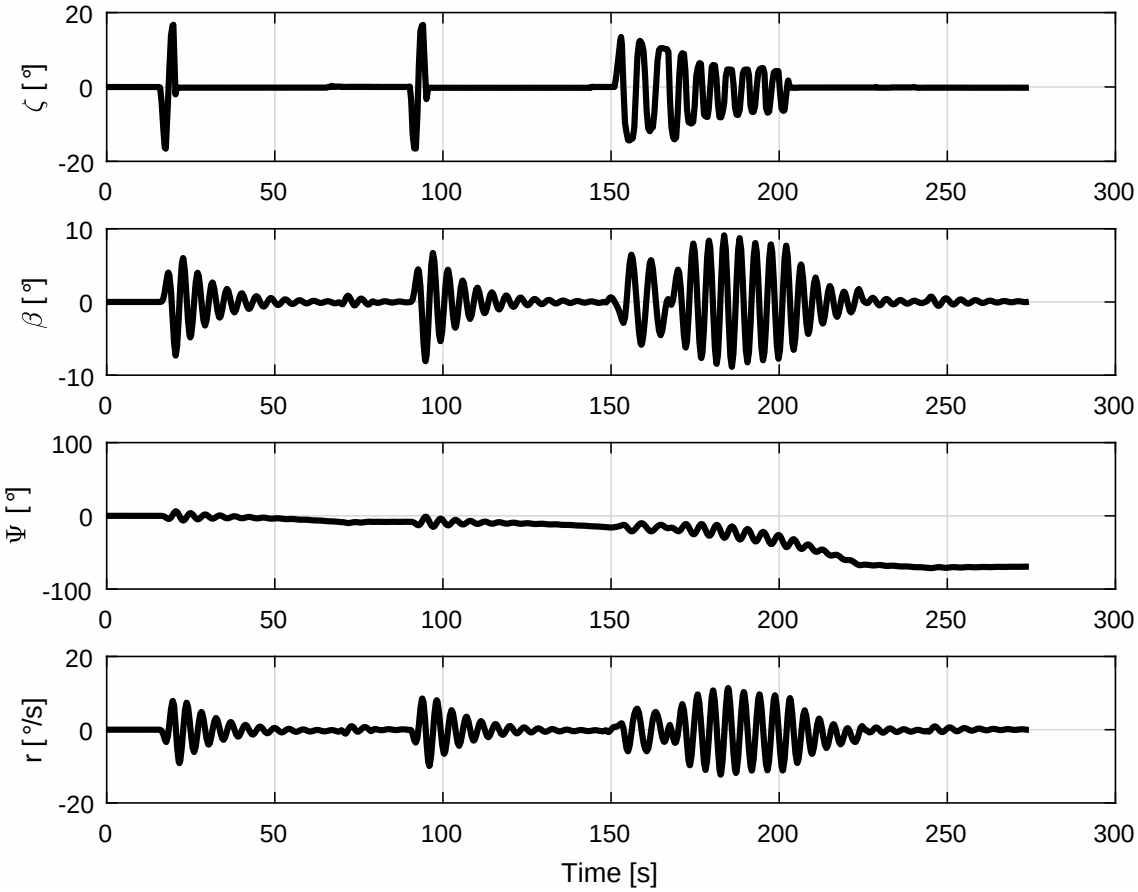

Figure F.55: Time histories of directional parameters

F.12 Dutch roll, pilot 2, rigid A/C – DR(2)R

Date: 09/02/2018 **Time start:** **Time stop:** 11:16

Test No:	DR(2)R	**Test hardware:**	EFS500 + Speedgoat
Test pilot:	(2)	**Model version:**	HARTEN_v1 (R)

Task:	Lateral / directional modes (Dutch roll mode) (DR)
Manoeuvre:	

Instrumentation:	
Relevant files:	{D_LOADS/D_SIM/D_STRUCT}.DAT @ 09/02/2018 11:16; DSCN9586.MOV

Flight velocity: 110 m/s **Flight altitude:** 10000 ft

Aircraft weight: 79 t **Aircraft CG:** 20% MAC

Rudder doublet

T_{damp}: N_{damp}:

Notes:

Forced Dutch roll

F: 4 sec period; 6 cycles to damp

Shape:

Notes:

Poor damping

Most intrusive mode

Notes (from audio recording):

Nil

Figure F.56: Test card (DR(2)R)

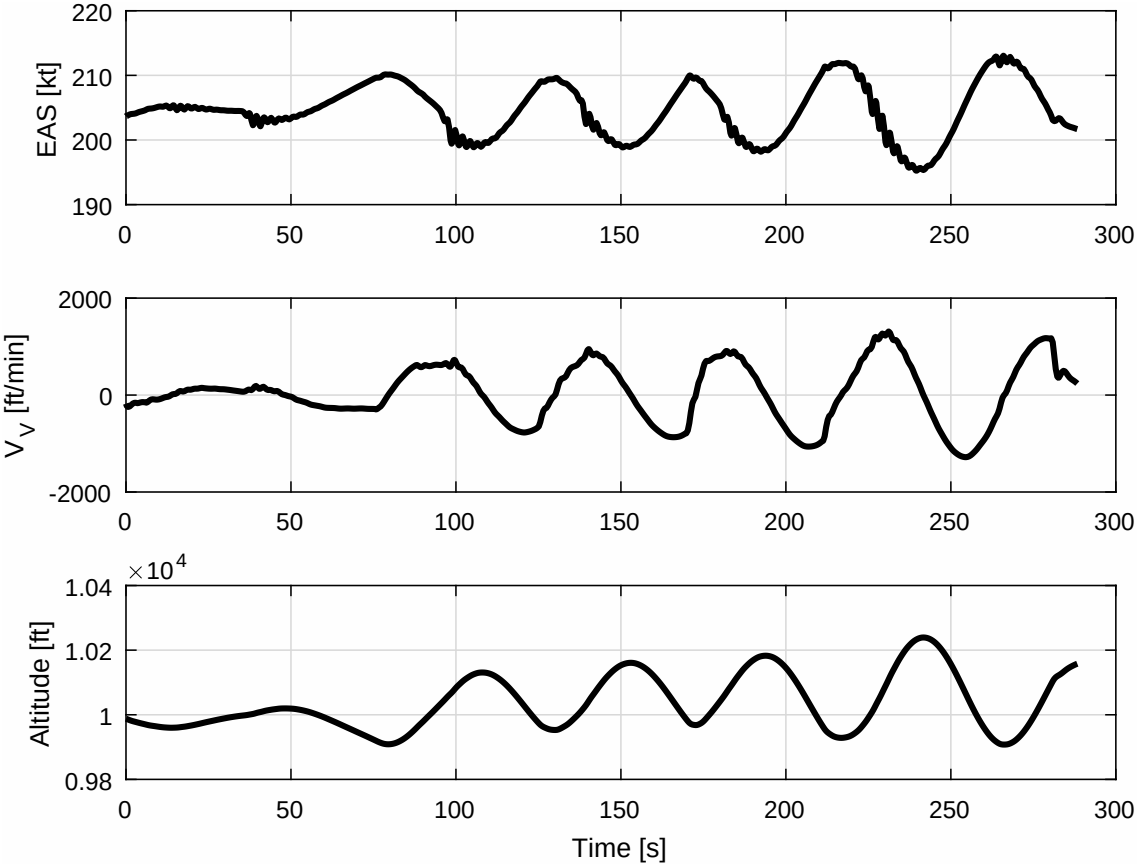

Figure F.57: Time histories of altitude and velocities

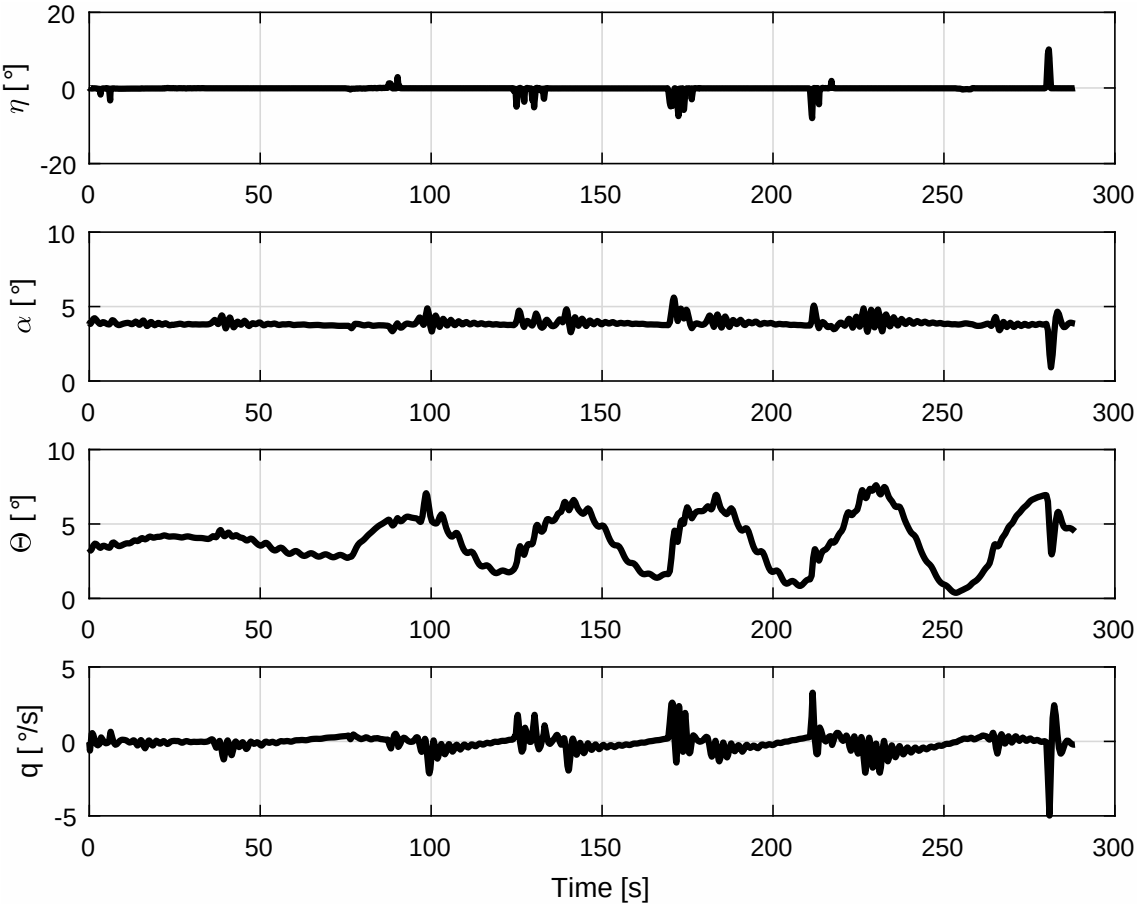

Figure F.58: Time histories of longitudinal parameters

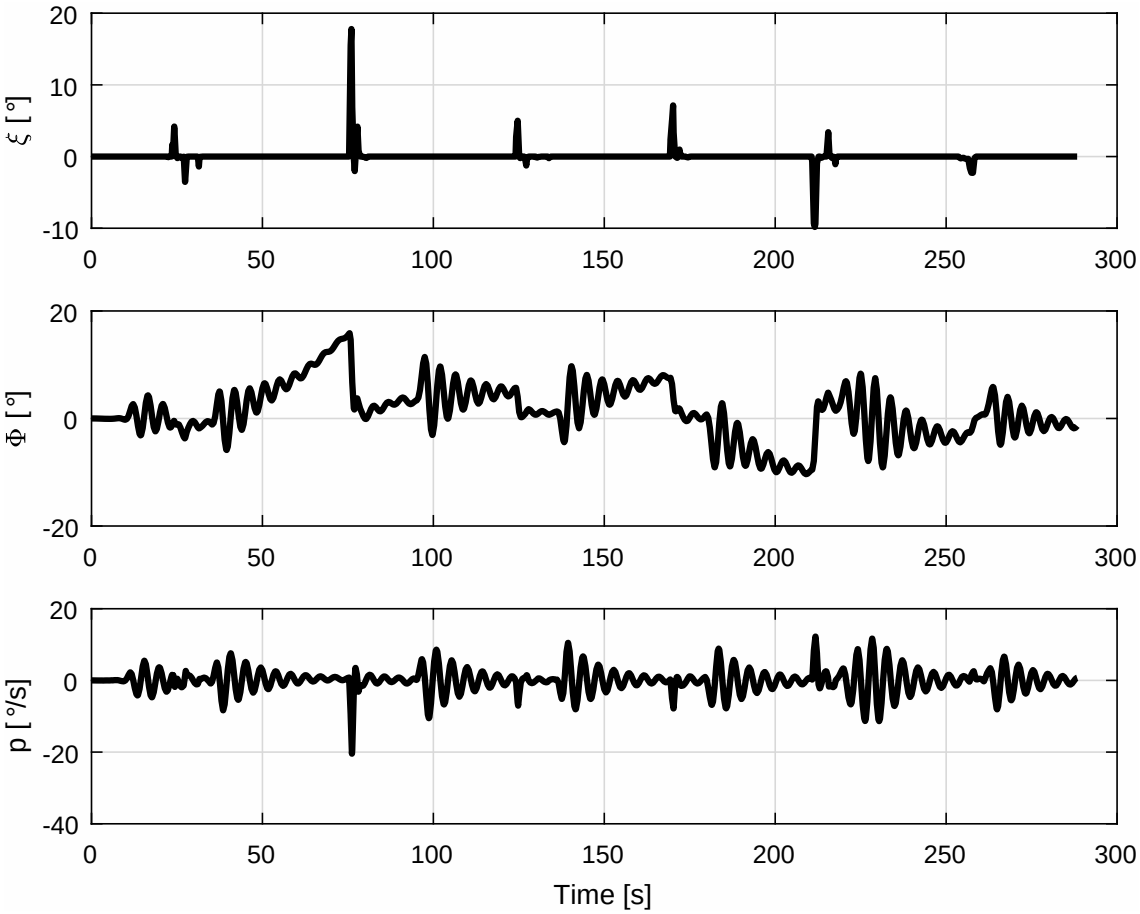

Figure F.59: Time histories of lateral parameters

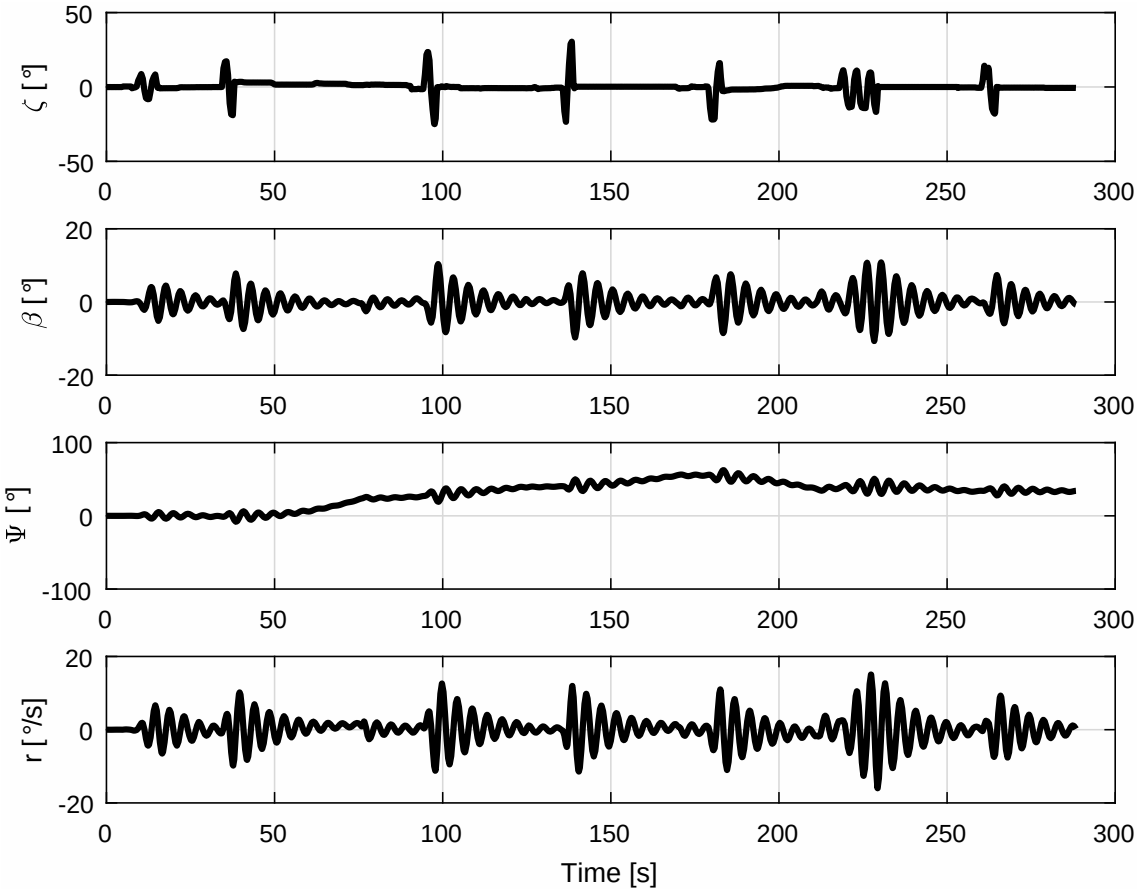

Figure F.60: Time histories of directional parameters

F.13 Dutch roll, pilot 2, flexible A/C – DR(2)F

Date: 09/02/2018 **Time start:** **Time stop:** 14:43

Test No:	DR(2)F	**Test hardware:**	EFS500 + Speedgoat
Test pilot:	(2)	**Model version:**	HARTEN_v1 (F)

Task:	Lateral / directional modes (Dutch roll mode) (DR)
Manoeuvre:	

Instrumentation:	
Relevant files:	{D_LOADS/D_SIM/D_STRUCT}.DAT @ 09/02/2018 14:43; DSCN9598.MOV

Flight velocity: 110 m/s **Flight altitude:** 10000 ft

Aircraft weight: 79 t **Aircraft CG:** 20% MAC

Rudder doublet

T_{damp}: 4 sec N_{damp}: very low

Notes:

Forced Dutch roll

F: 4 sec

Shape: 3/1 phi/beta

Notes:

A lot more roll, but same 4 sec; undamped;

Phi/beta ratio 3/1 → unpredictable, trigger to PIO → too much dihedral

Notes (from audio recording):

"Instead of 1/3 it is 3/1 phi/beta ratio – it is a huge change"

"Effectively undamped"

Figure F.61: Test card (DR(2)F)

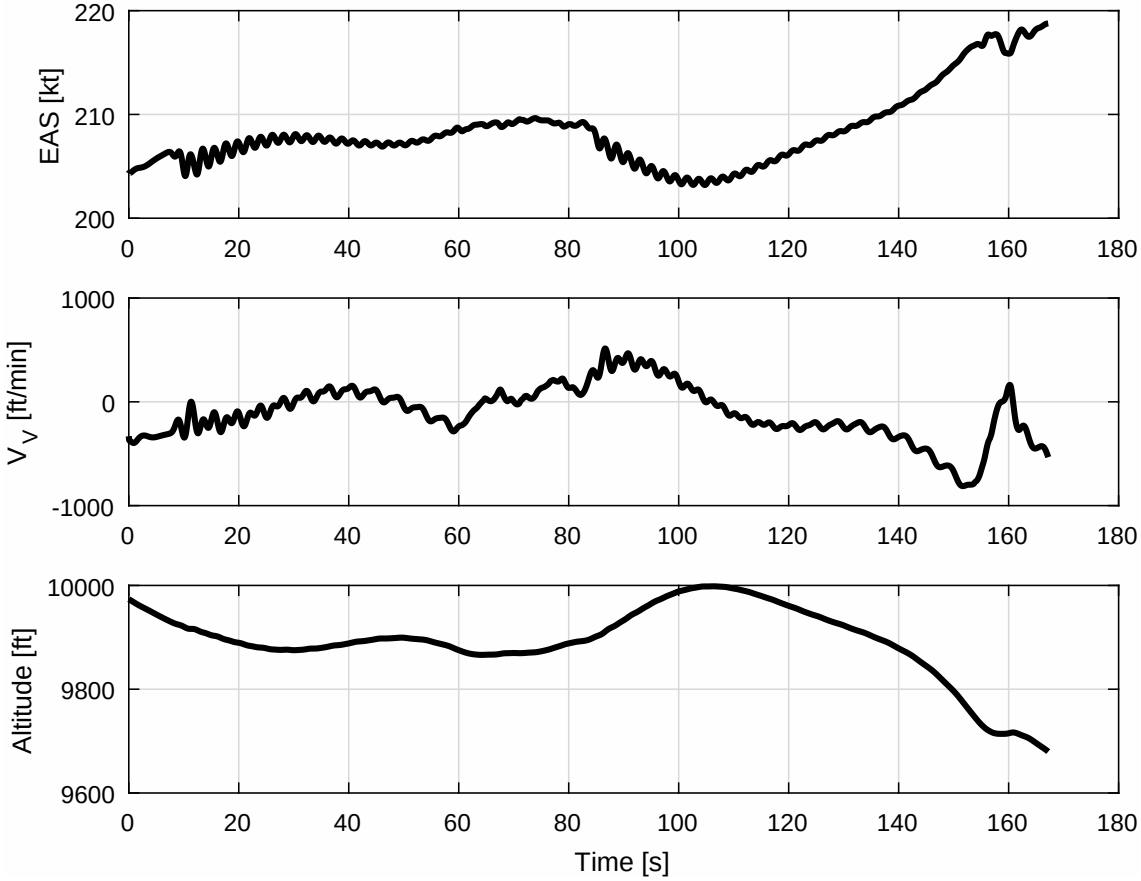

Figure F.62: Time histories of altitude and velocities

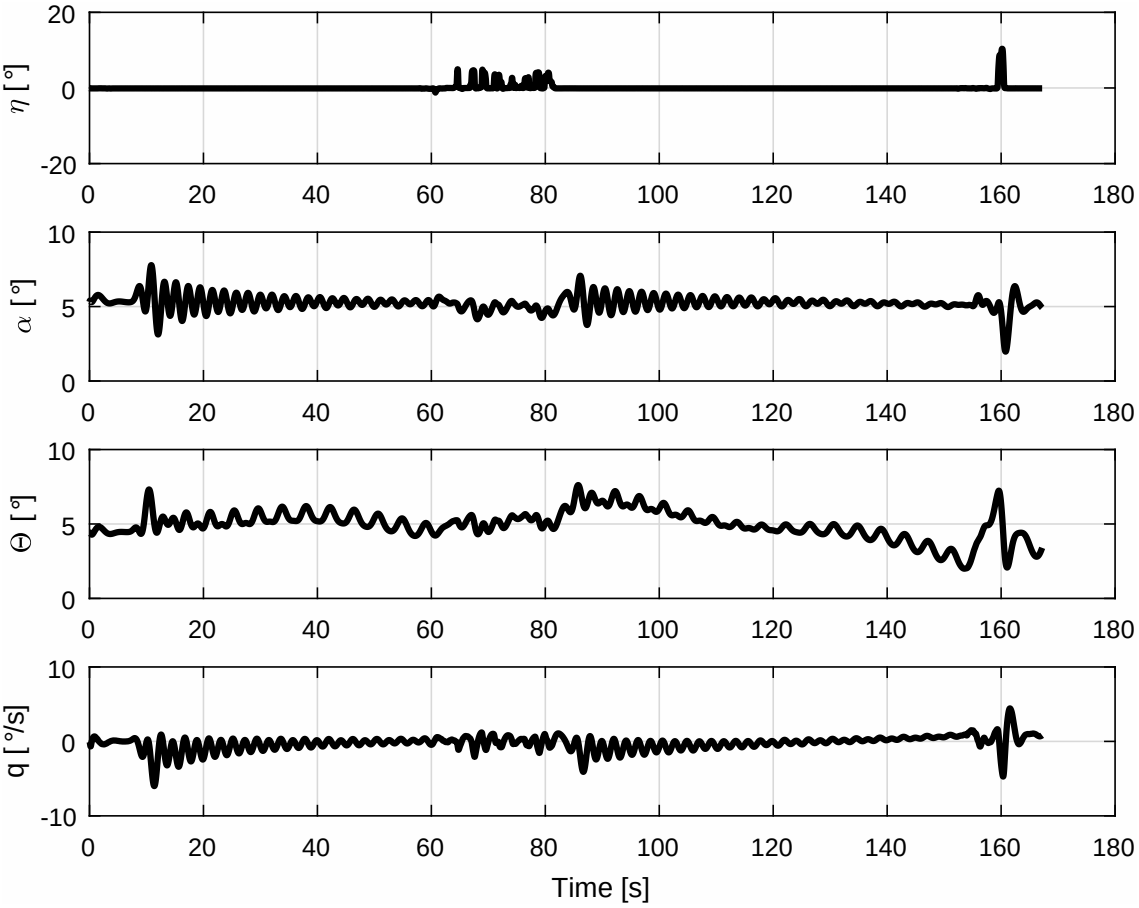

Figure F.63: Time histories of longitudinal parameters

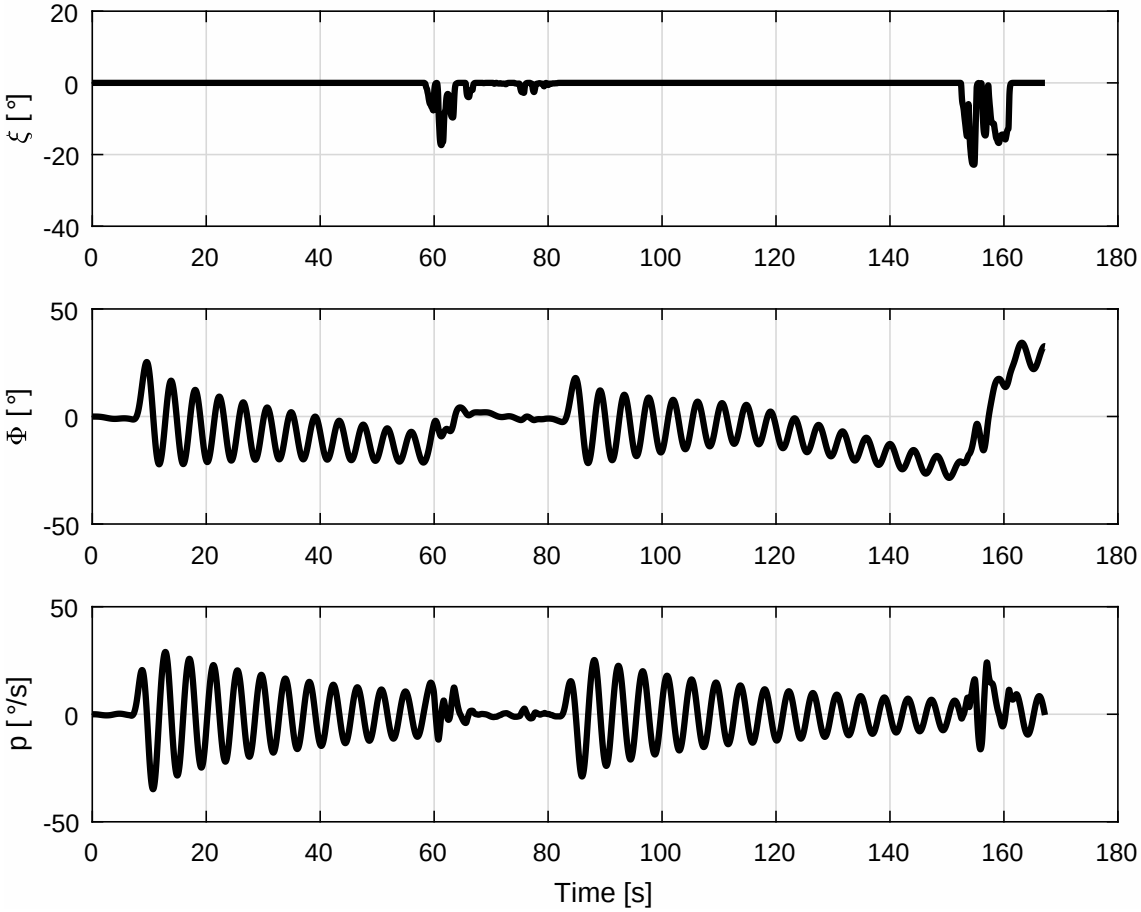

Figure F.64: Time histories of lateral parameters

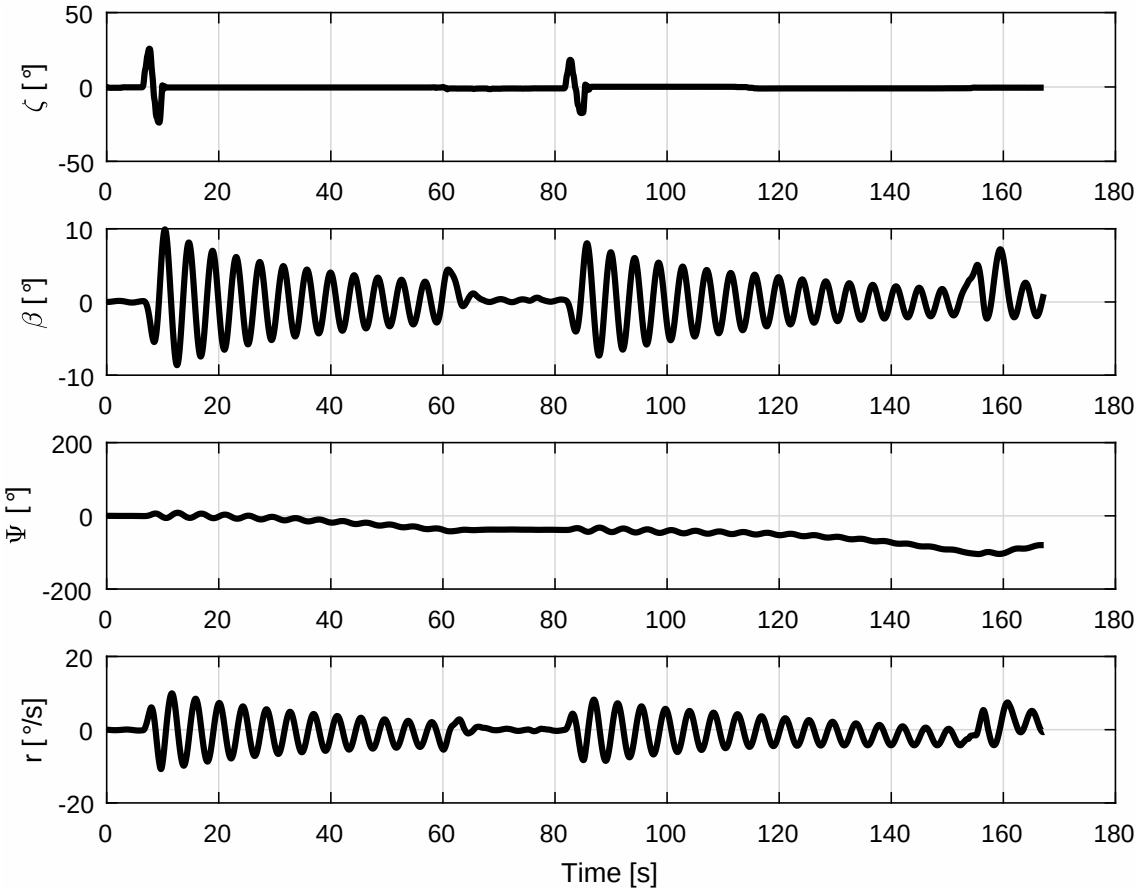

Figure F.65: Time histories of directional parameters

Appendix G

Slalom task simulation data

G.1 Slalom task, pilot 2, rigid A/C – SL(2)R

Date: 09/02/2018 **Time start:** **Time stop:** 11:31

Test No:	SL(2)R	**Test hardware:**	EFS500 + Speedgoat
Test pilot:	(2)	**Model version:**	HARTEN_v1 (R)

Task:	Slalom flying task (SL)
Manoeuvre:	

Instrumentation:	
Relevant files:	{D_LOADS/D_SIM/D_STRUCT}.DAT @ 09/02/2018 11:31; DSCN9587.MOV

Flight velocity: 110 m/s **Flight altitude:** 10000 ft

Aircraft weight: 79 t **Aircraft CG:** 20% MAC

Run	Long CHR	Lat/dir CHR	Comments
1	2	5	LAT/DIR CHANGING BECAUSE OF ADVERSE YAW EXCITING DUTCH ROLL.
2			LOW DUTCH ROLL FREQUENCY (POOR DIRECTIONAL STATIC STABILITY)
3			MEANS A/C SLOW TO STABILISE AFTER ROLL REVERSAL MANOEUVRE.
4			LOW PREDICTABILITY
5			
6			
7			
8			
9			
10			

Notes:

Very long forward fuselage destabilising – increase fin area to get rid of Dutch roll.

Notes (from audio recording):

“Pitch is not that difficult, bank angle control is most challenging”

“Combination of adverse yaw and Dutch roll that makes it hard”

Figure G.1: Test card (SL(2)R)

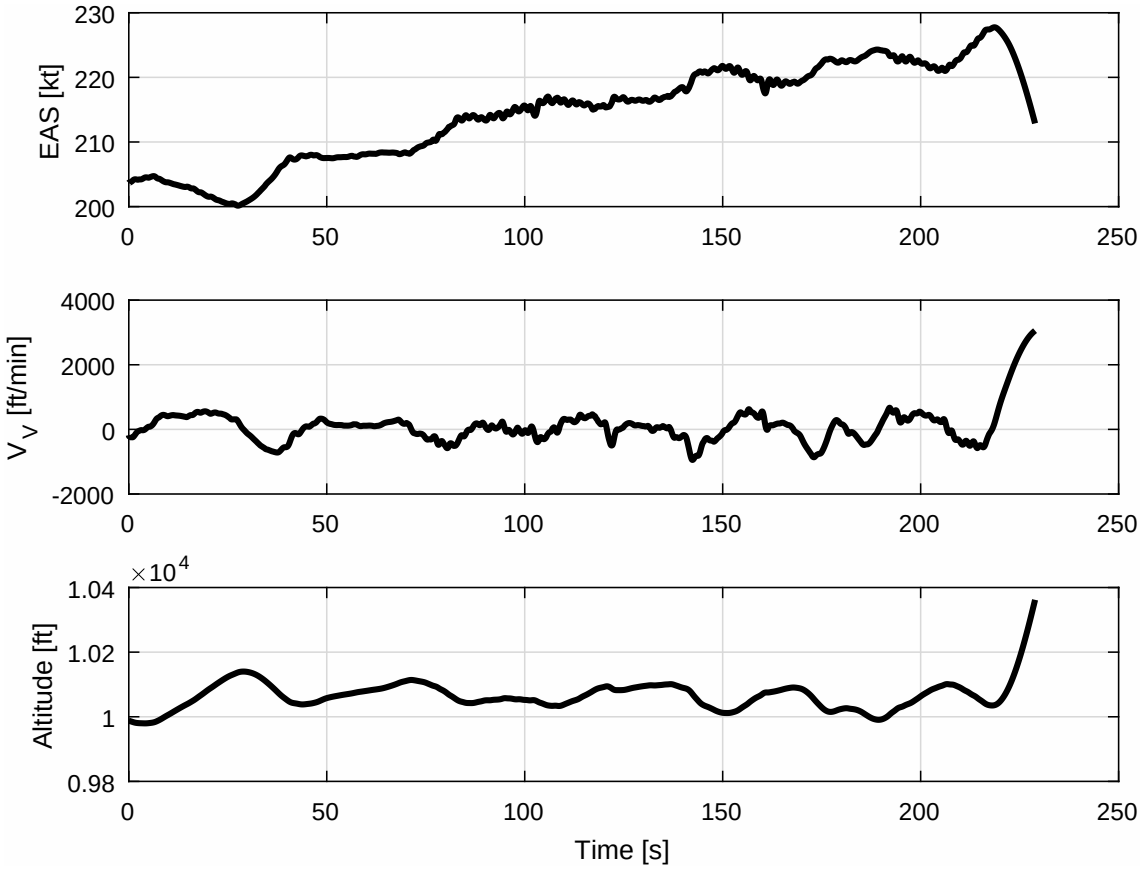

Figure G.2: Time histories of altitude and velocities

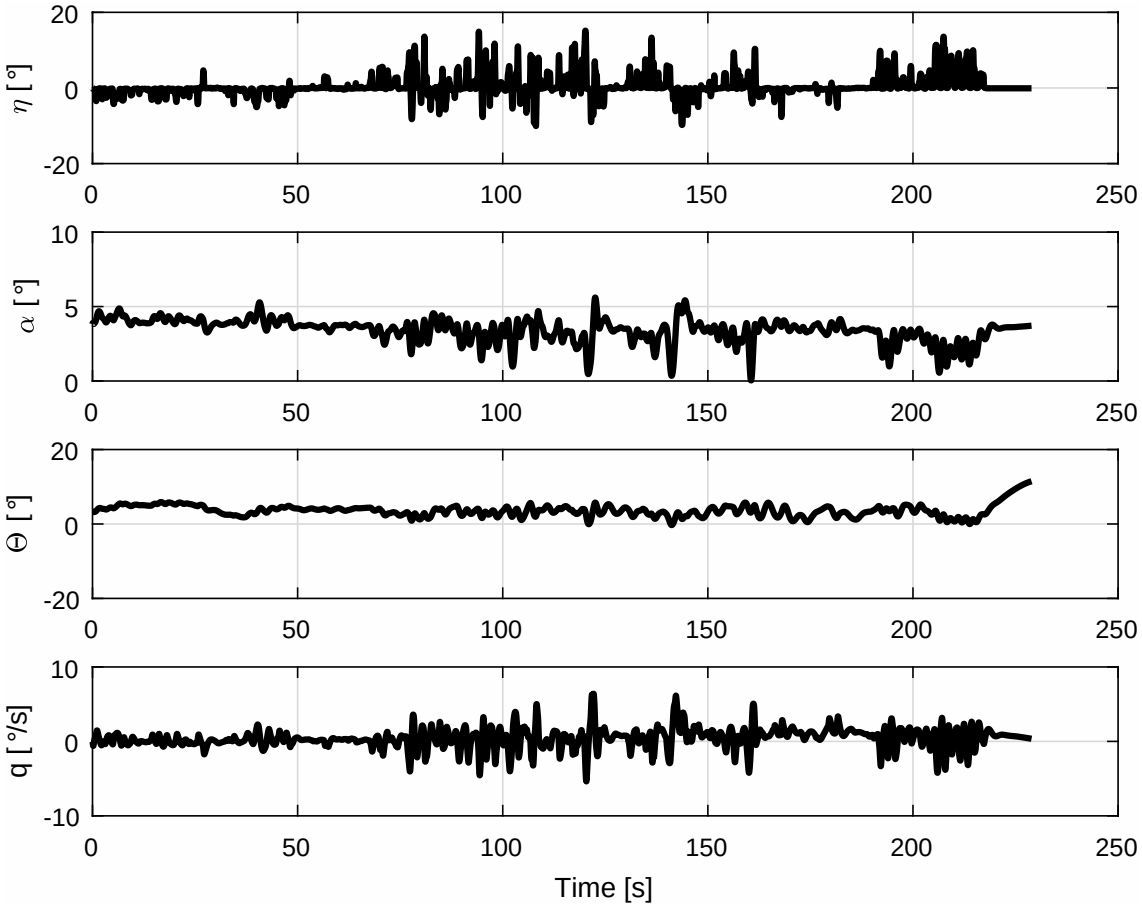

Figure G.3: Time histories of longitudinal parameters

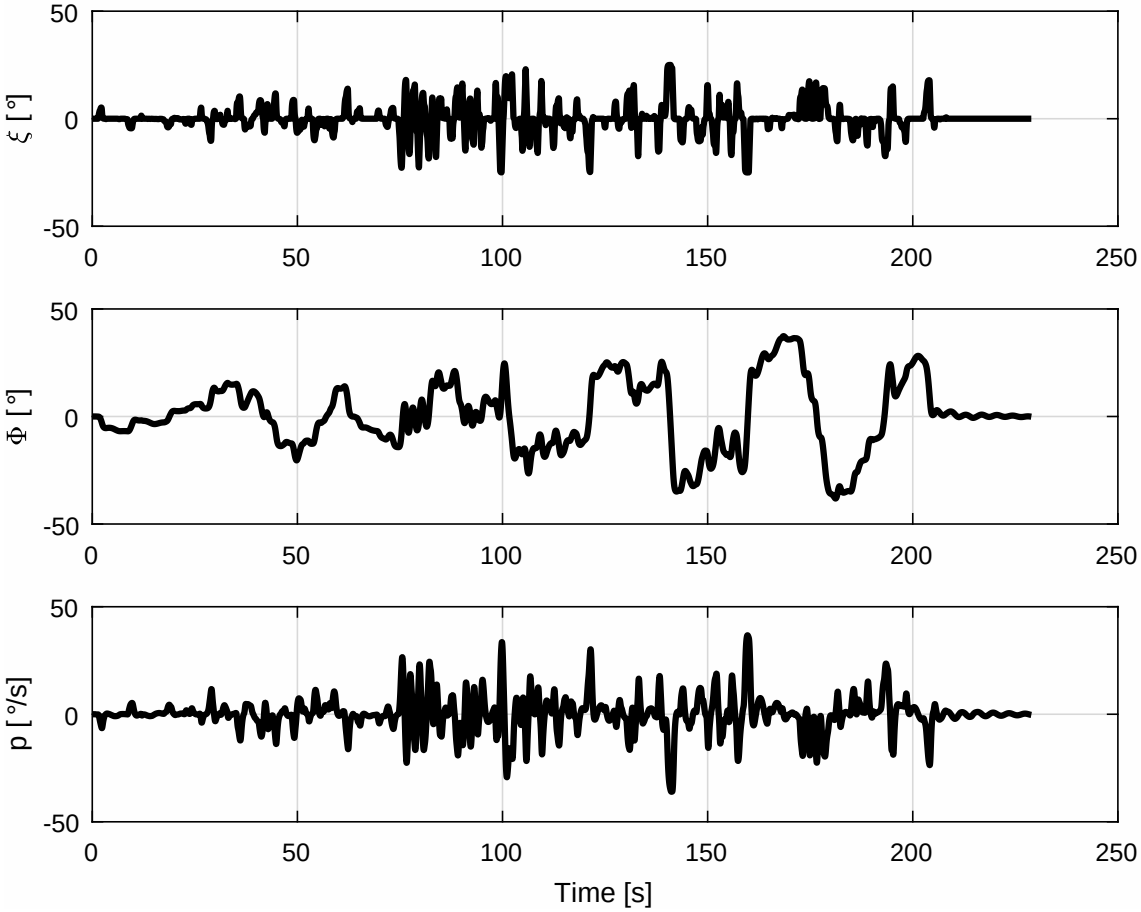

Figure G.4: Time histories of lateral parameters

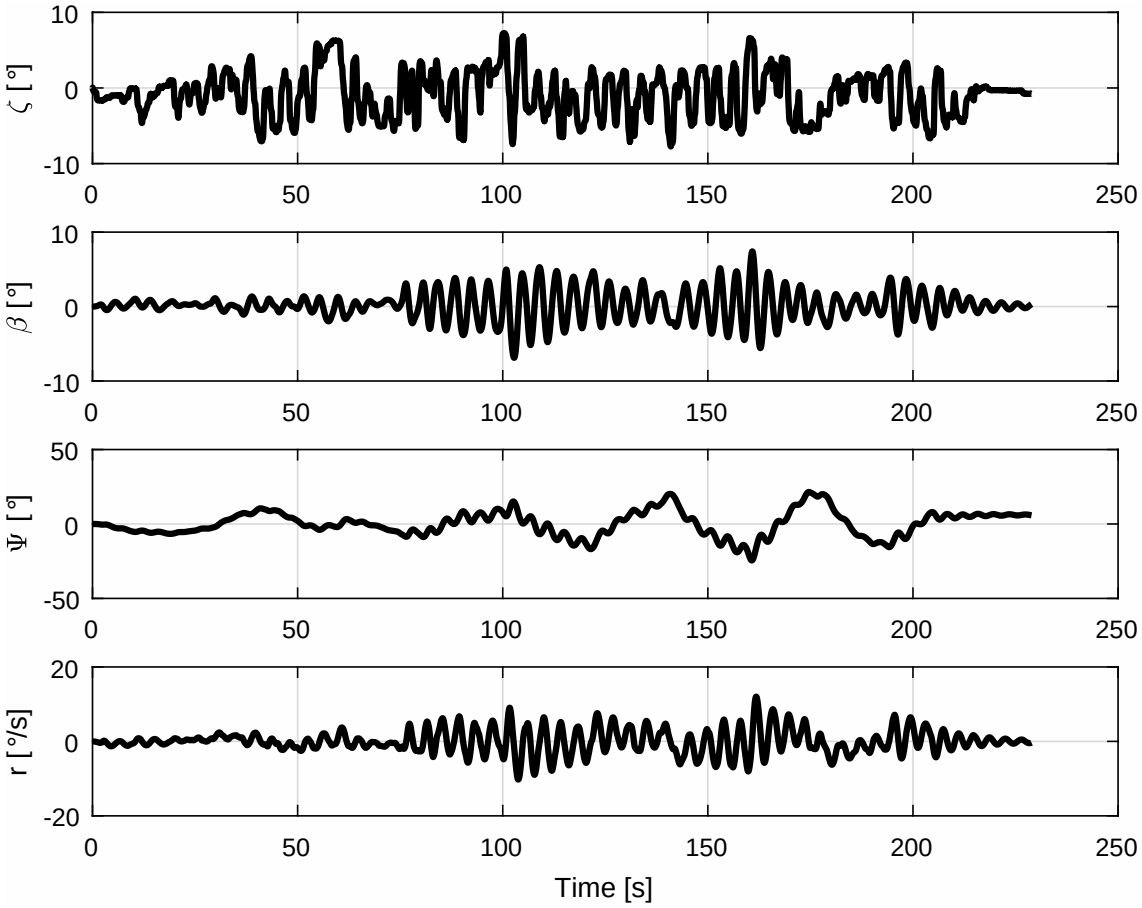

Figure G.5: Time histories of directional parameters

G.2 Slalom task, pilot 2, flexible A/C – SL(2)F

Date: 09/02/2018 **Time start:** **Time stop:** 15:05

Test No:	SL(2)F	**Test hardware:**	EFS500 + Speedgoat
Test pilot:	(2)	**Model version:**	HARTEN_v1 (F)

Task:	Slalom flying task (SL)
Manoeuvre:	

Instrumentation:	
Relevant files:	{D_LOADS/D_SIM/D_STRUCT}.DAT @ 09/02/2018 15:05; DSCN9600.MOV

Flight velocity: 110 m/s **Flight altitude:** 10000 ft

Aircraft weight: 79 t **Aircraft CG:** 20% MAC

Run	Long CHR	Lat/dir CHR	Comments
1	4	7	DUTCH ROLL VERY INTRUSIVE
2			
3			
4			
5			
6			
7			
8			
9			
10			

Notes:

Nil

Notes (from audio recording):

“How easy it is to naturally PIO”

Figure G.6: Test card (SL(2)F)

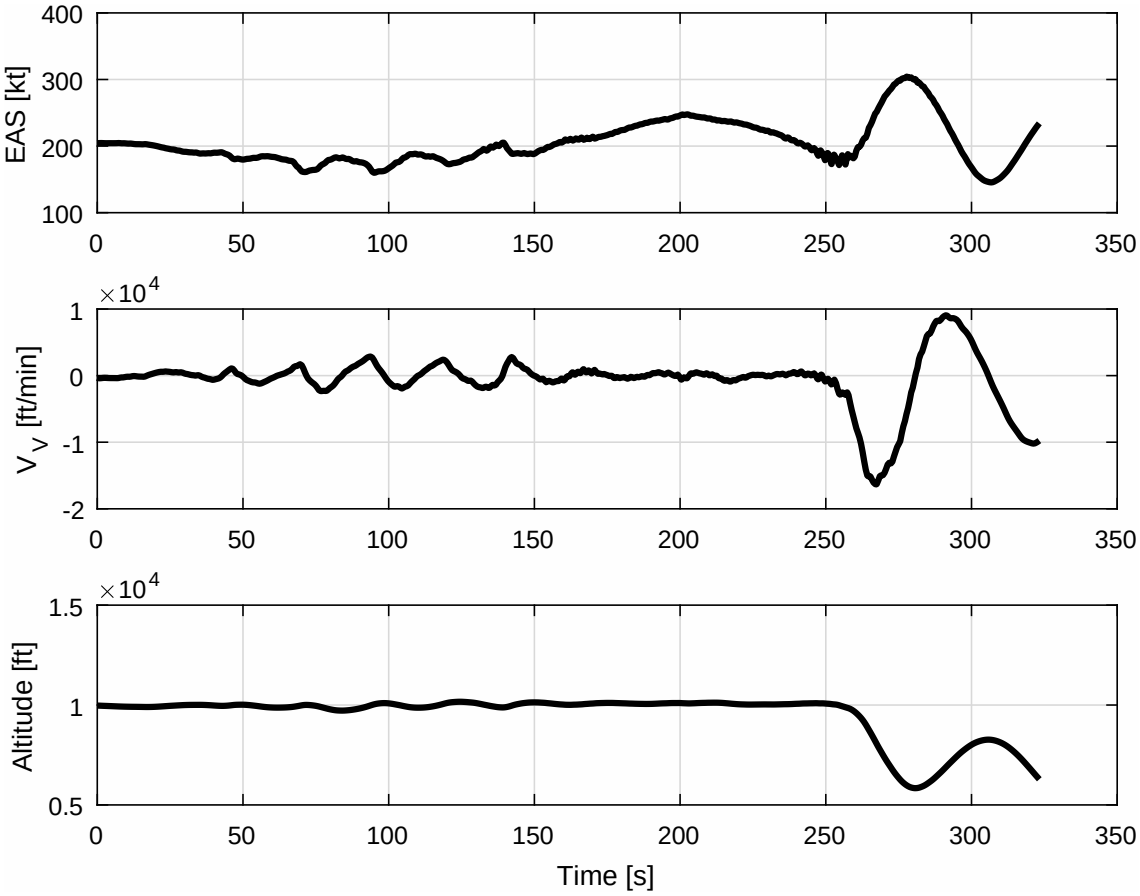

Figure G.7: Time histories of altitude and velocities

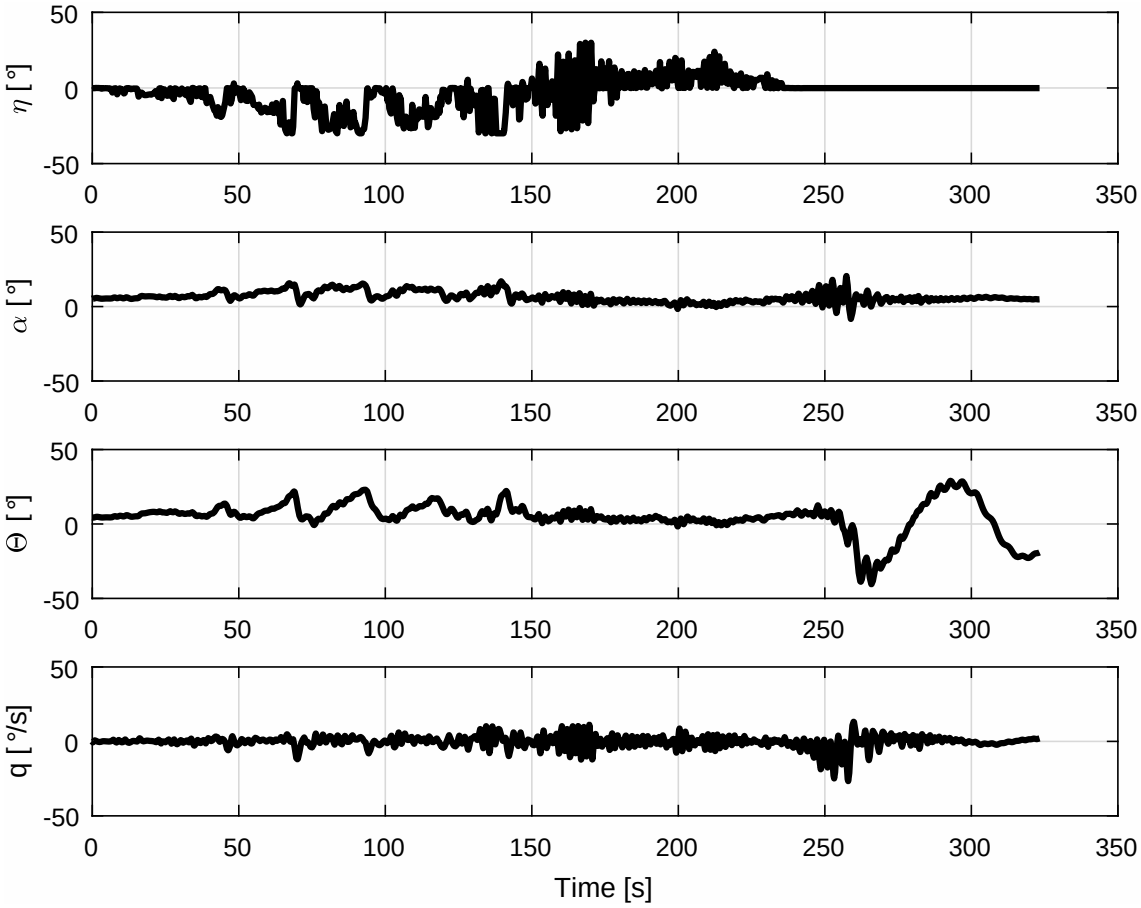

Figure G.8: Time histories of longitudinal parameters

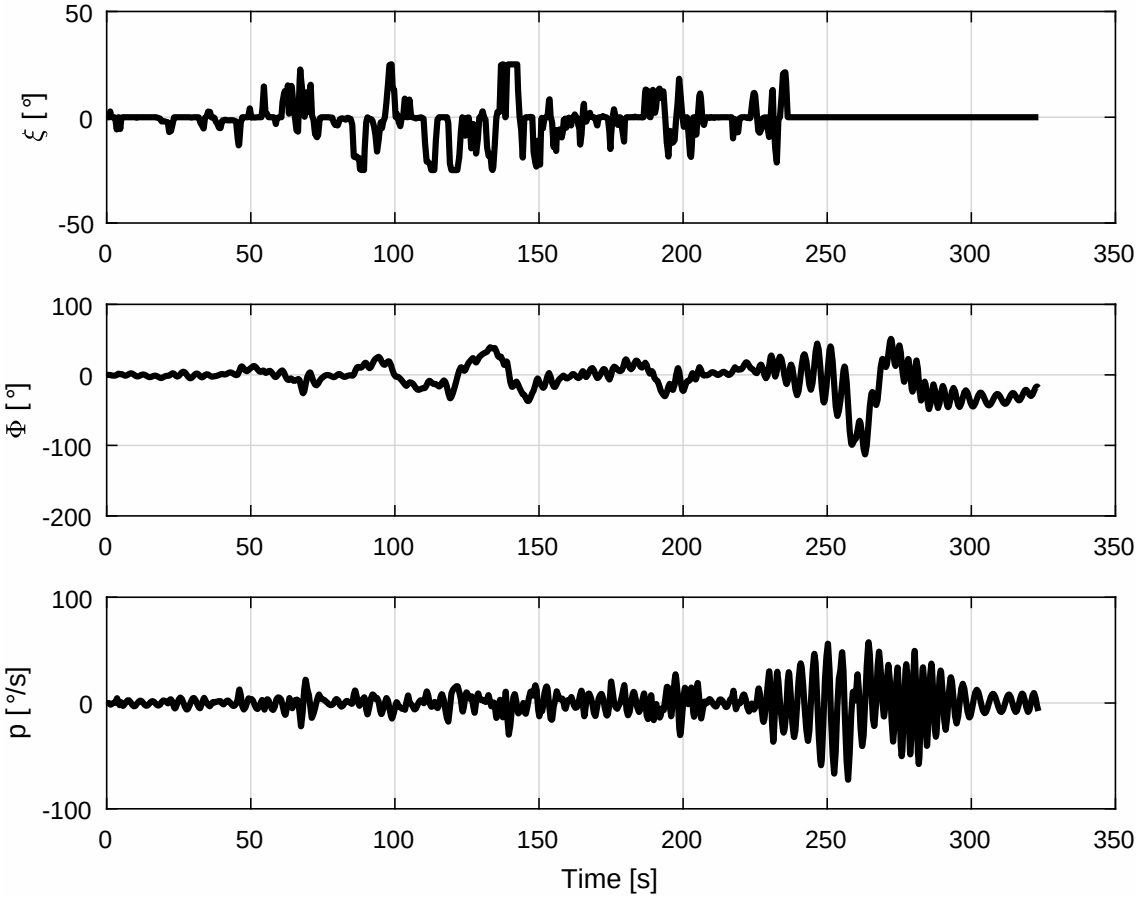

Figure G.9: Time histories of lateral parameters

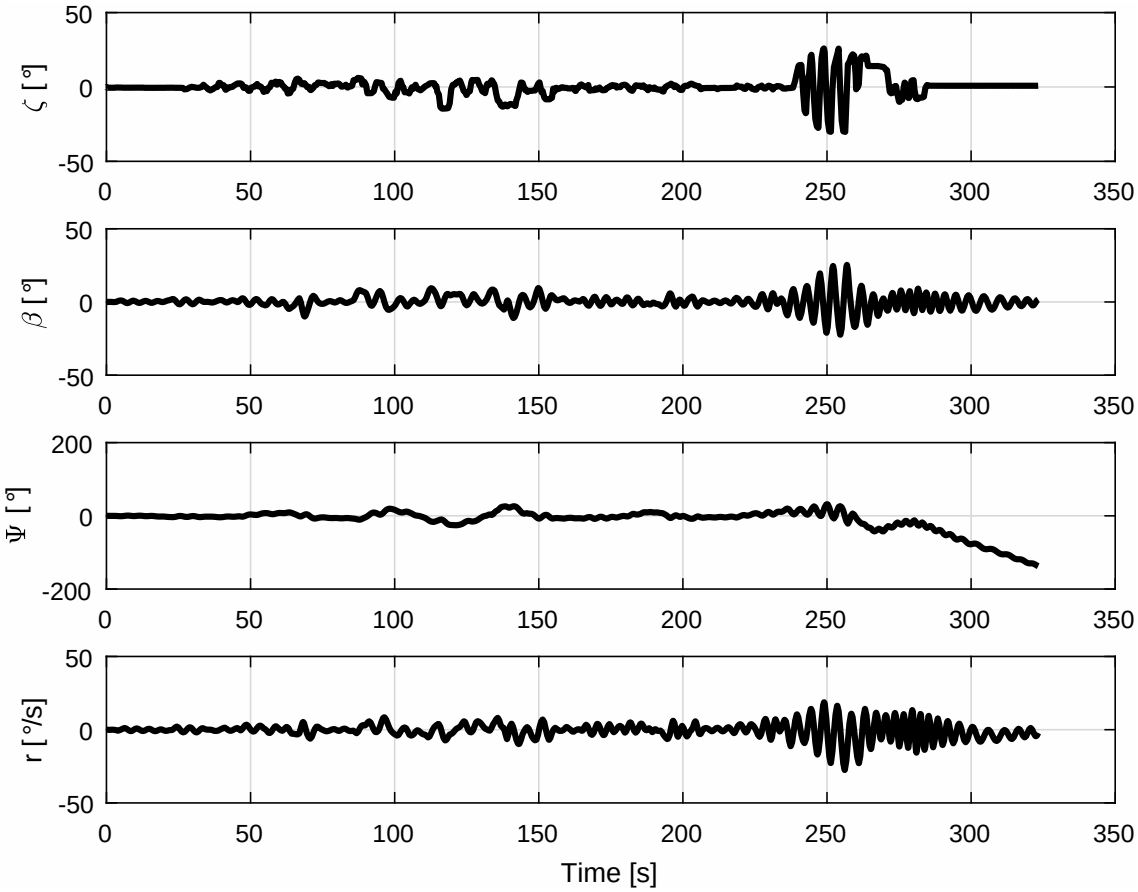

Figure G.10: Time histories of directional parameters

G.3 Slalom task, pilot 3, rigid A/C – SL(3)R

Date: 02/02/2018 **Time start:** **Time stop:** 14:29

Test No:	SL(3)R	**Test hardware:**	EFS500 + Speedgoat
Test pilot:	(3)	**Model version:**	HARTEN_v1 (R)

Task:	Slalom flying task (SL)
Manoeuvre:	

Instrumentation:	
Relevant files:	{D_SIM/D_STRUCT}.DAT @ 02/02/2018 14:29; DSCN9534.MOV

Flight velocity: 110 m/s **Flight altitude:** 10000 ft

Aircraft weight: 79 t **Aircraft CG:** 20% MAC

Run	Long CHR	Lat/dir CHR	Comments
1	8	8	Nil
2			
3			
4			
5			
6			
7			
8			
9			
10			

Notes:

Nil

Notes (from audio recording):

“Oscillating left and right” – after roll input

“I cannot put the nose where I want” – about lateral control

“Nose is pitching up and down and yawing left and right – it is hard to know what input to make”

“Sidestick is quite stiff”

Figure G.11: Test card (SL(3)R)

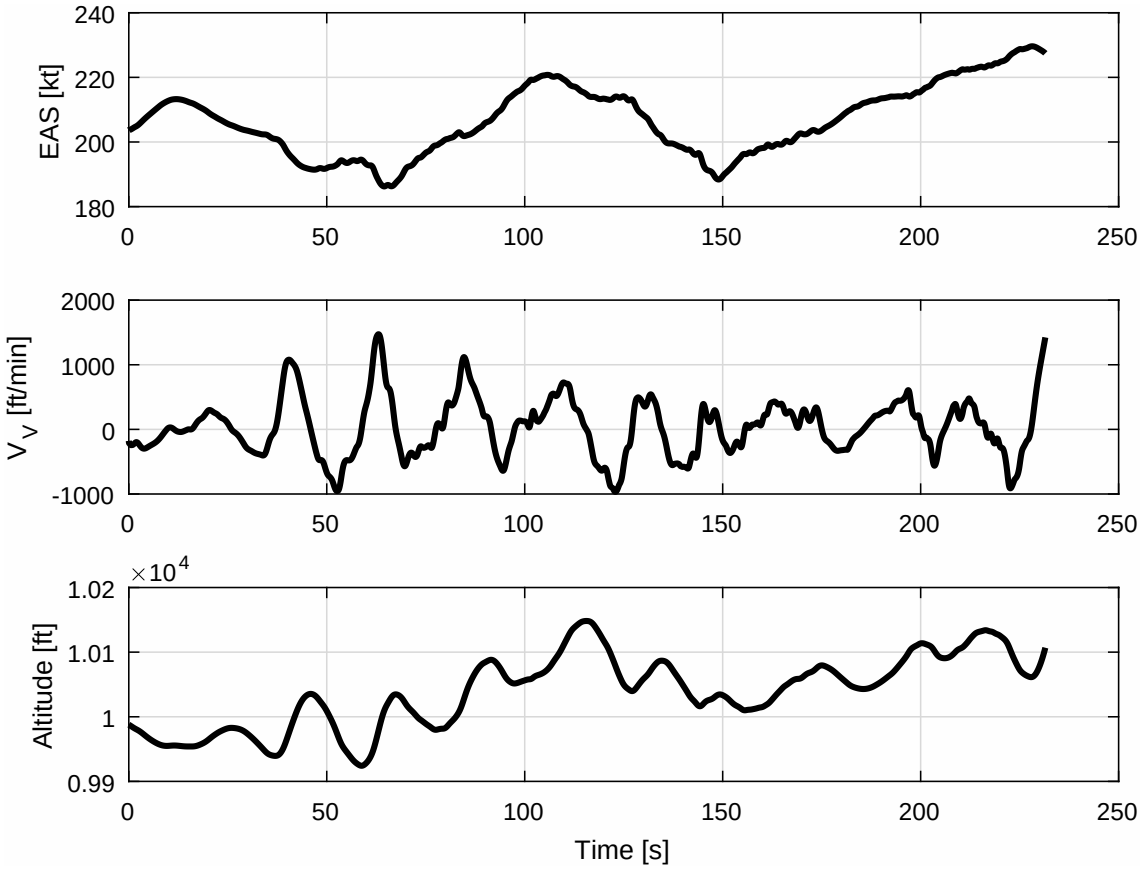

Figure G.12: Time histories of altitude and velocities

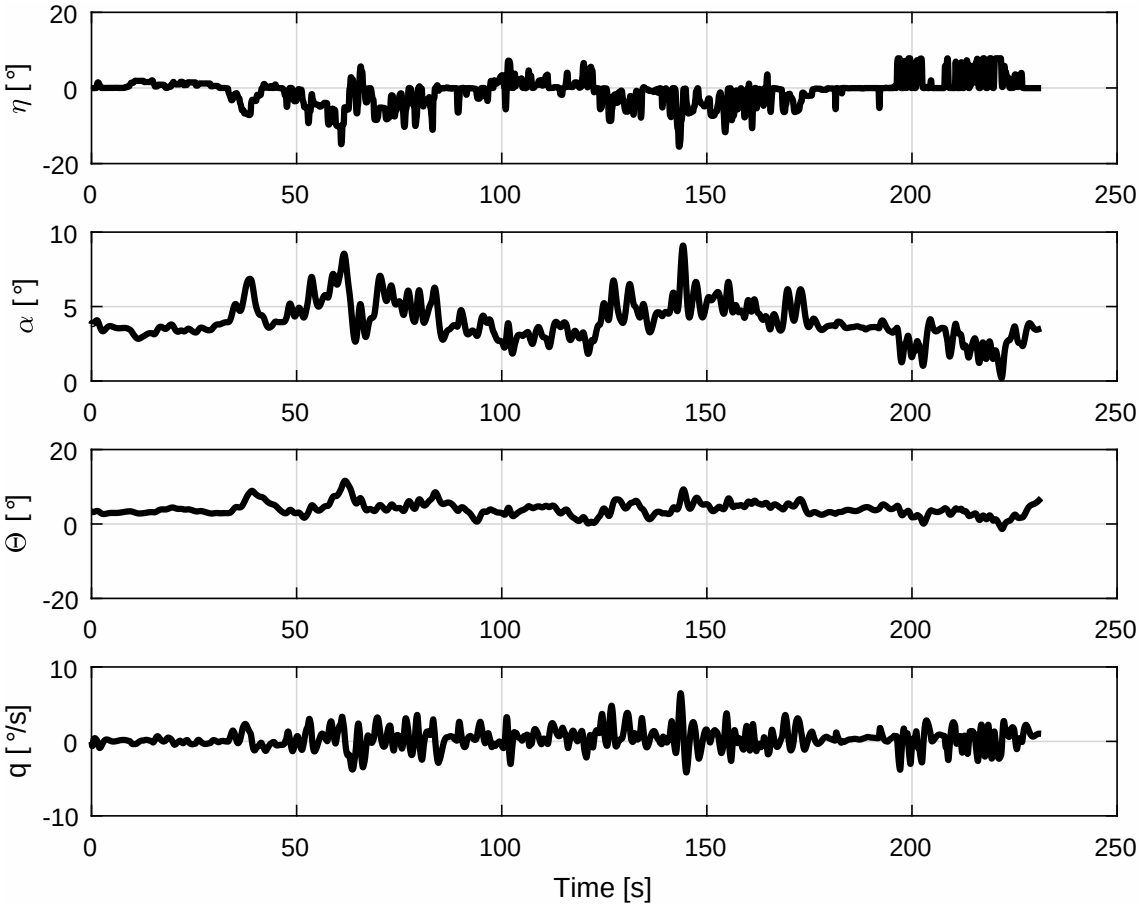

Figure G.13: Time histories of longitudinal parameters

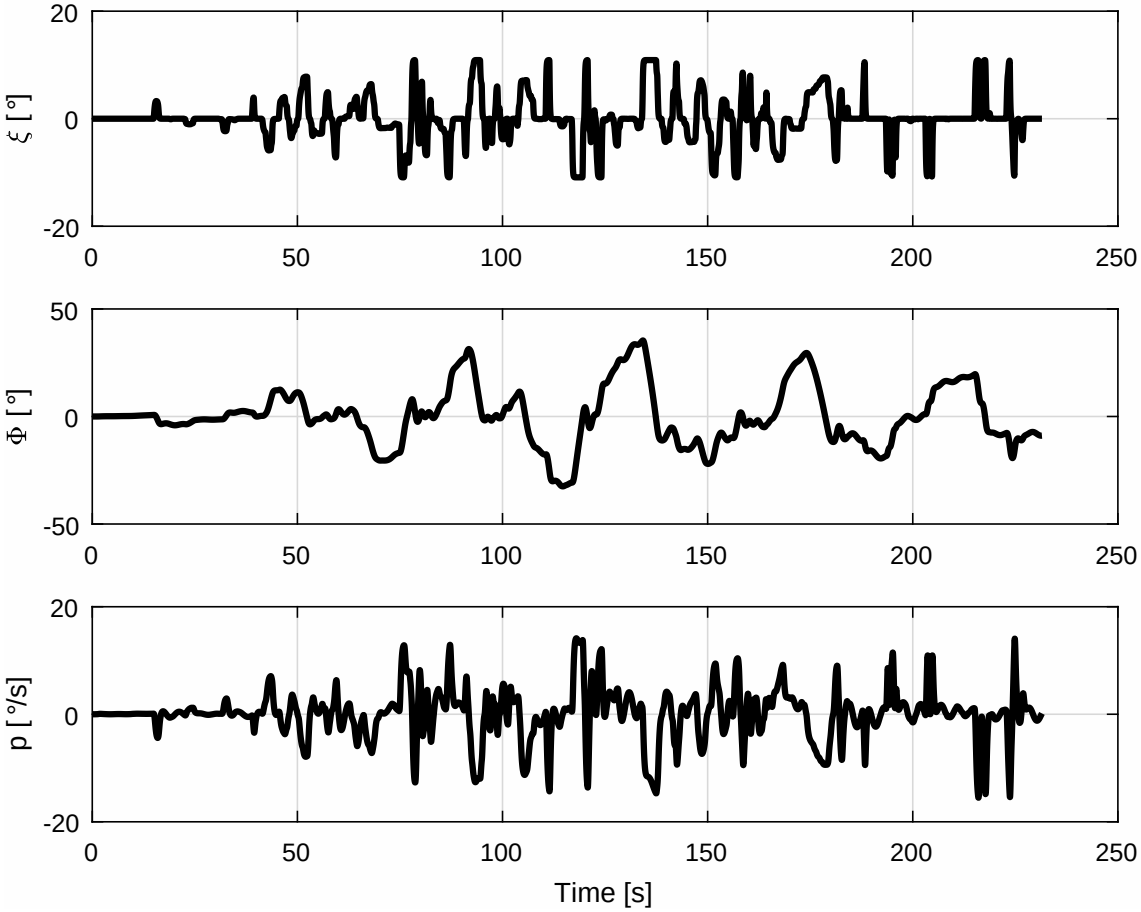

Figure G.14: Time histories of lateral parameters

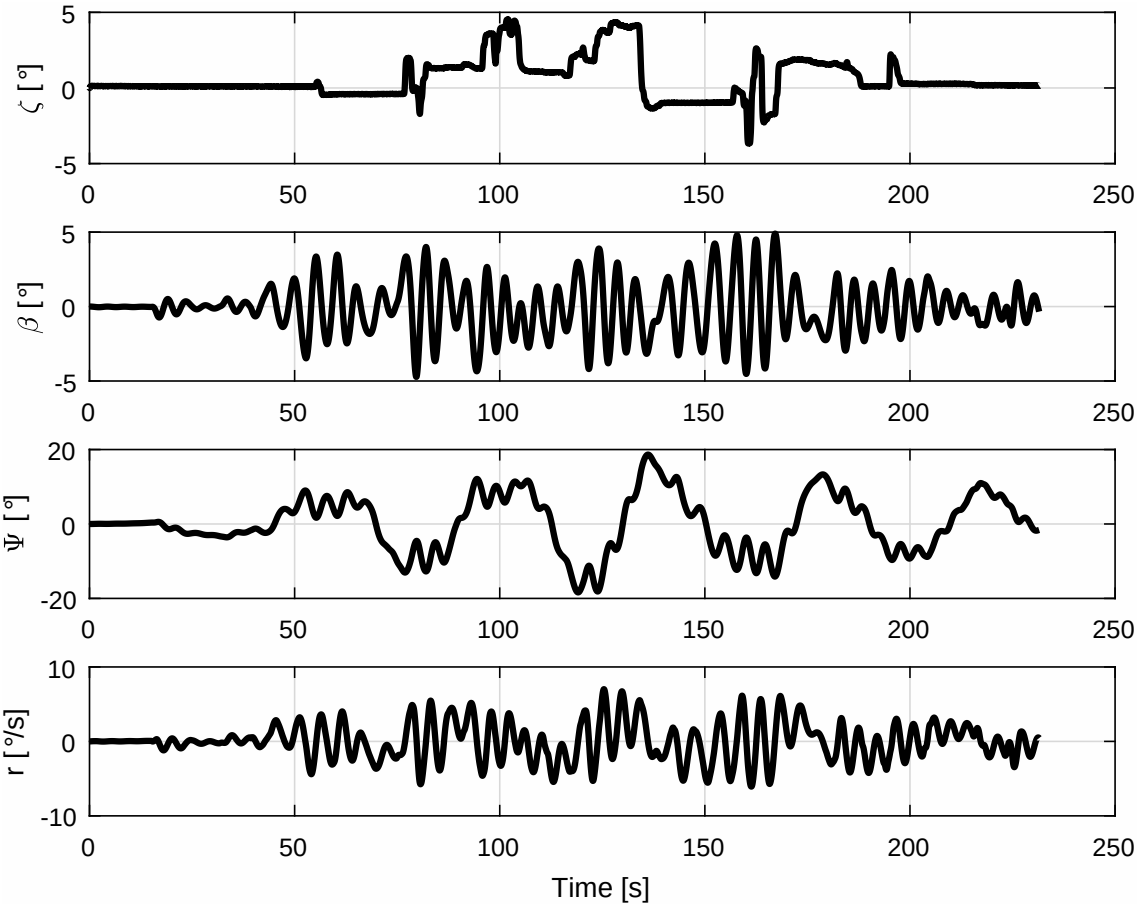

Figure G.15: Time histories of directional parameters

G.4 Slalom task, pilot 3, flexible A/C – SL(3)F

Date: 02/02/2018 **Time start:** **Time stop:** 14:46

Test No:	SL(3)F	**Test hardware:**	EFS500 + Speedgoat
Test pilot:	(3)	**Model version:**	HARTEN_v1 (F)

Task:	Slalom flying task (SL)
Manoeuvre:	

Instrumentation:	
Relevant files:	{D_SIM/D_STRUCT}.DAT @ 02/02/2018 14:46; DSCN9534.MOV

Flight velocity: 110 m/s **Flight altitude:** 10000 ft

Aircraft weight: 79 t **Aircraft CG:** 20% MAC

Run	Long CHR	Lat/dir CHR	Comments
1	10	10	Nil
2			
3			
4			
5			
6			
7			
8			
9			
10			

Notes:

Nil

Notes (from audio recording):

“A little bit unpredictable” – when aircraft rolls

“Feeling no motion cues” – about flying to aggressive, unnaturally

“A lot of roll oscillations for any lateral control input”

“Oscillating way to much” – about pitch oscillations

Figure G.16: Test card (SL(3)F)

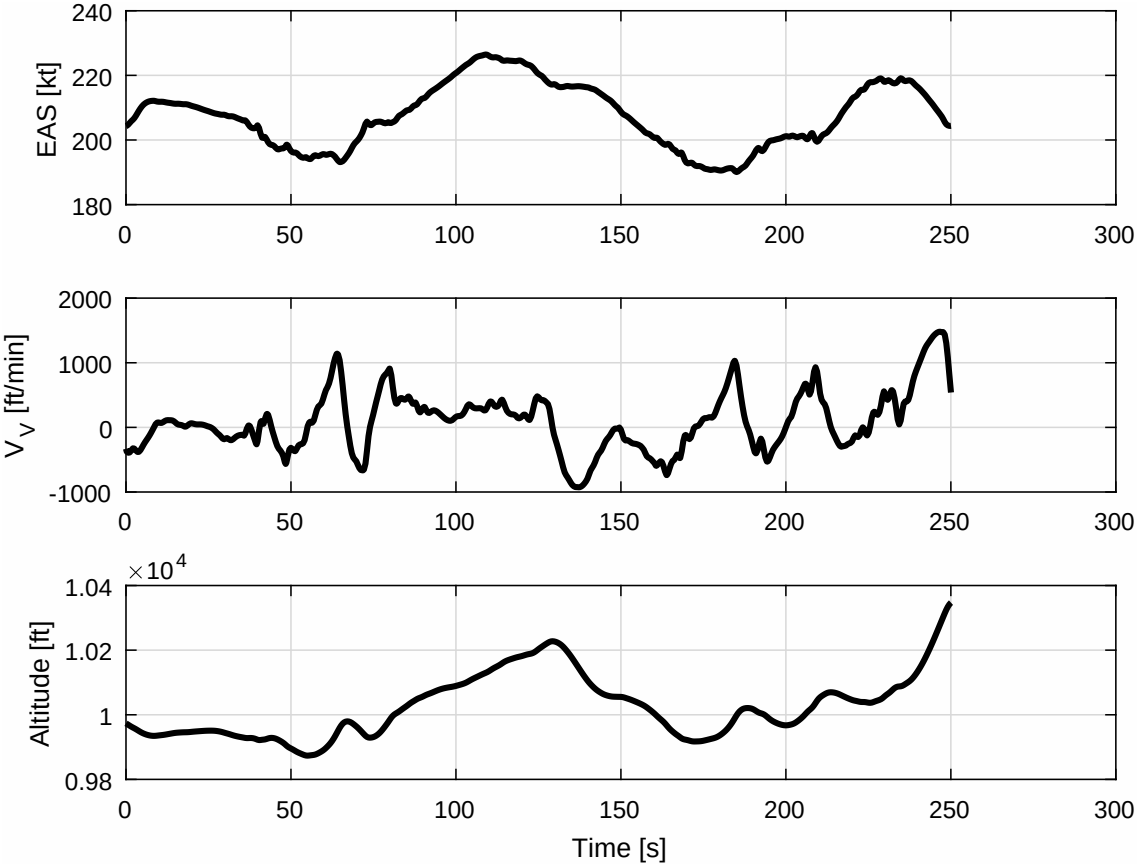

Figure G.17: Time histories of altitude and velocities

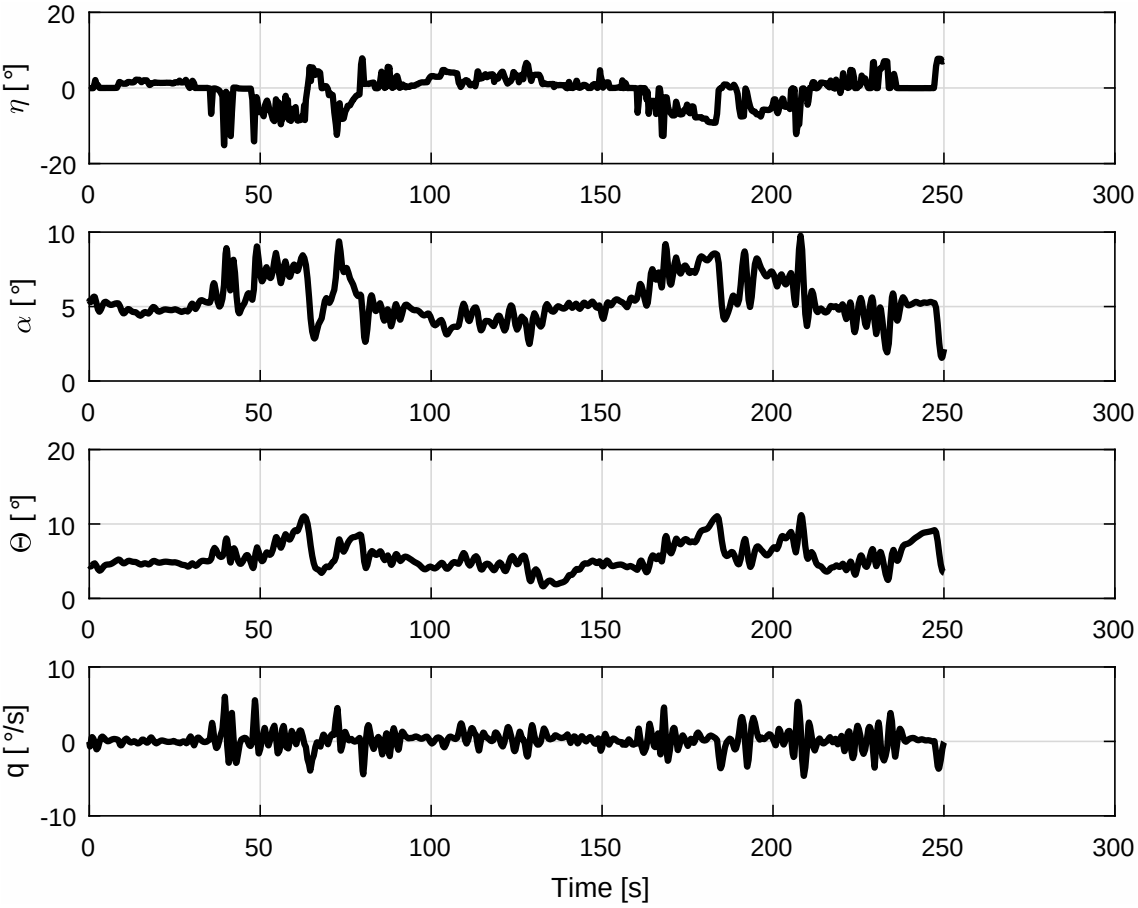

Figure G.18: Time histories of longitudinal parameters

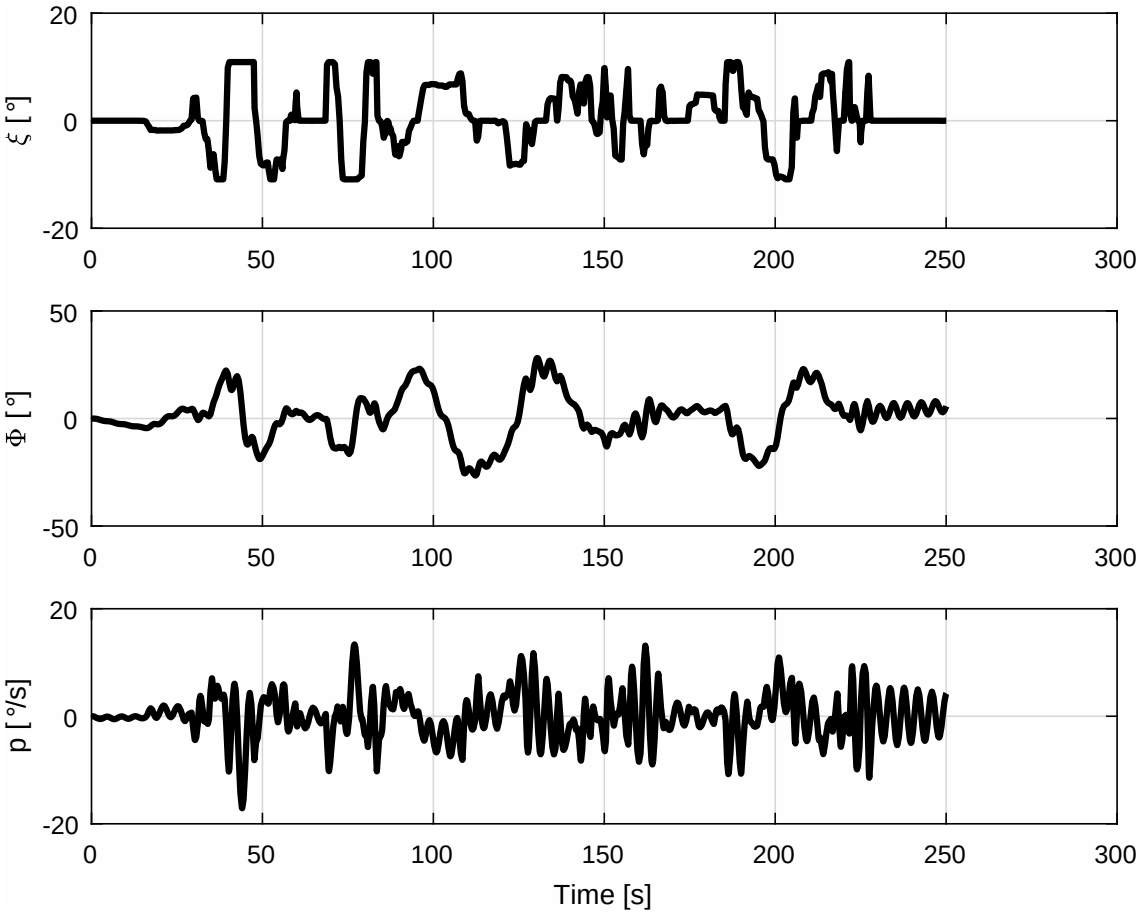

Figure G.19: Time histories of lateral parameters

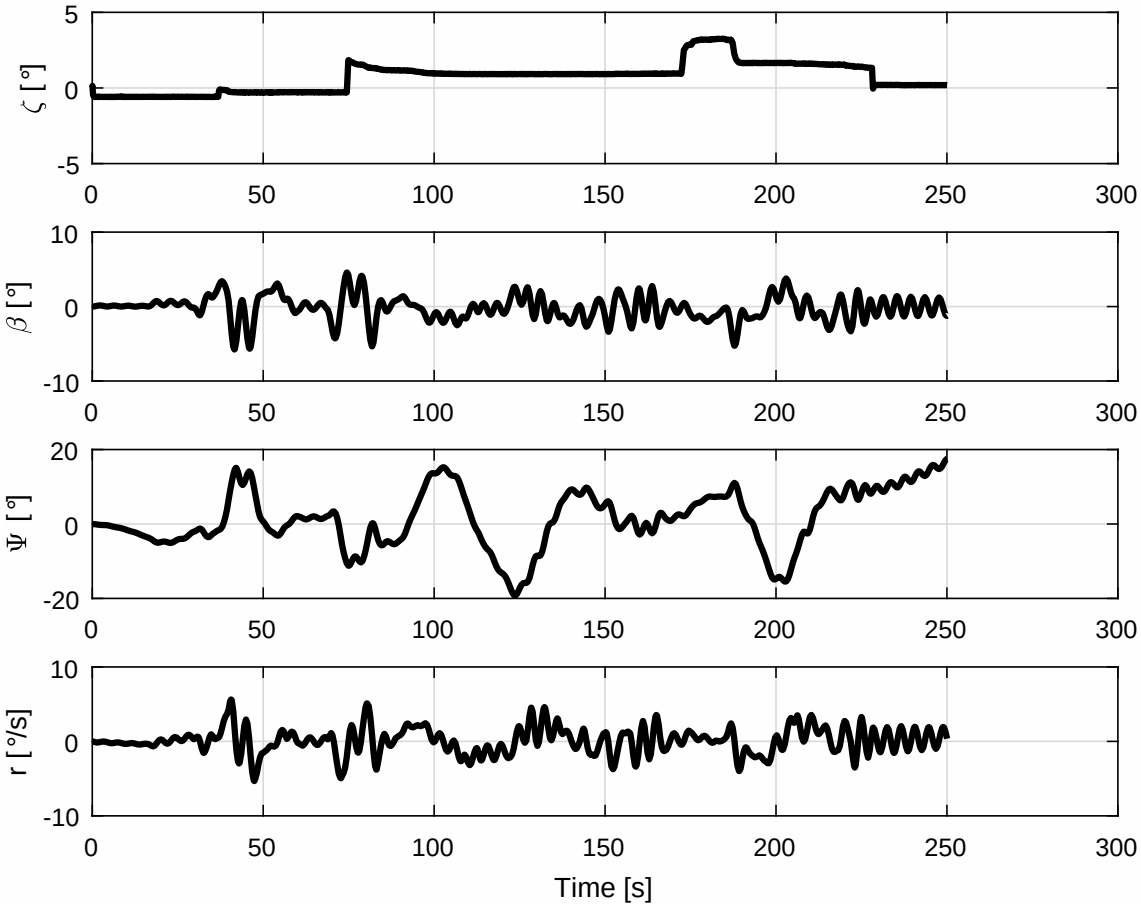

Figure G.20: Time histories of directional parameters